

**Head, trunk and in between –
the evolution and development of muscles in the head/trunk interface of
vertebrates**

Dissertation

To Fulfill the

Requirements for the Degree of

“doctor rerum naturalium” (Dr. rer. nat.)

**Submitted to the Council of the Faculty
of Biological Sciences
of the Friedrich Schiller University Jena**

by M.Sc., Benjamin Naumann

born on 02.03.1990 in Sömmerda

Date of defense: 24.08.2018

1. Reviewer: Prof. Dr. Lennart Olsson
Institut für Zoologie und Evolutionsforschung
Friedrich Schiller Universität, Jena, German
2. Reviewer: Prof. Dr. Dr. Martin S. Fischer
Institut für Zoologie und Evolutionsforschung
Friedrich Schiller Universität, Jena, Germany
3. Reviewer: Prof. Dr. Shigeru Kuratani
Evolutionary Morphology Laboratory
RIKEN Research Centre, Kobe, Japan

道場訓

- 一人格完戒に努める事
- 一誠の道を守る事
- 一努力の精神を養ふ事
- 一礼儀を重んずる事
- 一血氣の勇を戒める事

DÔJÔ- Kun

One: to strive for the perfection of character.

One: to defend the path of truth.

One: to foster the spirit of effort.

One: to honor the principles of etiquette.

One: to guard against impetuous courage.

English translation: Kanazawa, Hirokazu. S.K.I.
Kumite Kyôhan. 1987. Japan (no publishing
company)

Table of content

Summary.....	1
Zusammenfassung	3
Introduction	6
Evolutionary developmental biology – What is it good for?.....	6
The vertebrate head/trunk interface	10
The neural crest.....	14
The cardiopharyngeal field	18
The head and trunk myogenic program.....	21
Questions addressed in this study.....	25
Manuscript overview	26
Chapter 1	30
Naumann, B., Warth, P., Olsson, L., & Konstantinidis, P. (2017). The development of the cucullaris muscle and the branchial musculature in the Longnose Gar, (<i>Lepisosteus osseus</i> , Lepisosteiformes, Actinopterygii) and its implications for the evolution and development of the head/trunk interface in vertebrates. <i>Evolution & Development</i> , 19(6), 263-276.....	30
Chapter 2	45
Naumann, B., & Olsson, L. (2017). Three-dimensional reconstruction of the cranial and anterior spinal nerves in early tadpoles of <i>Xenopus laevis</i> (Pipidae, Anura). <i>Journal of Comparative Neurology</i> , 526(5), 836-857.....	45
Chapter 2 (Supplementary) – The developmental pattern of the cucullaris and diaphragmatico-branchialis muscles in <i>X. laevis</i>	68
Chapter 3	72
Naumann, B., Schmidt, J. & Olsson, L. <i>FoxN3</i> is involved in the development of the interatrial septum and the muscles in the head/trunk interface in the African clawed frog, <i>Xenopus laevis</i> (Pipidae: Anura: Lissamphibia). <i>Submitted</i>	72
Chapter 4	106

Naumann, & Olsson, L. “Escaping” the new head – Cranial neural crest cells inhibit early cardiac myogenesis in the Mexican axolotl, <i>Ambystoma mexicanum</i> (Ambystomatidae: Urodela: Lissamphibia). (<i>unpublished manuscript</i>).....	106
Discussion.....	133
Head, trunk and in between – The developmental and evolutionary pattern of the hypobranchial and cucullaris muscles	133
The role of the cardiac neural crest in amphibian heart development.....	140
Development and evolution of the muscles in the vertebrate head/trunk interface – “escaping” the circumpharyngeal crest	143
Method and techniques applied.....	146
A short note on the role of serendipity shaping this thesis	149
References	152
Eigenständigkeitserklärung (Declaration of authorship).....	170
CURRICULUM VITAE	171
Acknowledgements	177

Summary

The vertebrate head is often regarded as a discrete developmental unit, distinct from the trunk and governed by a different patterning mechanism. The head is patterned according to the branchial arches with patterning information primarily derived from the endoderm, a principle called “branchiomerism”. The trunk in contrast is patterned according to the somites, segmented blocks of mesoderm, a principle called “somitomerism”. The region of the vertebrate body where these two distinct patterning mechanisms meet is termed the head/trunk interface. The co-existence of two fundamentally different developmental patterning principles at the same axial level of the body is unique to vertebrates. As far as we know, the body architecture of all other animals is always based on one underlying patterning principle. The vertebrate head/trunk interface therefore offers a unique model to study how two different patterning principles interact in development and if this interaction might have played a special role in the evolutionary diversification of vertebrates.

During embryonic stages the vertebrate head/trunk interface is defined by the posterior-most population of cranial neural crest cells. At later stages it is still outlined by the vagal nerve dorsally and the hypoglossal nerve ventrally. Many unique structures develop close to the head/trunk interface, which is often denoted as the “neck region”. Examples are the vagal, accessory and hypoglossal nerves, the occipital bone, the pronephros, the heart, the shoulder girdle, and the muscles connecting the head and the trunk. Especially the muscles of the head/trunk interface have puzzled vertebrate comparative anatomists since the beginning of the 20th century. These muscles are divided into two groups, the ventral hypobranchial musculature and the dorsal cucullaris/trapezius muscle. Another very specialized muscle is derived from a common anlage with the cranial muscles, but has seldom been discussed in the context of the

vertebrate head/trunk interface. This muscle is the vertebrate heart and its close developmental relationship to the cranial muscles is reflected in the concept of the cardiopharyngeal field.

The aim of this study was to investigate the development and evolution of specific cardiopharyngeal field derivatives in two taxa, the highly derived tadpole of the frog species *Xenopus laevis* and the basal actinopterygian species *Lepisosteus osseus*. A comparison of the developmental pattern of the cucullaris and hypobranchial muscles of these species with data from other vertebrates indicates that the mechanisms that govern the early development of these muscle groups are conserved. Additional muscles in the two species are described, which span the head/trunk interface and show a developmental pattern highly similar to the cucullaris muscle. We examined Morpholino-mediated knock-down of *FoxN3*, a gene that plays a role in head but not trunk muscle patterning. It could be shown in *X. laevis* that the dorsal branchial muscles spanning the head/trunk interface are governed by the head developmental program. Defects in heart anatomy and development of these morphants were detected, adding more evidence to the close link between the heart and the head muscles. Recent study show that the vertebrate heart develops from two distinct mesodermal cell populations, the first and the second heart field. It is known that, as for head muscles, cranial neural crest cells are important for normal patterning and differentiation of second heart field-derived parts of the heart. Using the Mexican axolotl as a model, the role of cranial neural crest cells in the development of the early heart tube derived from the first heart field, was examined. In contrast to the second heart field, muscle differentiation is inhibited in cells derived from the first heart field. It is therefore speculated that this part of the heart pre-dates the evolution of neural crest cells and that the vertebrate head and chambered heart mainly evolved by interactions between the cranial neural crest, the second heart field and cranial muscle precursors.

Zusammenfassung

Der Kopf und der Rumpf der Wirbeltiere werden oft als eigenständige morphologische morphologische Einheiten betrachtet. Ihnen liegen unterschiedliche entwicklungsbiologische Musterbildungsprozesse zugrunde. Das der Kopfentwicklung zugrundeliegende Muster entstammt dem Endoderm und lässt sich in den Branchialbögen wiedererkennen. Ein Prinzip welches als „Branchiomerie“ bezeichnet wird. Das grundlegende Muster Rumpfungwicklung hingegen bilden segmentierte mesodermale Einheiten, die Somiten. Dieses Prinzip wird als „Somitomerie“ bezeichnet. Die Region des Wirbeltierkörpers in der beide Musterbildungsprozesse zusammentreffen bezeichnet man als „Kopf/Rumpf-Schnittstelle“ (im Englischen: „head/trunk-interface“). Die Koexistenz zweier grundlegend unterschiedlicher Musterbildungsprozesse in derselben Körperregion ist ein einzigartiges Merkmal der Wirbeltierentwicklung. Soweit bekannt basieren die Embryonalentwicklungen wirbelloser Tiere auf nur einem grundlegenden Musterbildungsprozess. Aus diesem Grund bietet die Kopf/Rumpf-Schnittstelle der Wirbeltiere ein einzigartiges Modell um die Interaktion zweier entwicklungsbiologischer Musterbildungsprozesse zu untersuchen. Dies ermöglicht die Fragestellung nach einer potentiellen Rolle dieser Interaktionen bei der evolutionären Diversifikation der Wirbeltiere.

Die Kopf/Rumpf-Schnittstelle des frühen Wirbeltierembryos ist definiert durch die posteriorste Population cranialer Neuralleistenzellen. In späteren Entwicklungsstadien zeichnet der Vagusnerv den dorsalen und der Hypoglossusnerv den ventralen Bereich dieser Schnittstelle nach. Viele einzigartige Strukturen entwickeln sich an dieser Schnittstelle, die oftmals auch als „Nackenregion“ bezeichnet wird. Beispiele sind der Vagus-, Accessorius- und Hypoglossusnerv, das Hinterhaupt (Occiput), der Pronephros, das Herz, der Schultergürtel und die Nackenmuskulatur, die eine Verbindung des Kopfes mit dem Rumpf darstellt. Seit Beginn des 20. Jahrhunderts sorgten vor allem die

Muskeln der Kopf/Rumpf-Schnittstelle für Diskussionen unter vergleichenden Anatomen. Die Muskulatur der Kopf/Rumpf-Schnittstelle lässt sich in zwei Gruppen unterteilen. Die hypobranchiale Muskulatur bildet die ventrale wohingegen die Cucullaris/Trapezius-Gruppe die dorsale darstellt. Ein anderer hochspezialisierter Muskel, der einer gemeinsamen Anlage mit der Kopfmuskulatur entspringt, entwickelt sich in derselben Region. Dieser Muskel ist das Herz der Wirbeltiere. Sein gemeinsamer entwicklungsbiologischer Ursprung mit der Kopfmuskulatur spiegelt sich in dem Begriff des „Cardiopharyngealen Feldes“ (im Englischen: „cardiopharyngeal field“) wieder.

Ziel dieser Studie ist die Untersuchung der Entwicklung und Evolution spezifischer Derivate des Cardiopharyngealen Feldes in zwei Taxa, der Kaulquappe des Froschlurchs *Xenopus laevis* und der basalen Actinopterygii-Spezies *Lepisosteus osseus*. Ein Vergleich der Entwicklungsmuster des Cucullaris und der hypobranchialmuskeln dieser beiden Arten mit Daten anderen Wirbeltieren deutet auf einen konservierten zugrundeliegenden Entwicklungsmechanismus. Weitere, die Kopf/Rumpf-Schnittstelle überbrückende Muskeln werden in beiden Arten beschrieben, Die Entwicklungsmuster dieser Muskeln weisen eine hohe Ähnlichkeit zu dem des Cucullaris/Trapezius-Muskels auf. Eine Untersuchung der Funktion des *FoxN3*-Gens in *X. laevis*, ein Gen unentbehrlich für eine normale Entwicklung der Kopf, jedoch nicht der Rumpfmuskulatur, zeigt eine craniale Herkunft dieser dorsalen „Schnittstellenmuskeln“. Zusätzlich wurden Defekte der Herzanatomie und -entwicklung festgestellt, die eine enge ontogenetische Verbindung des Herzes und der Kopfmuskulatur unterstützt. Aktuelle Untersuchungen zeigen eine entwicklungsbiologische Herkunft des Wirbeltierherzens von zwei unterschiedlichen Zellpopulationen, dem „Ersten und dem Zweiten Herzfeld“, auf. Wie für die Kopfmuskulatur, so ist die craniale Neuralleiste auch für die normale Entwicklung der

Zellen des Zweiten Herzfeldes unerlässlich. Eine potentielle Rolle der cranialen Neuralleiste in der Entwicklung des frühen Herzens, aufgebaut aus Zellen des Ersten Herzfeldes, wurde am Modellorganismus Axolotl untersucht. Im Gegensatz zum Zweiten Herzfeld wurde eine Inhibierung der Muskeldifferenzierung der Zellen des Ersten Herzfeldes festgestellt. Das erlaubt die Spekulation, des Vorhandenseins des Ersten Herzfeldes vor der Evolution der Neuralleistenzellen. Die Interaktion der cranialen Neuralleiste mit den Zellen des Zweiten Herzfeld und des Kopfmesoderms wäre demzufolge grundlegend für den evolutionären Ursprung des Kopfes und des gekammerten Herzens der Wirbeltiere.

Introduction

Evolutionary developmental biology – What is it good for?

Evolutionary developmental biology (or short “EvoDevo”) is a research program that requires an extensive interplay between what often has been independent paradigms, concepts and explanations, from different biological disciplines (Bonner et al., 2012; Love, 2003). The task of EvoDevo is to investigate developmental processes and place them in a phylogenetic framework to elucidate the sequence and mechanisms by which evolutionary changes occur over time. In my view, the interplay of the disciplines of comparative developmental anatomy and comparative developmental genetics creates one of the most fruitful theoretical frameworks to investigate the evolutionary origin and diversification of anatomical characters and offers the possibility to unravel “hidden” homologies.

The discipline of comparative developmental anatomy is in itself a blend of different approaches. Anatomy is the study of organic units or characters (e.g. organs) of the body of an organism. It describes the composition of an anatomical character and its arrangement (or position) in relation to the whole body (Fig. 1A) (Gegenbaur, 1889). Therefore, anatomy is based on pure empirical analysis. As stated by Gegenbaur, with increasing data about the anatomical characters of organisms it becomes tempting to compare these to each other (Gegenbaur, 1889; page 1). The comparison is a powerful method to determine similarities and dissimilarities between different organisms (Edgeworth, 1935; Gegenbaur, 1889; Hall, 2012). At this point, anatomy becomes comparative anatomy or “morphology” (Fig. 1B) (Gegenbaur 1889). Using the method of comparison, the task of morphology is to synthesize the empirical data of the purely analytical anatomy. This may result in the notion that an anatomical character, even if it is regarded as “the same” (homologous) in the different organisms, might show

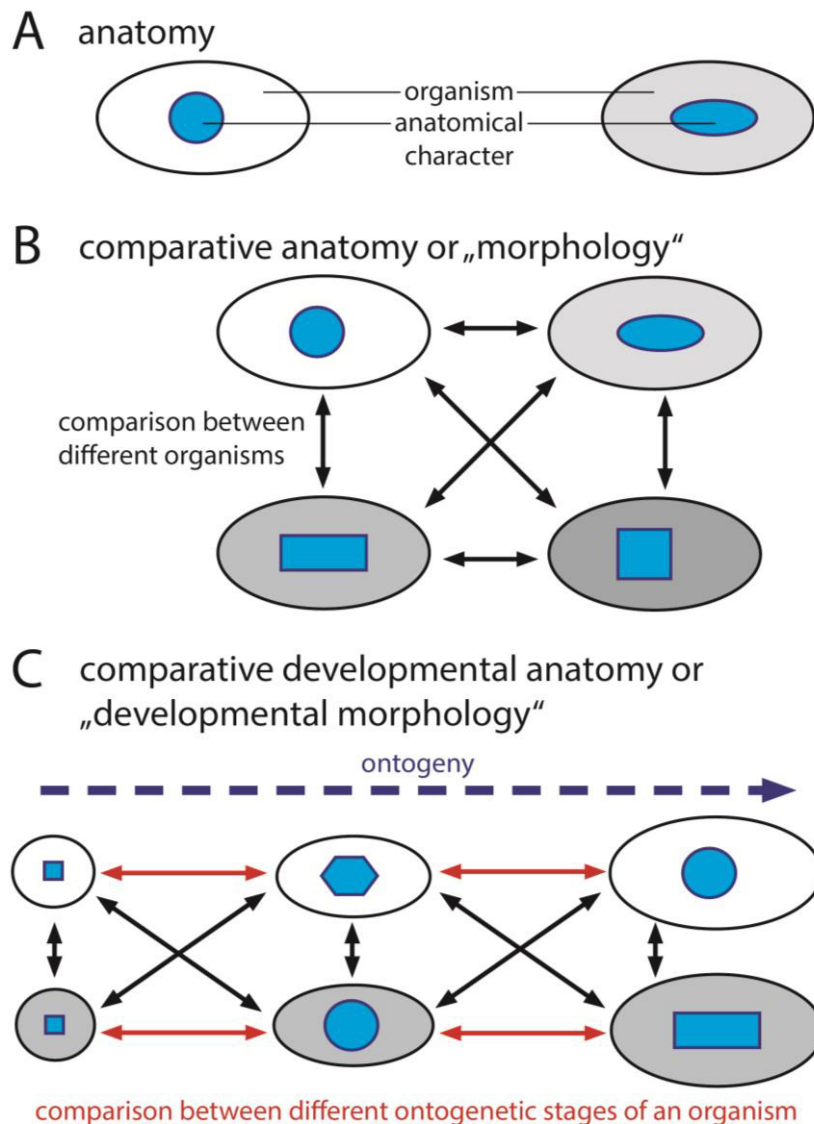


Figure 1: Schematic diagrams of practice in anatomy, morphology and developmental morphology. A, anatomy. The research field of anatomy is purely descriptive and does not compare between organisms. B, morphology. In morphology, comparisons are made between the anatomical descriptions of different organism. C, developmental morphology. In developmental morphology, comparisons are made between different ontogenetic/developmental stages of an organism and ontogenetic/developmental stages of different organism.

differences. That means, the same anatomical character might appear in different character states (Wagner, 2014). However, different character states might not only occur between organisms but also within one organism. Multicellular organisms have an ontogeny, i.e. they develop from a zygote into a multicellular, anatomically more complex adult (Haeckel, 1866). Similarly, the anatomical characters develop and change as the whole organism changes throughout its ontogeny. The developmental

trajectory of such a character is studied by comparative developmental anatomy (Fig. 1C). Comparative developmental anatomy or “developmental morphology” or “comparative embryology” (Wagner, 2007) is not purely analytical (as anatomy is), but rather a synthetic discipline. The reason is that describing the development of an anatomical character throughout ontogeny is always connected with a comparison of this character between different ontogenetic stages. Furthermore, developmental morphology enables us to compare the developmental trajectory of a character regarded to be the “same” in different organisms. By plotting the data gained from developmental morphology onto a pre-existing phylogenetic tree, it is possible to reconstruct the sequence of changes in the development or morphogenesis of an anatomical character. This allows asking questions about the evolution of an anatomical character regarded as the same in different organisms such as:

“Which parts of the developmental trajectory of a character are conserved and which parts have changed during the course of evolution?”

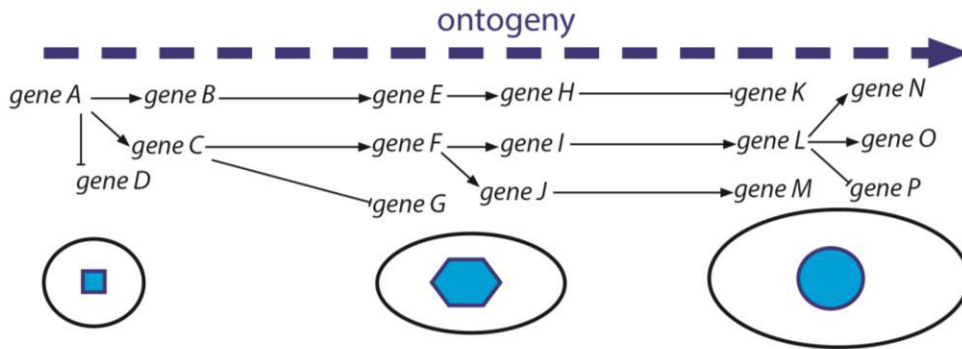
“What are the morphogenetic changes that led to the evolution of different character states of the same character across higher taxonomic groups?”

The second discipline important to the research program of EvoDevo is comparative developmental genetics. Developmental genetics examines how the genotype is transformed into the phenotype (Gilbert, 2013). In other words it asks the question:

“Which genes have to be expressed and how do their products interact to form a specific character during ontogeny?” (Fig. 2A).

The entirety of gene products interacting in the morphogenesis of a character forms a gene regulatory network (Davidson and Levin, 2005). The gene regulatory network underlies all processes involved in character morphogenesis such as cell proliferation,

A developmental genetics



B comparative developmental genetics

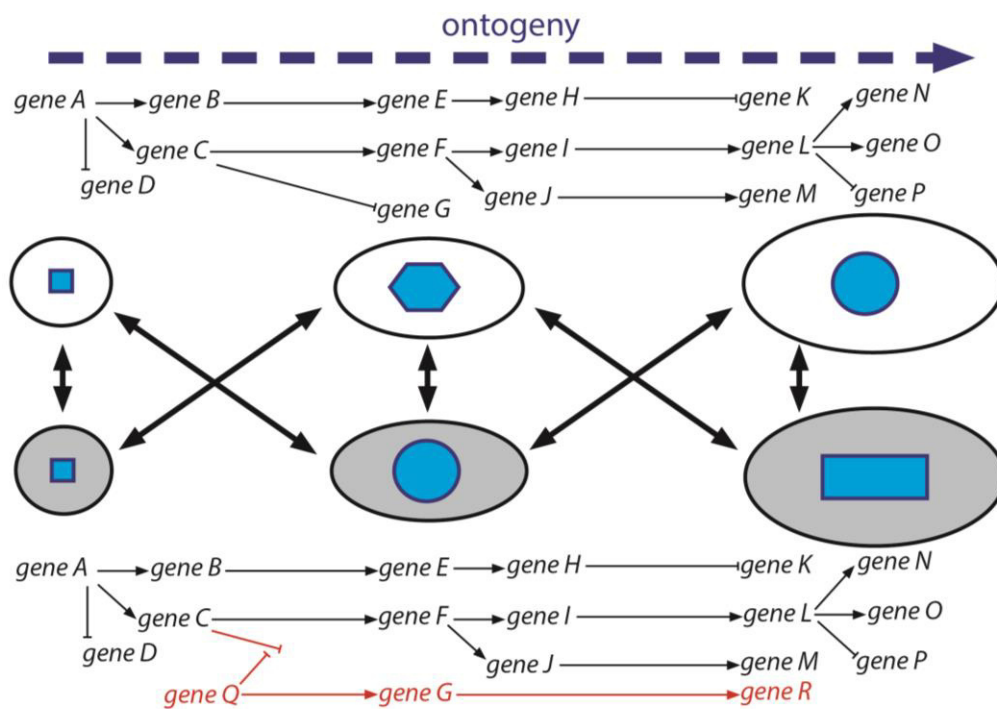


Figure 2: Schematic diagrams of practice in developmental genetics. A, developmental genetics. In the research field of developmental genetic, data about gene expression are compared between different ontogenetic/developmental stages of an organism. B, comparative developmental genetics. In comparative developmental genetics, comparisons are made between different ontogenetic/developmental stages of an organism and ontogenetic/developmental stages of different organism. Red genes and arrows represent “new” genes introduced in the defined developmental stages.

migration, induction, inhibition and differentiation. The examination of the gene regulatory networks underlying the development of the same character in different organisms makes it possible to elucidate the mechanisms responsible for the formation of different states of the same character (red genes and arrows in Fig. 2B). These

differences can be e.g. the introduction of "new" genes into a pre-existing network, differences in the time and place of the expression of a specific gene, or the level of the expression of a specific gene. At this point, developmental genetics becomes comparative developmental genetics. This has the potential to explain the mechanisms underlying the morphogenetic changes observed by developmental morphology and allows asking classical EvoDevo questions such as:

"Which genes influence the developmental changes (process) of an anatomical character (pattern) during evolution?" or "What is the mechanism underlying the development and evolution of different character states from the same anatomical character in different taxa?"

Using the research program of EvoDevo it might become possible to identify mechanisms that govern the development and evolution of the vertebrate head/trunk interface, also known as the "neck" region.

The vertebrate head/trunk interface

The idea of the head/trunk interface has been introduced by Shigeru Kuratani in 1997. It is based on the notion, that the vertebrate body is organized by two different patterning mechanisms. In the trunk a lot of anatomical structures, such as nerves, blood vessels, bones and muscles are patterned according the embryonic somites. Somites are distinct blocks of paraxial mesoderm which develop along the antero-posterior axis in a segmented manner (Gilbert, 2013). They give rise to the vertebrae, ribs, the epaxial as well as the limb musculature and the dermis underlying the skin. The term "somitomerism" (Fig. 3A) refers to the importance of these somites in trunk patterning (Kuratani, 1997). Since the "vertebral theory of the skull" (Goethe, 1820; Kuratani, 1997) many different opinions about the primary organization vertebrate head have been proposed. The prevailing opinion was that, as in the trunk, segmented blocks of

mesoderm (called somitomeres) lay down the primary pattern for the developing head (Goodrich, 1930; Jacobson, 1993; Kuratani, 2003; Meier, 1981; Olsson et al., 2005). However, the presence of somitomeres in the head has never been shown unambiguously. Nowadays it is thought that the organization of the vertebrate head is based on the segmental pattern of the visceral arches. The importance of the visceral arches in head patterning is reflected in the term “branchiomerism” (Fig. 3A) (Kuratani, 1997; Kuratani, 2003; Olsson et al., 2005).

Even though head and trunk show different patterning principles (branchiomerism vs. somitomerism) they do not develop completely separated from each other. The head/trunk interface (Kuratani, 1997) can be illustrated as an s-shaped line bordering the post-otic somites dorsally and the posterior pharyngeal arches ventrally (Fig. 3, dashed red line). In the embryo, the head/trunk interface is demarked by the cells originating from the posterior-most cranial neural crest (NC) on the axial level of the anterior-most post-otic somites (Fig. 3B). In contrast to the trunk neural crest cells (NCCs), which migrate ventrally through the posterior half of the overlaying somite, cranial NCCs are not able to migrate on this way. Instead, they migrate anteriorly in the direction of the developing otic capsule. Reaching the anterior-most somite, they curve ventrally and start to populate the posterior visceral arches in an anterior-to-posterior manner (Fig. 3B, white arrow) (Kuratani, 1997; Kuratani et al., 2018; Kuratani and Kirby, 1991). This curve around the post-otic somites represents the dorsal part of the head/trunk interface. Beneath the post-otic somites and posterior to the last visceral arch, there is a “partially encircling horseshoe-shaped ridge on the lateral body wall” (Kuratani, 1997). This so-called circumpharyngeal ridge has been shown to contain NCCs, equivalently named the circumpharyngeal crest cells (Kuratani and Kirby, 1991). The circumpharyngeal crest cells are the posterior-most population of the cranial NC.

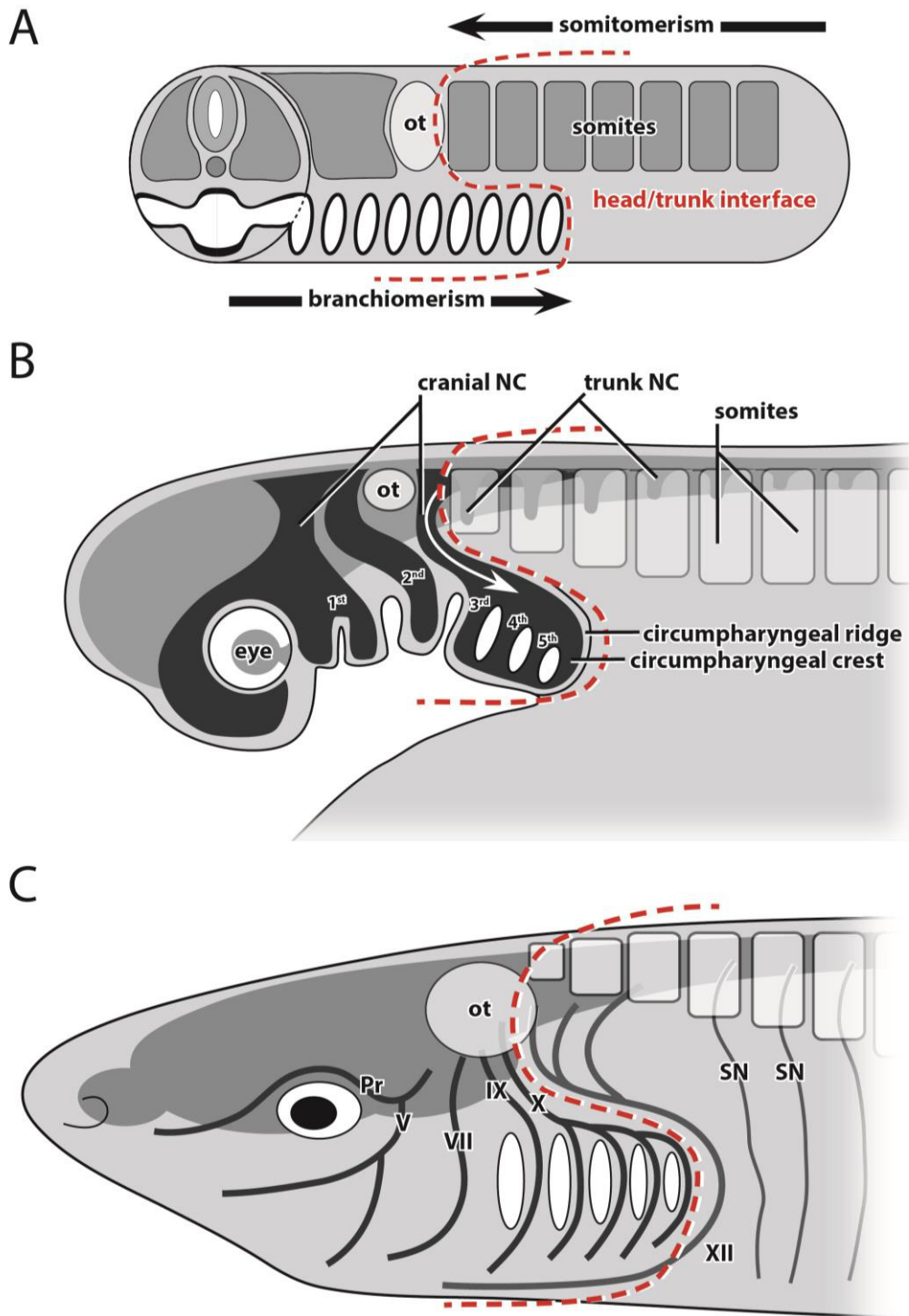


Figure 3: Schematic diagrams of the anterior body region of vertebrates. The dashed red line demarcates the head/trunk interface. A, hypothetical ancestral vertebrate. Two patterning mechanisms, the branchiomerism of the head and the somitomerism of the trunk meet at the head/trunk interface. Modified from Kuratani, 1997. B, later embryo from a lateral view. The migrating cranial neural crest cells (dark grey) invade the visceral arches. The posterior-most cranial neural crest cells gather in the circumpharyngeal ridge and are called the circumpharyngeal crest. Somites are depicted half-transparent to show the migrating trunk neural crest cells in the posterior half of each somite. Numbers refer to the visceral arches. The white arrow indicates the migration route of the posterior cranial neural crest cells. Embryo design modified from Kuratani et al., 2018. C, adult vertebrate from a lateral view. The head/trunk interface is still delineated by the vagal and hypoglossal nerves. V, trigeminal nerve; VII, facial nerve; IX, glossopharyngeal nerve; X, vagal nerve; XII, hypoglossal nerve; ot, otic capsule; Pr, profundal nerve; SN, spinal nerve.

They represent the ventral part of the head/trunk interface (Fig. 3B). In later developmental stages, after the NCCs have been differentiated into various structures, the head/trunk interface can still be illustrated by a similar s-shaped pattern. The dorsal part is now demarcated by the stem of the vagal nerve (Fig. 3C, X). The ventral part is lined by the course of the hypoglossal nerve, a compound nerve formed by the anterior post-otic spinal nerves (Fig. 3C, XII). The co-existence of two fundamentally different developmental patterning principles at the same axial level of the body is unique to vertebrates. To my best knowledge, the body architecture of all other animals is always based on one underlying patterning principle. Vertebrates therefore offer a unique model to study how two different patterning principles interact in development and if this interaction might have played a special role in the evolutionary diversification of vertebrates.

This special role is indicated by many unique structures that develop close to the head/trunk interface which is often denoted as the “neck region” (Ericsson et al., 2013; Kuratani, 2008). Examples are the vagal (X), accessory (XI) and hypoglossal (XII) nerves, the occipital bone, the pronephros, the shoulder girdle and the muscles connecting the head and the trunk (Edgeworth, 1935; Ericsson et al., 2013). Especially the muscles of the head/trunk interface have puzzled vertebrate comparative anatomists since the beginning of the 20th century (Edgeworth, 1911; 1935; Gegenbaur, 1889). They are divided in two groups, the ventral hypobranchial (or tongue) musculature and the dorsal cucullaris/trapezius muscle (Ericsson et al., 2013). Additionally, another very specialized muscle develops in the transition zone between the head and the trunk but was sparsely discussed in this context. This muscle is the vertebrate heart. To access the EvoDevo of muscles in the head/trunk interface, it is necessary to introduce three additional concepts in detail: the neural crest (and especially a sub-population of it: the

cardiac neural crest), the cardiopharyngeal field and the head and trunk myogenic program.

The neural crest

In 1886 the swiss embryologist Wilhelm His described a small population of cells present between the neural tube and the surface ectoderm in a chicken embryo (His, 1868). His named this cell population the “Zwischenstrang” (intermediate cord). This name has been switched to neural crest (NC) at the end of the 19th century, denoting the crest of the neural fold as its side of origin. After neural fold closure (Fig. 4 A, B) and subsidence of the neural tube (Fig. 4C), neural crest cells (NCCs) migrate ventrally to populate various regions of the body (Fig. 4D) (Gilbert, 2013). In the trunk region, NCCs migrate as single cells through the posterior half of each somite and differentiate into melanocytes, sympathetic as well as dorsal-root ganglia and chromaffin cells of the adrenal medulla (Hall, 1999). Cranial NCCs differ tremendously from their cognates in the trunk. In contrast to the trunk NCCs, cranial NCCs migrate ventrally in distinct streams (Fig. 1E, F). The most anterior, the mandibular (trigeminal) stream migrates around the eye and into the first visceral (mandibular) arch. The hyoid (facial) stream migrates into the second visceral (hyoid) arch. The posterior-most, the branchial (vagal) stream subdivides into several smaller streams migrating into the third to seventh visceral (first to fifth branchial) arches (Fig. 5). Cranial NCCs are able to differentiate into pigment cells, cartilage, bone, cranial neurons and glia cells as well as connective tissue surrounding and patterning the head muscles (Ericsson et al., 2004; Noden, 1983c; Rinon et al., 2007). The importance of the NC in vertebrate development gave it the status of a fourth germ layer additionally to the endo-, meso- and ectoderm, classifying vertebrates as “quadroblastic” animals (Hall, 2000). Not enough, the extensive contribution of cranial NC to craniofacial structures has led zoologists to propose that the evolution of “a new head” and the subsequent success of vertebrates are

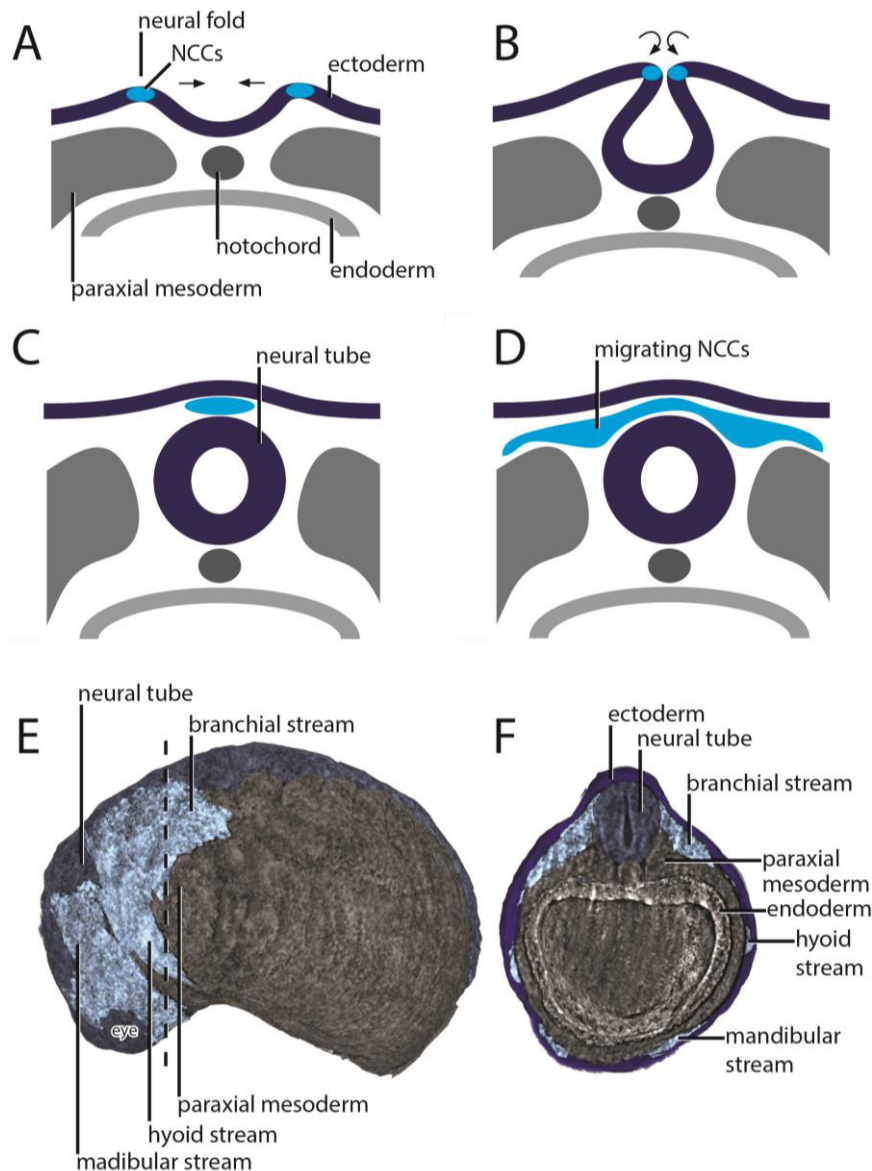


Figure 4: Neurulation and neural crest cells development. A-D, schematic cross sections through the dorsal region of a neurulating embryo. The dorsal ectoderm (dark blue) invaginates to form the neural tube. Neural crest cells (light blue) delaminate from the dorsal ectoderm in the neural folds and migrate ventrally. The arrows indicate the movement of the ectoderm. E and F, in-vivo phase contrast scans of an axolotl embryo at stage 24. The neural crest cells (light blue) migrate ventrally in discrete streams. E, lateral view with the ectoderm removed. The dashed line indicates the region of the cross section in F. NC, neural crest; NCCs, neural crest cells.

in huge parts due to the emergence of the cranial NCCs (Gans and Northcutt, 1983). Since its discovery in 1886 our understanding about the role of the NC in craniofacial patterning has increased tremendously. Many cellular and molecular mechanisms are known and much effort is made to completely dissect signaling cascades, migration mechanisms and interactions of NCCs with other tissues (Ericsson et al., 2004; Graham

et al., 1996; Green et al., 2015; Gross and Hanken, 2008; Jeong et al., 2004; Minoux and Rijli, 2010; Noden and Schneider, 2006; Santagati and Rijli, 2003; Schmidt et al., 2011; Trainor and Krumlauf, 2001).

During the 1980s a “novel” role of the NC in cardiovascular development has been described by Margaret Kirby and colleagues and was introduced as the concept of the cardiac NC (Kirby et al., 1983). The cardiac NC is a specific subpopulation of the branchial NC (Fig. 5A, B) located at the mid-otic level of the hindbrain. It patterns the visceral arch arteries and contributes to distinct parts of the heart (Fig. 5C) (Kirby and Waldo, 1995; Kuratani and Kirby, 1991; Waldo et al., 1998). The extent to which cardiac NCCs contribute to the heart varies greatly between different taxa (Fig. 6). In the chicken (*Gallus gallus*) and the mouse (*Mus musculus*), cardiac NCCs can be found in the visceral arch arteries and the septa of the outflow tract such as the aorticopulmonary septum (Jiang et al., 2000; Kirby et al., 1983; Kirby et al., 1985; Kirby and Waldo, 1995). In the African clawed frog (*Xenopus laevis*) the data are ambiguous. One study states that NCCs do not enter the outflow tract and do not contribute to its septation by the spiral septum (Lee and Saint-Jeannet, 2011). In another study it is shown that they also contribute to the outflow tract of *X. laevis* (Martinsen et al., 2004). Both of these studies report a cardiac NC contribution to the aortic sac and the visceral arch arteries. In the zebrafish (*Danio rerio*) cardiac NCCs populate the whole heart tube. They are found in the outflow tract, the ventricle and the atrium. Interestingly it has been reported, that cardiac NCCs can differentiate into muscle cells and contribute to the myocardium of the heart, a feature that has not been found in other vertebrates so far (Li et al., 2003; Sato and Yost, 2003).

Despite the cited studies, information about the direct and indirect interaction of the cardiac NC with cardiogenic mesoderm is scarce. It is known that the vertebrate heart

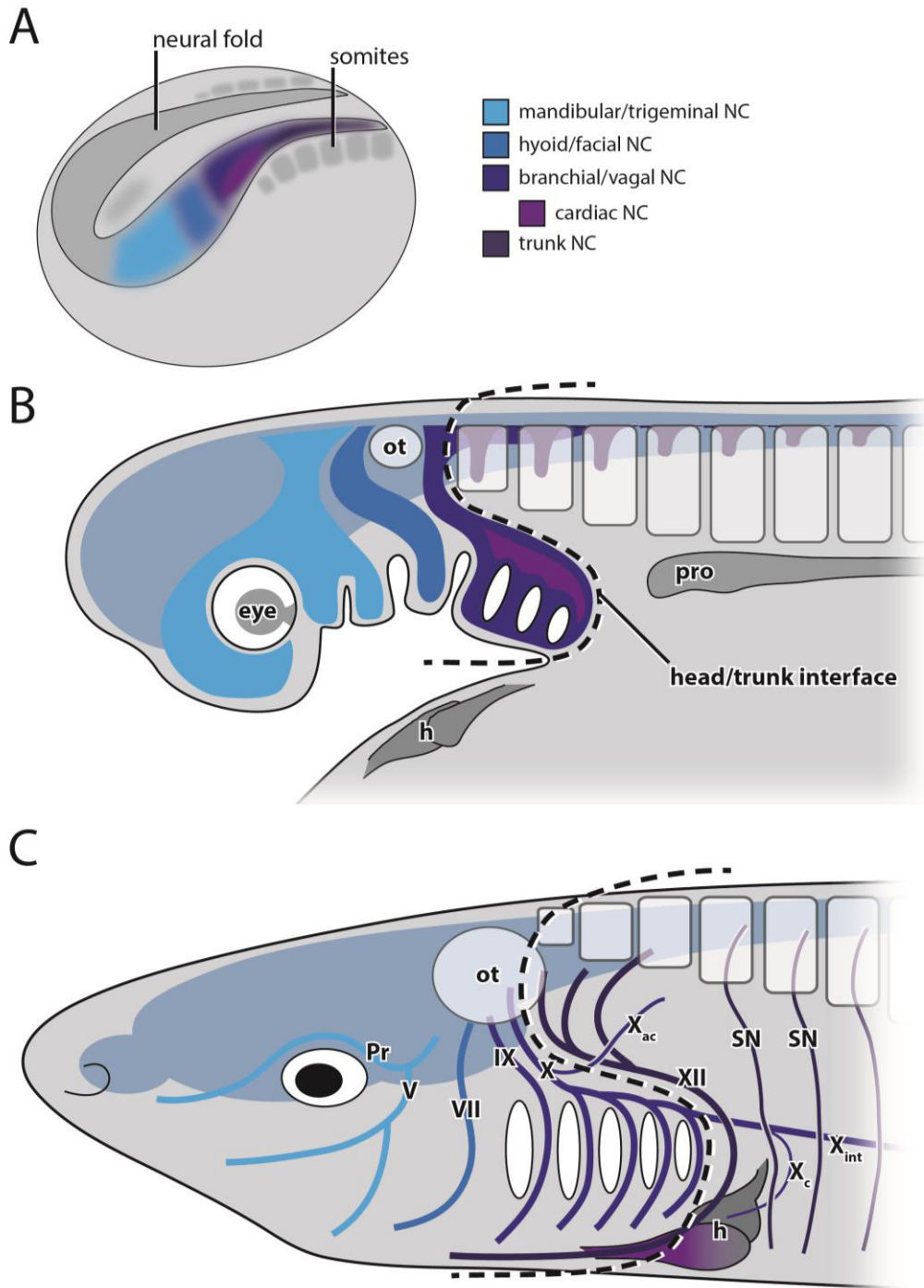


Figure 5: Schematic diagrams of different developmental stages of the anterior body region of vertebrates. Sub-populations of neural crest cells are colored in different shades of blue and purple. The dashed line demarcates the head/trunk interface. A, neurula stage. B, later embryo from a lateral view. C, adult vertebrate from a lateral view. The ramus accessorius and the intestinal and cardiac rami of the vagal nerve cross the head/trunk interface. V, trigeminal nerve; VII, facial nerve; IX, glossopharyngeal nerve; X vagal nerve; X_{ac}, X ramus accessorius; X_c, X ramus cardiopulmonaris; X_{int}, X ramus intestinalis; XII, hypoglossal nerve; h, heart; ot, otic capsule; Pr, profundal nerve; pro, pronephros; SN, spinal nerve.

forms at least from two different mesodermal cell populations. The first population forms the primary heart tube while the second forms the outflow tract and contributes to

various other chambers in later stages of heart development (Diogo et al., 2015). In chicken, it has been shown that cardiac NCCs interact with cells from the second mesodermal population (Waldo et al., 2005). Interactions of the NC with cells from the first cell population, forming the primary heart tube have not been studied.

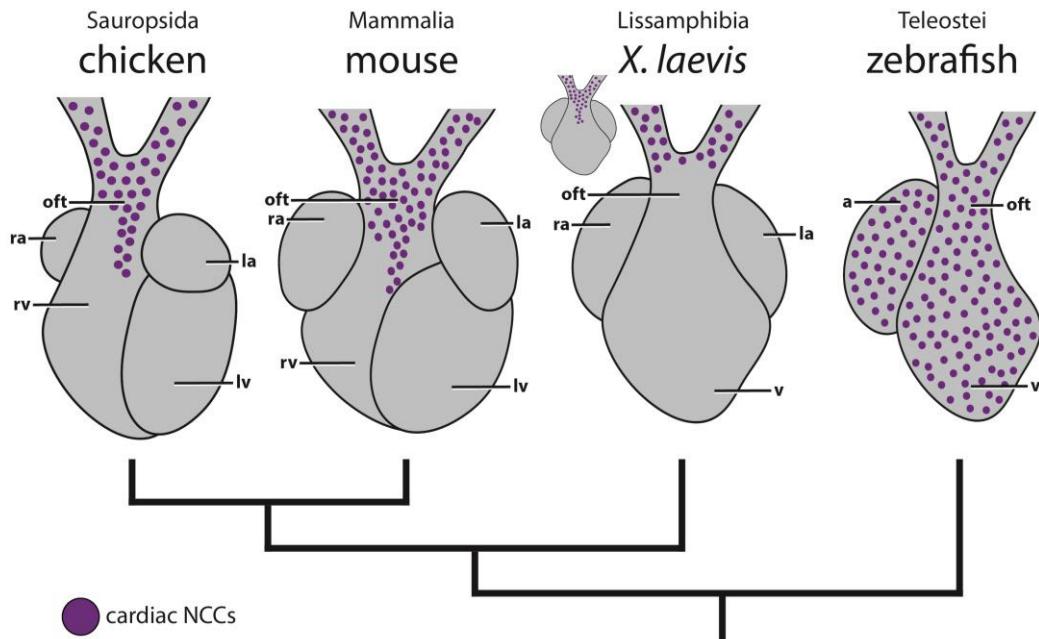


Figure 6: Schematic diagrams of the hearts of different vertebrate taxa. Neural crest cells (purple dots) contribute to the outflow tract in the chicken and mouse. In *Xenopus*, was reported by Sadaghiani and Thiébaud, 1987 (depicted as smaller diagram) but not found by Lee and Saint-Jeannet, 2011. In the zebrafish, neural crest cells contribute to all parts of the heart. a, atrium; la, left atrium; lv, left ventricle; NCCs, neural crest cells; oft, outflow tract; ra, right atrium; rv, right ventricle; v, ventricle.

The cardiopharyngeal field

In his Book “Vergleichende Anatomie der Wirbelthiere” the outstanding anatomist Carl Gegenbaur wrote, that the myocardium of the heart develops from the ventral parts of the lateral splanchnic mesoderm (Gegenbaur, 1889; page 343). The cranial splanchnic mesoderm is continuous with the cranial paraxial mesoderm, giving rise to most head muscles (Fig. 7). This implies a close link between the development of the heart and the head musculature. In recent years, the common developmental origin of the heart and head muscles has regained interest by the advent of new cell lineage and genetic labeling

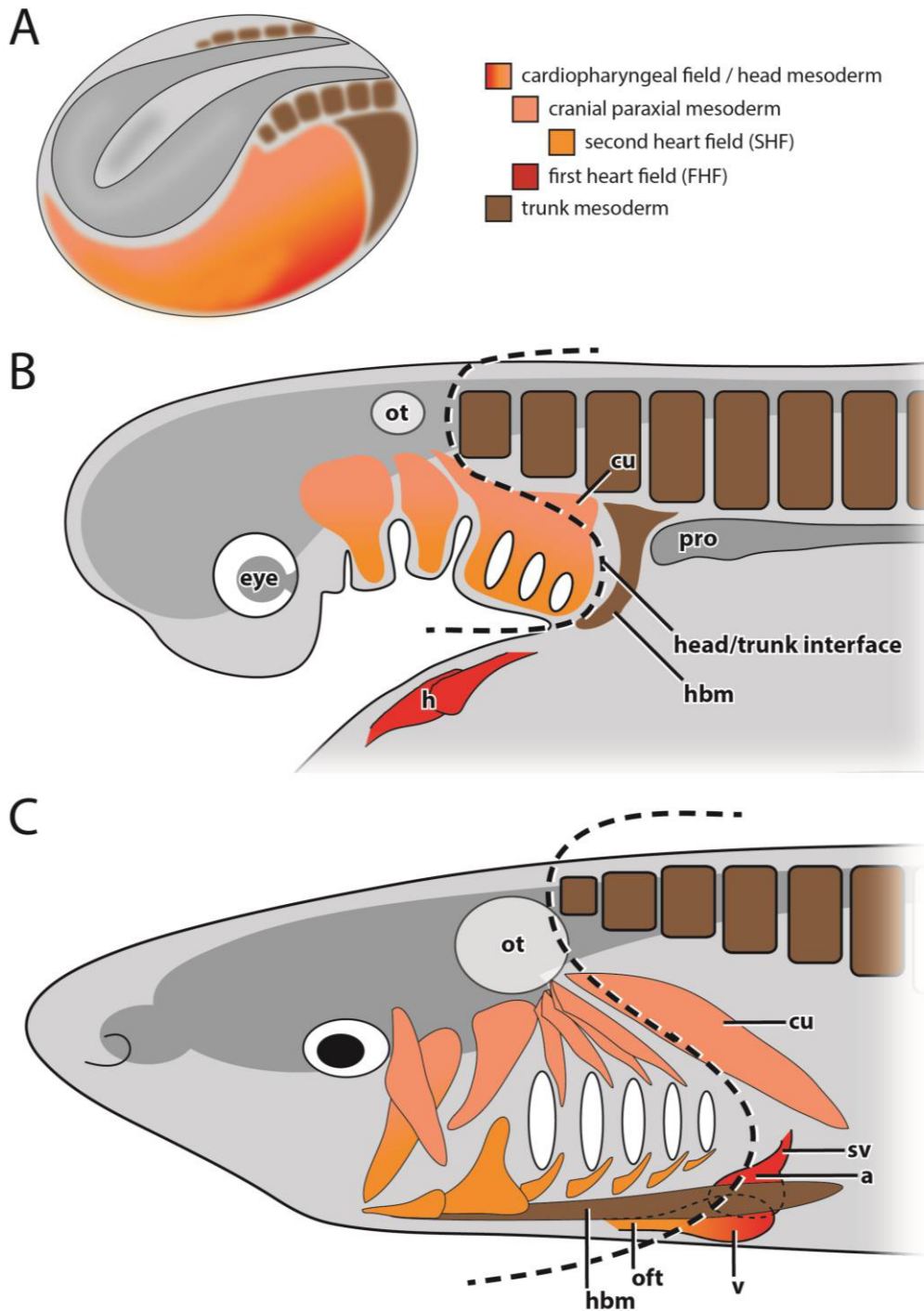


Figure 7: Schematic diagrams of different developmental stages of the anterior body region of vertebrates. Different sub-populations of the head mesoderm is colored in red, orange and yellow. The trunk mesoderm is colored in brown. The dashed line demarcates the head/trunk interface. A, neurula stage. B, later embryo from a lateral view. Migratory muscle precursors from the anterior-most somites migrate ventrally to form the hypobranchial musculature. The cucullaris anlage crosses the head/trunk interface. C, adult vertebrate from a lateral view. a, atrium; cu, cucullaris; h, heart; hbm, hypobranchial muscles; oft, outflow tract; ot, otic capsule; pro, pronephros; sv, sinus venosus; v, ventricle.

techniques (Tirosh-Finkel et al., 2006b). This led to the emergence of the idea of the cardiopharyngeal field (CPF). The CPF is a cell population that gives rise to the heart

and head muscles (Diogo et al., 2015). It is made up by the first heart field (FHF), the cranial paraxial mesoderm and the second heart field (SHF) (Fig. 7A). Cells of the FHF are located in the posterior region of the cranial splanchnic mesoderm (Fig. 7). They differentiate early and contribute to the linear heart tube, and later to parts of the atria and the left ventricle. The SHF is located anterior to the FHF and is continuous with the cranial paraxial mesoderm dorsally (Fig. 7). Cells from the SHF differentiate later and contribute to the myocardium of the outflow tract, the right ventricle and the atria as well as the ventral head muscles and, in mouse, parts of the dorsal head muscles in mouse (Tzahor, 2009). The cranial paraxial mesoderm however will give rise to the dorsal head muscles (Fig. 7) and, contributes the cardiac outflow tract in chicken (Fig. 8) (Diogo et al., 2015; Tzahor, 2009). Signals from the adjacent pharyngeal endoderm, surface ectoderm and the cranial neural crest control if cells from the cranial paraxial mesoderm differentiate into cardiac or skeletal muscles (Nathan et al., 2008; Tirosh-Finkel et al., 2006a; Tzahor and Evans, 2011; Tzahor and Lassar, 2001; Zhu et al., 2016). Additional evidence for the link between the heart and the head muscles is given by the similar regulatory factors involved in heart as well as head myogenesis (Diogo et al., 2015). The cardiogenic regulatory factors *Isl1* and *Nkx2-5* are expressed in the CPF and indispensable for either heart and head myogenesis (Bothe and Dietrich, 2006; Nathan et al., 2008; Sambasivan et al., 2011a). On the other hand, major factors involved in head muscle development such as *Tbx1* and *Pitx2* are also crucial for heart muscle formation (Sambasivan et al., 2011a; Tzahor, 2009).

The close relationship between the heart and the head muscles offers the interesting opportunity to discuss heart development in the context of the head/trunk interface as it has been done for the head muscles (Ericsson et al., 2013; Kuratani, 2008; Theis, 2010; Theis et al., 2010).

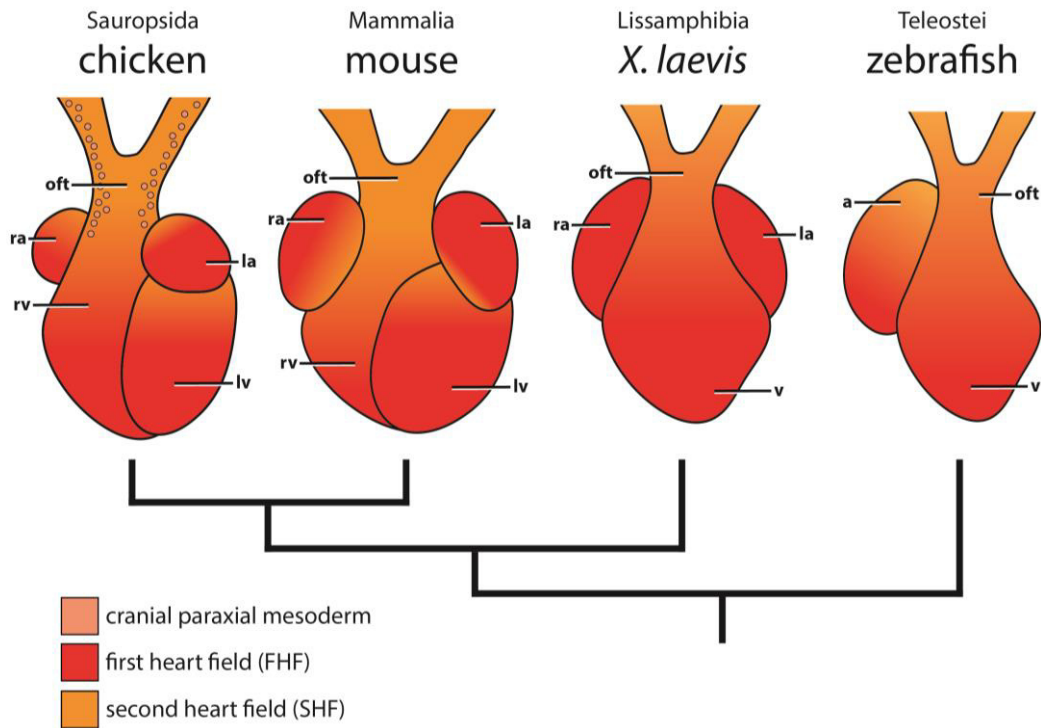


Figure 8: Schematic diagrams of the hearts of different vertebrate taxa. Colors indicate contributions of cells from the FHF and SHF to specific parts of the heart. In the chicken, cells from the cranial paraxial mesoderm contribute to the outflow tract. a, atrium; la, left atrium; lv, left ventricle; NCCs, neural crest cells; oft, outflow tract; ra, right atrium; rv, right ventricle; v, ventricle.

The head and trunk myogenic program

It has been shown, that heart and head muscle progenitors are dependent upon similar signaling molecules to enter their myogenic program. But what about the trunk muscles, developing posterior to the head/trunk interface? Despite sharing the same “core myogenic program”, early initiation of myogenesis in the head varies greatly to that in the trunk (Fig. 9) (Sambasivan et al., 2011b; Tzahor et al., 2003).

Head muscles (extra-ocular, visceral arch and some neck muscles) are innervated by cranial nerves and originate from the un-segmented paraxial mesoderm. They are often named “genuine head muscles” to distinguish them from the hypobranchial muscles with a trunk origin. The extra-ocular muscles show a different developmental program compared to the other genuine head muscles (Rios and Marcelle, 2009). Due to this, I will only refer to the visceral arch and neck muscles in this study. As mentioned earlier,

mesoderm giving rise to genuine head muscles is marked by genes such as *Isl1* (also *Islet1*) and *Nkx2-5*, *Tbx1* and *Pitx2* (Diogo et al., 2015). Genes like *Capsulin* and *Twist* prevent the myogenic progenitors from differentiation and keep them in a proliferative state. The onset of myogenic differentiation is marked by *Myf* and *MyoD* and further differentiation by *Myogenin* and myosin heavy chain (*MyHC*) (Theis et al., 2010). The differentiation of head muscles is delayed compared to trunk muscles (Theis, 2010). This is because BMP- and Wnt-Signals from the neural tube and dorsal ectoderm inhibit differentiation of head muscle progenitors (Theis, 2010). Wnt-inhibitors (e.g. *Frzb*) and BMP-inhibitors (e.g. *noggin*, *gremlin*) secreted by neural crest cells release head myoblasts from inhibition and promote differentiation (Tzahor et al., 2003). Neural crest cells also form the connective tissue, patterning and surrounding the head muscles (Ericsson et al., 2004; Matsuoka et al., 2005; Noden, 1983a).

Trunk muscles are innervated by the spinal nerves (Edgeworth, 1935). They originate from the somites in a segmented manner (Gilbert, 2013). Somitic myogenic progenitors express genes such as *Pax3* and *Pax7* (Buckingham, 2017; Buckingham and Relaix, 2007). *Pax3*, analogous to *Capsulin*, *Twist* and maybe *Tbx1* in the head, promotes cell proliferation and inhibits myogenic differentiation in trunk myoblasts (Theis, 2010). Additionally it activates *c-Met* which product initiates an epithelial to mesenchymal transition in some of the trunk myoblasts. These myoblasts migrate ventrally away from the somites to form the hypaxial, limb and hypobranchial musculature. The non-migratory paraxial trunk myoblasts will give rise to the epaxial muscles (Theis, 2010). After lineage specification *Myf5* and *MyoD* initiate the differentiation process as they do in the head. However the gene *MRF4* might also play a role in trunk muscle differentiation but is not expressed during head muscle development (Theis, 2010). Epaxial and hypobranchial trunk muscles are the first muscles developing in the embryo. It is suggested, that Wnt-signals from the neural tube promote trunk muscle

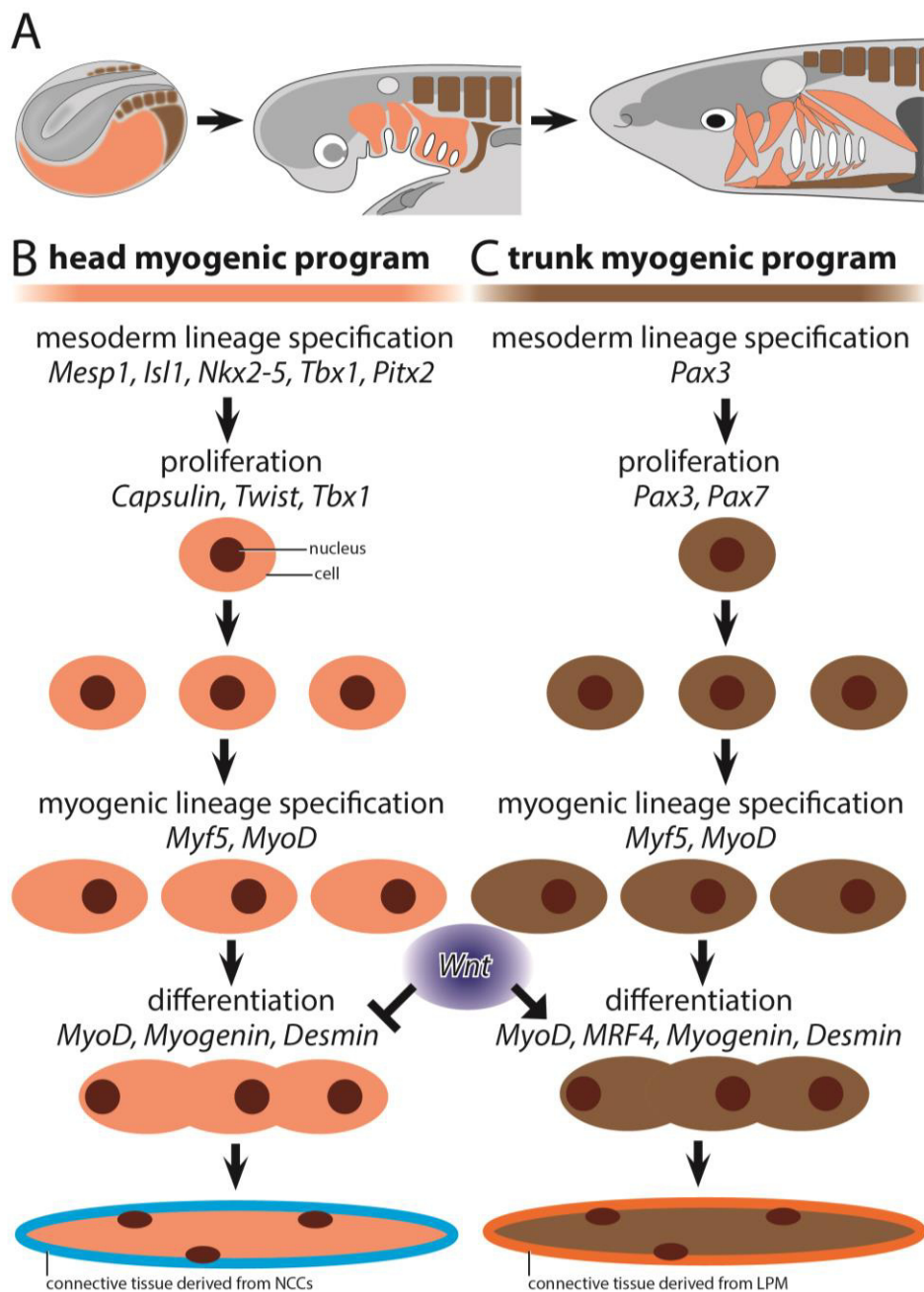


Figure 9: Head and trunk myogenic program. A, Schematic diagrams of different developmental stages of the anterior body region of vertebrates to illustrate the development of the head (flesh) and trunk musculature (brown). B, head myogenic program. C, trunk myogenic program. Wnt inhibits fiber formation in head myoblasts but activates the same process in trunk myoblasts. LPM, trunk lateral plate mesoderm; NCCs, neural crest cells.

differentiation in contrast to the inhibiting effect on head muscle differentiation (Fig. 9) (Theis, 2010). Another difference is the origin of the connective tissue surrounding the trunk muscles. It is derived from the trunk lateral plate mesoderm instead of neural crest cells.

These clearly defined characters of head and trunk muscles become fuzzy regarding the muscles developing in the head/trunk interface. While the hypobranchial musculature for example exhibit almost all of the typical trunk muscles characters, its associated connective tissue is derived from cranial neural crest cells (Ericsson et al., 2013). The cucullaris/trapezius muscle, occupying the dorsal area of the head trunk interface, is another example. Nowadays it is thought, that it originates from the head mesoderm (Ericsson et al., 2013; Sefton et al., 2016; Theis et al., 2010). In amniotes, this muscle is innervated by the accessory nerve (cranial nerve XI) which has shown to be neither a cranial nor a typical spinal nerve (Tada and Kuratani, 2015) and might get some additional innervation from cervical spinal nerves (Edgeworth, 1935). In the Mexican axolotl (*Ambystoma mexicanum*), it has been shown that neural crest cells, normally giving origin to the connective tissue of head muscles, do not contribute to the connective tissue of the cucullaris (Epperlein et al., 2012). This further indicates, that the head/trunk interface is more a transition zone than a border between the head and the trunk. However, most data available are from only a few tetrapod model organisms such as the chicken, mouse, African clawed frog and the Mexican axolotl. Data from much more species are needed to completely understand of the developmental diversity at the vertebrate head/trunk interface.

Questions addressed in this study

Is the developmental pattern of the cucullaris muscle of the basal actinopterygian Longnose gar, *Lepisosteus osseus*, similar to that observed in tetrapods?

Is the developmental pattern of the cucullaris muscle of the African clawed frog, *Xenopus laevis*, similar to that observed in other tetrapod taxa?

Answering these questions will test the explanatory scenario for the molecular mechanism governing the development of the tetrapod cucullaris muscle proposed by Theis et al., 2010.

What is the role of the *FoxN3* gene in the development of the heart and muscles of the head/trunk interface in *X. laevis*?

It has been mentioned that *FoxN3* might play a role in the EvoDevo of craniofacial structures in vertebrates. Addressing the aforementioned questions can help to test this idea and further understand the mechanisms controlled by this gene.

What mechanisms govern the early heart development in the head/trunk interface and are they similar to mechanisms that govern the development of head muscles that span the head/trunk interface?

It has been shown that heart and head muscles develop from a common cell population. Addressing this question will improve our understanding about the mechanisms that lead to the evolution of a chambered heart in the last common ancestor of vertebrates.

Manuscript overview

Chapter 1

Naumann, B., Warth, P., Olsson, L., & Konstantinidis, P. (2017). **The development of the cucullaris muscle and the branchial musculature in the Longnose Gar, (*Lepisosteus osseus*, Lepisosteiformes, Actinopterygii) and its implications for the evolution and development of the head/trunk interface in vertebrates.** *Evolution & Development*, 19(6), 263-276.

This paper describes the development of the branchial musculature in the basal actinopterygian *Lepisosteus osseus*, using classical histological techniques in combination with micro-computed tomography (μ CT), fluorescent antibody staining, confocal laser scanning microscopy and subsequent 3D reconstruction. We found that the cucullaris muscle of *L. osseus* had been misidentified in previous studies, maybe due to its late development. The observed developmental pattern of the cucullaris is similar to the pattern observed in the tetrapod cucullaris/trapezius muscle. Furthermore we described the development of the retractor dorsalis muscle which is similar to that of the cucullaris muscle. This suggests that the late development of the cucullaris might be a more general feature of head muscles spanning the vertebrate head/trunk interface.

Study design: B. Naumann, P. Konstantinidis, P. Warth

Acquisition of material: P. Konstantinidis, P. Warth

Data acquisition and experimental procedures: B. Naumann (90%), Peter Warth

3D reconstruction and illustration: B. Naumann

Writing of the manuscript: B. Naumann (60%), P. Warth, P. Konstantinidis, L. Olsson

Chapter 2

Naumann, B., & Olsson, L. (2017). **Three-dimensional reconstruction of the cranial and anterior spinal nerves in early tadpoles of *Xenopus laevis* (Pipidae, Anura).**

Journal of Comparative Neurology, 526(5), 836-857.

This paper provides a detailed description of the cranial nerve anatomy in the larva of the model organism *X. laevis*. We used a combination of classical and state of the art techniques to illustrate the cranial nerves in a 3D model and to give a detailed innervation map for each of them. We confirmed that the cucullaris muscle of *X. laevis* is innervated by a branch of the vagal nerve. Additionally, we described the diaphragmatico-branchialis muscle in *X. laevis*. As observed for the cucullaris, this muscle is innervated a branch of the vagal nerve and spans the head/trunk interface. In the supplement to this chapter we describe the developmental pattern of these two muscles. The cucullaris as well as the diaphragmatico-branchialis develop later than all other head muscles. Therefore, the developmental pattern of the cucullaris is similar to that in other tetrapods. The late development of the diaphragmatico-branchialis indicates that, as described in chapter 1, head muscles that span the head/trunk interface show a similar developmental pattern.

Study design: B. Naumann, Lennart Olsson

Acquisition of material: B. Naumann

Data acquisition and experimental procedures: B. Naumann

3D reconstruction and illustration: B. Naumann

Writing of the manuscript: B. Naumann (90%), L. Olsson

Chapter 3

Naumann, B., Schmidt, J. & Olsson, L. ***FoxN3* is involved in the development of the interatrial septum and the muscles in the head/trunk interface in the African clawed frog, *Xenopus laevis* (Pipidae: Anura: Lissamphibia).** *Submitted.*

FoxN3 morphants have been used to elucidate craniofacial development of *X. laevis* by Schmidt et al. 2011. We extended the analysis of these morphants onto to the heart and muscles of the head/trunk interface (the cucullaris and diaphragmatico-branchialis). We found that both, the cucullaris and diaphragmatico-branchialis muscles, are malformed. This is the first evidence for a head origin of these muscles in anurans since epaxial and hypaxial trunk muscles are unaffected by *FoxN3* knockdown. We further observed a delay in heart development, weak ventricular trabeculation and the absence of the interatrial septum. A few more inconsistent defects such as looping-failure and the reduction of the atrio-ventricular valves were also observed. Additionally, limb buds were absent. All these defects are similar to *HADC*-depleted zebrafish. This further adds evidence to the idea by Schuff et al. (2007) that *FoxN3* interacts with *HADC* in cell cycle control.

Study design: B. Naumann, L. Olsson

Acquisition of material: J. Schmidt

Data acquisition and experimental procedures: B. Naumann (data acquisition),

J. Schmidt (experimental procedures)

3D reconstruction and illustration: B. Naumann

Writing of the manuscript: B. Naumann (90%), L. Olsson

Chapter 4

Naumann, & Olsson, L. **“Escaping” the new head – Cranial neural crest cells inhibit early cardiac myogenesis in the Mexican axolotl, *Ambystoma mexicanum* (Ambystomatidae: Urodela: Lissamphibia).** (*unpublished manuscript*)

This manuscript describes the first data on the influence of cranial neural crest cells (NCCs) on the development of the early heart tube in the Mexican axolotl. We observed that the primary heart tube, derived from the first heart field (FHF), develops posteroventral to the head/trunk interface in the axolotl and many other vertebrates. It has been shown that NCCs are necessary for normal heart development both by direct and indirect interactions with cells derived from the second heart field (SHF). However, the primary heart tube develops at a time, when neural crest cells are still migrating and are not close to it. We transplanted cranial NCCs on top of the early heart primordium to test if factors secreted by these cells promote muscle differentiation, as is known for head muscles. Our results show, that cranial NCCs inhibit heart tube formation and muscle differentiation at early stages of heart development. At these early stages it is likely that only cells derived from the FHF are involved in heart tube formation. The inhibitory effect is compensated during later developmental stages, presumably when cells of the SHF enter the heart tube. We speculate that the FHF-derived heart tube can only develop outside of the head, due to the inhibitory effect of cranial NCCs. This leads to the assumption that the development of a chambered heart in vertebrates is due to the evolution of the interaction between the NC and the SHF.

Study design: B. Naumann, Lennart Olsson

Acquisition of material: B. Naumann

Data acquisition and experimental procedures: B. Naumann

3D reconstruction and illustration: B. Naumann

Writing of the manuscript: B. Naumann (90%), L. Olsson

Chapter 1

Naumann, B., Warth, P., Olsson, L., & Konstantinidis, P. (2017). **The development of the cucullaris muscle and the branchial musculature in the Longnose Gar, (*Lepisosteus osseus*, Lepisosteiformes, Actinopterygii) and its implications for the evolution and development of the head/trunk interface in vertebrates.** *Evolution & Development*, 19(6), 263-276.

The development of the cucullaris muscle and the branchial musculature in the Longnose Gar, (*Lepisosteus osseus*, Lepisosteiformes, Actinopterygii) and its implications for the evolution and development of the head/trunk interface in vertebrates

Benjamin Naumann¹  | Peter Warth¹ | Lennart Olsson¹ | Peter Konstantinidis²

¹ Institut für Spezielle Zoologie und Evolutionsbiologie mit Phyletischem Museum, Friedrich-Schiller-Universität, Jena, Germany

² Department of Fisheries and Wildlife, Oregon State University, Corvallis, Oregon

Correspondence

Benjamin Naumann, Institut für Spezielle Zoologie und Evolutionsbiologie mit Phyletischem Museum, Friedrich-Schiller-Universität, Jena, Germany.
Email: benjamin.naumann@uni-jena.de

Funding information

Volkswagen Foundation, Grant number: 184/825

The vertebrate head/trunk interface is the region of the body where the different developmental programs of the head and trunk come in contact. Many anatomical structures that develop in this transition zone differ from similar structures in the head or the trunk. This is best exemplified by the cucullaris/trapezius muscle, spanning the head/trunk interface by connecting the head to the pectoral girdle. The source of this muscle has been claimed to be either the unsegmented head mesoderm or the somites of the trunk. However most recent data on the development of the cucullaris muscle are derived from tetrapods and information from actinopterygian taxa is scarce. We used classical histology in combination with fluorescent whole-mount antibody staining and micro-computed tomography to investigate the developmental pattern of the cucullaris and the branchial muscles in a basal actinopterygian, the Longnose gar (*Lepisosteus osseus*). Our results show (1) that the cucullaris has been misidentified in earlier studies on its development in *Lepisosteus*. (2) Cucullaris development is delayed compared to other head and trunk muscles. (3) This developmental pattern of the cucullaris is similar to that reported from some tetrapod taxa. (4) That the retractor dorsalis muscle of *L. osseus* shows a delayed developmental pattern similar to the cucullaris. Our data are in agreement with an explanatory scenario for the cucullaris development in tetrapods, suggesting that these mechanisms are conserved throughout the Osteichthyes. Furthermore the developmental pattern of the retractor dorsalis, also spanning the head/trunk interface, seems to be controlled by similar mechanisms.

1 | INTRODUCTION

The vertebrate head is often regarded as a discrete developmental unit, distinct from the trunk and governed by a different developmental program (Ericsson, Knight, & Johanson, 2013; Kuratani, 2008; Theis et al., 2010). The

region of the vertebrate body where these distinct units, the head and the trunk, meet is termed the head/trunk interface (Kuratani, 1997). The evolution and development of the vertebrate head/trunk interface have attracted much less attention compared to the head and trunk on their own. However, with the advent of new methods the interest in this

transition area increased rapidly (Epperlein, Khattak, Knapp, Tanaka, & Malashichev, 2012; Ericsson et al., 2013; Huang, Zhi, Patel, Wilting, & Christ, 2000; Kuratani, 2008; Matsuoka et al., 2005; Oisi, Fujimoto, Ota, & Kuratani, 2015; Piekarski & Olsson, 2007; Sefton, Bhullar, Mohaddes, & Hanken, 2016; Tada & Kuratani, 2015; Theis et al., 2010; Trinajstić et al., 2013). The interface between the head and the trunk is defined by the posterior-most population of cephalic neural crest cells and can be demarcated by an s-shaped curve outlined by the vagal nerve dorsally and the spinal hypoglossal nerve ventrally (Kuratani, 1997). The development of the muscles (Kuratani, 2008), nerves (Tada & Kuratani, 2015), and the skeleton (Gegenbaur, 1889) of the head/trunk interface differ from those of the head and trunk by often showing a combination of head and trunk features (Ericsson et al., 2013). This is exemplified by the enigmatic cucullaris muscle. The cucullaris, and its amniote homolog the trapezius muscle (Edgeworth, 1935; Gegenbaur, 1889), spans across the head/trunk interface from its origin at the occiput to its insertion on the shoulder girdle. Based on anatomical and developmental evidence, its affiliation to either the head (Edgeworth, 1935) or the trunk (Couly, Coltey, & Le Douarin, 1993; Huang et al., 2000; Noden, 1983; Piekarski & Olsson, 2007) is controversially debated.

The innervation and embryonic origin of muscles are used as classical evidence in assessing homology. The sternohyoideus muscle for example is of somitic origin and starts forming in the trunk before migrating into the head. Its somitic origin can however still be inferred in adults, as it retains its original spinal innervation (Edgeworth, 1935). The cucullaris in non-amniote vertebrates is always innervated by a single ramus (sometimes called the ramus accessorius) of the vagal nerve (Edgeworth, 1935; Fürbringer, 1874; Gegenbaur, 1889). In contrast, in amniotes this branch is often treated as a discrete nerve (accessory nerve). In some taxa the cucullaris becomes additionally innervated by the anterior spinal nerves (Edgeworth, 1935; Ericsson et al., 2013), which might be due to the elongated neck in these taxa.

Another argument about the origin of the cucullaris muscle is based on its interaction with the cranial neural crest. The cranial neural crest is necessary for the differentiation of cranial muscles but has no influence on somite-derived trunk muscles (Ericsson, Cerny, Falck, & Olsson, 2004). A neural crest contribution to the connective tissue surrounding the cucullaris has been reported for two amniote taxa, chicken (Couly et al., 1993) and mouse (Matsuoka et al., 2005), but could not be confirmed in the non-amniote axolotl (Epperlein et al. 2012). Despite the contradicting data there are some consistent characters of the cucullaris muscle across vertebrates. First, it is governed by the head myogenic program (Sefton et al., 2016; Theis et al., 2010) and

second, its delayed differentiation in respect to all other muscles in the head or trunk (Edgeworth, 1935; Noden, 1983; Piekarski & Olsson, 2007; Theis et al., 2010; Ziermann & Diogo, 2013). A possible explanation for the peculiar developmental pattern of this muscle has been proposed by Theis et al. (2010), who argues that the crossing of the head/trunk interface exposes the cucullaris to the trunk myogenic program, delaying its differentiation.

However, most of the recent data are derived from model organisms such as axolotl (Piekarski & Olsson, 2007; Sefton et al., 2016), chicken (Huang et al., 2000; Theis et al., 2010) and mouse (Matsuoka et al., 2005). Consequently, the focus is shifted toward the tetrapod taxa. However, to understand the evolutionary history of the cucullaris and to address the controversy of its origin it is important to study a wider variety of taxa of different phylogenetic affiliations. Basal actinopterygians are of special interest as they presumably reflect a more ancestral condition than tetrapods, and in some characters show more basal character states than chondrichthyans (Zhu et al., 2016). Additionally some actinopterygians (e.g., lepisosteids) possess another muscle that is of special interest, the retractor dorsalis (Edgeworth, 1911). As the cucullaris, the retractor dorsalis of lepisosteids develops in the head trunk interface, is innervated by the vagal nerve and has been claimed to be derived from the anterior-most somites (Edgeworth, 1911) or head mesoderm (Edgeworth, 1929). Lepisosteids therefore are a suitable model to study these two muscles side by side and to evaluate the hypothesis of Theis et al. (2010) (see above). In this study, we approach this topic from a morphological view and investigate the developmental pattern of the cucullaris and the retractor dorsalis in relation to the branchial and the hypobranchial muscles in *Lepisosteus osseus*.

2 | MATERIALS AND METHODS

2.1 | Specimens

Specimens were collected on the Mattaponi River (Virginia) in 2013–2015 and preserved in 4% buffered paraformaldehyde at 4°C overnight before transferred to 70% ethanol for long-term storage. Staging of the embryos and larvae follows Long and Ballard (2001). All specimens are listed in Table 1.

2.2 | Terminology

For the terminology of the muscles we follow mainly the terminology used for Teleostei (Winterbottom, 1974) except for the protractor pectoralis and adductor arcus branchialium 4. For these muscles we use the terms cucullaris, instead of protractor pectoralis, and attractor arcus branchialium, instead of adductor arcus branchialium 4 according to Edgeworth (1935).

TABLE 1 List of specimens

Stage (Long & Ballard, 2001)	Length (SL,NL)	Specimen number	Method	VIMS number
27	n.A.	Lo023	FWAB	VIMS 310345
28	5.9 mm NL	Lo001	FWAB	VIMS 22688
29	7.2 mm NL	Lo002	FWAB	VIMS 22688
30	8.3 mm NL	Lo003	FWAB	VIMS 22688
31	9.5 mm NL	Lo004	FWAB	VIMS 22688
31	9.3 mm NL	Lo016	FWAB	VIMS 22688
31	9.7 mm NL	Lo005	FWAB	VIMS 22688
32	10.9 mm NL	Lo006	FWAB	VIMS 22688
32	10.7 mm NL	Lo017	FWAB	VIMS 22688
33	13.6 mm NL	Lo007	FWAB	VIMS 22688
34	16.1 mm SL	Lo008	FWAB	VIMS 22688
Juvenile	20.0 mm SL	Lo009	FWAB	VIMS 22688
Juvenile	21.0 mm SL	Lo011	FWAB	VIMS 22688
Juvenile	22.0 mm SL	Lo012	FWAB	VIMS 22688
Juvenile	24.0 mm SL	Lo010	FWAB	VIMS 22688
Juvenile	23.0 mm SL	Lo030	FWAB + AR	VIMS 31040
31/32	11.0 mm NL	LoSec001	His	n.A.
33	14.0 mm NL	LoSec002	His	n.A.
34	16.0 mm NL	LoSec003	His	n.A.
Juvenile	21.0 mm NL	LoSec004	His	n.A.
Juvenile	27.0 mm NL	LoSec005	His	n.A.
31/32	10.0 mm SL	n.A.	μ CT	VIMS 22684
32	12.8 mm NL	n.A.	μ CT	VIMS 22685
34	16.1 mm SL	n.A.	μ CT	VIMS 22686
Juvenile	22.0 mm SL	n.A.	μ CT	VIMS 22687

FWAB, fluorescent whole-mount antibody staining, FWAB + AR, FWAB and alizarin red; His, Azan-stained histological sections; n.A., not available; NL, normal length; SL, standard length; μ CT, micro-computed tomography.

2.3 | Histology

Specimens were embedded in paraffin, sectioned at 8 μ m in transverse orientation and stained after Heidenhain-Azan (Böck, 1989). Sections were digitalized with an Olympus BX51 microscope using the dotslide software 2.3 (Olympus Corporation, Tokyo, Japan).

2.4 | CT scan

For a μ CT scan and subsequent 3D reconstruction, a 22.0 mm juvenile gar was treated with phosphotungstic acid according to the procedure described earlier (Metscher, 2009). The specimen was scanned with an X-radia XCT scanner.

2.5 | Immunohistochemistry

Specimens were post-fixed in Dent's fixative and bleached in Dent's bleach. Antibody staining was conducted on whole mounts according to standard protocols (Klymkowsky &

Hanken, 1991) using monoclonal 12/101 (Developmental Studies Hybridoma Bank, diluted), or a combination of anti-desmin (Monosan, PS031) and anti-acetylated alpha-tubulin (Sigma–Aldrich, Darmstadt, Germany, T6793) primary antibodies at dilutions of 1:100 (12/101, anti-desmin) and 1:500 (anti-acetylated alpha tubulin) respectively in DAKO antibody diluent. Alexa 488 and Alexa 568 (Thermo Scientific, Darmstadt, Germany) were used as secondary antibodies at 1:200. Clearing was done using BABB (benzyl alcohol/benzyl benzoate, 2/1). To look at the connection of muscles to the bony pectoral girdle, a whole-mount specimen stained with an antibody against desmin was incubated with 0,01% Alizarin red in PBS overnight and cleared with BABB.

2.6 | Image acquisition and processing

Virtual sections of whole mounts were taken with a ZEISS LSM 510. 3D reconstructions on the basis of μ CT and clsm scans were performed using Amira 5.2 (FEI Visualization

Sciences Group, Bordeaux, France) and transferred to MAYA software (Autodesk GmbH, Munich, Germany) for visualization purposes. Background cleaning, contrast enhancement and color saturation of all images were adjusted using Adobe Photoshop CS6.

3 | RESULTS

3.1 | Development of the hypobranchial musculature

In *L. osseus*, the hypobranchial musculature is represented solely by the sternohyoideus muscle (rectus cervicis muscle in Edgeworth, 1935). It inserts on the hypohyal via a strong tendon anteriorly (Figures 1a and 1b). Posteriorly, it is first attached to the scapulocoracoid until stage 32 but changes to the cleithrum at stage 33 and, in part, becomes continuous with the hypaxonic trunk musculature in older larvae (Figures 1a and 1b).

At stage 30, the sternohyoideus muscle appears at the anterior end of the yolk sac, ventral to the branchial arches and dorsal to the heart. It is sub-divided into three distinct segments (Figure 1c, white arrows). The sternohyoideus is slightly curved posteriorly and not attached to any skeletal elements.

At stage 31, the muscle is elongated compared to the previous stage but neither its posterior nor its anterior end is

attached to the corresponding skeletal element as it is described in older stages (Figure 1d). It is sub-divided into three to four (depicted specimen) distinct segments, while the anterior-most segment is smaller compared to the three subsequent segments (Figure 1d, gray arrows).

At stage 32, the sternohyoideus has extended farther anteriorly (Figure 1e), and its anterior end tapers into a tendon that attaches to the hypohyal cartilage. The posterior end of the muscle inserts on the scapulocoracoid, embracing the dorsal quarter of the heart together with its antimere (Figure 1e).

At stage 33, the posterior insertion of the sternohyoideus is now on the ossifying cleithrum, showing the juvenile/adult condition (Figure 1b). The posterior ends of the left sternohyoideus encase the ventral half of the heart now, which is due to the elongation of the snout and the consumption of the yolk sac (Figure 1f),

3.2 | Development of the ventral branchial muscles

At stage 29 (Figures 2a and 2a'), regions with higher levels of autofluorescence indicate formation of branchial arches 1–3 (Figure 3a'). The anlagen of the obliqui ventrales 1–3 (Figures 4a–4c) are distinct compact cell masses adjacent to the ventral ends of branchial arches 1–3 as inferred from histological sections.

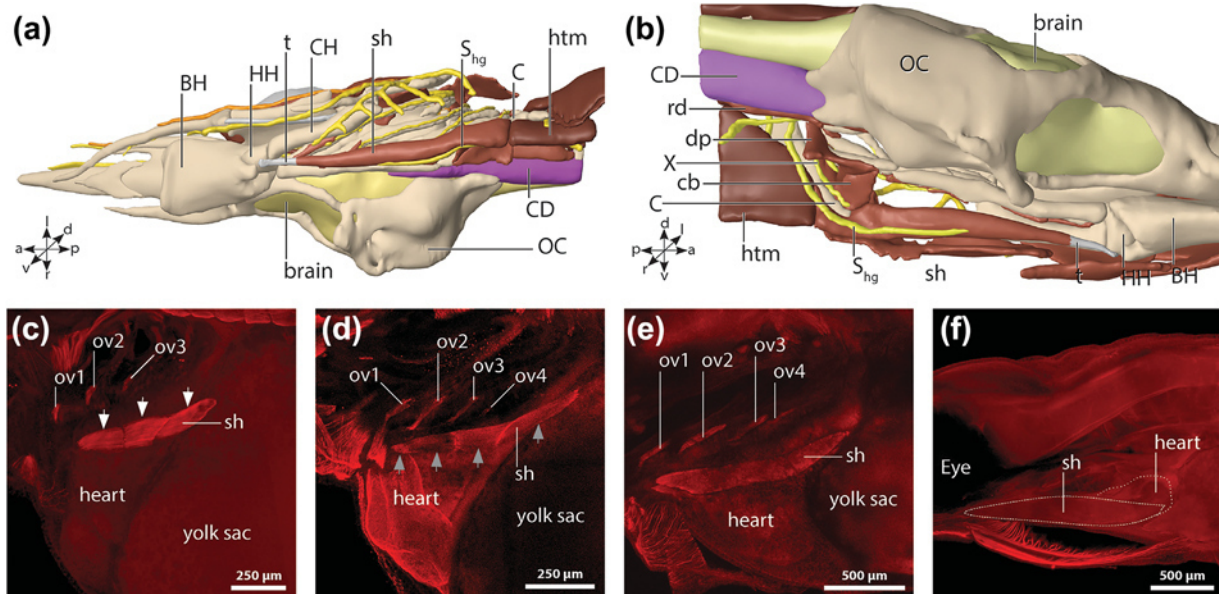


FIGURE 1 (a–b) 3D reconstruction of a μ CT scan of a juvenile 22 mm *L. osseus* (VIMS 22687). (a) Ventral view. (b) Medial view. Muscles and nerves are reconstructed on the left side, while the skeletal elements are reconstructed in total. The different structures have been colored as follows: nerves, yellow to orange; brain, light yellow; muscles, dark flesh; skeletal elements, beige; chorda dorsalis, violet. (c–f) Maximum intensity projections of whole mount antibody stainings of *L. osseus* larvae. The ventral branchial region is shown from a lateral view. Muscles are colored in red. (c) Stage 30 (VIMS 22688). (d) Stage 31 (VIMS 22688). (e) Stage 32 (VIMS 22688). (f) Stage 33 (VIMS 22688). X, vagal nerve; a, anterior; BH, basihyal toothplate (Grande, 2010); C, cleithrum; cb, coracobranchialis; CD, chorda dorsalis; CH, ceratohyal; d, dorsal; dp, dilatator pharyngeus; HH, hypohyal; htm, hypaxonic trunk muscles; l, left; OC, otic capsule; ov1–ov4, obliquus ventralis 1–4; p, posterior; r, right; rd, retractor dorsalis; S_{hg} , spinal hypoglossal nerve; sh, sternohyoideus; t, tendon of the sternohyoideus; v, ventral

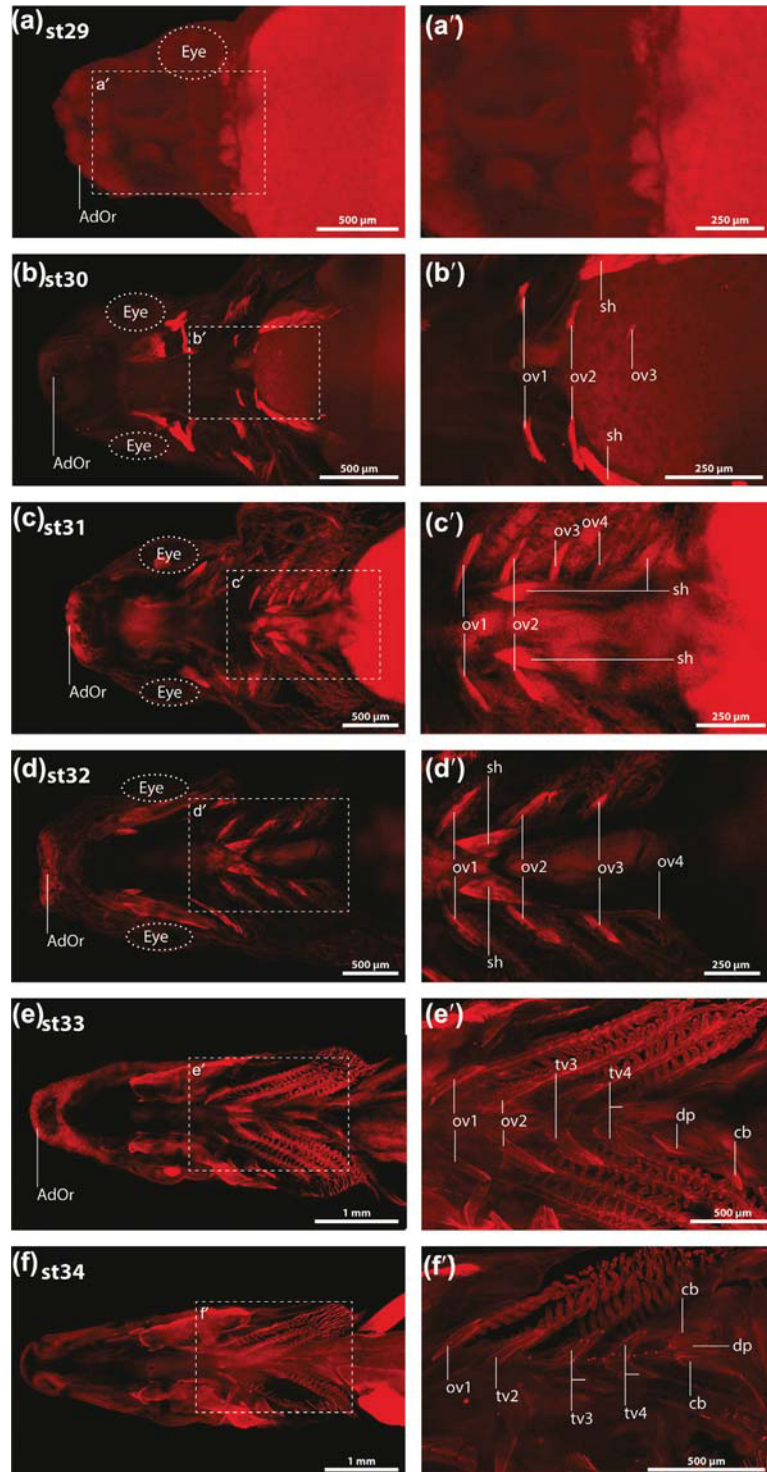


FIGURE 2 Maximum intensity projections of whole mount antibody staining of *L. osseus* larvae from a ventral view. Muscles are depicted in red. (a) Stage 29 (VIMS 22688). (a') Close-up of the area marked by the dashed line in (a). (b) Stage 30 (VIMS 22688). (b') Close-up of the area marked by the dashed line in (b). (c) Stage 31 (VIMS 22688). (c') Close-up of the area marked by the dashed line in (c). (d) Stage 32 (VIMS 22688). (d') Close-up of the area marked by the dashed line in (d). (e) Stage 33 (VIMS 22688). (e') Close-up of the area marked by the dashed line in (e). (f) Stage 34 (VIMS 22688). (f') Close-up of the area marked by the dashed line in (f). AdOr, adhesive organ; cb, coracobranchialis; dp, dilatator pharyngeus; ov 1–4, obliquus ventralis 1–4; sh, sternohyoideus; tv 2–4, transversus ventralis 2–4

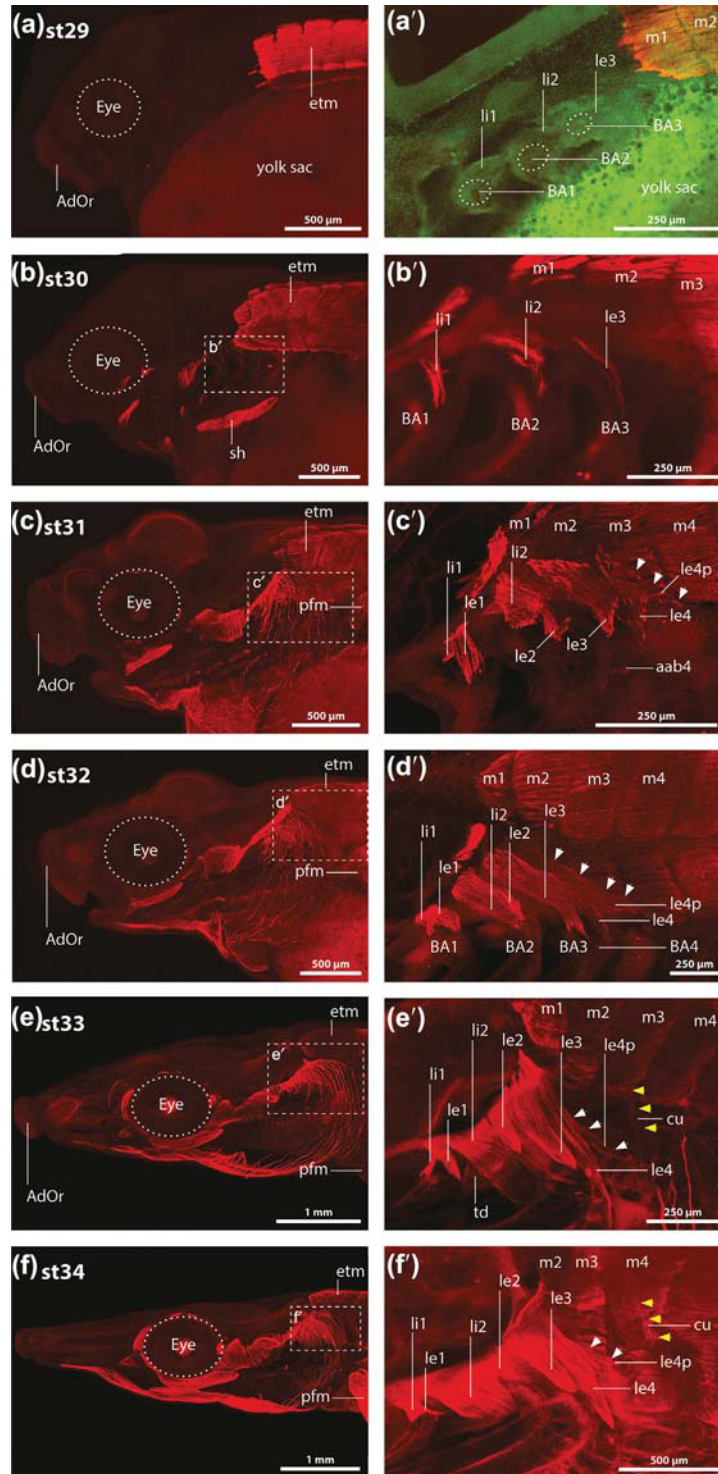


FIGURE 3 Maximum intensity projections of whole mount antibody stainings of the same *L. osseus* larvae as in Figure 2 from a lateral view. Muscles are depicted in red. (a) Stage 29 (VIMS 22688). (a') Dorsolateral view of the brachial arches of the same specimen depicted in (a) using autofluorescence of the tissue at 488 nm (green). (b) Stage 30 (VIMS 22688). (b') Close-up of the area marked by the dashed line in (b). (c) Stage 31 (VIMS 22688). (c') Close-up of the area marked by the dashed line in (c). (d) Stage 32 (VIMS 22688). (d') Close-up of the area marked by the dashed line in (d). (e) Stage 33 (VIMS 22688). (e') Close-up of the area marked by the dashed line in (e). (f) Stage 34 (VIMS 22688). (f') Close-up of the area marked by the dashed line in (f). White arrows indicate the posterior portion of the levator externus 4. Yellow arrows indicate the cucullaris. AdOr, adhesive organ; BA 1–4, branchial arch 1–4; cu, cucullaris; etm, epaxonic trunk muscles; htm, hypaxonic trunk muscles; le 1–4, levator externus 1–4; le4p, posterior portion of the levator externus 4; li 1–2, levator of internus 1–2; m 1–4, myotome 1–4; pfm, pectoral fin muscles; td, transversus dorsalis

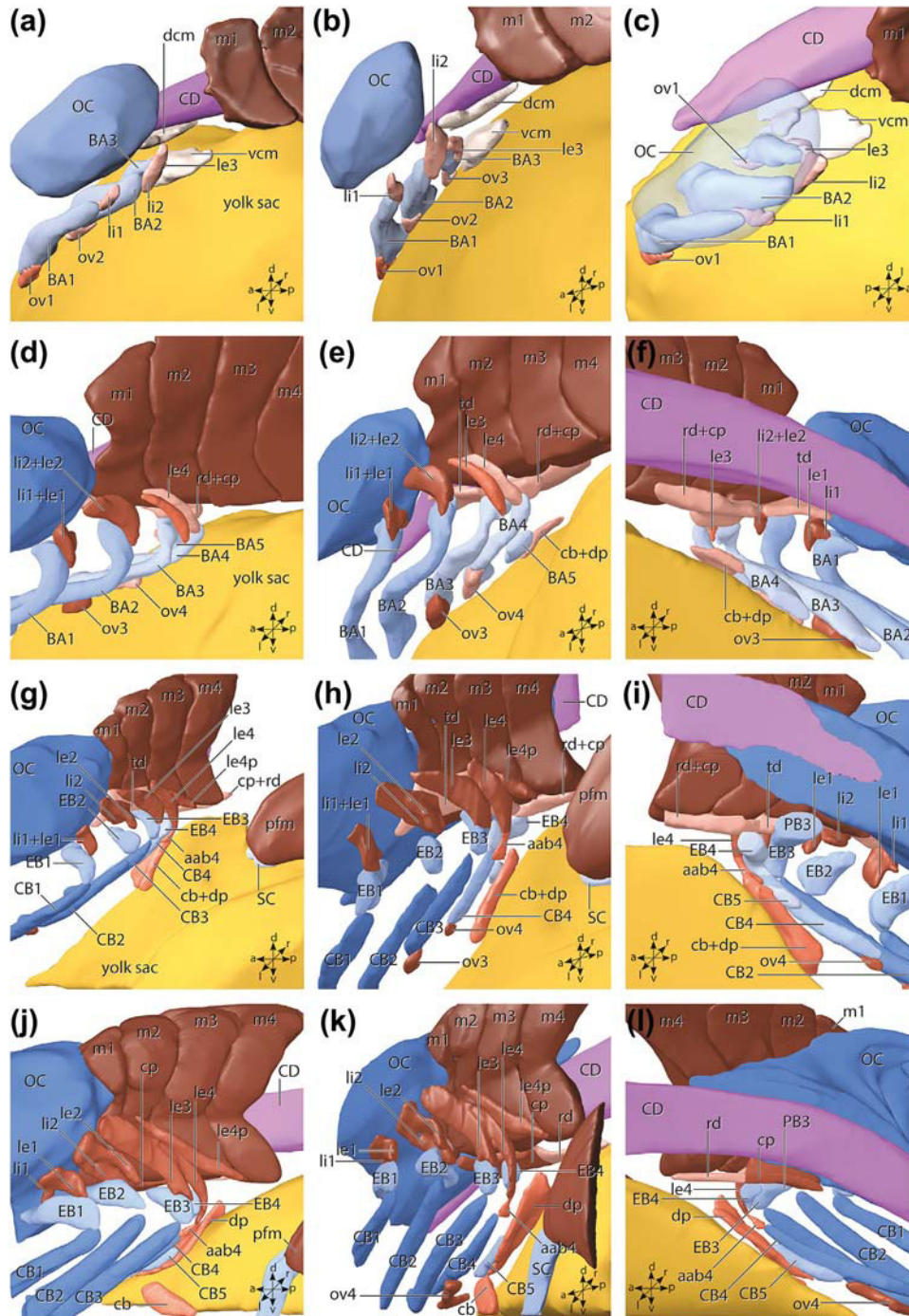


FIGURE 4 3D reconstructions based on fluorescent whole mount antibody stainings of *L. osseus* larvae. The different structures have been color as follows: Yolk, yellow; chorda dorsalis, violet; trunk muscles, brown; undifferentiated muscle anlagen, light flesh; differentiating muscles already showing some muscle fibers, flesh; differentiated muscles, dark flesh; cartilage anlagen, light blue; differentiating cartilage, blue; differentiated cartilage, dark blue; undifferentiated cell mass, light beige. (a–c) Stage 29 (VIMS 22688). (a) Lateral view. (b) Posterolateral view. (c) Dorsal view, the otic capsule has been made transparent. (d–f) Stage 30 (VIMS 22688). (d) Lateral view. (e) Posterolateral view. (f) Medial view. (g–i) Stage 31 (VIMS 22688). (g) Lateral view. (h) Posterolateral view. (i) Medial view. (j–l) Stage 32 (VIMS 22688). (j) Lateral view. (k) Posterolateral view. (l) Medial view. a, anterior; aab4, attractor arcus branchialium 4; BA1–BA5, branchial arch 1–5; cb, coracobranchialis; CB1–CB5, ceratobranchial 1–5; CD, chorda dorsalis; cp, constrictor pharyngeus; d, dorsal; dcm, dorsal cell mass; dp, dilatator pharyngeus; EB1–EB4, epibranchial 1–4; le1–le4, levator externus 1–4; le4p, posterior portion of the levator externus 4 (cucullaris *sensu* Edgeworth, 1911); l, left; li1–li2, levator internus 1–2; m1–m4, myotome 1–4; OC, otic capsule; ov1–ov4, obliquus ventralis 1–4; p, posterior; pfm, pectoral fin muscles; r, right; rd, retractor dorsalis; td, transversus dorsalis; v, ventral

At stage 30 (Figure 2b), the obliqui ventrales 1–3 are thin fiber bands attached to the ventral surface of the respective ceratobranchial anlagen (Figure 2b'). The anlage of the obliquus ventralis 4 (Figures 4d and 4e) is a small population of myoblasts located in the ventral area of the fourth branchial arch. A second distinct population of myoblasts is present at the ventral surface of the fifth branchial arch and adjacent to the myoblasts surrounding the pharynx (Figure 4f). We interpret this cell mass as the anlage of the coracobranchialis and dilatator pharyngeus muscles.

At stage 31 (Figure 2c), the obliquus ventralis 1 is elongated and reaches its insertion point at the anterior end of the basibranchial copula (Figure 2c'). The obliqui ventrales 2 and 3 are elongated too, but do not reach the basibranchial copula (Figure 2c'). The obliquus ventralis 4 has formed muscle fibers (Figure 2c'). The common anlage of the coracobranchialis and dilatator pharyngeus is elongated in anteroventral and posterodorsal direction (Figures 4g–4i) and the first muscle fiber formation is evident by a weak antibody signal. The anterior part of the anlage is slightly bent posteriorly. This part will form the coracobranchialis muscle.

At stage 32 (Figure 2d), all obliqui ventrales muscles are curved in a sharper angle to the basibranchial copula due to the elongation of the snout (Figure 2d'). The common anlage of the coracobranchialis and dilatator pharyngeus is divided into two distinct muscles (Figures 4j–4l). The anterior end of the coracobranchialis muscle points toward the developing ceratobranchial 5 and the posterior end toward the developing scapulocoracoid (Figure 4j).

At stage 33 (Figure 2e), the obliquus ventralis 2 has reached the medial side of the basibranchial. The obliqui ventrales 3 and 4 have met their antimeres and form per definition the transversi ventrales 3 and 4 now (Figure 2e').

At stage 34 (Figure 2f) the obliquus ventralis 1 and the transversi ventrales 2–4 are in an increased pointed angle to the branchial midline correlated with the advanced elongation of the snout in juvenile *L. osseus* (Figures 2f' and 2f'').

3.3 | Development of the dorsal branchial and pectoral muscles

At stage 29 (Figure 3a), dense cell areas are present, dorsal to the first three branchial arches. We interpret these cells as the anlagen of the levatores interni 1 and 2 and the levator externus 3 (Figure 3a'). The muscle anlagen adhere to the posterodorsal end of the corresponding branchial arch (Figures 4a–4c).

At stage 30 (Figure 3b) the anlagen of the levator muscles of the anterior three branchial arches, levator internus 1 and 2 and the levator externus 3, are distinct (Figure 3b'). Muscle fibers are already present in all three levator muscles. The levator externus 3 is less developed than the first two levatores and consists of only a few differentiated muscle fibers

(Figure 3b'). All three muscles are attached to the posterodorsal surface of the corresponding branchial arch (Figures 4d and 4e). The levator externus 4 still consists of a small mass of myoblasts at the dorsal area of the fourth branchial arch and can be seen in histological sections as well as scans with a high laser intensity. The skeletal elements of the first and second branchial arches show first signs of chondrification. The third and fourth arches still appear as a dense mass with little extra-cellular matrix (Figures 4d–4f). A muscle anlage is present anteroventral to the first myomere, representing the anlage of the transversus dorsalis muscle (Figure 4f). Another muscle anlage is located ventrolateral to the chorda dorsalis. It starts at the level of myomere one and continues posteriorly until the level of myomere 3 (Figures 4e and 4f). Its anterior part consists of a population of myoblasts extending from the branchial arches in a medial direction and meets the anlage of its antimeres in the midline ventral to the chorda dorsalis. Due to its position between branchial arches 2 and 3, we interpret the anterior part as the anlage of the transversus dorsalis and the posterior part as the anlage of the retractor dorsalis and constrictor pharyngeus muscle (Figures 4d–4f). The anlage appears continuous and no signs of segmentation are recognizable.

At stage 31 (Figure 3c), the levator internus 1 of the first branchial arch has reached its point of origin at the lateroventral surface of the otic capsule. The levator externus 1 has split from the levator internus 1 and inserts distally on epibranchial 1 (Figures 3c', 4g, and 4h). The levator internus 2 approaches the otic capsule but does not insert on it yet. Its posterior end extends posteroventrally. It inserts on the epibranchial two forming the levator externus 2 (Figures 3c', 4g, and 4h). It is a more massive muscle, compared to the previous stage (Figure 3c'). The levator externus 3 is broader compared to the previous stage (Figure 3c'). In close connection to the levator externus 3, the anlage of levator externus 4 has formed the first muscle fibers (Figure 3c') and extends ventrally, reaching the area where the epibranchial 4 and ceratobranchial 4 will be in contact. This extension represents the anlage of the attractor arcus branchialium 4 (Figures 3c' and 4h). Another muscle appears, originating from the levator externus 4 and running posteroventral into the direction of the developing shoulder girdle (Figure 3c', white arrows). We call this muscle the posterior portion of the levator externus 4.

At stage 32 (Figure 3d) the levatores interni and externus two have reached their point of origin at the surface of the otic capsule, posterodorsal to the first levator muscle (Figures 3d', 4j, and 4k). The posterior portion of the levator externus 4 has become broader and extends farther posteriorly (Figure 3d'). Its anterior end seems separate from the fourth branchial levator in the specimen used for the 3D reconstruction (Figure 4j) but appears connected in another specimen of almost the same size, and in larvae of later stages. The

posterior portion of the levator externus 4 is innervated by a ramus of the vagal nerve exiting the posterior vagal ganglion close to the vagal ramus of the fourth branchial arch (Figure 5). First muscle fibers are present in the anlage of the transversus dorsalis. The common anlage of the constrictor pharyngeus and retractor dorsalis muscles shows an anterior-to-posterior differentiation. Its anterior part shows first muscle fibers, while its posterior part still consists of myocytes (Figures 4k and 4l).

At stage 33 (Figure 3e), all the dorsal muscles of the branchial arches are present. The attractor arcus branchialium 4 has split from the ventral end of the fourth levator muscle, bridging the joint between epi- and ceratobranchial 4 (Figure 6a). The transversus dorsalis has formed more muscle fibers (Figure 3e'). The posterior portion of the levator externus 4 ends in the lateral skin (Figure 3e'). Posterodorsally, the anlage of the cucullaris appears close to the developing cleithrum and already shows muscle fiber formation (Figure 3e', yellow arrows; Figure 6a).

At stage 34 (Figure 3f), the dorsal levator muscles as well as the attractor arcus branchialium 4 show no differences compared to older specimens (Figure 3f'). The posterior portion of the levator externus 4 is smaller compared to earlier stages but still inserts in the skin anterior to the pectoral girdle (Figure 3f', white arrows; 6B, C, green arrows). The cucullaris has formed more muscle fibers (Figures 3f', 6d, and 6f) and is attached to the occiput via a dorsal fascia in juveniles older than stage 34 (Figure 6f, also shown in Figure 7a). The ramus accessorius of the vagal nerve runs posterodorsally and innervates the cucullaris muscle (Figure 6g). A complete innervation scheme of all the branchial muscles, derived from whole mount antibody stainings as well as histological sections, is given in Figure 5.

4 | DISCUSSION

4.1 | Development of the hypobranchial musculature

The sternohyoideus is the only hypobranchial muscle present in *L. osseus*. Edgeworth (1935) reported that the muscle has seven to nine “inscriptions,” implying an origin from seven to nine anterior somites. In contrast to Edgeworth's finding, we found that the sternohyoideus muscle consists of three to four segments. An origin from the anterior-most three to four somites gains further support from our observation on the composition of the spinal hypoglossal nerve. Three spino-occipital nerves exit the occiput through distinct foramina and fuse to form a single nerve. In turn, this compound nerve becomes accompanied by fibers from the first spinal nerve (Figures 5b and 5c) which might increase the sensory component of the spinal hypoglossal nerve (Edgeworth, 1935). An innervation of the sternohyoideus, consisting of

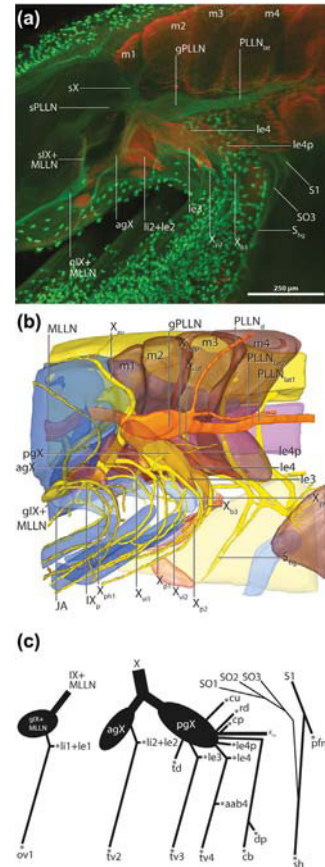


FIGURE 5 Maximum intensity projections of a whole mount antibody staining of a *L. osseus* larva at stage 32 (VIMS 22688). The posterior branchial region is shown from a lateral view. Muscles are depicted in red, nerves are depicted in green. (b) 3D reconstruction of the same data set as shown in (a). Coloring as described for Figure 4, nerves are depicted in yellow to orange. Muscles and skeletal elements have been made transparent to show the underlying nerves. (c) Innervation scheme of the branchial and anterior pectoral muscles deduced from Whole mount antibody stainings as well as histological sections. IX + MLLN, glossopharyngeal and middle lateral line nerve; IX_p, post-trematic ramus of IX; X, vagal nerve; X_{aur}, ramus auricularis of X; X_{b3}, branchial ramus 3 of X; X_{cut}, cutaneous ramulus of X; X_{int}, ramus intestinalis of X; X_{le4p}, X motor ramus innervating the posterior portion of the levator externus 4; X_{p1}-X_{p2}, post-trematic ramus 1–2 of X; X_{ph1}-X_{ph2}, pharyngeal ramus 1–2 of X; X_{vi1}-X_{vi2}, visceral ramus 1–2 of X; aab4, attractor arcus branchialium 4; agX, anterior vagal ganglion; cb, coracobranchialis; cp, constrictor pharyngeus; cu, cucullaris; dp, dilatator pharyngeus; gIX + MLLN, ganglion of the glossopharyngeal and middle lateral line nerve; gPLLN, ganglion of the posterior lateral line nerve; le1-le4, levator externus 1–4; le4p, posterior portion of the levator posterior 4; li1-li2, levator internus 1–2; m1-m4, myotome 1–4; MLLN, middle lateral line nerve; ov1, obliquus ventralis 1; pfm, pectoral fin muscles; pgX, posterior ganglion of the vagal nerve; PLLN, posterior lateral line nerve; PLLN_d, dorsal ramus of PLLN; PLLN_{lat1}-PLLN_{lat2}, lateral ramus 1–2 of PLLN; rd, retractor dorsalis; sIX + MLLN, stem of IX and MLLN; sX, stem of X; S1, spinal nerve 1; SC, scapulocoracoid; sh, sternohyoideus; SO1-SO3, spino-occipital nerve 1–3; sPLLN, stem of the PLLN; td, transversus dorsalis; tv2-tv4, transversalis ventralis 2–4

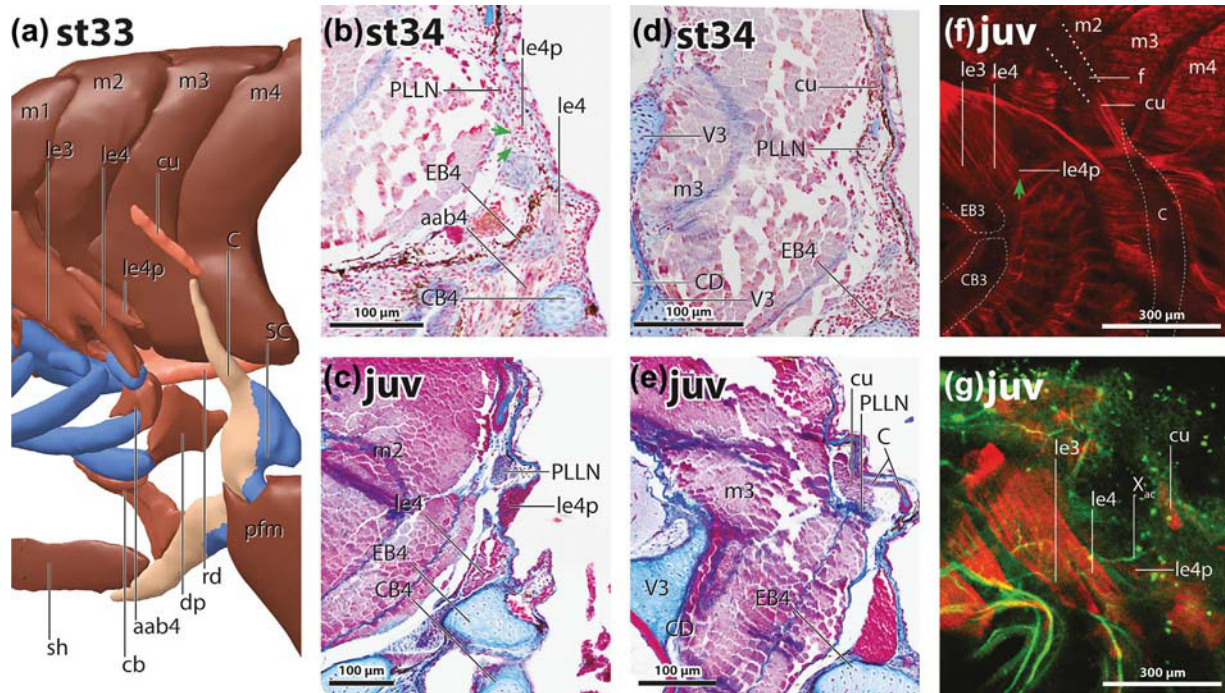


FIGURE 6 (a) 3D reconstruction based on fluorescent whole mount antibody staining of *L. osseus* larva at stage 33 (VIMS 22688). The posterior branchial region and the pectoral girdle are shown from a posterolateral view. Coloring as described for Figure 4, the ossified cleithrum is colored in beige. (b–e) Histological section through the posterior branchial region of *L. osseus* larvae. (b and d) Stage 34 (LoSec003). (c and e) Juvenile (27 mm, LoSec005). (f) (20.0 mm, VIMS 22688) and (g) (22.0 mm, VIMS 22688), Maximum intensity projections of whole mount antibody stainings of a juvenile *L. osseus*. The position of skeletal elements and the fascia is indicated by dotted lines. Muscles are depicted in red, nerves are depicted in green. Green arrows indicate the posterior portion of the levator externus 4. X_{ac} , ramus accessories of the vagal nerve; aab4, attractor arcus branchialium 4; C, cleithrum; cb, coracobranchialis; CB3–4, ceratobranchial 3–4; CD, chorda dorsalis; dp, dilatator pharyngeus; EB3–4, epibranchial 3–4; f, fascia; le3–4, levator externus 3–4; le4p, posterior portion of the levator externus 4; m1–m4, myotome 1–4; pfm, pectoral fin muscles; PLLN, posterior lateral line nerve; rd, retractor dorsalis, V3, vertebra 3

three to four muscular segments, correlates with the observed composition of the spinal hypoglossal nerve by three spino-occipital and one spinal nerve. Fate mapping experiments in actinopterygians, similar to tetrapods (Piekarski & Olsson, 2007; Theis et al., 2010) are needed to draw the final conclusion of how many somites form the sternohyoideus in *L. osseus*.

4.2 | Development of the branchial muscles

As described by Edgeworth (1911, 1929, 1935), we also found a single dorsal and ventral muscle anlage (muscle plate in Edgeworth, 1935) for each branchial arch (Figures 4a–4c). These anlagen give rise to the levatores interni and externi dorsally and the obliqui ventrales ventrally (Edgeworth, 1911, 1935). Furthermore, we were able to describe developmental stages of *L. osseus* in which the attractor arcus branchialium 4 is still connected to the levator externus 4 (Figures 4g–4l), confirming the origin of the attractor from this branchial levator muscle (Edgeworth, 1929). We also confirm Edgeworth's description of the developmental pattern of the ventral branchial muscles. As stated by Edgeworth (1911, 1935) they

begin to develop as obliqui ventrales. As development proceeds, the second to fourth obliqui ventrales alter their orientation, grow toward the branchial mid-line and fuse to their antimeres forming transversi ventrales (Figure 2).

4.3 | Development of the cucullaris muscle

Previous information on the cucullaris muscle in *Lepisosteus* is conflicting. Edgeworth (1935) reported a cucullaris originating from the levator externus 4 in *Lepisosteus* (probably also *L. osseus*). According to Edgeworth (1935), it forms directly posterior the levator externus 4, running posteriorly and ending in the skin without attaching to the pectoral girdle. Norris (1925) in contrast described a cucullaris in *L. osseus*, originating from the occipital fascia, running posteriorly and inserting on the cleithrum. Other authors (Greenwood & Lauder, 1981; Jessen, 1972) reported the absence of the cucullaris muscle in some *Lepisosteus* species including *L. osseus*. Our results show that the muscle interpreted as the cucullaris by Edgeworth (1911) in *Lepisosteus* is a posterior portion of the levator externus 4 (Figures 3c', 4g, and 4h) and probably was misidentified because of (1) its origin (together

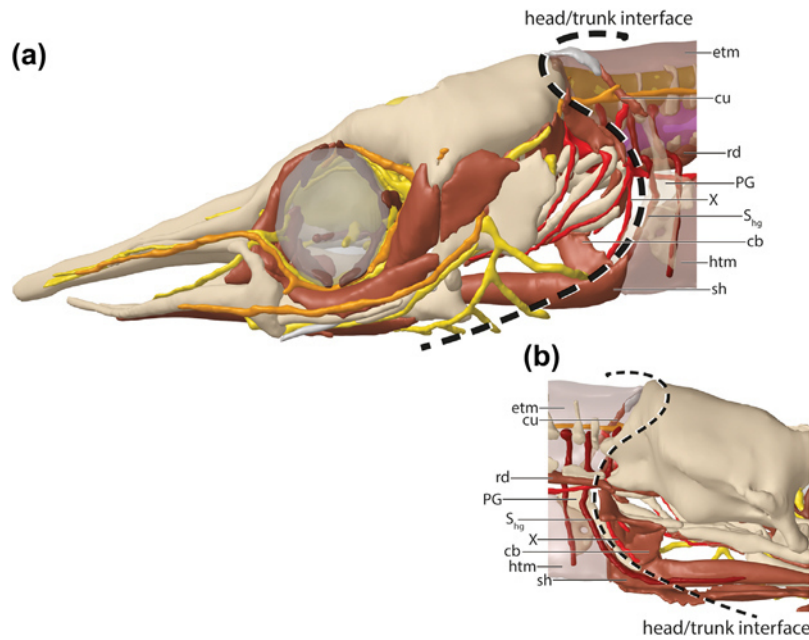


FIGURE 7 The same 3D reconstruction as shown in Figure 1 (VIMS 22687). Coloring as described for Figure 1. The dashed line indicates the head/trunk interface, outlined by the vagal (light red) and spinal hypoglossal (dark red) nerves. The head-derived cucullaris and retractor dorsalis muscles extend into the trunk, crossing the head/trunk interface, while the coracobranchialis muscle is situated anterior to that interface. (a) Lateral view. (b) Median view of the posterior branchial region. X, vagal nerve; cb, coracobranchialis; cu, cucullaris; PG, pectoral girdle; rd, retractor dorsalis; S_{hg} , spinal hypoglossal nerve; sh, sternohyoideus

with the levator externus 4) at the otic capsule and posteriorly directed course and (2) the absence of the “real” cucullaris muscle in the specimens studied by Edgeworth (1911) due to the delayed differentiation of the cucullaris compared to the other head muscles. The muscle we identified as the cucullaris muscle in *L. osseus* is congruent with the description of this muscle by Norris (1925). He determined the cucullaris based on its origin and insertion as well as the innervation by the vagal nerve. Because he did not observe the posterior portion of the levator externus 4 in his specimens, the conclusion that the cucullaris muscle develops from the levator externus 4 (Edgeworth, 1911) could not be refuted. The reported absence of the cucullaris in some specimens investigated by Jessen (1972) could be due to the inconspicuousness of this delicate muscle in or its reduction in larger animals. We show that the cucullaris and the posterior portion of the levator externus 4 as described by Edgeworth (1911) are present simultaneously but independent from each other (Figure 3e', f', and 6a) in *L. osseus* from stage 35 on to early juveniles. We never observed a connection between them in any of our specimens. Our investigation clarifies the identity of the cucullaris, and also disproves Edgeworth's statement about the first appearance of the cucullaris muscle in synchrony with the levator externus 4 in *L. osseus*. However, important questions remain. (1) What is the function and evolutionary significance of the posterior portion of the levator externus 4? (2) What is the embryonic origin of the cucullaris and why does it form so late (see hypothesis below)?

4.4 | The retractor dorsalis muscle

According to Edgeworth (1929, 1935), in *Lepisosteus* the retractor dorsalis originates from the constrictor pharyngeus and is therefore of cranial origin, whereas other authors (Allis, 1897; Wiedersheim & Weismann, 1904) reported an origin from the trunk myotomes. Interestingly, all authors reported an innervation by the vagal nerve, while an origin from trunk myotomes (Wiedersheim & Weismann, 1904) would imply a spinal innervation. Our observation concurs with Edgeworth that the muscle is a derivative of the constrictor pharyngeus and therefore of cranial origin (Figure 4f).

Further, we observed a delay in muscle fiber formation within the retractor dorsalis portion compared to the constrictor pharyngeus portion (Figure 4l). This delayed timing of the muscle fiber development resembles the delayed fiber formation in the cucullaris. It is conspicuous, that the retractor dorsalis of *Lepisosteus* shows a developmental pattern very similar to that of the cucullaris muscle and therefore raises the same question: Why does it form so late?

4.5 | Developmental pattern of the muscles in the head/trunk interface

The trunk myogenic program is activated early in development (Theis et al., 2010). It promotes the differentiation of trunk-derived muscles (e.g., the hypobranchial musculature) via the expression of *Pax3* but inhibits differentiation of

head-derived muscles (Mootoosamy & Dietrich, 2002; Sambasivan, Kuratani, & Tajbakhsh, 2011; Tzahor et al., 2003). In the head, the migrating neural crest cells activate head muscle differentiation by inhibiting myogenic suppressors such as *Wnts* and *BMPs* (Theis et al., 2010; Tzahor et al., 2003). To reach its attachment site on the pectoral girdle, the anlage of the cucullaris muscle has to grow out from the head into the trunk, crossing the head/trunk interface. Thereby, the cucullaris/trapezius changes from the head myogenic environment into the trunk myogenic environment (Theis et al., 2010). The trunk myogenic program inhibits differentiation of the cucullaris muscle until it is downregulated or migrating cranial neural crest cells reach the cucullaris anlage, promoting an activating stimulus (Theis et al., 2010). At the time when the cucullaris starts to form muscle fibers, all other head and trunk muscles are already differentiated (Ericsson et al., 2013; Theis et al., 2010).

By investigating the timing of the muscles developing in the head/trunk interface of *Lepisosteus*, we can test this “tetrapod-based” hypothesis using our data gained from a basal actinopterygian species. In *L. osseus* a coracobranchialis and a retractor dorsalis muscle connect the head to the trunk in addition to the hypobranchial and cucullaris muscles.

Despite its insertion on the pectoral girdle, the coracobranchialis muscle does not cross the head/trunk interface outlined by the vagal and spinal hypoglossal nerve (Figures 7a and 7b). In contrast, the retractor dorsalis and the cucullaris, both innervated by the vagal nerve, originate from the head, cross the head/trunk interface and insert on structures situated in the trunk, like the third and fourth vertebrae (retractor dorsalis) or the cleithrum (cucullaris) (Figures 7a and 7b). Based on what is known in tetrapods (Theis et al., 2010), we propose, that the anlagen of the cucullaris and retractor dorsalis muscles are under the inhibiting influence of the trunk myogenic program (Figure 8a, green gradient). In the head, migrating cranial neural crest cells (Figure 8b) inhibit the trunk myogenic program, promoting the differentiation of the head muscles (Figure 8c, blue gradient within the branchial arches). In the posterior head region the circumpharyngeal crest cells migrate around the posterior-most branchial arch along the head/trunk interface (Figure 8c). They reach the coracobranchialis muscle, promoting its differentiation, but not the more posterior anlagen of the cucullaris and retractor dorsalis (Figure 8d). The late differentiation of these two muscles can be explained in two different ways. First, only a small population of cranial neural crest cells reaches the anlagen,

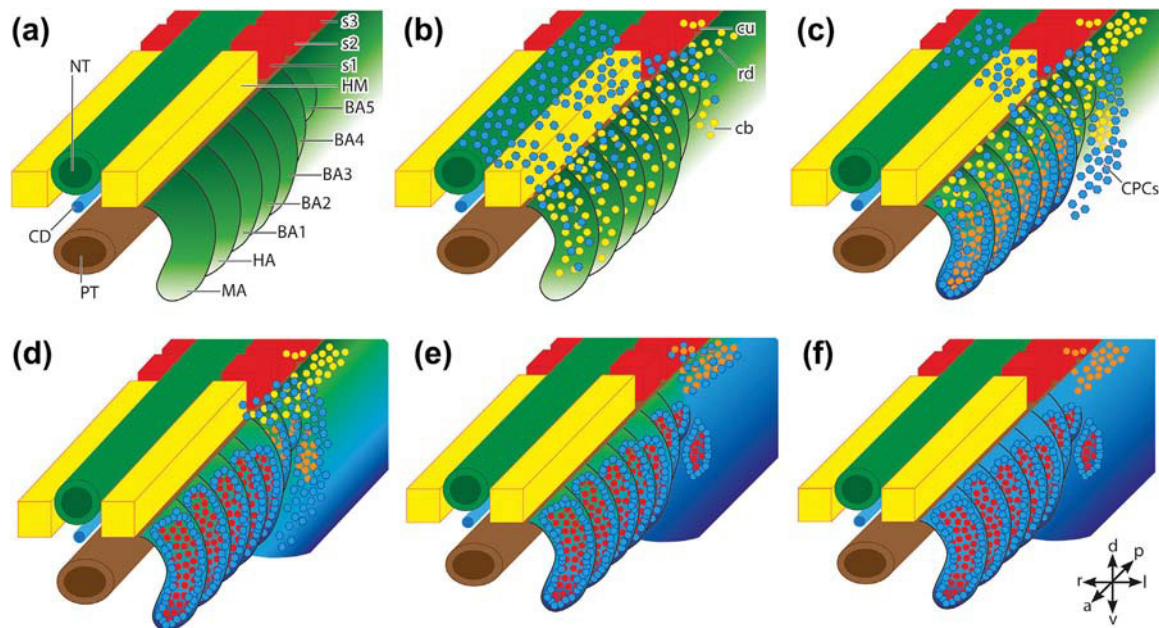


FIGURE 8 A possible explanatory scenario for the developmental pattern of the muscles of the head/trunk interface of *L. osseus*. (a–d) Show the successive progression from the early migration of the myogenic progenitor cells (myoblasts; yellow dots) and neural crest cells (blue hexagons) in the branchial arches. In the branchial arches, the myoblasts differentiate into myocytes (orange dots), which later form functioning muscle fibers (red dots). *Wnts* and *BMPs* genes (green gradient) are expressed from the neural tube and the overlaying ectoderm inhibiting head muscle formation. In the trunk the expression of *Pax3* initiates the trunk myogenic program unimpaird of *Wnts* and *BMPs*. In the branchial arches, *Wnt* and *BMP* inhibitors are expressed by neural crest cells (blue gradient), activating the head myogenic program. (e and f) Are two possible explanations, which could also act side-by-side, for the late differentiation of the cucullaris and retractor dorsalis muscle. The cross in the lower right corner shows the axis orientations (a, anterior; p, posterior; d, dorsal; v, ventral; l, left; r, right). BA1 to 5, branchial arch 1–5; cb, coracobranchialis; CD, chorda dorsalis; CPCs, circumpharyngeal crest cells; cu, cucullaris; HA, hyoid arch; HM, head mesoderm; MA, mandibular arch; NT, neural tube; PT, pharyngeal tube; rd, retractor dorsalis

resulting in a slower inhibition of the trunk myogenic program (Figure 8e) or no neural crest cells reach the anlagen of the retractor dorsalis and cucullaris and muscle formation starts when the trunk myogenic program becomes down-regulated (Figure 8f). Fate mapping studies of the neural crest and anterior-most somites in basal actinopterygians as well as gene expression studies for *Pax3*, *Wnts*, and *BMPs* are needed to test this scenario.

Our results on the delayed differentiation of the cucullaris and retractor dorsalis muscles are similar to the pattern observed for the trapezius muscle in tetrapod taxa (e.g., Theis et al., 2010). We therefore speculate that the mechanisms underlying the developmental pattern of the muscles in the head/trunk interface might be conserved throughout, at least, the Osteichthyes.

ACKNOWLEDGMENTS

We would like to thank P. McGrath and E. Loose for their help in the field to collect and preserve larval and juvenile gars. We would like to thank Katja Felbel for help with histological sections. We are grateful to E. Hilton for supporting our research, offering his lab to us and for the countless discussions. We thank Sarah K. Huber for curatorial assistance. We also thank the two anonymous reviewers for valuable comments on the manuscript. The monoclonal antibodies obtained from the Developmental Studies Hybridoma Bank were developed under the auspices of the NICHD and maintained by The University of Iowa, Department of Biological Sciences, Iowa City, IA 52242, USA. This project was supported by the Volkswagen Foundation, Germany (project no. I84 / 825 to P Konstantinidis).

ORCID

Benjamin Naumann  <http://orcid.org/0000-0003-0970-2431>

REFERENCES

- Allis, E. P. (1897). The cranial muscles and first spinal nerves in *Amia calva*. *Journal of Morphology*, 12, 487–772.
- Böck, P. (1989). *Romeis mikroskopische technik*. München: Urban & Schwarzenberg.
- Couly, G. F., Coltey, P. M., & Le Douarin, N. M. (1993). The triple origin of skull in higher vertebrates: A study in quail-chick chimeras. *Development*, 117(2), 409–429.
- Edgeworth, F. H. (1911). Memoirs: On the morphology of the cranial muscles in some vertebrates. *Journal of Cell Science*, 2(222), 167–316.
- Edgeworth, F. H. (1929). The development of some of the cranial muscles of ganoid fishes. *Philosophical Transactions of the Royal Society of London. Series B, Containing Papers of a Biological Character*, 217, 39–89.
- Edgeworth, F. H. (1935). *The cranial muscles of the vertebrates*. Cambridge: Cambridge University Press.
- Epperlein, H. H., Khattak, S., Knapp, D., Tanaka, E. M., & Malashichev, Y. B. (2012). Neural crest does not contribute to the neck and shoulder in the axolotl (*Ambystoma mexicanum*). *PLoS ONE*, 7(12), e52244. <https://doi.org/10.1371/journal.pone.0052244>
- Ericsson, R., Cerny, R., Falck, P., & Olsson, L. (2004). Role of cranial neural crest cells in visceral arch muscle positioning and morphogenesis in the Mexican axolotl, *Ambystoma mexicanum*. *Developmental Dynamics*, 231(2), 237–247. <https://doi.org/10.1002/dvdy.20127>
- Ericsson, R., Knight, R., & Johanson, Z. (2013). Evolution and development of the vertebrate neck. *Journal of Anatomy*, 222(1), 67–78. <https://doi.org/10.1111/j.1469-7580.2012.01530.x>
- Fürbringer, M. (1874). Zur vergleichenden anatomie der schultermuskeln. II theil. *Jenaische Zeitschrift für Naturwissenschaften*, 8, 175–280.
- Gegenbaur, C. (1889). *Vergleichende Anatomie der Wirbelthiere: mit Berücksichtigung der Wirbellosen*. Leipzig: W. Engelmann.
- Grande, L. (2010). An empirical synthetic pattern study of gars (Lepisosteiformes) and closely related species, based mostly on skeletal anatomy. The resurrection of Holosteii. *Copeia*, 10(2A), 1.
- Greenwood, P. H., & Lauder, G. V. (1981). Protractor pectoralis muscle and the classification of teleost fishes. *Bulletin. Zoology series-British Museum (Natural History) Dept. of Zoology*.
- Huang, R., Zhi, Q., Patel, K., Wilting, J., & Christ, B. (2000). Contribution of single somites to the skeleton and muscles of the occipital and cervical regions in avian embryos. *Anatomy and Embryology*, 202(5), 375–383.
- Jessen, H. L. (1972). Schultergürtel und Pectoralflosse bei Actinopterygiern [Shoulder girdle and pectoral fin in actinopterygians]. *Fossils and Strata*, 1, 1–101.
- Klymkowsky, M. W., & Hanken, J. (1991). Whole-mount staining of *Xenopus* and other vertebrates. *Methods in Cell Biology*, 36, 419–441.
- Kuratani, S. (1997). Spatial distribution of postotic crest cells defines the head/trunk interface of the vertebrate body: Embryological interpretation of peripheral nerve morphology and evolution of the vertebrate head. *Anatomy and Embryology*, 195(1), 1–13.
- Kuratani, S. (2008). Evolutionary developmental studies of cyclostomes and the origin of the vertebrate neck. *Development, Growth and Differentiation*, 50(Suppl 1), S189–S194. <https://doi.org/10.1111/j.1440-169X.2008.00985.x>
- Long, W. L., & Ballard, W. W. (2001). Normal embryonic stages of the longnose gar, *Lepisosteus osseus*. *BMC Developmental Biology*, 1, 6.
- Matsuoka, T., Ahlberg, P. E., Kessaris, N., Iannarelli, P., Dennehy, U., Richardson, W. D., ... Koentges, G. (2005). Neural crest origins of the neck and shoulder. *Nature*, 436(7049), 347–355. <https://doi.org/10.1038/nature03837>
- Metscher, B. D. (2009). MicroCT for comparative morphology: Simple staining methods allow high-contrast 3D imaging of diverse non-mineralized animal tissues. *BMC Physiology*, 9, 11. <https://doi.org/10.1186/1472-6793-9-11>
- Mootoosamy, R. C., & Dietrich, S. (2002). Distinct regulatory cascades for head and trunk myogenesis. *Development*, 129(3), 573–583.
- Noden, D. M. (1983). The embryonic origins of avian cephalic and cervical muscles and associated connective tissues. *American Journal of Anatomy*, 168(3), 257–276. <https://doi.org/10.1002/aja.1001680302>

- Oisi, Y., Fujimoto, S., Ota, K. G., & Kuratani, S. (2015). On the peculiar morphology and development of the hypoglossal, glossopharyngeal and vagus nerves and hypobranchial muscles in the hagfish. *Zoological Letters*, *1*, 6. <https://doi.org/10.1186/s40851-014-0005-9>
- Piekarski, N., & Olsson, L. (2007). Muscular derivatives of the cranialmost somites revealed by long-term fate mapping in the Mexican axolotl (*Ambystoma mexicanum*). *Evolution and Development*, *9*(6), 566–578. <https://doi.org/10.1111/j.1525-142X.2007.00197.x>
- Sambasivan, R., Kuratani, S., & Tajbakhsh, S. (2011). An eye on the head: The development and evolution of craniofacial muscles. *Development*, *138*(12), 2401–2415. <https://doi.org/10.1242/dev.040972>
- Sefton, E. M., Bhullar, B. A., Mohaddes, Z., & Hanken, J. (2016). Evolution of the head-trunk interface in tetrapod vertebrates. *Elife*, *5*, e09972. <https://doi.org/10.7554/eLife.09972>
- Tada, M. N., & Kuratani, S. (2015). Evolutionary and developmental understanding of the spinal accessory nerve. *Zoological Letters*, *1*, 4. <https://doi.org/10.1186/s40851-014-0006-8>
- Theis, S., Patel, K., Valasek, P., Otto, A., Pu, Q., Harel, I., . . . Huang, R. (2010). The occipital lateral plate mesoderm is a novel source for vertebrate neck musculature. *Development*, *137*(17), 2961–2971. <https://doi.org/10.1242/dev.049726>
- Trinajstić, K., Sanchez, S., Dupret, V., Tafforeau, P., Long, J., Young, G., . . . Ahlberg, P. E. (2013). Fossil musculature of the most primitive jawed vertebrates. *Science*, *341*(6142), 160–164. <https://doi.org/10.1126/science.1237275>
- Tzahor, E., Kempf, H., Mootosamy, R. C., Poon, A. C., Abzhanov, A., Tabin, C. J., . . . Lassar, A. B. (2003). Antagonists of Wnt and BMP signaling promote the formation of vertebrate head muscle. *Genes & Development*, *17*(24), 3087–3099. <https://doi.org/10.1101/gad.1154103>
- Wiedersheim, R., & Weismann, A. (1904). *Ueber das Vorkommen eines Kehlkopfes bei Ganoiden und Dipnoern: sowie über die Phylogenie der Lunge*. Verlag von Gustav Fischer.
- Winterbottom, R. (1974). Descriptive synonymy of striated muscles of teleostei. *Proceedings of the Academy of Natural Sciences of Philadelphia*, *125*(12), 225–317.
- Zhu, M., Ahlberg, P. E., Pan, Z., Zhu, Y., Qiao, T., Zhao, W., . . . Lu, J. (2016). A Silurian maxillate placoderm illuminates jaw evolution. *Science*, *354*(6310), 334–336. <https://doi.org/10.1126/science.aah3764>
- Ziermann, J. M., & Diogo, R. (2013). Cranial muscle development in the model organism *Ambystoma mexicanum*: Implications for tetrapod and vertebrate comparative and evolutionary morphology and notes on ontogeny and phylogeny. *Anatomical Record-Advances in Integrative Anatomy and Evolutionary Biology*, *296*(7), 1031–1048. <https://doi.org/10.1002/ar.22713>

How to cite this article: Naumann B, Warth P, Olsson L, Konstantinidis P. The development of the cucullaris muscle and the branchial musculature in the Longnose Gar, (*Lepisosteus osseus*, Lepisosteiformes, Actinopterygii) and its implications for the evolution and development of the head/trunk interface in vertebrates. *Evolution & Development*. 2017;19:263–276. <https://doi.org/10.1111/ede.12239>

Chapter 2

Naumann, B., & Olsson, L. (2017). **Three-dimensional reconstruction of the cranial and anterior spinal nerves in early tadpoles of *Xenopus laevis* (Pipidae, Anura).** *Journal of Comparative Neurology*, 526(5), 836-857.

RESEARCH ARTICLE

WILEY

The Journal of
Comparative Neurology

Three-dimensional reconstruction of the cranial and anterior spinal nerves in early tadpoles of *Xenopus laevis* (Pipidae, Anura)

Benjamin Naumann  | Lennart Olsson

Institut für Spezielle Zoologie und Evolutionsbiologie mit Phyletischem Museum, Friedrich-Schiller-Universität, Jena, Germany

Correspondence

Benjamin Naumann, Institut für Spezielle Zoologie und Evolutionsbiologie mit Phyletischem Museum, Friedrich-Schiller-Universität, Jena 07745, Germany
Email: benjamin.naumann@uni-jena.de

Funding information

Deutsche Forschungsgemeinschaft, Grant Number: DFG-OL 134/10-2 (to LO)

Abstract

Xenopus laevis is one of the most widely used model organism in neurobiology. It is therefore surprising, that no detailed and complete description of the cranial nerves exists for this species. Using classical histological sectioning in combination with fluorescent whole mount antibody staining and micro-computed tomography we prepared a detailed innervation map and a freely-rotatable three-dimensional (3D) model of the cranial nerves and anterior-most spinal nerves of early *X. laevis* tadpoles. Our results confirm earlier descriptions of the pre-otic cranial nerves and present the first detailed description of the post-otic cranial nerves. Tracing the innervation, we found two previously undescribed head muscles (the processo-articularis and diaphragmatico-branchialis muscles) in *X. laevis*. Data on the cranial nerve morphology of tadpoles are scarce, and only one other species (*Discoglossus pictus*) has been described in great detail. A comparison of *Xenopus* and *Discoglossus* reveals a relatively conserved pattern of the post-otic and a more variable morphology of the pre-otic cranial nerves. Furthermore, the innervation map and the 3D models presented here can serve as an easily accessible basis to identify alterations of the innervation produced by experimental studies such as genetic gain- and loss of function experiments.

KEYWORDS

cranial nerves, three-dimensional reconstruction, *Xenopus laevis*

Abbreviations: Aa, anterior auditory lateral line; Al, anterior lower lateral line; ALLN, anterior lateral line nerve; An, angular lateral line; Ao, aortic lateral line; Asc, anterior semicircular canal; Atr, Atrium; AV+Shg, anastomosis of the V and the Shg; AV+VII, anastomosis of the V and the VII; cabII, Musculus constrictor arcum branchiarium II; cabIII, Musculus constrictor arcum branchiarium III; cabIV, Musculus constrictor arcum branchiarium IV; Ccr, common crus; CD, Notochord; CO, chiasma opticum; COE, ciliary olfactory epithelium; cp, Musculus constrictor pharyngeus; dALLN, dorsal anterior lateral line nerve; dALLNaa, ramulus acusticus anterioris of the dALLNbu; dALLNao, ramus oticus anterioris of the dALLN; dALLNbu, ramus buccalis of the dALLN; dALLNso, ramus ophthalmicus superficialis of the dALLN; db, Musculus diaphragmatico-branchialis; DiC, Diencephalon; dl, Musculus dilatator larynges; DRG, dorsal root ganglion; drS2-S5, dorsal root of S2-S5; epm, epaxonic trunk musculature; gdALLN, ganglion of the dALLN; gh, Musculus geniohyoideus; gIX, ganglion of the IX; gIX+X, common ganglion of the IX and X; gPLLN, ganglion of the PLLN; gPr, profundal ganglion; gPr+V, fused ganglion of the Pr and V (Ganglion gasserii); gV, ganglion of the V; gvALLN, ganglion of the vALLN; gVII+vALLN, common ganglion of the VII and vALLN (geniculate-lateral ganglion); gVIIIaa, ganglion of the VIIIaa; gVIIIap, ganglion of the VIIIap; Hm, hyomandibular lateral line; I, nervus olfactorius; Id, I ramus lateralis; ih, Musculus interhyoideus; II, nervus opticus; III, nervus oculomotorius; IIIoi, III ramus obliquus inferioris; IIIos, III ramus obliquus superioris; IIIri, III ramus rectus inferioris; IIIrl, III ramus rectus lateralis; IIIrm, III ramus rectus medialis; IIIrs, III ramus rectus superioris; Im, I ramus medius; im, Musculus intermandibularis; lo, infra-orbital lateral line; lp, I ramus medialis; IV, nervus trochlearis; IX, nervus glossopharyngeus; IXcut, ramus cutaneus of the IXb; IXcVII, ramus communicans IX cum VII; IXlabI, ramuli levator arcum branchiarium I of the IX; IXp, post-trematic ramus of the IX; IXph, ramus pharyngeus of the IX; IXsr, ramus subarcualis rectus of the IX; IXvi, ramus visceralis of the IX; lab I-IV, Musculus levator arcus branchialis I to IV (fused to one); Lag, Lagena; Lm, lagenar macula; lma, Musculus levator mandibulae articularis; lmc, levator mandibulae complex; lme, Musculus levator mandibulae externus; lmi, Musculus levator mandibulae internus; lmlp, Musculus levator mandibulae longus profundus; lmls, Musculus levator mandibulae longus superior; LoO, bulbus olfactorius; Lsc, lateral semicircular canal; m1-m5, myotome 1 to 5; Mi, middle lateral line; MLLN, median lateral line nerve; MLLNsb, ramus suprabranchialis of the MLLN; MLLNsot, ramus supraoticus of the MLLN; Mn, mandibular lateral line; MsC, Mesencephalon; MtC, Metencephalon muscular sheet in *X. laevis*; Mv, median ventral lateral line; Mx, maxillary lateral line; MyC, Myelencephalon; NC, Neurocranium; NM, Neuromast; Oc, occipital lateral line; OC, otic capsule; oh, Musculus orbitohyoideus; oi, Musculus obliquus inferioris; os, Musculus obliquus superioris; Pa, posterior auditory lateral line; par, Musculus processo-articularis; Pl, posterior lower lateral line; PLLN, posterior lateral line nerve; PLLNd, ramus dorsalis of the PLLN; PLLNlat, ramus lateralis of the PLLN; PLLNv, ramus ventralis of the PLLN; PLLNva, ramulus ventralis anterior of the PLLNv; PLLNvp, ramulus ventralis posterior of the PLLNv; PN, Pronephros; Pr,

1 | INTRODUCTION

Since the mid-20th century, the African clawed frog, *Xenopus laevis*, has become one of the most widely used model organisms in biology (Harland & Grainger, 2011; Porro & Richards, 2017). Especially in neurobiology, *Xenopus* embryos, tadpoles, and adults are used as models in pathological, developmental, physiological, and behavioral studies (Cannatella & De Sa, 1993; Cervino, Paz, & Frontera, 2017; Cline & Kelly, 2012; Dong et al., 2009; Edwards-Faret et al., 2017; Frankenhaeuser & Huxley, 1964; Gouchie, Roberts, & Wassersug, 2008; Katz, Potel, & Wassersug, 1981; Lee-Liu, Méndez-Olivos, Muñoz, & Larrain, 2016; McKeown, Sharma, Sharipov, Shen, & Cline, 2013; Moreno, Tapia, & Larrain, 2014; Pieper, Eagleson, Wosniok, & Schlosser, 2011; Pratt & Khakhalin, 2013; Roberts, Walford, Soffe, & Yoshida, 1999; Schlosser & Northcutt, 2000; Simmons, Costa, & Gerstein, 2004; Wassersug & Hessler, 1971; Young & Poo, 1983). It is therefore surprising, that only one study (Paterson, 1939) on the anatomy of the cranial nerves of *X. laevis* tadpoles exists. This study was based on rather destructive techniques like histological paraffin sectioning and dissections which limit the detection of very fine nerve branches. Using more sensitive, non-destructive techniques such as fluorescent whole-mount antibody staining and micro-computed tomography in combination with traditional histological sectioning, we reinvestigated the anatomy of the cranial nerves in *X. laevis* tadpoles. We confirm earlier descriptions of the "pre-otic" cranial nerves (Paterson, 1939) and present the first detailed description and illustration of the "post-otic" cranial and anterior spinal nerves in *X. laevis* tadpoles. An innervation map (as prepared for *DiscoGLOSSUS pictus* by Schlosser & Roth, 1995) and freely rotatable three-dimensional (3D) models (3pdfs are available as Supporting Information

material 1 to 3) of the major nerve branches can serve as an easily accessible basis for evaluation of experimental studies, for example, genetic gain- and loss-of-function analyses. A detailed comparison between the cranial nerve anatomy of *D. pictus* and *X. laevis* shows a relatively conserved pattern at least for the larvae of non-neobatrachian frogs.

2 | MATERIALS AND METHODS

Animals

Xenopus laevis tadpoles were obtained from the breeding colony at the Institut für Spezielle Zoologie, Friedrich-Schiller-University, Jena, Germany. A total of 12 larvae were staged according to the normal table (Nieuwkoop & Faber, 1994), anesthetized, and either fixed in 4% saline-buffered para-formaldehyde (4% PFA) or in Dent's fixative (four parts 100% methanol, one part dimethyl sulfoxide). The specimens investigated are listed in Table 1.

2.1 | Micro-computed tomography

One larva was fixed in 4% PFA and treated with phosphotungstic acid (PTA) as described by Metscher (2009). The specimen was scanned using a phoenix nanotom m (GE Sensing & Inspection Technologies GmbH, Wunstorf, Germany).

2.2 | Fluorescent whole mount antibody staining

Specimens were fixed in Dent's fixative for a minimum of one day and bleached in Dent's bleach (10% hydrogen peroxide in Dent's fixative)

nervus profundus; Prcu, ramus cutaneus of the Pr; Prcut, diverse cutaneous ramuli of the Pr; Prln, ramulus narium lateralis of the Prna; Prna, ramus narium of the Pr; Prnm, ramulus naris medialis of the Prna; Psc, posterior semicircular canal; Pt, parietal lateral line; qha, Musculus quadrato-hyoangularis; ra, Musculus rectus anterioris; rALLN, root of the ALLN; ReC, Rhombencephalon; ri, Musculus rectus inferioris; rIX+MLLN, root of the IX and MLLN; rp, Musculus rectus posterioris; rPLLN, root of the PLLN; rPr+V, common root of the Pr and V; rs, Musculus rectus superioris; rVII+VIII, common root of the VII and VIII; rX, root of the X; S1-S5, spinal nerve 1-5; S2a, anterior ramulus of the S2v; S2d-S5d, dorsal ramulus of the S1-S5; S2p, posterior ramulus of the S2v; S2v-S5v, ventral ramulus of the S1-S5; S4c-S5c, ramulus cutaneus of the S4v-S5v; S5m, ramulus muscularis of the S5v; sa, Musculus suspensorio-angularis; Sac, Sacculus; SC, spinal cord; sdALLN, stem of the dALLN; Sgh, ramulus geniohyoideus of the Shg; Shg, nervus hypoglossus (hypoglossal nerve); Sm, saccular macula; So, supra-orbital lateral line; sPr+V, common stem of the Pr and V; sr, Musculus subarcualis rectus I; Src, ramuli rectus cervicis of the Shg; Sve, sinus venosus; ; sVII+vALLN, common stem of the VII and vALLN; sVIII, stem of the VIII; Te, tentacular lateral line; TeC, Telencephalon; TR, trabecula crani; Tra, truncus arteriosus; tvII, Musculus transversus ventralis II; Um, utricular macula; Up, upper lateral line; Utr, Utriculus; V, nervus trigeminus; Va, ventral anastomosis of the IX and the X; vALLN, ventral anterior lateral line nerve; vALLNan, ramus angularis of the vALLN; vALLNhm, ramus hyomandibularis of the vALLN; vALLNm, ramus mandibularis of the vALLN; Ven, Ventriculus; VI, nervus abducens; VII, nervus facialis; VIIcut, ramulus cutaneus of the VII; VIIhm, VII ramus hyomandibularis; VIIhy, VII ramus hyoideus; VIII, nervus vestibulochochlearis; VIIIaa, VIII ramus acusticus anterior; VIIIac, ramulus canalis semicircularis anterior of the VIIIaa; VIIIap, VIII ramus acusticus posterior; VIIIlc, ramulus canalis semicircularis lateralis of the VIIIaa; VIIIpa, ramulus ampullaris posterior of the VIIIap; VIIIpc, ramulus canalis semicircularis posterior of the VIIIap; VIIIme, ramulus mandibularis externus of the VIIIhm; VIIImi, ramulus mandibularis internus of the VIIIhm; VIIoh, ramuli orbitohyoideus of the VIIhy; VIIpa, VII ramus palatinus; VIIpl, VII ramus palatinus lateralis; VIIpm, VII ramus palatinus medialis; VIIqha, ramulus quadrato-hyoangularis of the VIIhy; VIIsa, ramulus suspensorio-angularis of the VIIhy; Vim, ramuli intermandibularis of the Vmm; VIm, ramulus levator mandibulae 1 of the Vmm; VIme, ramulus levator mandibulae 2 of the Vmm; Vmm, ramus maxillomandibularis of the V; Vmn, ramus mandibularis of the V; ; Vmu, ramulus mucosus of the Vmm; Vmx, ramus maxillaris of the V; Vpar, ramulus processo-articularis of the Vmm; Vpl, ramulus palatinus of the Vmm; Vre, ramulus cutaneus recurrens of the Vmm; vrS1-S5, ventral root of S1-S5; Vte1, ramulus temporalis 1 of the Vmm; Vte2, ramulus temporalis 2 of the Vmm; X, nervus vagus; Xac, ramulus accessorius of the X; Xaud, ramulus auricularis dorsalis of Xaur; Xaul, ramulus auricularis lateralis of Xaur; Xaur, ramus auricularis of the X; Xb1, ramus branchialis 1 of the X; Xb2, ramus branchialis 2 of the X; Xb3, ramus branchialis 3 of the X; XcabII, ramulus constrictor arcum branchiarium II of the Xb1; XcabIII, ramulus constrictor arcum branchiarium III of the Xb2; Xcard, cardiac ramulus of the Xcpu; Xcp, ramulus constrictor pharyngeus of the X; Xcpu, ramus cardiopulmonaris of the X; Xcut1, ramus cutaneus of the Xb1; Xcut2, ramus cutaneus of the Xb2; Xcut3, ramus cutaneus of the Xb3; Xdb, ramulus diaphragmatico-branchialis of the X; Xdl, ramulus dilatator laryngeus of the X; ; Xin, ramus intestinalis of the X; Xinm, ramus intestinalis medialis of the X; XlabII, ramulus levator arcum branchiarium II of the Xb1; XlabIII, ramulus levator arcum branchiarium III of the Xb2; XlabIV, ramulus levator arcum branchiarium IV of the Xb3; Xp1, post-trematic ramus of the Xb1; Xp2,, post-trematic ramus of the Xb2; Xph1, ramus pharyngeus 1 of the X; ; Xph2, ramus pharyngeus 2 of the X; Xpul, pulmonary ramulus of the Xcpu; XtvII, ramulus transversus ventralis II of the Xb1; Xvi1, ramus visceralis 1 of the Xb1; Xvi2, ramus visceralis 2 of the Xb2.

TABLE 1 Summary of the specimens investigated in this study. Methods used: histology (H), μ CT (C), fluorescent whole mount antibody staining (F)

NF stage	46	46	47	47	47/48	46	46	47	47	47	47/48	47/48
Method	H	H	H	H	C	F	F	F	F	F	F	F

for 4 hr under a normal desk lamp. All incubations were carried out at room temperature (21–25°C). Antibody staining was conducted on whole mounts according to standard protocols (Klymkowsky & Hanken, 1991). After bleaching, specimens were washed three times in PBS + 0,1% TritonX-100 for 20 min each. They were then blocked for 2 hr in DAKO antibody diluent. Anti-desmin (Monosan, PS031) and anti-acetylated alpha-tubulin (Sigma, T6793) antibodies at dilutions of 1:100 (12/101, anti-desmin) and 1:500 (anti-acetylated alpha tubulin) were applied and incubated overnight. On the next day specimens were washed again three times in PBS + 0,1% TritonX-100 for 20 min each and blocked in DAKO antibody diluent for 2 hr. Afterward, Alexa488-anti-mouse (Thermo Fisher Scientific, Product # R37120) and Alexa568-anti-rabbit (Thermo Fisher Scientific, Product # A-11011) were applied as secondary antibodies (1:500 in DAKO antibody diluent) and incubated overnight. Stained specimens were dehydrated two times in 100% methanol for 10 min each and cleared and stored in BABB (benzyl alcohol/benzyl benzoate, 1/2).

2.3 | Image processing and 3D reconstruction

Digital stacks from the antibody stainings were obtained using a Zeiss LSM510 confocal microscope and processed with ZEN 2012. Different image sequences were isolated from the complete stacks and shown as maximum intensity projections or 3D depth coding views, in which structures close to the observer are depicted in warmer (red, orange, yellow) and structures away from the observer in colder colors (green, blue). The real measure of the z axis is shown by a color scale for each image separately. The background was cleaned and brightness, contrast, and color balance were adjusted using Adobe Photoshop CS6. Optical noise, produced by antibody precipitate in the tissue, was reduced using Fiji (GitHub, Inc.). 3D reconstructions were performed using Amira 5.2 3D-analysis software (FEI Visualization Sciences Group) and transferred to MAYA software (Autodesk, Inc.) for surface renderings.

2.4 | Histology

Specimens were fixed in 4% PFA for at least 24 hr, embedded in paraffin and sectioned into 7 μ m transverse sections using a HM360 Microm (Germany). The sections were stained using the standard Heidenhein-Azan technique (Böck, 1989). Single sections were digitalized with an Olympus BX51 microscope using the dotslide software 2.3 (Olympus Corporation, Tokyo, Japan).

2.5 | Terminology

For muscles and skeletal elements, we used the terminology for *X. laevis* in Ziermann and Olsson (2007), which is mainly based on the

muscular terminology of Edgeworth (1935). For the cranial, spinal and lateral line nerves we adopted the terminology of Schlosser and Roth (1995). For the lateral lines we used the terminology of Shelton (1970). Furthermore, we use the term “visceral arches” to refer to mandibular (first), hyoid (second), and the four posterior (three to six) gill-bearing arches. The latter four are referred to as branchial arches (one to four).

3 | RESULTS

3.1 | The lateral lines

The lateral line system of *X. laevis* has been described for tadpoles at NF stage 55 and 57 (Quinzio & Fabrezi, 2014; Shelton, 1970). To examine the innervation pattern of the lateral line nerves (LLNs) of younger tadpoles (NF stage 47/48), we re-examined the distribution of lateral lines in *X. laevis*. Phosphotungstic acid accumulates in the hair cells of single neuromasts making them visible as white dots in a volume rendering of the μ CT data set. We identified all the lateral lines described by Shelton (1970) for older tadpoles. The lateral lines are depicted in Figure 1. Ventral to the infraorbital lateral line, a cluster of four single neuromasts can be seen in whole-mount antibody stainings but not in the μ CT scan. We identified this cluster as the angular lateral line, as described by Schlosser and Roth (1995) for tadpoles of *Discoglossus pictus* (Figure 1a; black asterisks).

3.2 | The cranial muscles

Using fluorescent whole-mount antibody stainings in combination with confocal laser scanning microscopy we obtained new data about the head muscles of *X. laevis*. The Musculus diaphragmatico-branchialis is present in *X. laevis*. It originates from the posterior edge of the levator arcus branchiarum complex and the ceratobranchial 4, runs posteroven-trally and becomes continuous with the hypaxial trunk musculature. It is innervated by the ramulus diaphragmatico-branchialis of the third branchial ramus of the vagal nerve (Figure 8k). The Musculus processio-articularis of *X. laevis* is a very small muscle in the anterior head region, close to the mandibular levator muscles. It is attached to the palatoquadrate cartilage on both sides and innervated by a small ramulus of the ramus maxillomandibularis of the trigeminal nerve (Figure 6d–f). Additionally, we confirm the presence of a small cucullaris muscle (Ziermann & Diogo, 2014) originating from the otic capsule via a fascia, at the level of the first myotome (Figure 8c; blue arrow). Its posterior end is still loose. It is innervated by the ramus accessorius of the vagal nerve (Figure 8l).

3.3 | The cranial nerves

The root of the anterior lateral line nerve (ALLN) originates from the anterior rhombencephalon, slightly dorsal to the common root of the

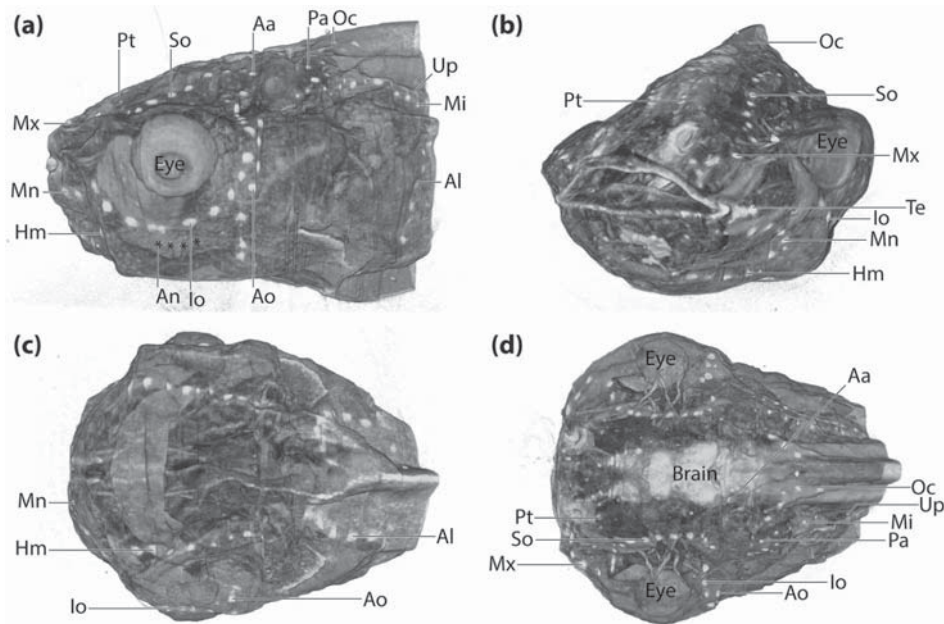


FIGURE 1 Volume rendering of a μ CT-scan of a PTA-stained *Xenopus laevis* tadpole at NF stage 47/48. The neuromasts are visible as white dots in the gray skin of the specimen. (a) lateral view. The four neuromasts of the angular lateral line are not visible in the scan but their positions are indicated by black asterisks. (b) frontolateral view. (c) ventral view. (d) dorsal view

facial and vestibulocochlear nerves. Immediately after exiting the brain it splits into the dorsal ALLN (dALLN) and the ventral ALLN (vALLN). The dALLN (Figure 2a–c) runs anteriorly, medial to the otic capsule and close to the dorsal surface of the trigeminal nerve. It enters a ganglion slightly posterodorsal to the fused profundal/trigeminal ganglion (Figure 3a,b,g). A superficial ophthalmic ramus and a buccal ramus originate from the anterior end of the dALLN ganglion. The superficial ophthalmic ramus runs anteriorly, dorsal to the eye, innervating the neuromasts of the supraorbital, and the parietal lateral lines (Figures 2 and 3c). The buccal ramus gives off a small ramulus, innervating the few neuromasts of the anterior auditory lateral line (Figures 2 and 3c). The remaining main trunk runs anteriorly, curving around the eye and supplies the infraorbital lateral line (Figures 2 and 3c). The vALLN runs ventrally and joins the facial/vestibulocochlear nerve stem (Figures 3a,b). They leave the otic capsule, entering the ganglion geniculi (Figure 3g) which is positioned slightly proximal to the unfused trigeminal part of the profundal/trigeminal ganglion. After leaving the ganglion, the fibers of the vALLN are closely associated with the fibers of the facial nerve (Figures 2 and 3b). This compound nerve curves anteroventrally medial to the eye, dividing into the ramus hyomandibularis and ramus hyoideus. The vALLN becomes closely associated with the hyomandibular ramus (Figure 3g). It gives rise to the ramulus angularis of the vALLN (Figure 3d). This ramulus describes a curve, runs posteriorly and innervates the four neuromasts of the angular lateral line. The remaining nerve trunk splits off into several ramuli. Only the ramuli carrying a lateral line component are described here. The ramulus mandibularis of the vALLN innervates the lateral line organs of the anterior head region (the mandibular, maxillary, and tentacular lateral lines). It leaves the main nerve trunk together with the ramulus mandibularis internus of the

facial nerve and runs anteriorly in the direction of the mouth opening (Figure 3d). The ramulus hyomandibularis of the vALLN runs posteroventrally, supplying the hyomandibular lateral line (Figure 3d). A single neuromast anterior to the hyomandibular lateral line is innervated by a branchlet, originating from the ramulus mandibularis externus of the facial nerve. Therefore, it seems that this nerve also carries fibers of the vALLN (Figure 7f, red arrow). A schematic innervation map of the ALLN is given in Figure 3i. The root of the medial lateral line nerve (MLLN; Figure 2) exits the rhombencephalon with the root of the glossopharyngeal nerve. They form a common nerve stem running posteriorly (Figure 3a) along the ganglion of the PLLN and the ganglion of the vagal nerve. These post-otic ganglia are grouped together as the post-otic ganglionic complex. It is not clear whether the glossopharyngeal/MLLN only runs along this ganglionic complex or if they contact each other. However, no separate ganglion of the MLLN could be found. After a short distance a distinct MLLN branches off from the common glossopharyngeal/MLLN stem and curves anteriorly. A small ramus supraoticus separates from the main trunk of the MLLN. It runs posterodorsally innervating the posterior acoustic lateral line (Figure 3e). The main trunk of the MLLN curves anteroventrally, posterior to the ramus buccalis of the dALLN. This so-called ramus suprabranchialis of the MLLN innervates the aortic lateral line (Figure 3e). A schematic innervation map of the MLLN is given in Figure 3j. The root of the posterior lateral line nerve (PLLN; Figure 2) exits the rhombencephalon anterodorsal to the glossopharyngeal/MLLN and vagal roots (Figure 3a). It runs posteroventrally entering a ganglion on top of the glossopharyngeal/vagal ganglion (Figure 3b,h). The ganglion of the PLLN may fuse to some degree with the glossopharyngeal/vagal ganglion, since the ventral ramus of the PLLN originates close to the vagal branches supplying

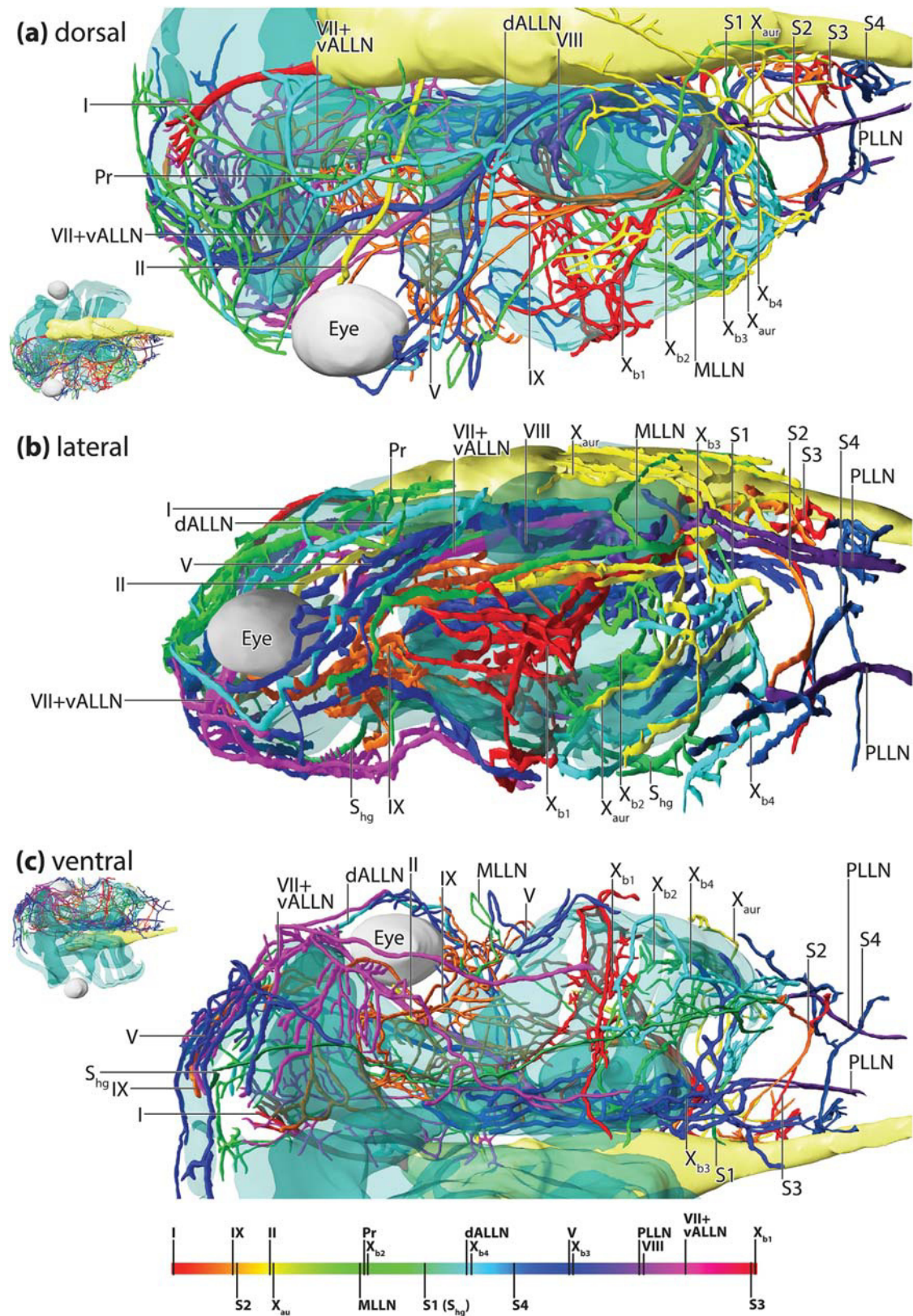


FIGURE 2 3D reconstruction of a dorso-ventral scan of a whole mount antibody staining against acetylated- α tubulin of a *Xenopus laevis* larva at NF stage 47/48. The nerves have been reconstructed only on the left side. Cranial nerves are color-coded according to a rainbow color map. The brain is shown in light yellow, the eye in white, and the cartilaginous head skeleton in transparent blue. A smaller overview of the whole 3D model is shown in the lower left corner. (b) lateral view. (c) ventral view. A smaller overview of the whole 3D model is shown in the upper left corner [Color figure can be viewed at wileyonlinelibrary.com]

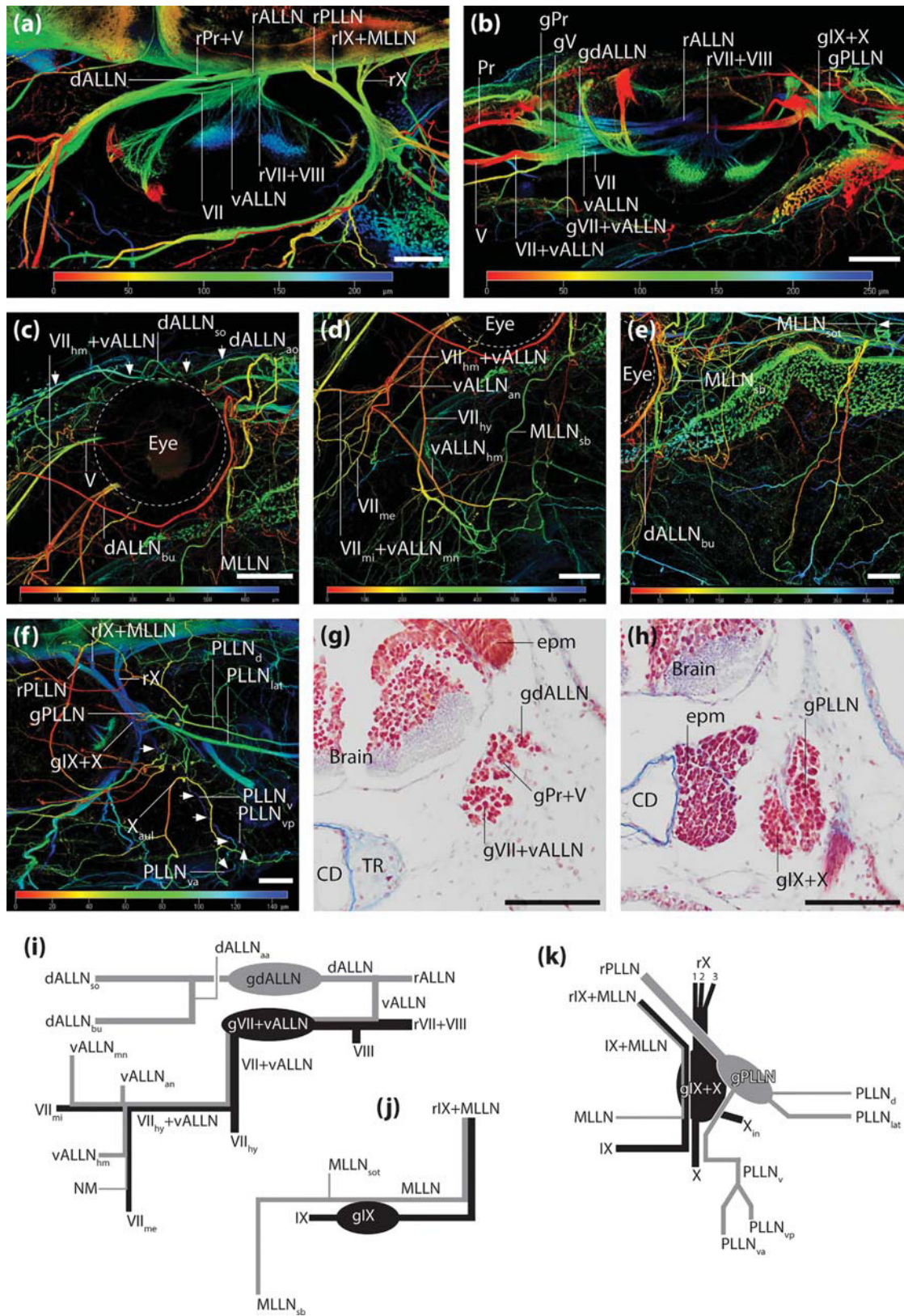


FIGURE 3.

the third and fourth branchial arches. This ventral ramus curves dorsally and divides into an anterior and a posterior ramulus (Figure 3f). The anterior ramulus innervates the anterior lower lateral line, while the posterior ramulus supplies posterior lower and the median ventral lateral line. The part of the nerve which does not enter the glossopharyngeal/vagal ganglion leaves the PLLN ganglion in a posterior direction. It immediately divides into a smaller ramus dorsalis and a larger ramus lateralis (Figure 3f). The ramus dorsalis supplies the upper line, while the ramus lateralis supplies the middle lateral line. A schematic innervation map of the PLLN is given in Figure 3k.

The olfactory nerve (nervus olfactorius, I) of *X. laevis* originates from axons in the olfactory mucosa of the naris. It runs posterodorsally, entering the bulbus olfactorius at the anterior edge of the telencephalon (Figures 2 and 4a). Three distinct ramuli unite to the main trunk of the olfactory nerve shortly after leaving the olfactory mucosa. The ramus lateralis originates from the distal-most part of the olfactory mucosa. The ramus medius originates from the middle part, while the ramus medialis originates from the proximal part of the olfactory mucosa (Figure 4a1).

The optic nerve (nervus opticus, II) originates from the joining axons of the retinal ganglion cells (Figure 4b–b3). The bundled nerve trunk runs medially performing a slight dorsal curve. It crosses the optic nerve from the contralateral side, forming the chiasma opticum, before it enters the optic tract (Figure 4b3).

The oculomotor nerve (Nervus oculomotorius, III) originates from the lateral surface of the mesencephalon. It runs anterodistally crossing the course of the profundal nerve ventrally (Figure 5a). A thin ramus branches off from the oculomotor nerve, innervating the Musculus rectus superioris (Figure 5a1). The main ramus runs laterodistally in proximity to the Musculus rectus inferioris. On its way to the eyeball, it bifurcates. One ramus innervates the Musculus rectus inferioris and the Musculus obliquus inferioris, while the other ramus runs anteroventrally, supplying the Musculus rectus medialis. (Figure 5a1).

The trochlear nerve (nervus trochlearis, IV) originates from the dorso-lateral surface of the medullar velum. This delicate nerve runs anteriorly alongside the lateral brain wall (Figure 5b). When it reaches the level of the optic nerve, it crosses it dorsally and describes a distally bent curve. The trochlear nerve continues in a ventrodistal direction almost parallel to the optic nerve. It bifurcates when it reaches the Musculus obliquus superioris. One ramus runs dorsally, supplying the upper, and the other ramus runs ventrally, supplying the lower part of the muscle (Figure 5b1).

The stem of the profundal and trigeminal nerve (nervus profundus and nervus trigeminus, V; Figure 2) originates from the medulla, ventral

to the stem of the dALLN (Figure 3a). The profundal and trigeminal ganglia are closely associated. While they are fused in the posterior region, they appear separated anteriorly, with the profundal ganglion laying dorsomedially to the trigeminal ganglion (Figure 6a). The fused ganglia form the so-called gasserian ganglion (Figure 3g). The profundal nerve arises from the separated profundal part of the gasserian ganglion. It runs in an anterior direction, giving off a few very small ramuli supplying the skin before it crosses the trochlear as well as the optic nerves dorsally and gives off the ramus cutaneus, supplying the skin dorsal to the eye (Figure 6b). The remaining nerve trunk, the ramus narium, runs further anteriorly. At the level of the anterior bulbus olfactorius, it divides into the ramus narium medialis and the ramus narium lateralis (Figure 6b). The ramus narium medialis runs antero-medially, supplying the skin and maybe the olfactory mucosa of the dorsal narial region. The ramus narium lateralis runs anterodistally in the direction of the lateral narial region, innervating the skin and maybe the olfactory mucosa of the lateral narial region. Both ramuli give off a few small cutaneous ramuli on the way to their terminal region. A prominent nerve trunk, the ramus maxillomandibularis, originates from the separated trigeminal part of the gasserian ganglion (Figure 2). Directly after it leaves the trigeminal ganglion, a ramulus temporalis 1 branches off and curves proximally, supplying the skin posterolateral to the eye (ramulus mandibularis 1 in Paterson, 1939). A ramulus temporalis 2 (ramulus mandibularis 2 in Paterson, 1939) branches off from the maxillomandibularis, slightly anterior to the ramulus temporalis 1 and curves around the posterior edge of the eyeball (Figures 2 and 6b). The main trunk of the ramus maxillomandibularis continues in an anterior direction behind the eyeball (Figure 6c). Because of the high absorbance of the eye pigment no signal of the nerve can be seen from a lateral view. Immediately anterior to eye, even before it subdivides into its two major branches, the ramus mandibularis and maxillaris, the nerve gives off three motor ramuli. The first one runs ventrally along the Musculus levator mandibulae complex and innervates the Musculus levator mandibulae longus superior, Musculus levator mandibulae internus and Musculus levator mandibulae longus posterior (Figure 6d,e,f; V_{lm1}). The second ramulus curves anteromedially, innervating the Musculus levator mandibulae articularis and the Musculus levator mandibulae externus (Figure 6d,e,f; V_{lm2}). The two nerves communicate with each other via an anastomosis. The ventral-most and smallest ramulus supplies the small Musculus processo-articularis (Figure 6e,f; red arrows). The main trunk of the maxillomandibular nerve divides into the ramus maxillaris and the ramus mandibularis (Figures 2 and 6c). A small ramulus emerges at exactly the same level, and makes it

FIGURE 3 The lateral line nerves. (a–f) 3D depth coding views of a whole mount antibody staining (acetylated alpha-tubulin) of a NF stage 47/48 *X. laevis* tadpole. (a) dorsal view of the region of the otic capsule. (b) lateral view of the region of the otic capsule. (c) lateral view of the eye region. (d) lateral view of the region ventral to the eye. (e) lateral view of the brachial region. (f) dorsal view of the posterior head region. The dotted line outlines the course of the ventral posterior lateral line nerve lying under the lateral auricular nerve. (g and h) transverse sections of a *X. laevis* tadpole at NF stage 46. (g) section through the region posterior to the eye to show the ganglia of the anterior lateral line nerve, the profundal and trigeminal nerves and the facial nerve. (h) section through the region posterior to the otic capsule to show the ganglia of the posterior lateral line nerve and the glossopharyngeal and vagal nerves. (i–k) schematic diagrams illustrating the rami and ramuli of the lateral line nerves. Components of the lateral line nerves are colored in gray, while components of the associated cranial nerves are colored in black. (i) anterior lateral line nerve. (j) middle lateral line nerve. (k) posterior lateral line nerve. White scale bar is 200 μm . Black scale bar is 100 μm [Color figure can be viewed at wileyonlinelibrary.com]

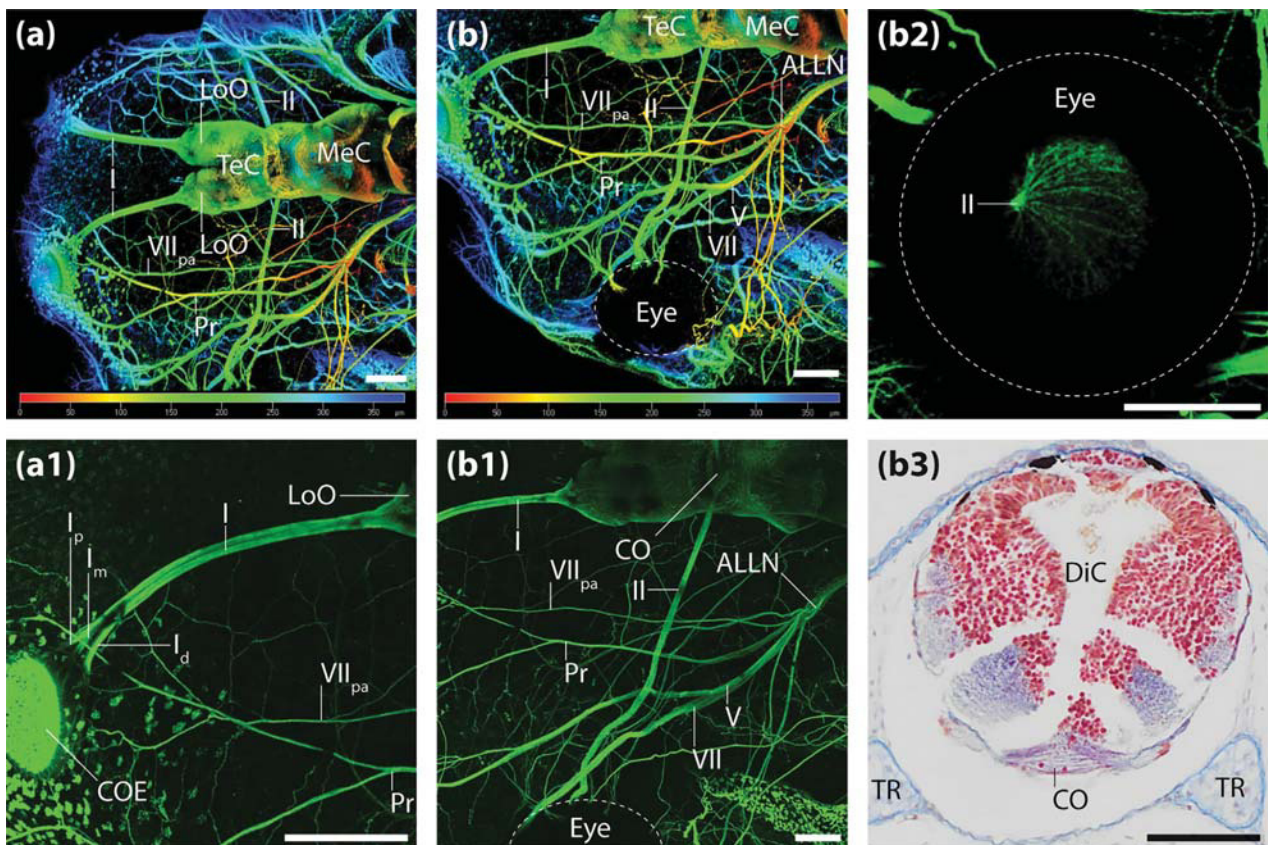


FIGURE 4 The olfactory and optic nerves. (a and b) 3D depth coding views of a whole mount antibody staining (acetylated alpha-tubulin) of a NF stage 47/48 *X. laevis* tadpole. (a) dorsal view of the anterior head region. (a1) maximum intensity projection of the same digital stack. Dorsal view of the olfactory nerve (I). (b) dorsal view of the anterior head region around the eye. (b1) maximum intensity projection of the same digital stack. Dorsal view of the optic nerve (II). (b2) 3D projection of the same digital stack. Lateral view of the eye to show the convergence of the optic fibers toward the optic papilla. (b3) histological section through the diencephalic region of a *X. laevis* tadpole at NF stage 46. The Chiasma opticum is closely associated with the ventral region of the diencephalon. Black and white scale bars are 200 μm [Color figure can be viewed at wileyonlinelibrary.com]

impossible to observe if it branches off from the ramus maxillaris or mandibularis. We therefore treat it as a ramulus of the maxillomandibular trunk in our description. The ramulus runs ventrally, describing a curve of approximately 90 degree in the posterior direction and turns ventrally again (Figure 6c). On its way it sends a few small ramuli into the skin as well as anastomosing fibers to the ramus hyomandibularis of the facial nerve, before it terminates in the skin of the lower jaw. Due to its peculiar course, we denominate this nerve branchlet as the ramulus cutaneus recurrens. Almost immediately, the ramus maxillaris divides into two ramuli. The first, the ramulus palatinus, runs anterodorsally and terminates in the mucosa and maybe the skin of the upper jaw (Figure 6c). We can confirm Paterson's statement (1939) that no anastomosing fibers between the ramulus palatinus of the facial nerve and the ramulus palatinus of the trigeminal nerve are detectable. The second nerve, the ramulus cutaneus, runs anteroventrally, and supplies the skin of the lower jaw overlaying the Musculus intermandibularis (Figure 6c). The ramus mandibularis runs anteroventrally, giving off a few small ramuli innervating the skin posterior to the mouth opening (Figure 6h). It also gives off a small ramulus, which runs straight in a ventral direction, anastomoses with the hypoglossal nerve and

eventually innervates the skin in this area (Figure 6h; A_{V+Shg}). The main trunk of the mandibular ramus continues anteroventrally, curving in a medial direction. At the level of the Musculus intermandibularis it becomes very delicate and difficult to follow. We observed a cutaneous ramulus and a few small ramuli innervating the intermandibular muscle (Figure 6g,h,i). The nerve terminates as the ramulus mucosus in the mucosa of the anterior lower jaw area (Figure 6i). A schematic innervation map of the profundal and trigeminal nerves is given in Figure 10a.

The abducens nerve (nervus abducens, VI) originates from the lateroventral surface of the myelencephalon. It leaves the brain posteromedial to the common root of the facial/vestibulocochlear nerves. The thin nerve runs anteroventrally joining the the profundal nerve (Figure 5c). It runs alongside this nerve and is not distinguishable from it until shortly before it reaches the optic nerve. It becomes recognizable as a distinct nerve running distally close to the oculomotor nerve. It innervates the Musculus rectus lateralis (Figure 5c1).

The facial nerve (nervus facialis, VII) originates from a common root with the vestibulocochlear nerve (Figure 2). This root enters the rhombencephalon posterior to the root of the profundal/trigeminal

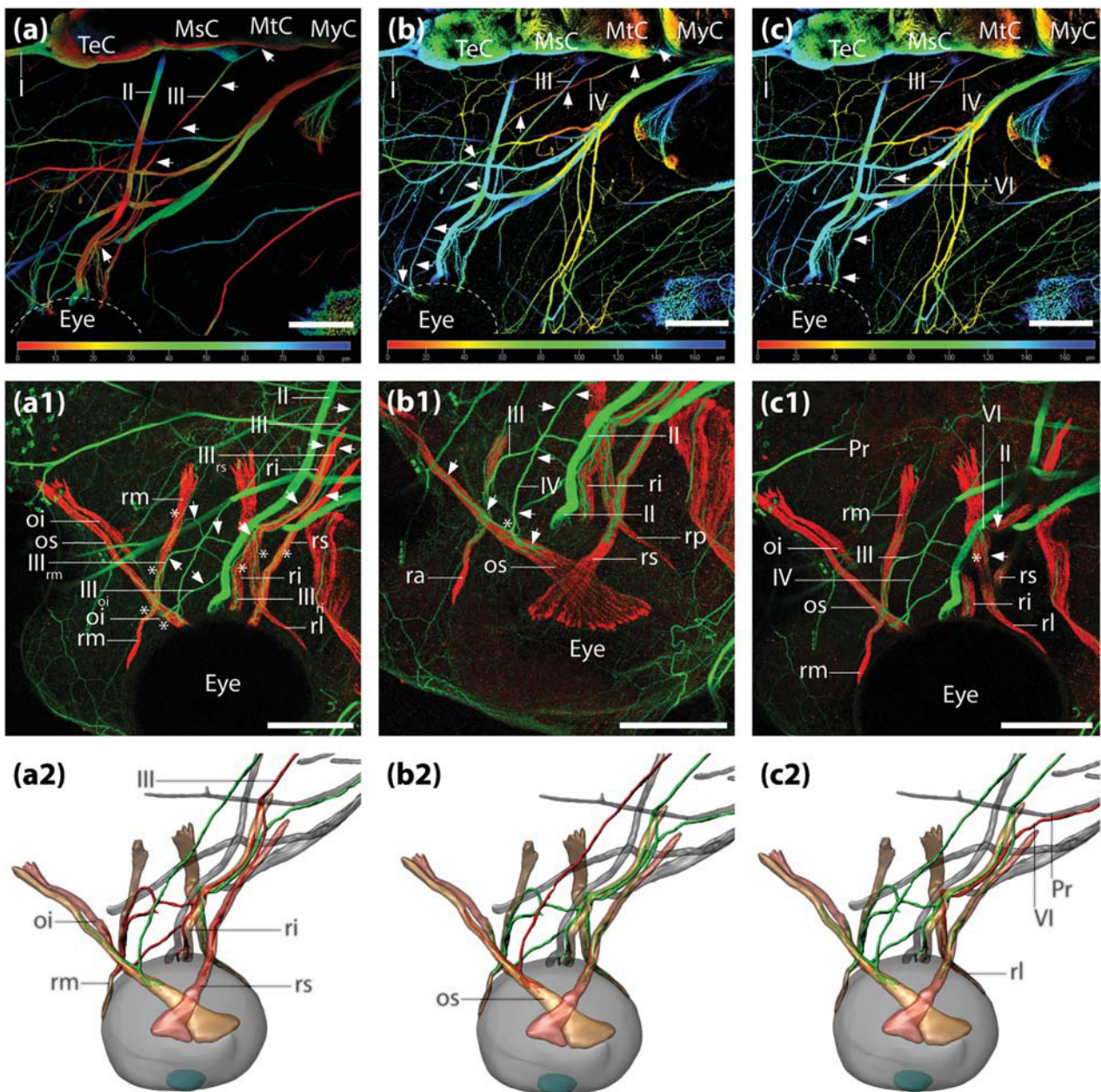


FIGURE 5 The nerves innervating the extra-ocular muscles. Whole mount antibody staining of the nerves (anti-acetylated alpha-tubulin) and muscles (anti-desmin) of a NF stage 47/48 *X. laevis* tadpole. (a and b) 3D depth coding views of the anterior head region. (a) dorsal view. The route of the oculomotor nerve (III) is indicated by the white arrows. (a1) dorsal view of the anterior head region around the eye. Nerves are shown in green and muscles are shown in red. The white arrows indicate the route of the III. The white asterisks indicate its innervation sites. (a2) 3D reconstruction of the extra-ocular muscles and nerves of the same specimen in dorsal view. The oculomotor nerve is shown in red. (b) dorsal view. The route of the trochlear nerve (IV) is indicated by the white arrows. (b1) dorsal view of the anterior head region around the eye. Nerves are shown in green and muscles are shown in red. The white arrows indicate the route of the IV. The white asterisks indicate its innervation site. (b2) 3D reconstruction of the extra-ocular muscles and nerves of the same specimen in dorsal view. The trochlear nerve is shown in red. (c) dorsal view of the border region between the metencephalon and myelencephalon. Nerves are shown in green. The white arrows indicate the routes of the abducens nerve (VI). (c1) dorsal view of the anterior head region around the eye. Nerves are shown in green and muscles are shown in red. The white arrows indicate the route of the VI. (c2) 3D reconstruction of the extra-ocular muscles and nerves of the same specimen in dorsal view. The abducens nerve is shown in red. The white scale bar is 200 μm [Color figure can be viewed at wileyonlinelibrary.com]

nerve (Figure 3a). Proximal to the facial/vestibulocochlear root the stem of the nerves fuses with the stem of the vALLN and enters the otic capsule. Immediately after entering the otic capsule, the fibers of

the facialis/vALLN split from the vestibulocochlear nerve and run in an anterior direction within the proximal part of the otic capsule (Figure 7a). After the nerve exits the otic capsule it enters the so-called

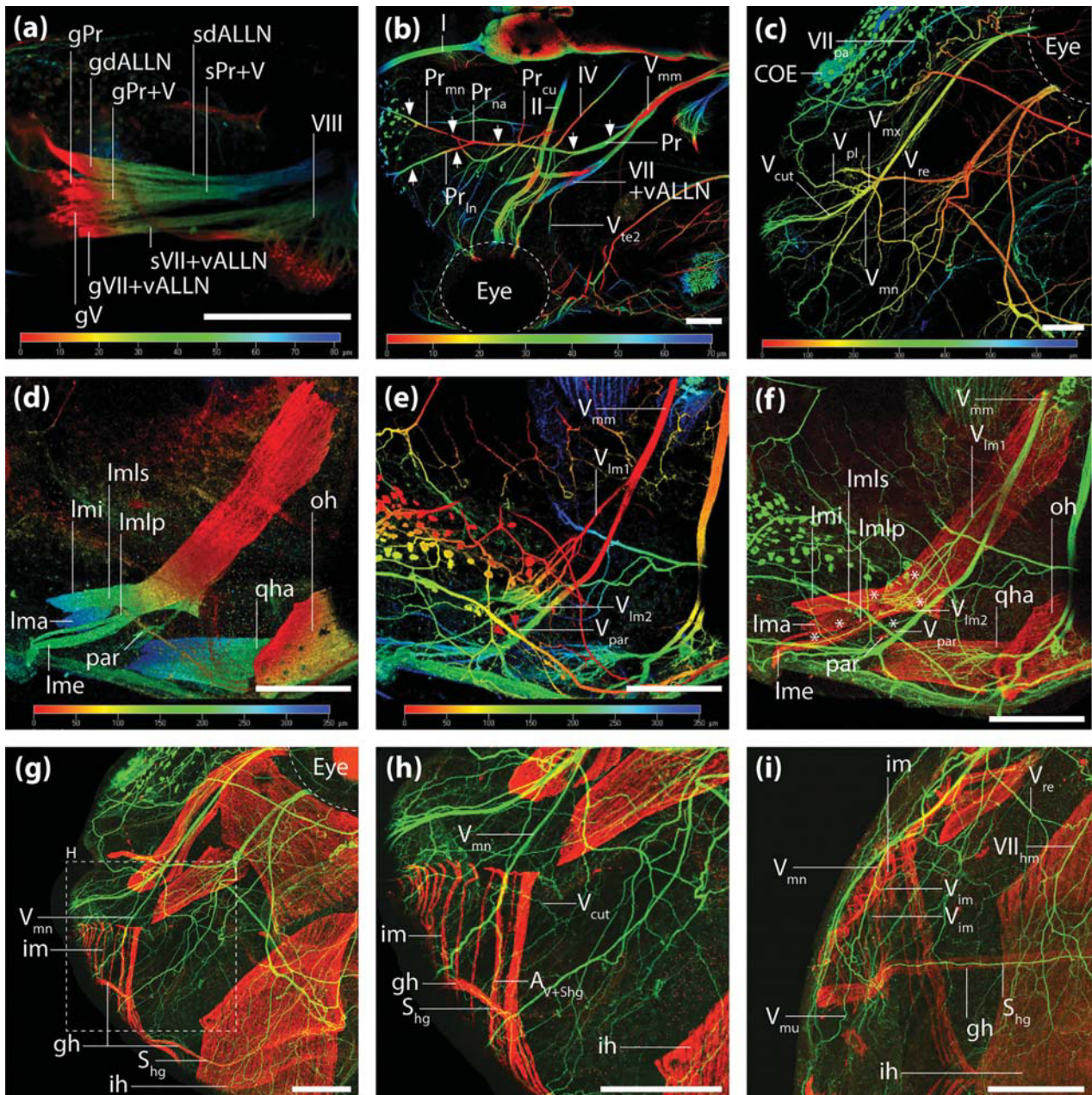


FIGURE 6 The profundal and trigeminal nerves. Whole mount antibody staining of the nerves (anti-acetylated alpha-tubulin) and muscles (anti-desmin) of a NF stage 47/48 *X. laevis* tadpole. (a-e) 3D depth coding views of the nerves. (a) lateral view of the ganglia of the anterior cranial nerves. (b) dorsal view of the anterior head region. (c) lateral view of the anterior head region between the mouth opening and the eye. (d) dorsal view of the levator mandibulae muscles. (e) dorsal view of the same area as in (d) showing the nerves innervating the levator mandibulae muscles. (f-i) nerves are shown in green, muscles are shown in red. (f) merged image from (d) and (e). The white asterisks indicate the innervation sites of the levator mandibulae muscles by ramuli of the trigeminal nerve. (g) lateral view of the ventral anterior head region. (h) magnification of the area surrounded by the strippled rectangle in (g). (i) ventral view of the anterior head region. The white scale bar is 200 μm [Color figure can be viewed at wileyonlinelibrary.com]

geniculate-lateral ganglion, a complex ganglion consisting of the fused ganglia of the facial and vALLN (Figure 7a; gVII + vALLN) and located directly ventral to the gasserian ganglion (Figure 3g). A part of this ganglion gives rise to the ramus palatinus of the facial nerve (Figure 7a). This nerve runs anteriorly along the medial surface of the palate, crossing the dALLN, the oculomotor, and optic nerve ventrally. The ramus palatinus medialis branches off from the palatine ramus and continues

anteromedially. It bifurcates into one ramulus, running in a median direction and fusing with its counterpart from the contralateral side, and another ramulus, curving anterolaterally fusing back to the main trunk of the ramus palatinus (Figure 7b). The palatine nerve continues as the ramus palatinus lateralis in the direction of the narial region (Figure 7b) innervating the mucosa of this area. The remaining part of the facialis/vALLN forms a prominent nerve trunk, leaving the geniculate-

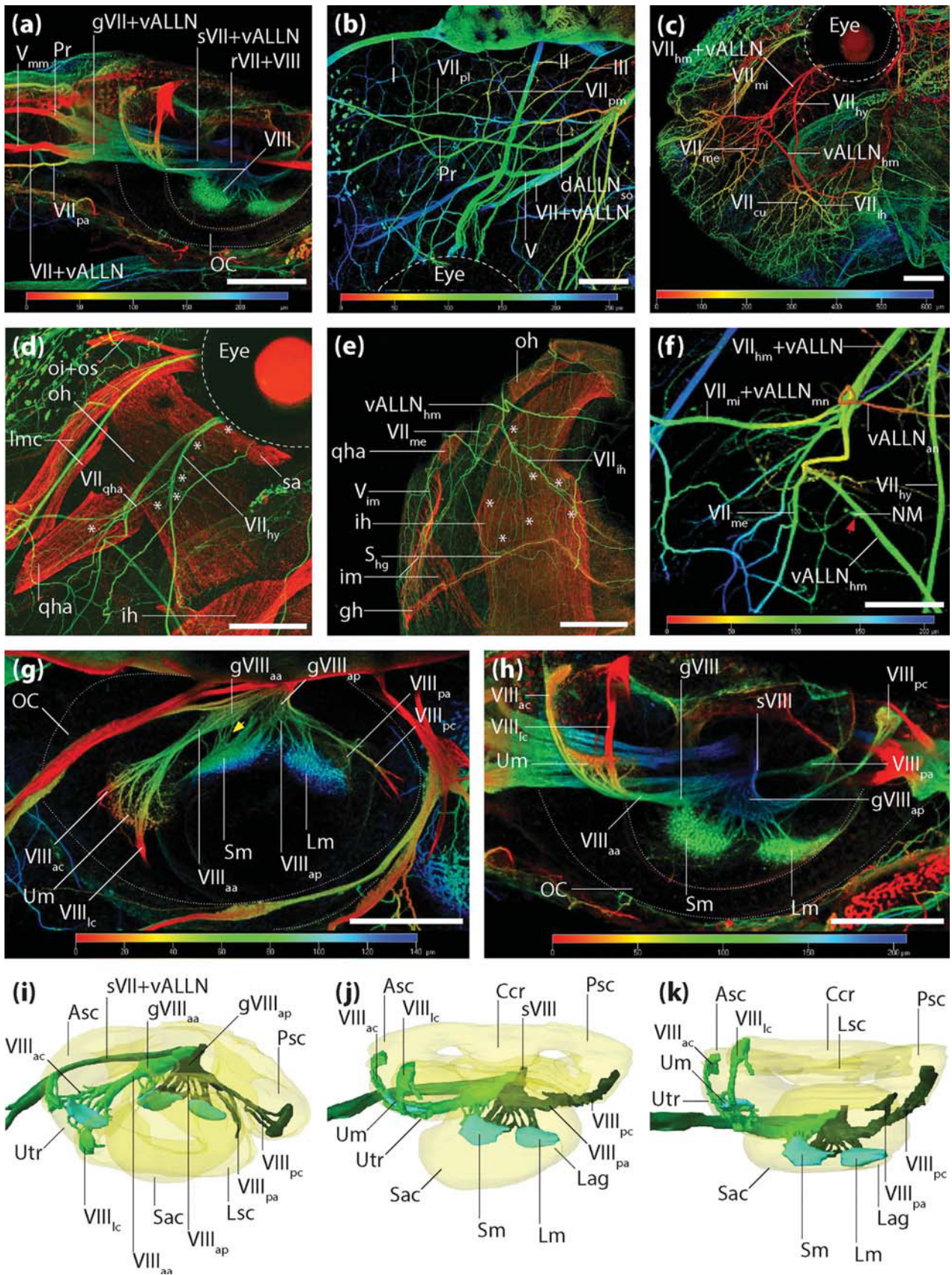


FIGURE 7.

lateral ganglion proximal to the ramus palatinus (Figure 7a). The nerve continues in a steep decline behind the eye until it reaches the ventral-most quarter of the eyeball (Figure 7c, dotted line). At the anterior margin of the eyeball the ramus hyoideus splits off from the nerve trunk, which contains fibers of the vALLN and the ramus hyomandibularis (Figure 7c). The ramus hyoideus runs ventrally, giving off a few small ramuli. The first ramulus innervates the *Musculus suspensorio-angularis* anteroventral to the eye (Figure 7d). The other small ramuli of the ramus hyoideus innervate the large orbitohyoideus muscle (Figure 7d). Further ventrally, a thin but long ramulus splits off from the ramus hyoideus, runs anteroventrally and innervates the *Musculus quadrato-hyoangularis* (Figure 7d). The major trunk of the ramus hyoideus continues ventromedially. It splits into a cutaneous ramulus, running slightly anteroventrally and a motor ramulus, the ramulus interhyoideus, running posteroventrally (Figure 7c). The ramulus interhyoideus gives off a multitude of delicate branchlets, fans out and supply different regions of the *Musculus interhyoideus*, or anastomose with ramuli of the trigeminal nerve (Figure 7e). The compound trunk of the ramus hyomandibularis and the vALLN runs anteroventrally (Figure 7c). It splits off into four main ramuli. Two of them are components of the vALLN and are described in the section on lateral line nerves. One of the remaining two ramuli is the ramulus mandibularis internus (Figure 7f). It is a compound nerve since it also carries a lateral line component, the fibers of the ramus mandibularis of the vALLN. It runs anteriorly, giving off the fibers of the ramus mandibularis of the vALLN and terminates in the mucosa of the floor of the mouth. The ramulus mandibularis externus (Figure 7c,f) runs anteroventrally, terminating in the skin of the lower jaw (Figure 7c,e). On its way it gives off a few cutaneous ramuli and some which anastomose with ramuli of the trigeminal nerve. A schematic innervation map of the facial nerve is given in Figure 10b.

The vestibulocochlear nerve (*nervus vestibulocochlearis*, VIII) of *X. laevis* can be divided into the ramus acusticus anterior and the ramus acusticus posterior. (Figure 7g). The ramus acusticus anterior is made up of two ramuli. The ramulus canalis semicircularis anterior originates from nerve fibers in the crest of the anterior semicircular canal. It runs posteromedially innervating the utricular macula and anastomoses with fibers of the ramulus canalis semicircularis lateralis (Figure 7g–k). The latter one originates from nerve fibers of the crest of the lateral semicircular canal. It runs lateromedially innervating the utricular macula and fuses with the ramulus canalis semicircularis anterior. The fused nerve trunk runs further medially entering a common ganglion (Figure

7g–k). A few small fibers emerge from this ganglion and innervate the saccular macula (Figure 7g, yellow arrow). The main ramus leaves the ganglion in a medial direction fusing with the ramus acusticus posterior. The ramus acusticus posterior originates from nerve fibers in the posterior semicircular canal (Figure 7g–k). The fibers run anteromedially where they fuse with the ramulus ampullaris posterior, coming from the ampullar region of the sacculus.

The glossopharyngeal nerve and the vagal nerves (*nervus glossopharyngeus et nervus vagus*, IX and X). The glossopharyngeal and vagal nerves originate from the posterior-most region of the rhombencephalon, posteroventrally to the root of the PLLN. At least four rootlets can be distinguished. The first is located distinctly anterior to the other three and can be assigned to the glossopharyngeus and the MLLN (Figure 8a). The remaining three rootlets fuse to form the stem of the vagal nerve (Figure 8a, Arabic numbers). The stem of the glossopharyngeus and MLLN runs posteroventrally, hidden under the stem of the PLLN, which runs in the same direction (Figure 8a). The joined roots of the vagus form a common stem, running lateroventrally and meeting the stem of the glossopharyngeus/MLLN. Before they enter a common ganglion which, together with the ganglion of the PLLN, forms the so-called post-otic ganglionic complex, the vagal nerve stem gives off the ramus auricularis (Figure 2). This nerve starts to run in a posterior direction before it splits into two main ramuli. The ramulus auricularis dorsalis describes an anterodorsally directed curve to innervate the skin of the dorsal branchial region. The ramus auricularis lateralis curves anterolaterally and innervates the skin overlaying the posterior branchial arches (Figure 8a). The glossopharyngeal nerve innervates structures assigned to the first branchial arch. After exiting the postotic ganglionic complex it curves around the otic capsule and enters its own independent ganglion (Figure 8b). From this glossopharyngeal ganglion the nerve trunk runs anteriorly and splits into two rami at the level of the anterior margin of the otic capsule. The dorsal ramus *communicans IX cum IV* runs anteriorly, almost parallel to the brain, and anastomoses with the main trunk of the *facialis/vALLN* (Figure 8a). The other one represents the main ramus of the glossopharyngeus. It runs anteroventrally, and divides into two branches. Both branches continue to run anteriorly until they reach the thymus gland. One branch runs medioventrally, innervating the visceral area of the upper jaw. It might represent the pre-trematic ramus of the glossopharyngeus and is therefore identified as the ramus pharyngeus (Figure 8a). The other ramus runs anterodistally, giving off a few small branchlets, innervating the anterior part of

FIGURE 7 The facial and vestibulocochlear nerves. (a–h) Whole mount antibody staining of the nerves (anti-acetylated alpha-tubulin) and muscles (anti-desmin) of a NF stage 47/48 *X. laevis* tadpole. (a–c) and (f–h) 3D depth coding views of the nerves. (a) lateral view of the ganglia of the cranial nerves anterior to the otic capsule. (b) dorsal view of the anterior head region. (c) lateral view of the anterior head region. (d and e) maximum intensity projections of the same digital stack. Nerves are shown in green, muscles are shown in red. (d) lateral view of the anterior head region close to the eye. The white asterisks indicate the innervation sites of the *Musculus orbitohyoideus* and the *Musculus quadrato-hyoangularis* by ramuli of the facial nerve (VII). (e) ventral view of the anterior head region. The white asterisks indicate the innervations sites of the *Musculus interhyoideus* by the ramulus interhyoideus of the VII. (f) lateral view of the anterior head region, anteroventral to the eye. (g) dorsal view of the area of the otic capsule. The yellow arrows mark anastomosing fibers between the anterior and the posterior portions of the vestibulocochlear nerve (VIII). (h) lateral view of the same area shown in (g). (i–k) 3D reconstructions of the labyrinth organ and the components of the VIII, prepared from the z-stack of the whole mount antibody staining. The anterior branch of the VIII is colored in light green and the posterior branch in dark green. The labyrinth organ is shown half-transparent and colored in yellow while the maculae are colored in turquoise. (i) dorsal view. (j) dorsolateral view. (k) lateral view. The white scale bar is 200 μm [Color figure can be viewed at wileyonlinelibrary.com]

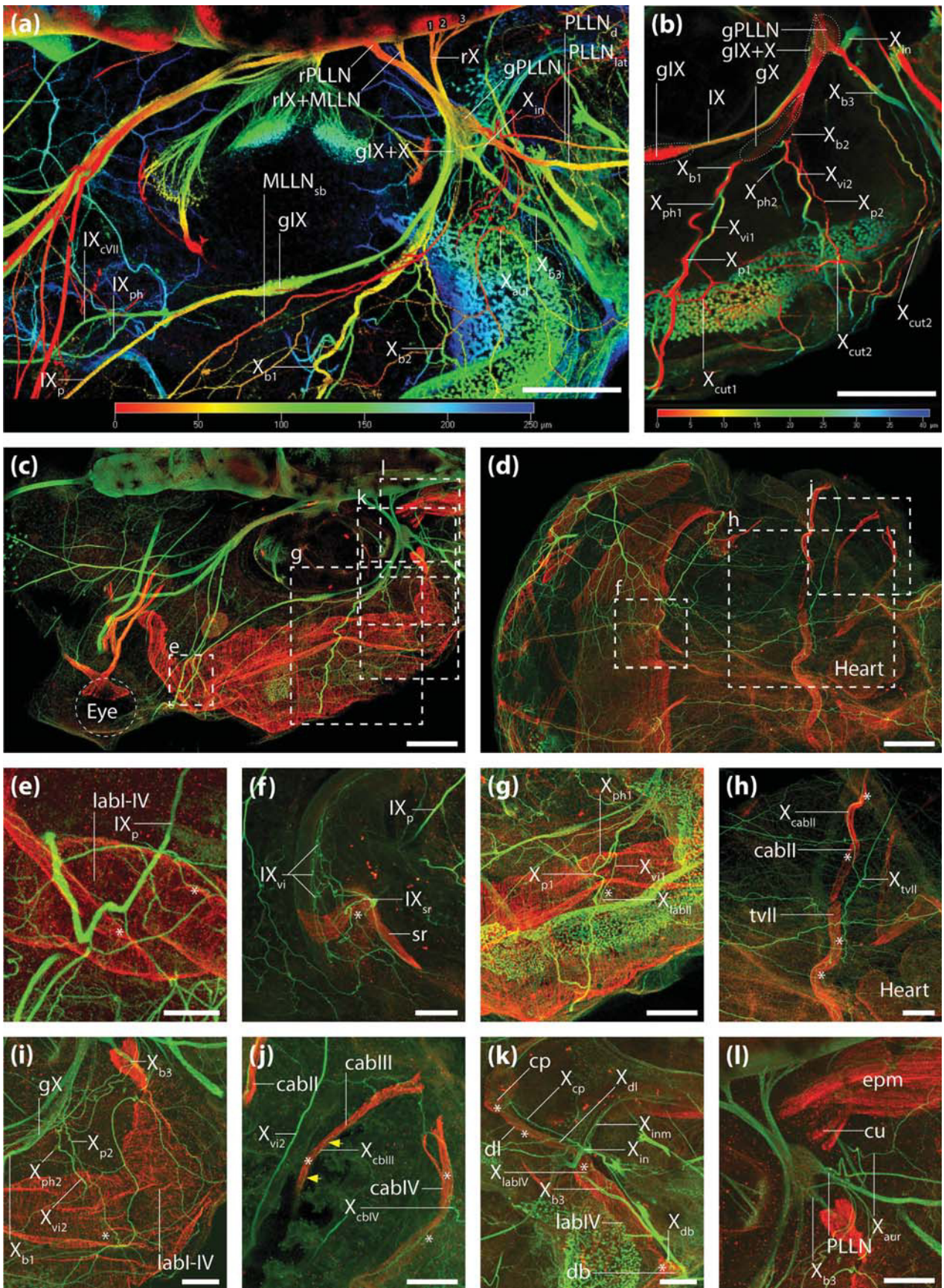


FIGURE 8.

the branchial levator muscle sheet, representing the *Musculus levator arcum branchiarium I* (Figure 8e). It therefore might represent the post-trematic ramus of the glossopharyngeus. It curves further ventromedially, following the interior gills within the first branchial arch. Reaching the ventral limit of the arch, the remainder of the post-trematic branch divides into the ramus subarcualis rectus, innervating the *Musculus subarcualis rectus* and the ramus visceralis innervating the ventral epithelium of the pharynx (Figure 8f). The ramus visceralis also anastomoses with fibers of the ramus visceralis 1 of the vagal nerve. A laryngeal branch of the glossopharyngeus, reported for tadpoles of *Discoglossus* (Schlosser & Roth, 1995), was not found in *X. laevis*. A nerve trunk originates from the glossopharyngeal/vagal component of the postotic ganglionic complex. It runs anteriorly, directly ventral to the glossopharyngeal nerve and enters a second ganglion (Figure 8b). This ganglion gives rise to the nerve components supplying structures of the second and third (Figure 2) branchial arches. The first branchial trunk of the vagal nerve leaves the ganglion at its anterior end. It immediately splits into two branches. The thinner branch immediately bifurcates again. The first, the ramus pharyngeus 1, runs ventromedially supplying the pharyngeal mucosa and anastomoses with ramuli of the glossopharyngeal nerve (Figure 8h). The second branch, the ramus visceralis 1, runs ventromedially following the interior gills, giving off a small ramulus to each gill filament. It terminates in the mucosa of the pharyngeal floor, anastomosing with ramuli of the glossopharyngeus and the second branchial trunk of the vagus. The largest post-trematic branch, the ramus branchialis 1, runs lateroventrally along the branchial levator muscle complex, giving off the ramulus levator arcum branchiarium II, innervating the levator muscle (Figure 8g). While the nerve continues to run ventrally, it gives off a ramulus innervating the *Musculus constrictor branchiarium II* before it terminates, innervating the *Musculus transversus ventralis* (Figure 8h). The second branchial trunk of the vagal nerve leaves the ganglion posterior to the first branchial trunk. The first ramus branches off from the main trunk and soon splits into the ramus pharyngeus 2 and the ramus visceralis 2 (Figures 8b and 2). Both nerves take ways similar to the ramus pharyngeus 1 and the ramus visceralis 1 described earlier. The post-trematic branch of the nerve is thinner, compared with the post-trematic branch of the first vagal trunk. It curves lateroventrally along the branchial levator complex, giving off the ramulus levator arcum branchiarium III, innervating the muscle (Figure 8i). The nerve continues its ventral course along the second branchial arch and terminates as a thin ramulus innervating the *Musculus constrictor arcum branchiarium III* (Figure 8j, yellow arrows). The pattern of third branchial trunk of the vagus differs from that of the first and second branchial trunks (Figure 2). Neither a distinct

pharyngeal/visceral nor a post-trematic ramus can be identified. The nerve originates from the glossopharyngeal/vagal part of the postotic ganglionic complex and runs posteriorly in a combined nerve trunk together with the ramus intestinalis. This common nerve trunk soon splits into its components, the ramus branchialis 3 and the ramus intestinalis (Figure 8b). The ramus branchialis 3 runs lateroventrally, giving off the ramulus levator arcum branchiarium IV that innervates the posterior-most region of branchial levator complex (Figures 8k and 2). Reaching the ventral margin of the levator muscle complex the ramus branchialis 3 turns medially, sending out a ramulus innervating the small diaphragmatico-branchialis muscle (Figure 8k) before it supplies the *Musculus constrictor arcum branchiarium IV* (Figure 8j). Immediately after the ramus branchialis 3 splits off from the ramus intestinalis, the latter one sends out a delicate ramulus accessorius, innervating the *Musculus cucullaris* (Figure 8l). The ramus intestinalis runs further ventromedially, sending out a ramulus dilatator laryngeus and a ramulus constrictor pharyngeus innervating the corresponding muscles (Figure 8k). It then gives off a small ramus, running posteromedially (ramus intestinalis medialis) and a ramus cardiopulmonaris. The ramus cardiopulmonaris runs ventrally and divides into two ramuli. One ramulus runs posteriorly, innervating the lung primordium, whereas the other one runs further ventrally supplying the Sinus venosus, Atrium, Ventriculum, and Truncus arteriosus. A schematic innervation map of the glossopharyngeal and vagal nerves is given in Figure 10c.

The anterior spinal nerves. The first spinal nerve (S1) is located slightly posteroventral to the post-otic ganglionic complex. It has only a ventral root that originates from the posterior rhombencephalon (Figures 9a and 2). It curves along the inter-myotomal septum between the small myomere one and the larger myomere two (Figure 9b). The S1 then curves ventrally, directly anterior to the pronephros (Figure 9a). Ventral to the pronephros, a delicate ramulus communicates with a ramulus of the second spinal nerve (S2) (Figure 9e; blue arrow). We could not show this exactly in our reconstruction since the 3D model was prepared from a dorso-ventral scan (compare Figures 9e and 2). In this scan, it was not possible to follow all ramuli of the spinal nerves. There may also be some fiber contribution from the third spinal nerve (S3) since S2 and S3 already anastomosed further dorsally (Figure 9b; pink arrow). From this point on we refer to the S1 as the hypoglossal nerve. The hypoglossal nerve runs further anteroventrally until it reaches the posterior edge of the ventral gill arches. It gives off a small ramulus running posteriorly to the anterior-most area of the hypaxial trunk musculature. Here it anastomoses with a ramulus from the S2 (Figure 9e; yellow arrow). Additionally, the hypoglossal nerve sends out a ramulus which further ramifies and innervates the *Musculus rectus*

FIGURE 8 The glossopharyngeal and vagal nerves. Whole mount antibody staining of the nerves (anti-acetylated alpha-tubulin) and muscles (anti-desmin) of a NF stage 47/48 *X. laevis* tadpole. (a and b) 3D depth coding views of the nerves. (a) dorsal view of the region of the otic capsule. (b) dorsal view of the distal branchial region. (c–l) maximum intensity projections of the same digital stack. Nerves are shown in green, muscles are shown in red. (c) dorsal overview of head and branchial region. (d) ventral overview of the head and branchial region. (e–l) magnifications of the areas marked by the striped rectangles in (c) and (d). The white asterisks indicate the innervation sites of the branchial muscles by rami/ramuli of the glossopharyngeal (IX) and vagal nerves (X). The yellow arrows indicate the route of the ramulus constrictor arcus branchiarium III of the X. (l) dorsal view of the cucullaris muscle. The white scale bar in (c) and (d) is 200 μm , in (e) to (l) 50 μm [Color figure can be viewed at wileyonlinelibrary.com]

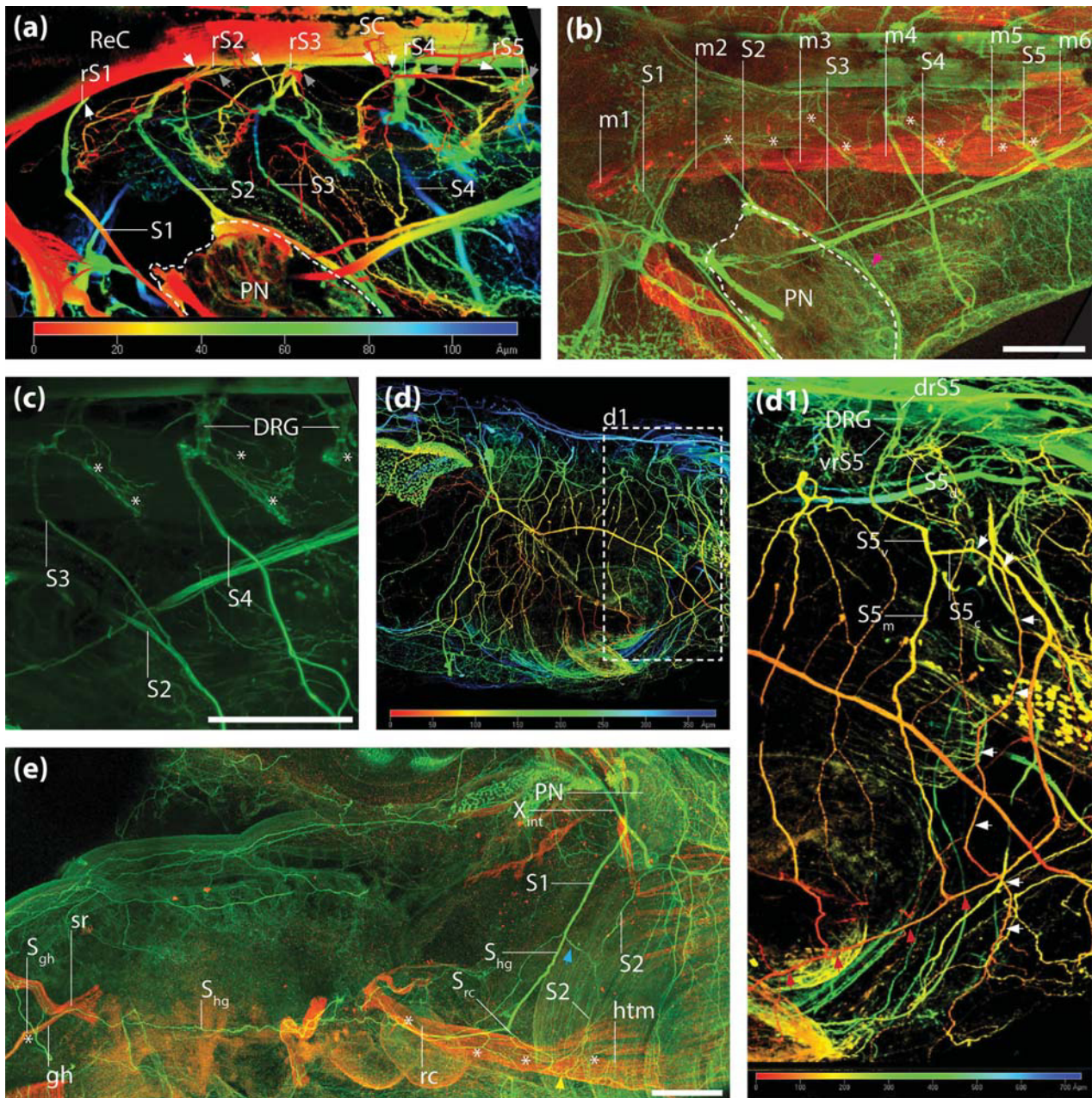


FIGURE 9 The anterior spinal nerves. Whole mount antibody staining of the nerves (anti-acetylated alpha-tubulin) and muscles (anti-desmin) of a NF stage 47/48 *X. laevis* tadpole. (a) 3D depth coding view of the nerves. Dorsal view of the posterior head region. The white arrows indicate the ventral spinal roots while gray arrows indicate the dorsal spinal roots. The spinal nerve 1 has no dorsal root. (b) maximum intensity projections of the same digital stack. Dorsal view of the posterior head region. Nerves are shown in green, muscles are shown in red. The white asterisks mark the fibers of the spinal nerves innervating the myotomes of the epaxial trunk musculature. Spinal nerve 1 does not innervate any myotome. The pink arrow indicates the point where the second and third spinal nerves fuse. (c) dorsal close-up of the roots of the third to fifth spinal nerves. The white asterisks mark the fibers of the spinal nerves innervating the myotomes of the epaxial trunk musculature. (d) 3D depth coding view of the nerves. Lateral overview of the trunk region. d1, magnification of the area surrounded by the strippled rectangle in (d). The white arrows indicate the route of the cutaneous ramus of the fifth spinal nerve. (e) maximum intensity projections of the same digital stack. lateral view of the ventral head region. Nerves are shown in green, muscles are shown in red. The blue arrow indicates the fibers of spinal nerve 2 (and maybe 3) joining spinal nerve 1 and becoming the hypoglossal nerve. The yellow arrow indicates the anastomosis between fibers of the hypoglossal nerve and spinal nerve 2. The white asterisks indicate the innervation sites of the hypoglossal muscles by the hypoglossal nerve. The white scale bar is 200 μm [Color figure can be viewed at wileyonlinelibrary.com]

cervicis (Figure 9e). The main trunk of the nerves continues running anteriorly, supplying the Musculus geniohyoideus (Figure 9e). The dorsal and the ventral root of the S2 exit the spinal cord (Figure 9a). No

dorsal root ganglion is present in the S2. After the ventral and the dorsal root have merged, a small dorsal ramus leaves the nerve, running dorsally to innervate myomere two as well as the skin (Figure 9b). The

ventral ramus of the S2 runs ventrally, along the posterior border of the pronephric glomeruli (Figure 9b). A small ramulus coming from the S3 joins the ventral ramus of the S2. The ventral rami of the S2 and S3 run ventrally very close to each other and then fuse. Ventral to the pronephros, they separate and the ventral ramus of the S2 sends a ramulus to the first spinal nerve (Figure 9e; blue arrow). The main trunk of the ventral ramus continues running ventrally and innervates the hypaxial trunk musculature (Figure 9e). The S3 also originates from a dorsal and a ventral root. Like in the S2 before, no dorsal root ganglion was detected (Figure 9A). The dorsal ramus of the S3 innervates myotome three as well as the skin above it (Figure 9b). Altogether, only a few small ramuli of the dorsal rami of the S2 and S3 seem to end in the epidermis. The major sensory innervation in that region is supplied by the ramus auricularis dorsalis of the vagal nerve. The ventral ramus of the S3 is very thin, running lateroventrally and joining the ventral ramus of the S2 at the level of the posterior edge of the pronephric glomeruli (Figure 9b). After they have anastomosed, the S3 continues to run ventrally, innervating the hypaxial trunk musculature. The fourth (S4) and fifth (S5) spinal nerves are the first spinal nerves that show the “normal,” metameric, pattern of the trunk spinal nerves. After the dorsal root of the S4 exits the spinal cord, it enters the dorsal root ganglion (Figure 9a,c). The S4 gives off a dorsal ramus innervating myotome four and the skin, and a ventral ramus. The ventral ramus runs anteroventrally and splits into three rami. The anterior-most ramus runs in the direction of the Anlage of the limb bud, anastomosing with S3. The posterior-most ramus curves ventrally and innervates the skin (Figure 2), while the middle ramus runs ventrally, innervating the hypaxial trunk musculature. The S5 is patterned like all the following lumbal spinal nerves, without anastomosing ramuli to the hypoglossal or brachial plexus. The dorsal root enters a dorsal root ganglion before it fuses with the ventral root (Figure 9a,c). It then gives off the dorsal ramus, supplying myotome five and the skin (Figure 9B), as well as a ventral ramus (Figure 9d,d1). The ventral ramus divides further into a ramulus muscularis and a ramulus cutaneus. Both ramuli run side-by-side in a ventral direction (Figure 9d1). The ramulus muscularis innervates the hypaxial trunk musculature while the ramulus cutaneus innervates the overlying lateroventral skin area. The ventral rami of the hypoglossal nerve and the posterior spinal nerves are all connected via a profound anastomosis (Figure 9d1; red arrows). A schematic innervation map of the five anterior-most spinal nerves is given in Figure 10d.

4 | DISCUSSION

4.1 | The cranial muscles

The development and anatomy of the cranial muscles of *X. laevis* have been described in detail by Ziermann and Olsson (2007) and Schmidt et al. (2011). Using fluorescent antibody staining in combination with confocal laser scanning microscopy, we detected an additional muscle in the anterior head region, the Musculus processo-articularis. This small muscle has previously only been found in tadpoles of *Discoglossus pictus* (Schlosser & Roth, 1995). Similar to *D. pictus*, the processo-articularis muscle of *X. laevis* was only found within a short

developmental period (NF stage 46–48). Its function remains unclear because of its peculiar position and attachment at the palatoquadrate. Due to its short appearance and its curious attachment it could be a vestige with no anatomical function. Another muscle, first described for *X. laevis* by Ziermann and Olsson (2007), is the Musculus transversus anterior. These authors were not able to trace the innervation of this muscle using traditional techniques such as histology and preparation. We could detect this muscle (but not its innervation) using whole mount antibody staining. Information about its innervation pattern are needed since the homology of this muscle to muscles in other anuran species is not clear (Ziermann & Olsson, 2007). Using whole mount antibody staining and a PTA stained μ CT scan we describe another branchial muscle, the Musculus diaphragmatico-branchialis, in *X. laevis*. The diaphragmatico-branchialis muscle is innervated by a ramulus of the ramus branchialis 3 of the vagal nerve. It is therefore regarded as a branchial muscle derived from the head mesoderm. In *X. laevis* it is positioned posterior to the vagal and hypoglossal nerves. This border, delineated by the routes of these two nerves, is the head/trunk interface (Kuratani, 1997). It marks the zone, in which the head and trunk myogenic programs overlap (Ericsson, Knight, & Johanson, 2013). Another muscle described for *X. laevis* tadpoles by Ziermann and Diogo (2014) is the Musculus cucullaris (also named Musculus protractor pectoralis or Musculus trapezius). It is found in specimens at NF stage 45 where it already shows muscle fiber formation. In the specimens we investigated (NF stage 46–48), we were also able to detect this muscle using fluorescent whole mount antibody staining. It originates from the posterior edge of the otic capsule via a fascia and runs posteroventrally, in the direction of the future limb bud. Its posterior end is still loose, which might be due to the late development of its future insertion site on the scapular cartilage. It is innervated by a small ramulus, branching off from the ramus intestinalis of the vagal nerve. Like the diaphragmatico-branchialis, the cucullaris muscle develops posterior to the head/trunk interface marked by the vagal and hypoglossal nerves. Information about the developmental pattern of these two muscles would be of great value, as it is known that the myogenic program of the trunk inhibits muscle fiber differentiation in myoblasts derived from the head (Tzahor et al., 2003). This could enable the muscles to grow and insert on skeletal structures that form late in development, such as the scapular cartilage (Theis et al., 2010). Further studies on the differentiation pattern of the diaphragmatico-branchialis and cucullaris muscles will clarify if their differentiation pattern is prolonged compared to other head muscles.

The lateral lines and the lateral line nerves. Most neuromasts of *X. laevis* tadpoles are organized in distinct rows, the so-called lateral lines. In *X. laevis* tadpoles at NF stage 46 to 48 we confirmed the pattern of lateral lines reported previously (Shelton, 1970). We found four additional neuromasts, grouped in a row slightly ventral to the infra-orbital lateral line. This grouping of neuromasts cannot be seen in the μ CT scan, but is clearly visible in whole mount antibody stainings. Due to its position and innervation by a ramus of the vALLN, we propose this line to be homologous to the angular lateral line of *Discoglossus pictus* tadpoles, described by Schlosser and Roth (1995). Since a similar line has been described in an earlier study (Quinzio & Fabrezi, 2014), we

pre-otic and jugular ganglionic complexes. As described for *D. pictus* (Schlosser & Roth, 1995), we could confirm the existence of a group of neuromasts, situated directly anterodorsal to the otic capsule. In tadpoles of *X. laevis*, this group was recognized as a distinct lateral line and named the anterior auditory lateral line by Shelton (1970). While in *D. pictus*, this group of neuromasts is innervated by a ramulus of the ramus buccalis of the dALLN (Schlosser & Roth, 1995), no precise information about its innervation is available for *X. laevis*. Shelton (1970) depicted some ramuli, emerging from the main trunk of the dALLN and running posterodorsal to the anterior auditory lateral line. We reinvestigated the innervation of this lateral line and found a small ramulus of the ramus buccalis, running anterodorsally and supplying the neuromasts of this line, similar to the pattern observed in *D. pictus*. Paterson (1939) reported a nerve branch that separates from the ramus mandibularis of the trigeminal nerve and runs posteroventrally to innervate the neuromasts of the aortic lateral line. In the area of the aortic lateral line, we observed a high density of nerve fibers. The main part of these fibers belongs to the first temporal ramulus of the ramus maxillomandibularis of the trigeminal nerve. Despite the large extent to which the skin of this region is innervated by the ramulus temporalis 1, no neuromast is supplied by this nerve. Due to the high resolution of the digital z-stacks of fluorescent whole mount antibody stainings, we could identify this lateral line component of the trigeminal nerve, reported by Paterson (1939), as the MLLN of *X. laevis*. It is closely associated with the glossopharyngeal nerve and innervates the neuromasts of the aortic and posterior-auditory lateral lines. The MLLN was classified as a distinct lateral line nerve by Northcutt (1989) and Song and Northcutt (1991), retaining a separate ganglion while fusing or anastomosing with the glossopharyngeal nerve (Song and Northcutt, 1991; see Schlosser and Roth, 1995 for more references). In amphibians, no distinct ganglion of the MLLN is present in larval or adult animals, although it is clearly separate at embryonic stages (Schlosser & Ahrens, 2004; Schlosser & Northcutt, 2000; Schlosser & Roth, 1995). We confirm this by observing no separate ganglion of the MLLN in *X. laevis* tadpoles. But since the MLLN is situated close to the glossopharyngeal/vagal ganglion and the separate glossopharyngeal ganglion, it seems likely that its ganglion fuses with one of these two ganglia during late embryonic development. Data on the developmental anatomy of the cranial nerves in late embryonic/early larval stages are needed to obtain information about the developmental fate of the MLLN ganglion. The innervation of the aortic lateral line in *X. laevis* by the MLLN supports the suggestion in Schlosser and Roth (1995), that the suprabranchial lateral line of *D. pictus* is homologous to the aortic lateral line of *X. laevis*. The innervation pattern of the posterior lateral lines by the PLLN is similar to the pattern described for *D. pictus* (Schlosser & Roth, 1995). It supplies the occipital (auricular in *D. pictus*), upper and middle (dorsal and lateral in *D. pictus*) and the anterior and posterior lower (ventral in *D. pictus*) lateral lines. In contrast to further studies of *Xenopus* (Paterson, 1939) or *Discoglossus* (Schlosser & Roth, 1995), we found a separate root by which the PLLN leaves the rhombencephalon (see Figure 3a).

The profundal and trigeminal nerves. The branching pattern of the profundal and trigeminal nerves of *X. laevis* is very similar to the pattern described for *D. pictus* (Schlosser & Roth, 1995) and *Rana* (Strong,

1895). The ganglion of the profundal nerve is closely associated with the ganglion of the trigeminal nerve, forming the gasserian ganglion (Gegenbaur, 1889). Both originate from different placodes that fuse later in development (Schlosser & Ahrens, 2004; Schlosser & Northcutt, 2000). The profundal nerve shows the same ramification pattern as described for *Discoglossus pictus* (Schlosser & Roth, 1995). Schlosser and Roth (1995) described a few temporal ramuli, originating from the ramus maxillomandibularis and innervating the skin in *D. pictus*. In *Xenopus*, the number of these ramuli is much lower. We found only two ramuli, the ramulus temporalis 1 and the ramulus temporalis 2, which correspond to the mandibular ramulus 1 and 2 in Paterson's description (1939). The division of the ramus maxillomandibularis of *X. laevis* into the ramus maxillaris and mandibularis appears further "downstream" compared to *D. pictus*. The ramus maxillaris of *X. laevis* therefore is a rather short nerve compared to the maxillaris of other amphibians. It must have been this special feature, which led Paterson (1939) to the statement, that no ramus maxillaris is present in *X. laevis* (Paterson, 1939, p. 203). Later in the same study (page 208), he assigned one remaining ramus of the ramus mandibularis to be homologous to the ramus maxillaris of other amphibians. Furthermore, Paterson compared the origin and branching pattern to those in different urodele amphibians (*Siren*: Norris 1913; *Proteus*: Benedetti 1933; *Salamandra*: Francis, 1934). He argued that the branching pattern of the ramus maxillaris of *X. laevis* is more similar to the pattern found in urodeles than in other anurans. By using whole mount antibody staining, we found a pattern of the ramus maxillaris in *X. laevis* more similar to the pattern described for *D. pictus* (Schlosser & Roth, 1995). We also confirmed the absence of an anastomosis between the ramus maxillaris and the ramus palatinus of the facial nerve as reported by Paterson (1939). In *D. pictus*, the ramus mandibularis divides from the ramus maxillaris after giving off a motor ramus, supplying the levator mandibulae anterior, levator mandibulae posterior profundus and levator mandibulae posterior superficialis. After it has split from the common maxillomandibular trunk, it sends a ramulus to each of the levator mandibulae externus, levator mandibulae anterior articularis, processo-articularis, and levator mandibulae externus, before terminating in the intermandibularis (Figure 11). This innervation sequence resembles the one we found in *X. laevis*. The first muscles, innervated by the ramulus levator mandibulae 1 are the levator mandibulae longus profundus, levator mandibulae internus, and the levator mandibulae longus superficialis. Despite the different names, it seems that these muscles are homologous (Schlosser and Roth for *D. pictus* and Ziermann and Olsson for *X. laevis*). The following mandibular muscles of *D. pictus* are innervated by a single ramulus originating from the ramus mandibularis. For the levator mandibulae externus, Schlosser and Roth (1995) reported two innervating ramuli (Figure 11). In *X. laevis*, the levator mandibulae externus and levator mandibulae articularis are innervated by the ramulus levator mandibulae 2, which bifurcates to supply both muscles. We did not find a second innervating ramulus of the levator mandibulae externus in *X. laevis*, as described in *D. pictus* by Schlosser and Roth (1995). The next muscle innervated in both species is the small and transient processo-articularis. In *X. laevis*, the ventral mandibular musculature only consists of an intermandibularis muscle, while three muscles can be distinguished in *D. pictus* (*Musculus*

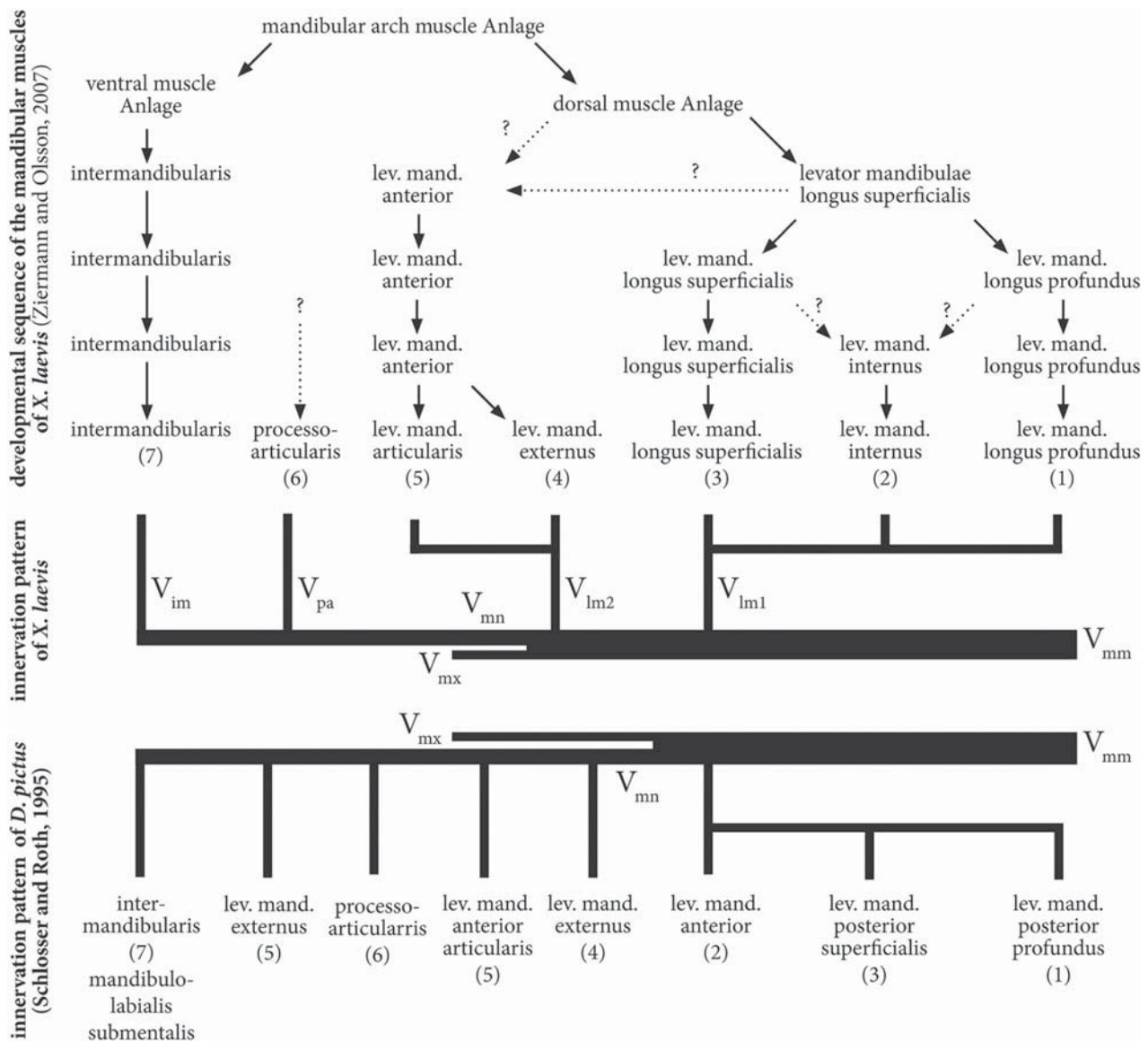


FIGURE 11 Scheme of the developmental sequence of the mandibular muscles of *Xenopus laevis* and their innervation pattern compared to the innervation pattern described for *Discoglossus pictus*. Black arrows indicate the sequence of differentiation. Dotted arrows with an interrogation mark indicate an unsure or unknown origin of the muscle. Numbers in brackets indicate muscles which might be homologous in both species. The names of the predicted homologous muscle are different since Schlosser and Roth (1995) used the terminology of Edgeworth (1935) while Ziermann and Olsson (2007) used their own terminology

intermandibularis, M. mandibulo-labialis, M. submentalis; Schlosser and Roth 1995). It is therefore not surprising, that the motor fibers of the ramus mandibularis terminate in the single intermandibularis muscle in *X. laevis*, while they branch an additional time in *D. pictus* to innervate the three ventral muscles (branching scheme simplified for *D. pictus* in Figure 11). Since the gross anatomy of the ramus mandibularis follows a phylogenetically highly conserved pattern (Schlosser & Roth, 1995; Song & Boord, 1993) it might be possible that some variation occurs in the fine ramuli, supplying different subdivisions of a muscle, for example, the adductor mandibulae of Tetraodontiformes (Nakae & Sasaki, 2004) or the levator mandibulae of anuran tadpoles (Haas, 2001; Schlosser & Roth, 1995). Nakae and Sasaki (2004), in their study on

tetraodontiformes, state that the innervation patterns are not “stand-alone” criteria for inferences of homology. They propose to combine innervation data with topological information to establish more stable hypotheses of homology. Nonetheless, regarding the very large morphological differences between the jaw apparatus of the filter-feeding *Xenopus* and the grazing *Discoglossus* tadpoles, and the accompanying changes to the mandibular musculature, innervation seems to be relatively stable even at the level of the fine ramuli. Another possible explanation, in addition to the different tadpole anatomies, might be a methodological artifact. The innervation patterns may be similar but appear different because single neurons cannot be traced within a nerve bundle by the technique we used. For example, the ramulus levator mandibulae 2 could

also be present in *D. pictus*. It might branch off from the ramus mandibularis but the motor axons, innervating the levator mandibulae anterior articularis, stay so close to the mandibular nerve trunk until they reach their muscle, that they appear to be a single ramulus.

The facial nerve. The general innervation pattern is similar (but not identical, see below) to the pattern described by Paterson (1939) and confirms the pattern described for other anuran tadpoles (Schlosser & Roth, 1995; Strong, 1895). We found separate motor ramules, innervating the suspensorio-angularis, the orbitochoydeus and the quadrato-hyoangularis muscles (see Figure 7d). These larval muscles are the precursors of the mandibular depressor muscle in adult frogs (Schlosser & Roth, 1995). A similar pattern has been observed in *Discoglossus pictus* (Schlosser & Roth, 1995) but not in *Rana* (Strong, 1895), where all these larval muscles are innervated by a single nerve branch. *Xenopus* (Pipidae) and *Discoglossus* (Discoglossidae) are thought to represent relatively basal taxa, while *Rana* (Ranidae) is grouped with more derived taxa into the Neobatrachia (Frost et al., 2006; Pyron & Wiens, 2011). It is possible that the pattern of facial motor innervation found in *Xenopus* and *Discoglossus* is the plesiomorphic condition, while *Rana* (and maybe all other neobatrachians) represent a more derived innervation pattern. Traditionally, the facial nerve was thought to not contain any general cutaneous fibers. Therefore it was assumed, that all general cutaneous fibers of the facial nerve originated from the trigeminal and glossopharyngeal nerves entering the facialis via anastomoses (Schlosser & Roth, 1995). While these two anastomoses were reported for many different amphibian taxa (Schlosser & Roth, 1995; Strong, 1895), the presence of an anastomosis between the trigeminal and facial nerve was rejected for *X. laevis* (Paterson, 1939). Paterson (1939) stated that the ramus hyomandibularis of the facial nerve receives all its general cutaneous fibers from the ramus communicans IX cum VII of the glossopharyngeal nerve. Taking advantage of the high resolution of fluorescent whole mount antibody stainings, we found delicate ramuli of the ramus cutaneus recurrens of the trigeminal nerve anastomosing with the ramus mandibularis externus of the hyomandibular nerve (see Figure 7c). Assuming that this anastomosis delivers some general cutaneous fibers from the trigeminus to the ventral part of the hyomandibular ramus of the facial nerve, it is possible to apply the general, dual anastomosis-pattern of other anurans to *X. laevis*.

The glossopharyngeal and vagal nerves. The ganglia of the glossopharyngeus and vagus nerves are often regarded as having fused into a common ganglion (Paterson, 1939; Schlosser & Roth, 1995). In *X. laevis* tadpoles at NF stages 46–48 the distinct stem of the glossopharyngeus is still recognizable throughout the ganglion. The pattern of the glossopharyngeal nerve corresponds to the pattern reported for many other vertebrates (Coghill, 1902; Gegenbaur, 1889; Kuratani, 1990; Norris & Hughes, 1918; Northcutt & Bemis, 1993; Schlosser & Roth, 1995). However, there are some differences regarding Paterson's (1939) interpretation of the routes of the glossopharyngeal nerve. While her description of the ramus communicans IX cum VIII and the ramus pharyngeus (pre-trematic branch) fits well with our observations, there are some differences regarding the post-trematic ramus. She reported an anteroventral route of this ramus, ventral to the ramus buccalis of the ALLN (truncus infra-orbitalis in Paterson, 1939) and with a constrictor

branchialis muscle (levator arcus branchiarium in our nomenclature) between them. Additionally, Paterson reported an innervation of the muscoli constrictor branchialis I and II and the muscoli subarcualis recti I and II (Paterson, 1939, p. 219). An innervation of the dorsal musculature of the second branchial arch seems unlikely, because we found no motor ramuli supplying this region but some very thin cutaneous branches, which could be interpreted as motor ramuli innervating the levator arcus branchiarium II (constrictor branchialis II in Paterson's description). A delicate visceral ramulus originates from the post-trematic ramus of the glossopharyngeus. It innervates the ventral mucosa of the pharynx and anastomoses with the ramus pharyngeus of the glossopharyngeus as well as the ramus visceralis 1 of the vagal nerve. The main trunk of the glossopharyngeus supplies a single subarcualis rectus muscle, and not two, as stated by Paterson (1939). Despite the extensive amount of plexus formation in the ventral pharyngeal region, no dorsal anastomosis between the facial, glossopharyngeal, and vagal nerves was observed in our whole mount immunostainings. It therefore confirms the absence of a Jacobson's anastomosis in *X. laevis* reported by Paterson (1939). The first and the second branchial trunks of the vagal nerve consist of three major rami: A post-trematic branch (supplying motor innervation to the associated muscles as well as sensory innervation to the skin), a pharyngeal ramus and a visceral ramus. This corresponds to the pattern observed in *D. pictus* (Schlosser & Roth, 1995) and *Rana* (Strong, 1895). As mentioned in Schlosser and Roth (1995) all these rami are post-trematic in the sense that they always take their course posterior to the corresponding gill cleft. Since pre-trematic vagal rami exist in most other vertebrates, it has been suggested that the profundal branchial rami in *D. pictus* (visceral rami in *X. laevis*) might be homologous to this pre-trematic branches observed in other vertebrates (Schlosser & Roth, 1995). If this is correct, our data on the absence of pre-trematic rami in *X. laevis* add further evidence that the absence of vagal pre-trematic rami in anurans is due to a positional shift of the very early outgrowing axons in relation to the corresponding gill cleft. Since no transient pre-trematic branches have been found in the development of the vagal nerve in *D. pictus* (Schlosser & Roth, 1995), it would be interesting to investigate the development of the vagal nerve in *X. laevis* to clarify if the positional shift of the prospected pre-trematic branches is a common feature within the Anura.

The anterior spinal nerves. As has been reported for tadpoles of *Discoglossus pictus* (Schlosser & Roth, 1995) and *Rana* (Gaupp, 1896/1899), a distinct first spinal nerve is present in tadpoles of *X. laevis*. This is in contrast to adults of most frog species, which lack a distinct first spinal nerve (Fürbringer, 1874; Oka, Takeuchi, Satou, & Ueda, 1987; Schlosser & Roth, 1995, 1997). The peripheral part of the first spinal nerves has only been described in tadpoles of *D. pictus* (Schlosser & Roth, 1995). As a foundation for a broader comprehensive dataset, we describe the peripheral course of the anterior-most spinal nerves in the tadpole of *X. laevis*. Like in *D. pictus*, we found that the first two, maybe even three, spinal nerves contribute fibers to the formation of the hypoglossal nerve. A contribution of the first two spinal nerves to the hypoglossal nerve has been reported for many urodeles (Coghill, 1902; Norris, 1913; Wake, Roth, & Wake, 1983) and caecilians (Wake, 1992, 1993). This fits with the report of two motor nuclei within the spinal cord. An anterior motor

nucleus, assigned to spinal nerve 1 supplying the geniohyoid muscle and a posterior motor nucleus, assigned to the second spinal nerve supplying the sternohyoid muscle, which is derived from the larval rectus cervicis muscle in larval anurans (Oka et al., 1987; Schlosser & Roth, 1995). Therefore, it seems that if the third spinal nerve contributes to the formation of the hypoglossal nerve it might only be through the contribution of a few sensory fibers. The overall pattern of the anterior spinal nerves found in tadpoles of *X. laevis* is similar to that reported for *D. pictus* (Schlosser & Roth, 1995). Dorsal root ganglia are first present in spinal nerve four and more posterior spinal nerves.

ACKNOWLEDGMENTS

We are thankful to Paul Lukas for giving access to additional serial sections of *Xenopus laevis* tadpoles. We also thank Gerhard Schlosser and two anonymous reviewers for critical reading of an earlier form of the manuscript. This project was funded by the Deutsche Forschungsgemeinschaft (Grant Number: DFG-OL 134/10-2 to LO).

AUTHOR CONTRIBUTION

All authors had full access to all the data in the study and take responsibility for the integrity of the data and the accuracy of the data analysis. Study concept and design: BN. Acquisition of data: BN. Analysis and interpretation of data: BN. Drafting of the manuscript: BN and LO.

ORCID

Benjamin Naumann  <http://orcid.org/0000-0003-0970-2431>

REFERENCES

- Allis, E. P. (1897). The cranial muscles and cranial and first spinal nerves in *Amia calva*. *Journal of Morphology*, 12, 487–769.
- Altman, J. S., & Dawes, E. A. (1983). A cobalt study of medullary sensory projections from lateral line nerves, associated cutaneous nerves, and the VIIIth nerve in adult *Xenopus*. *The Journal of Comparative Neurology*, 213(3), 310–326. <https://doi.org/10.1002/cne.902130307>
- Benedetti, E. (1933). *Il cervello ei nervi cranici del Proteus anguineus Laur.* Stabilimento tipografico nazionale.
- Böck, P. (1989). *Romeis mikroskopische Technik*. München, Germany: Urban & Schwarzenberg.
- Cannatella, D. C., & De Sa, R. O. (1993). *Xenopus laevis* as a model organism. *Systematic Biology*, 42(4), 476–507.
- Cervino, A., Paz, D., & Frontera, J. (2017). Neuronal degeneration and regeneration induced by axotomy in the olfactory epithelium of *Xenopus laevis*. *Developmental Neurobiology*, 77(11), 1308–1320.
- Cline, H. T., & Kelly, D. (2012). *Xenopus* as an experimental system for developmental neuroscience: Introduction to a special issue. *Developmental Neurobiology*, 72(4), 463–464.
- Coghill, G. E. (1902). The cranial nerves of *Amblystoma tigrinum*. *Journal of Comparative Neurology*, 12, 207–289.
- Dong, W., Lee, R. H., Xu, H., Yang, S., Pratt, K. G., Cao, V., ... Aizenman, C. D. (2009). Visual avoidance in *Xenopus* tadpoles is correlated with the maturation of visual responses in the optic tectum. *Journal of Neurophysiology*, 101(2), 803–815.
- Edgeworth, F. H. (1935). *The cranial muscles of the vertebrates*. Cambridge: Cambridge University Press.
- Edwards-Faret, G., Muñoz, R., Méndez-Olivos, E. E., Lee-Liu, D., Tapia, V. S., & Larrain, J. (2017). Spinal cord regeneration in *Xenopus laevis*. *Nature Protocols*, 12(2), 372–389.
- Ericsson, R., Knight, R., & Johanson, Z. (2013). Evolution and development of the vertebrate neck. *Journal of Anatomy*, 222(1), 67–78. <https://doi.org/10.1111/j.1469-7580.2012.01530.x>
- Francis, E. T. B. (1934). *The anatomy of the salamander* (Vol. 2). At the Clarendon Press.
- Frankenhaeuser, B., & Huxley, A. (1964). The action potential in the myelinated nerve fibre of *Xenopus laevis* as computed on the basis of voltage clamp data. *The Journal of Physiology*, 171(2), 302–315.
- Frost, D. R., Grant, T., Faivovich, J., Bain, R. H., Haas, A., Haddad, C. F. B., ... Wheeler, W. C. (2006). The amphibian tree of life. *Bulletin of the American Museum of Natural History*, 297, 8–370. [https://doi.org/10.1206/0003-0090\(2006\)297\[0001:Tatol\]2.0.Co;2](https://doi.org/10.1206/0003-0090(2006)297[0001:Tatol]2.0.Co;2)
- Fürbringer, M. (1874). Zur vergleichenden Anatomie der Schultermuskeln. II Theil. *Jenaische Zeitschrift für Naturwissenschaften*, 8, 175–280.
- Gaupp, G. (1896/1899). *Anatomie des Frosches*. 1. Abteilung: Lehre vom Skelet und vom Muskelsystem. (3rd ed.). 2. Abteilung: Lehre vom Nerven- und Gefäßsystem. (2nd ed.). Braunschweig: Vieweg.
- Gegenbaur, C. (1889). *Vergleichende Anatomie der Wirbelthiere: mit Berücksichtigung der Wirbellosen*. Leipzig, Germany: W. Engelmann.
- Gouchie, G., Roberts, L., & Wassersug, R. (2008). The effect of mirrors on African clawed frog (*Xenopus laevis*) larval growth, development, and behavior. *Behavioral Ecology and Sociobiology*, 62(11), 1821–1829.
- Haas, A. (2001). Mandibular arch musculature of anuran tadpoles, with comments on homologies of amphibian jaw muscles. *Journal of Morphology*, 247(1), 1–33. [https://doi.org/10.1002/1097-4687\(200101\)247:1<1::AID-JMOR1000>3.0.CO;2-3](https://doi.org/10.1002/1097-4687(200101)247:1<1::AID-JMOR1000>3.0.CO;2-3)
- Harland, R. M., & Grainger, R. M. (2011). *Xenopus* research: Metamorphosed by genetics and genomics. *Trends in Genetics : TIG*, 27(12), 507–515.
- Katz, L. C., Potel, M. J., & Wassersug, R. J. (1981). Structure and mechanisms of schooling intadpoles of the clawed frog, *Xenopus laevis*. *Animal Behaviour*, 29(1), 20–33.
- Klymkowsky, M. W., & Hanken, J. (1991). Whole-mount staining of *Xenopus* and other vertebrates. *Methods in Cell Biology*, 36, 419–441.
- Kuratani, S. (1990). Development of glossopharyngeal nerve branches in the early chick embryo with special reference to morphology of the Jacobson's anastomosis. *Anatomy and Embryology*, 181(3), 253–269.
- Kuratani, S. (1997). Spatial distribution of postotic crest cells defines the head/trunk interface of the vertebrate body: Embryological interpretation of peripheral nerve morphology and evolution of the vertebrate head. *Anatomy and Embryology*, 195(1), 1–13.
- Lee-Liu, D., Méndez-Olivos, E. E., Muñoz, R., & Larrain, J. (2016). The African clawed frog *Xenopus laevis*: A model organism to study regeneration of the central nervous system. *Neuroscience Letters*, 652, 82–93.
- McKeown, C. R., Sharma, P., Sharipov, H. E., Shen, W., & Cline, H. T. (2013). Neurogenesis is required for behavioral recovery after injury in the visual system of *Xenopus laevis*. *Journal of Comparative Neurology*, 521(10), 2262–2278.
- Metscher, B. D. (2009). MicroCT for comparative morphology: Simple staining methods allow high-contrast 3D imaging of diverse non-mineralized animal tissues. *BMC Physiology*, 9, 11. <https://doi.org/10.1186/1472-6793-9-11>
- Moreno, M., Tapia, K., & Larrain, J. (2014). Neural regeneration in *Xenopus* tadpoles during metamorphosis. In M. Kloc & J. Z. Kubiak (Eds.), *Xenopus development* (pp. 293–308). Oxford: John Wiley & Sons.
- Nakae, M., & Sasaki, K. (2004). Homologies of the adductor mandibular muscles in Tetraodontiformes as indicated by nerve branching patterns. *Ichthyological Research*, 51(4), 327–336. <https://doi.org/10.1007/s10228-004-0238-2>

- Nieuwkoop, P. D., & Faber, J. (1994). *Normal table of Xenopus laevis (Daudin). A systematical and chronological survey of the development from the fertilized egg till the end of metamorphosis* (2nd ed.): New York, NY: Garland publishing.
- Norris, H. W. (1913). The cranial nerves of *Siren lacertina*. *Journal of Morphology*, 24, 245–316.
- Norris, H. W., & Hughes, S. P. (1918). The cranial and anterior spinal nerves of caecilian amphibians. *Journal of Morphology*, 31(3), 489–560.
- Northcutt, R. G. (1993). A reassessment of Goodrich's model of cranial nerve phylogeny. *Acta Anatomica*, 148(2–3), 71–80.
- Northcutt, R. G. (1989). The phylogenetic distribution and innervation of craniate mechanoreceptive lateral lines. In S. Coombs, P. Görner, & H. Münz (Eds.), *Neurobiology and Evolution of the Lateral Line System* (pp. 17–78). New York: Springer.
- Northcutt, R. G., & Bemis, W. E. (1993). Cranial nerves of the coelacanth, *Latimeria chalumnae* [Osteichthyes: Sarcopterygii: Actinistia], and comparisons with other craniata. *Brain, Behavior and Evolution*, 42(Suppl 1), 1–76.
- Oka, Y., Takeuchi, H., Satou, M., & Ueda, K. (1987). Cobaltic lysine study of the morphology and distribution of the cranial nerve efferent neurons (motoneurons and preganglionic parasympathetic neurons) and rostral spinal motoneurons in the Japanese toad. *The Journal of Comparative Neurology*, 259(3), 400–423. <https://doi.org/10.1002/cne.902590308>
- Paterson, N. F. (1939). The head of *Xenopus laevis*. *Journal of Cell Science*, s2–81(322), 161–232.
- Pieper, M., Eagleson, G. W., Wosniok, W., & Schlosser, G. (2011). Origin and segregation of cranial placodes in *Xenopus laevis*. *Developmental Biology*, 360(2), 257–275. <https://doi.org/10.1016/j.ydbio.2011.09.024>
- Porro, L. B., & Richards, C. T. (2017). Digital dissection of the model organism *Xenopus laevis* using contrast-enhanced computed tomography. *Journal of Anatomy*, 231, 169–191.
- Pratt, K. G., & Khakhalin, A. S. (2013). Modeling human neurodevelopmental disorders in the *Xenopus tadpole*: From mechanisms to therapeutic targets. *Disease Models & Mechanisms*, 6(5), 1057–1065.
- Pyron, R. A., & Wiens, J. J. (2011). A large-scale phylogeny of Amphibia including over 2800 species, and a revised classification of extant frogs, salamanders, and caecilians. *Molecular Phylogenetics and Evolution*, 61(2), 543–583. <https://doi.org/10.1016/j.ympev.2011.06.012>
- Quinzio, S., & Fabrezi, M. (2014). The lateral line system in anuran tadpoles: Neuromast morphology, arrangement, and innervation. *The Anatomical Record*, 297(8), 1508–1522. <https://doi.org/10.1002/ar.22952>
- Roberts, A., Walford, A., Soffe, S., & Yoshida, M. (1999). Motoneurons of the axial swimming muscles in hatching *Xenopus tadpoles*: Features, distribution, and central synapses. *The Journal of Comparative Neurology*, 411(3), 472–486.
- Schlosser, G., & Ahrens, K. (2004). Molecular anatomy of placode development in *Xenopus laevis*. *Developmental Biology*, 271(2), 439–466. <https://doi.org/10.1016/j.ydbio.2004.04.013>
- Schlosser, G., & Northcutt, R. G. (2000). Development of neurogenic placodes in *Xenopus laevis*. *The Journal of Comparative Neurology*, 418(2), 121–146.
- Schlosser, G., & Roth, G. (1995). Distribution of cranial and rostral spinal nerves in tadpoles of the frog *Discoglossus pictus* (Discoglossidae). *Journal of Morphology*, 226(2), 189–212. <https://doi.org/10.1002/jmor.1052260207>
- Schlosser, G., & Roth, G. (1997). Evolution of nerve development in frogs. II. Modified development of the peripheral nervous system in the direct-developing frog *Eleutherodactylus coqui* (Leptodactylidae). *Brain, Behavior and Evolution*, 50(2), 94–128.
- Schmidt, J., Schuff, M., & Olsson, L. (2011). A role for FoxN3 in the development of cranial cartilages and muscles in *Xenopus laevis* (Amphibia: Anura: Pipidae) with special emphasis on the novel rostral cartilages. *J Anat*, 218(2), 226–242. <https://doi.org/10.1111/j.1469-7580.2010.01315.x>
- Shelton, P. M. (1970). The lateral line system at metamorphosis in *Xenopus laevis* (Daudin). *Journal of Embryology and Experimental Morphology*, 24(3), 511–524.
- Simmons, A. M., Costa, L. M., & Gerstein, H. B. (2004). Lateral line-mediated rheotactic behavior in tadpoles of the African clawed frog (*Xenopus laevis*). *Journal of Comparative Physiology A*, 190(9), 747–758.
- Song, J., & Boord, R. L. (1993). Motor components of the trigeminal nerve and organization of the mandibular arch muscles in vertebrates. Phylogenetically conservative patterns and their ontogenetic basis. *Cells Tissues Organs*, 148(2–3), 139–149.
- Song, J. K., & Northcutt, R. G. (1991). The primary projections of the lateral-line nerves of the Florida gar, *Lepisosteus platyrhincus*. *Brain, Behavior and Evolution*, 37(1), 38–63.
- Strong, O. S. (1895). The cranial nerves of Amphibia. *Journal of Morphology*, 10, 101–230.
- Theis, S., Patel, K., Valasek, P., Otto, A., Pu, Q., Harel, I., ... Huang, R. (2010). The occipital lateral plate mesoderm is a novel source for vertebrate neck musculature. *Development*, 137(17), 2961–2971. <https://doi.org/10.1242/dev.049726>
- Tzahor, E., Kempf, H., Mootoosamy, R. C., Poon, A. C., Abzhanov, A., Tabin, C. J., ... Lassar, A. B. (2003). Antagonists of Wnt and BMP signaling promote the formation of vertebrate head muscle. *Genes & Development*, 17(24), 3087–3099. <https://doi.org/10.1101/gad.1154103>
- Wake, D. B., Roth, G., & Wake, M. H. (1983). Tongue evolution in lungless salamanders, family plethodontidae. III. Patterns of peripheral innervation. *Journal of Morphology*, 178(3), 207–224. <https://doi.org/10.1002/jmor.1051780302>
- Wake, M. H. (1992). Patterns of peripheral innervation of the tongue and hyobranchial apparatus in caecilians (Amphibia: Gymnophiona). *Journal of Morphology*, 212(1), 37–53. <https://doi.org/10.1002/jmor.1052120105>
- Wake, M. H. (1993). Evolutionary diversification of cranial and spinal nerves and their targets in the gymnophione amphibians. *Cells Tissues Organs*, 148(2–3), 160–168.
- Wassersug, R., & Hessler, C. M. (1971). Tadpole behaviour: Aggregation in larval *Xenopus laevis*. *Animal Behaviour*, 19(2), 386–389.
- Young, S. H., & Poo, M.-M. (1983). Rapid lateral diffusion of extrajunctional acetylcholine receptors in the developing muscle membrane of *Xenopus tadpole*. *Journal of Neuroscience*, 3(1), 225–231.
- Ziermann, J. M., & Diogo, R. (2014). Cranial muscle development in frogs with different developmental modes: Direct development versus biphasic development. *Journal of Morphology*, 275(4), 398–413.
- Ziermann, J. M., & Olsson, L. (2007). Patterns of spatial and temporal cranial muscle development in the African clawed frog, *Xenopus laevis* (Anura: Pipidae). *Journal of Morphology*, 268(9), 791–804. <https://doi.org/10.1002/jmor.10552>

SUPPORTING INFORMATION

Additional Supporting Information may be found online in the supporting information tab for this article.

How to cite this article: Naumann B, Olsson L. Three-dimensional reconstruction of the cranial and anterior spinal nerves in early tadpoles of *Xenopus laevis* (Pipidae, Anura). *J Comp Neurol*. 2017;00:1–22. <https://doi.org/10.1002/cne.24370>

Chapter 2 (Supplementary) – The developmental pattern of the cucullaris and diaphragmatico-branchialis muscles in *X. laevis*

The development of the cranial muscles of *X. laevis* has been described in detail in an earlier study (Ziermann and Olsson, 2007). However, the development of the cucullaris and diaphragmatico-branchialis muscles has not been described so far.

The anlage of the cucullaris muscle is first detectable at late NF stage 44/ early 45 (Ziermann & Olsson stage 18). At this stage it consists of a few muscle fibers, originating from a tendon from the otic capsule. It is closely associated with the dilatator larynges muscle (Fig. S1A, A'). The anlage of the cucullaris muscle is extending in a posteroventral direction in the direction of the fore limb field. The investigation stopped at NF stage 47/48 (older than Ziermann & Olsson stage 20). At this stage the posterior end of the cucullaris is not attached due to the late development of the pectoral girdle in anuran larvae (Fig. S1B).

At early NF stage 45 (Ziermann & Olsson stage 18) a small cell population is visible at the posterior end of the developing branchial basket (Fig. S1C). It consists of a few myocytes closely associated with the levator arcus branchialium complex (Fig. S1C'). We interpret this cell population as the anlage of the diaphragmatico-branchialis muscle according to its position and the position of the muscle at later developmental stages. At NF stage 46 (Ziermann & Olsson stage 20) the muscle anlage has separated from the levator arcus branchialium complex and extends in a postero-ventral direction (Fig. S1D and D'). First muscle fibers are recognizable. It is not in contact with the hypaxonic trunk muscles. NF stage 47/48 the muscle has increased in size. It has extended in a postero-ventral direction and is in contact with the hypaxonic trunk muscles. A strong desmin signal is recognizable (Fig. S1E).

The cucullaris muscle of *X. laevis* develops late in comparison to other branchial and trunk muscles (Table S1). The only other branchial muscle that develops that late is the transversus anterior, first described by Ziermann and Olsson (2007). Unfortunately, neither its developmental origin nor its innervation is known.

In summary it can be stated, that the cucullaris muscle of *X. laevis* shows a developmental pattern similar to that in other vertebrates (Naumann et al., 2017a; Theis, 2010; Theis et al., 2010; Ziermann and Diogo, 2013; Ziermann et al., 2017). The diaphragmatico-branchialis muscle of *X. laevis* also develops late albeit not as late as the cucullaris. The late development of these two muscles might be connected to the delayed development of pectoral and fore limb structures in anuran tadpoles. It has been shown by Tzahor and colleagues, that signals from the dorsal ectoderm and neural tube inhibit head muscle development (Tzahor et al., 2003). A larger distance from the inhibitors secreted by the dorsal ectoderm and neural tube might play a role in the earlier differentiation of myofibers in the diaphragmatico-branchialis compared to the cucullaris. We therefore speculate, that the mechanism underlying the development of the cucullaris and diaphragmatico-branchialis muscle of *X. laevis* is similar to the mechanism in other vertebrate taxa (Chapter 1).

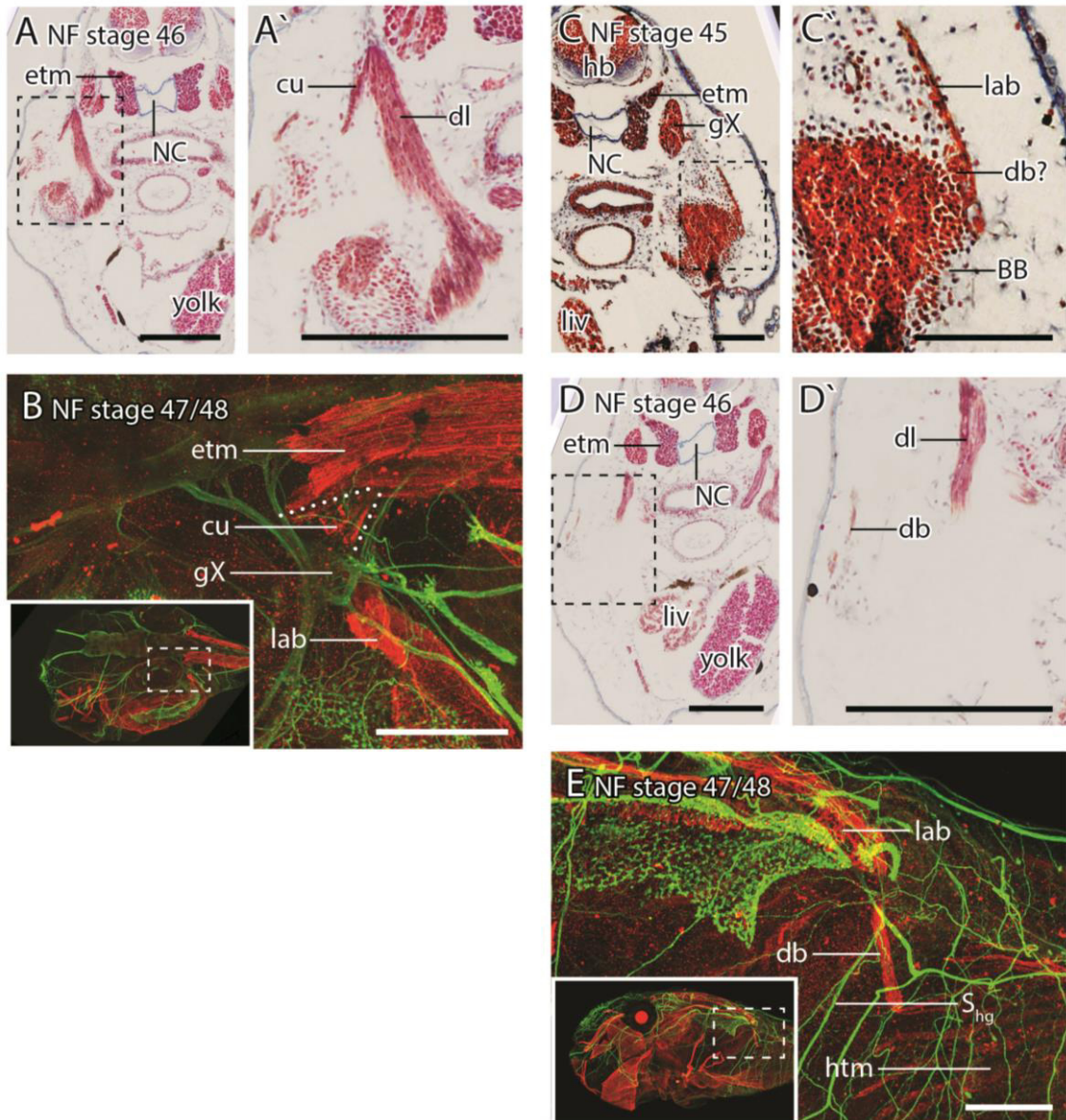


Figure S1: A, cross section through an *X. laevis* larva at stage NF 46. The dashed rectangle indicates the region in A'. A', the cucullaris originates from a tendon at the otic capsule close to the dilatator laryngis. B, whole mount antibody staining of a *X. laevis* larva at stage NF 47/48 in a dorsal view. Muscles are stained with an antibody against desmin (red) and nerves with an antibody against acetylated alpha-tubulin (green). The rectangle in the lower left image shows the region of the cucullaris muscle. C, cross section through an *X. laevis* larva at stage NF 45. The dashed rectangle indicates the region in C'. C', the cell population proximal to the levator arcus branchialium is interpreted as the anlage of the diaphragmatico-branchialis muscle (db?). D, cross section through an *X. laevis* larva at stage NF 46. The dashed rectangle indicates the region in D'. D', the diaphragmatico-branchialis muscle extends in an postero-ventral direction. E, whole mount antibody staining of a *X. laevis* larva at stage NF 47/48 in a dorsal view. Muscles are stained with an antibody against desmin (red) and nerves with an antibody against acetylated alpha-tubulin (green). The rectangle in the lower left image shows the region of the diaphragmatico-branchialis muscle. BB, branchial basket; cu, cucullaris; db, diaphragmatico-branchialis; dl, dilatator laryngis; etm, epaxial trunk muscles; gX, ganglion of the vagal nerve; hb, hind brain; htm, hypaxial trunk muscles; lab, levator arcum branchialium-complex; liv, liver diverticulum; NC, notochord; S_{hg}, spinal hypoglossal nerve. The scale bar in A, A', B, D, D' is 200 μ m. The scale bar in C, C' is 100 μ m.

NF	35/36-37/38	37/38	39	39-40	40	40-41	40-41	41	41-42	42	43	43-44	44	44-45	45	45-46	47/48	reference	
ZO	5	6	7	8	9	10	11	12	13	14	15	16	17	18	19	20	/	ZO (2007)	
VA 3																		levator arcus branchialium I	ZO (2007)
VA 3																		subarcualis rectus I	ZO (2007)
VA 3																		transversus anterior	ZO (2007)
VA 4																		levator arcus branchialium II	ZO (2007)
VA 4																		constrictor branchialis II	ZO (2007)
VA 4																		transversus ventralis II	ZO (2007)
VA 5																		levator arcus branchialium III	ZO (2007)
VA 5																		constrictor branchialis III	ZO (2007)
VA 6																		levator arcus branchialium IV	ZO (2007)
VA 6																		constrictor branchialis IV	ZO (2007)
?																		constrictor laryngis	ZO (2007)
?																		dilatator laryngis	ZO (2007)
?														n.a.	n.a.	n.a.		cucullaris	N
?														n.a.	n.a.			diaphragmatico-branchialis	N
somitic																		rectus cervicis	ZO (2007)
somitic																		geniohyoideus	ZO (2007)
somitic																		epaxonic trunk muscles	N
somitic																		hypaxonic trunk muscles	N

Table S1: Timing of the branchial muscle development in *X. laevis*. Embryos are stages according to, Nieuwkoop & Faber, 1994 (NF) or Ziermann & Olsson, 2007 (ZO). Light grey, myoblasts; grey, myocytes; dark grey, myofibers. References: ZO (2007), Ziermann and Olsson, 2007; N, own observations in this chapter. n.a., not attached to the insertion site; VA4-6, visceral arch 4 to 6; ?, developmental origin not known.

Chapter 3

Naumann, B., Schmidt, J. & Olsson, L. ***FoxN3* is involved in the development of the interatrial septum and the muscles in the head/trunk interface in the African clawed frog, *Xenopus laevis* (Pipidae: Anura: Lissamphibia). *Submitted.***

***FoxN3* is involved in the development of the interatrial septum and the muscles in the head/trunk interface in the African clawed frog, *Xenopus laevis* (Lissamphibia: Anura: Pipidae).**

Benjamin Naumann*, Jennifer Schmidt, Lennart Olsson

Institut für Zoologie und Evolutionsforschung, Friedrich-Schiller-Universität, 07743
Jena, Germany

*author for correspondence: benjamin.naumann@uni-jena.de

Abstract

The *fork-head box* (*Fox*) genes are a large family of transcription factors sharing a common DNA binding domain, the fork head box, and play diverse roles in the immune system, metabolism, cancer, cell cycle and animal development. Recently, *FoxN3* has been shown to be indispensable for normal craniofacial development in other vertebrates such as the mouse and the African clawed frog. The knockdown of *FoxN3* in *X. laevis* delays overall development of early tadpole stages, causes eye defects, the absence of some cranial nerve branches and malformations of the cranial skeleton and genuine head muscles while the hypoglossal and other trunk muscles are unaffected. We report malformations of muscles developing in the head/trunk interface of *X. laevis*, the cucullaris and diaphragmatico-branchialis muscle. This gives the first evidence for a dependence on the head myogenic program of the cucullaris muscle in an anuran species. Furthermore we describe defects in the heart such as the absence of the interatrial septum and weak trabeculation. This is in compliance with the recent emergence of the concept of the cardiopharyngeal field and further supports the developmental and evolutionary link of the vertebrate heart and the head.

Keywords: *FoxN3*, interatrial septum, cardiogenesis, cucullaris, *Xenopus laevis*

Introduction

The *fork-head box* (*Fox*) genes are a large family of transcription factors sharing a common DNA binding domain, the fork head box, and play diverse roles in the immune system, metabolism, cancer, cell cycle and animal development (Carlsson and Mahlapuu, 2002; Samaan et al., 2010). Deletions in the human *FoxN3* gene at the chromosomal locus 14(q24.3q32.1) for example, are linked to various congenital craniofacial defects (Byth et al., 1995; Karnitis et al., 1992; Schlade-Bartusiak et al., 2008; Yamamoto et al., 1986). More recently, *FoxN3* has been shown to be indispensable for normal craniofacial development in other vertebrates such as the mouse (*Mus musculus*) and the African clawed frog, *Xenopus laevis* (Samaan et al., 2010; Schmidt et al., 2011; Schuff et al., 2007). Morpholino-mediated knockdown of *FoxN3* in *X. laevis* delays overall development of early tadpole stages and causes eye defects and absence of some cranial nerve branches (Schuff et al., 2007). Additionally, these so-called morphants (Egger, 2000) exhibit severe malformations of the neural crest-derived cartilaginous head skeleton (Schmidt et al., 2011; Schuff et al., 2007) as well as the associated jaw and branchial musculature (Schmidt et al., 2011). Head muscle development depends on neural crest cells (NCCs), forming a scaffold of connective tissue patterning these muscles (Ericsson et al., 2004; Tokita and Schneider, 2009). This led to the interpretation that the head muscle defects in *X. laevis FoxN3* morphants are mainly due to patterning effects originating from the *FoxN3*-depleted NCCs or increased apoptosis of NCCs (Schmidt et al., 2013). This hypothesis is supported by the fact that the epaxial and hypaxial trunk muscles, not patterned by the neural crest (NC), develop normally in *FoxN3* morphants (Schuff et al., 2007). However, the role of *FoxN3* in the development of the muscles between the head and the trunk has not been investigated so far. The origin of the musculature developing in this head/trunk interface (Kuratani, 1997) has long been of special interest to

developmental morphologists (Edgeworth, 1935). For the ventral (hypobranchial) muscles, it is known that they are innervated by spinal nerves, originate from the somites in the trunk, migrate into the head and are patterned by NC-derived connective tissue (Edgeworth, 1935; Ericsson et al., 2013; Gegenbaur, 1889). The dorsal musculature, mainly represented by the cucullaris/trapezius muscle, in contrast has been at the center of much debate. While innervated by the vagus or accessory nerve, either an origin from the unsegmented head mesoderm (Edgeworth, 1935; Ericsson et al., 2013; Matsuoka et al., 2005; Naumann et al., 2017; Rylkoff, 1924; Sefton et al., 2016; Theis et al., 2010; Ziermann and Diogo, 2013) or the somites in the trunk (Huang et al., 2000; Noden, 1983a; Piekarski and Olsson, 2007) has been proposed in a variety of vertebrate taxa. We investigated the development of the cucullaris and the diaphragmatico-branchialis muscle in *FoxN3* morphant *X. laevis*. The diaphragmatico-branchialis has been described recently in *X. laevis* as a muscle similar to the cucullaris by spanning the head/trunk interface and being innervated by the vagal nerve (Naumann and Olsson, 2017). Additional to these features, malformations of the cucullaris and diaphragmatico-branchialis in *FoxN3* morphants would indicate their cranial origin. Additionally to the cucullaris, diaphragmatico-branchialis and the epaxial trunk musculature another muscle develops at the head/trunk interface. This muscle is the heart.

Recently, the heart has been linked to the cranial muscles, including the cucullaris/trapezius muscle, by originating from a common mesodermal precursor cell population called the cardiopharyngeal field (Diogo et al., 2015; Lescroart et al., 2015). In contrast to head muscle development, cranial NCCs might not contribute directly to the heart tissue in *X. laevis* (Lee and Saint-Jeannet, 2011). However, a study in chicken has shown that signals from cranial NCCs are needed for the early normal development of parts of the cardiopharyngeal field. Cells from a sub-population of the

cardiopharyngeal field, the second heart field, fail to migrate and populate the developing heart tube. This causes disturbed loop-formation and weakened myocardia of the outflow tract and ventricle (Waldo et al., 2005).

We investigated the heart morphology and development in *FoxN3* morphants of *X. laevis* to evaluate whether an increased rate of apoptosis in the mesoderm cells of the cardiopharyngeal field or decreased signaling of the cranial NCCs can explain the observed head muscle malformations as well as the effects on heart development.

Materials and Methods

Specimens

Thirty-seven histological sections of *Xenopus laevis* embryos and larvae prepared in a previous study (Schmidt et al. 2011) were re-investigated. For fluorescent whole-mount antibody stainings of *FoxN3*-MO injected specimens and controls, embryos were obtained from the breeding colony at the Institut für Zoologie und Evolutionsforschung (Jena, Germany) by temperature-induced spawning from adult *X. laevis*. All embryos and larvae were staged according to the normal table of development (Nieuwkoop and Faber, 1994).

Morpholino injections

Fertilized eggs were rinsed in 0.1 x MBSH for three times. The eggs were then de-jellied in 2 % cysteine-hypochloride (pH 7.5) for 4 minutes and then rinsed with 0.1 x MBSH for three times again. To assure comparability and because of the previous specificity tests we injected the same *FoxN3* Morpholino used in the previous studies (sequence: 5'-ACTAGGAGGGCATGACTAGGACCCAT-3'; Schmidt et al. 2011, Schuff et al. 2007). Morpholino injections were performed in 4 % Ficoll/0.1 x MBSH. The Morpholino was diluted in 0,1 % saccharose solution and injected in doses of

around 15-17 ng into one or both cells of *X. laevis* embryo at the two-cell stage. For control, a standard control Morpholino against human beta-globulin mRNA (sequence: 5'-CCTCTTACCTCAGTTACAATTTATA-3'; Gene Tools) was injected under identical conditions.

Histology

Specimens were fixed in 4% para-formaldehyde (PFA) for at least 24 hours, embedded in paraffin and sectioned into 7 µm transverse sections using a HM360 Microm (Germany). The sections were stained using the standard Heidenhein-Azan technique (Böck, 1989). Single sections were digitalized with an Olympus BX51 microscope using the dotslide software 2.3 (Olympus Corporation, Tokyo, Japan). Images were converted to greyscale for a better visualization and brightness and contrast were adjusted using ImageJ.

Fluorescent whole mount antibody staining

Specimens were fixed in Dent's fixative (4 parts 100 % methanol, 1 part dimethyl sulfoxide) for a minimum of one day and bleached in Dent's bleach (10% hydrogen peroxide in Dent's fixative) for 4 hours under a normal desk lamp. All incubations were carried out at room temperature (21 to 25°C). Antibody staining was conducted on whole mounts according to standard protocols (Klymkowsky and Hanken, 1991). After bleaching, specimens were washed 3 times in PBS + 0.1 % TritonX-100 for 20 minutes each. They were then blocked for 2 hours in DAKO antibody diluent. An antibody against desmin (Monosan, PS031) was applied as primary antibody (1:200 in DAKO antibody diluent) and incubated overnight. On the next day specimens were washed again 3 times in PBS + 0.1 % TritonX-100 for 20 minutes each and blocked in DAKO antibody diluent for 2 hours. Afterwards, Alexa568-anti-rabbit (Thermo Fisher

Scientific, Product # A-11011) was applied as secondary antibody (1:500 in DAKO antibody diluent) and incubated overnight. Stained specimens were dehydrated two times in 100 % methanol for 10 minutes each and cleared and stored in BABB (benzyl alcohol/ benzyl benzoate, 1/2). Digital stacks from the antibody stainings were obtained using a Zeiss LSM510 confocal microscope and processed with ZEN 2012.

Micro-computed tomography (μ CT)

Three larvae (un-injected control, uni- and bilateral injected specimens) were fixed in 4% PFA and treated with phosphotungstic acid (PTA) as described by (Metscher, 2009). The specimens were scanned using the Xradia MicroCT system at the Department of Theoretical Biology, University of Vienna, Austria.

3D reconstruction

Three-dimensional reconstructions were performed from digital stacks of μ CT scans as well as fluorescent whole mount antibody stainings using Amira 5.2 3D-analysis software (FEI Visualization Sciences Group) and transferred to MAYA software (Autodesk, Inc.) for surface renderings or to VGStudioMax 2.0 (Volume Graphics) for volume renderings.

Whole mount *in situ* hybridization

Whole mount *in situ* hybridizations were done according to the standard procedures (Harland, 1991). Digoxigenin labeled antisense probes were synthesized using FoxN3 cDNA (Schuff et al., 2006).

Results

The anatomy and development of the heart of *X. laevis* have been described in detail by Kolker et al. (2000) and Mohun et al. (2002). For a better evaluation of the heart

anatomy and development after *FoxN3* knockdown we give short descriptions of the heart anatomy in stage-matched, un-injected control embryos. A list of all specimens and their observed malformations is given in table 1.

Morpholino-mediated knockdown of *FoxN3* leads to absence of the interatrial septum in tadpoles at Nieuwkoop and Faber (NF) stage 46/47

Un-injected controls (Fig. 1A) - Heart morphogenesis is complete and all parts of the tadpole heart are now present. The systemic blood circuit enters the right atrial chamber via the sinus venosus, while the pulmonary blood circuit enters the smaller left atrial chamber via the pulmonary vein. The right and the left atrial chambers are incompletely separated by the interatrial septum. It originates from the dorso-posterior atrial wall and extends anteroventrally into the atrial lumen. The ventro-laterally located opening of the atrium into the ventricle is surrounded by the atrio-ventricular valves (AV-valves). The ventricle is coated with a strong myocardial wall, from which muscular trabeculae extend into the ventricular lumen. Anteroventral to its connection with the atrium, the ventricle opens into the outflow tract. Like the ventricle, the outflow tract is coated with a strong myocardium. It runs in a postero-anterior direction, performing a “mirrored s”-shaped curve. The spiral septum, extending from the myocardial wall into the lumen, divides the outflow tract along its anterior-posterior axis. At its anterior end, the outflow tract bifurcates into two arterial main trunks which further split into the aortic arch arteries. Figure 2A to E show different sections of the same 3D reconstruction as in Figure 1A from a ventral view.

FoxN3-morphants (Fig. 1B) – The systemic blood flow enters the atrium via the sinus venosus. Both the interatrial septum and the pulmonary vein are missing. Due to this, the atrium appears as one undivided chamber. Morphants at this developmental stage completely lack a pulmonary blood circuit, which is present in stage-matched un-

injected control specimens. In most of the morphants, the AV-valves, surrounding the passage from the atrium into the ventricle, are greatly reduced or absent. This results in partial blood back flow from the ventricle into the atrium during ventricular contraction. While the myocardium of the ventricle is normally developed, the trabeculae originating from it appear stout and much more compact than the control specimens. The outflow tract myocardium as well as the spiral septum show no differences compared to the same structures in un-injected control specimens. Other malformations in addition to the absence of the interatrial septum can be observed in some specimens. The AV-valves can be reduced or completely absent. In many specimens slightly abnormal heart looping formation was recognized by a more lateral exit of the outflow tract from the ventricle and a more lateral placement of the atrium in relation to the rest of the heart, in contrast to the right-sided dorsolateral position in un-injected control specimens. Figure 2F to J show different section planes of the same 3D reconstruction as in Figure 1B from a ventral view.

Morpholino-mediated knockdown of *FoxN3* delays early heart development and inhibits the formation of the interatrial septum.

NF stage 36-37

Un-injected controls – At this stage, the myocardium is completely closed. The heart tube has become twisted in an s-shaped curve. The Outflow tract, ventricle, atrium and sinus venosus are only faintly delimited along the anteroposterior-axis. The part of the future atrium and sinus venosus lay slightly dorsally, compared to the future ventricle and Outflow tract. Loop-formation of the heart tube has started to displace the ventricular region away from the midline. Due to this, the heart tube is forming a counterclockwise curved spiral.

FoxN3 morphants – Morphant phenotypes of *FoxN3* knockdown are not recognizable at these stages of development.

NF stage 39-40

Un-injected controls (Fig. 3A) – The spiral looping of the heart is more compressed along the anterior-posterior axis. As a result, the atrial region is positioned dorsolateral to the ventricular region. The myocardium of the ventricular region and the Outflow tract has thickened while in the atrial region it is only weakly developed.

FoxN3 morphants (Fig. 3E) – Morphant phenotypes are first recognizable at these stages by a decrease in eye size. Heart morphogenesis is delayed in uni- and bilaterally injected specimens compared to un-injected control embryos at the same NF stage. The heart tube is still twisted in an s-shaped curve. The Outflow tract, ventricle, atrium and sinus venosus are only weakly delineated along the antero-posterior axis. No difference in the thickness of the myocardium can be recognized among the areas of the future chambers. The stage of heart development of *FoxN3* morphants at NF stage 39-40 resembles the stage of heart development in un-injected control embryos at stage 36-37.

NF stage 42

Un-injected controls (Fig. 3B) – The atrium has shifted further dorsally and is now positioned directly on top of the ventricle. Two small bulges, representing the developing AV-valves, are present at the passage from the atrium to the ventricle. The myocardial wall of the ventricle has thickened and the first small trabeculae have started to form on its outer left side (Fig. 2B, blue arrows). The myocardium of the Outflow tract has also thickened and the developing spiral septum has become visible.

FoxN3 morphants (Fig. 3F) – The development of the heart shows a delay of around two stages in uni- as well as bilaterally injected specimens. The heart tube resembles the

one of un-injected control embryos at NF stage 40. Loop formation of the heart tube has started. As the result the atrial region is positioned lateral to dorso-lateral to the ventricular region. The myocardium of the ventricle and outflow tract has started to thicken but no developing trabeculae are visible. The myocardial wall of the atrium is still weakly developed. Neither the AV-valves and spiral septum nor the interatrial-septum are recognizable.

NF stage 44

Un-injected controls (Fig. 3C) – The interatrial-septum has started to form extending from the posterodorsal myocardial wall into the lumen of the atrium. It divides the atrium incompletely into a right and a smaller left chamber (Fig. 2D, red arrows). The AV-valves are completely developed and the ventricle shows a rich trabeculation. The myocardium of the Outflow tract has continued to increase its thickness and the spiral septum is much more distinct compared to earlier stages.

FoxN3 morphants (Fig. 3G) – From this stage on, unilaterally injected specimens show similar heart morphologies to un-injected control specimens. In bilaterally injected specimens no interatrial septum can be recognized. The AV-valves are only weakly developed or absent. The ventricular trabeculation is sparse and compact. The outflow tract is developed normally and a distinct spiral septum can be recognized.

NF stage 46

Un-injected controls (Fig. 3D) – At this stage, morphogenesis of the heart of the tadpole of *X. laevis* is complete. The interatrial septum has grown further into the lumen of the atrium, still dividing the right and left chambers incompletely (Fig. 2D, red arrows). The AV-valves as well as the spiral septum are completely differentiated.

FoxN3 morphants (Fig. 3H) – The interatrial septum is absent and no presumptive anlage is recognizable in bilaterally injected specimens. Like in earlier stages, AV-valves are weakly developed or absent. In many specimens, the ventricular trabeculae are reduced and do not show the typical “spongy” architecture as visible in un-injected control specimens at the same developmental stage.

Normal NC migration in *FoxN3* morphants

It has been shown by Schuff et al. (2007) that NC migration is normal in *FoxN3*-depleted *X. laevis* using and EosFP RNA as a fluorescent marker. However, normal migration of NCCs was only shown in anterior parts of the head. We specifically examined NC migration in the branchial region by *in situ* hybridization of *Sox9* mRNA. *Sox9* is a well-known marker for migrating NCCs (Hall, 1999). No differences of *Sox9* expression were detected in *FoxN3* morphants compared to un-injected control embryos (Fig. 4).

Morpholino-mediated knockdown of *FoxN3* leads to malformations of the muscles in the head/trunk interface of *X. laevis*

In un-injected control specimens at NF stage 46/47 (Fig. 5A), the cucullaris muscle originates from the posterolateral wall of the otic capsule. It runs posteroventrally in the direction of the developing limb bud. At this developmental stage its posterior end is still loose (Fig. 5A'). The diaphragmatico-branchialis muscle originates from the posterodorsal margin of the ceratobranchial 4. It runs posteroventrally, becoming continuous with the hypaxial trunk musculature (Fig. 5A'). In *FoxN3*-MO injected specimens the cucullaris as well as the diaphragmatico-branchialis muscle are seriously malformed (Fig. 5B). The cucullaris is not in contact with the wall of the otic capsule. It is much shorter and curves in a dorsolateral direction (Fig. 5B'). Its normal target, the

forelimb bud, is absent in *FoxN3* morphants of *X. laevis*. The diaphragmatico-branchialis muscle cannot be clearly identified. It is either totally absent or sometimes represented by a small muscle cell population at the posterodorsal margin of ceratobranchial 4 (Fig. 5B`).

Discussion

NCCs migrate normal in *FoxN3*-depleted embryos of *X. laevis*

It is known that the NC contributes to the aortic arch arteries and the aortic sac in *X. laevis* (Lee and Saint-Jeannet, 2011). Using *Sox9* as a marker for migrating NCCs we showed, that NCCs migrate normally into the posterior branchial arches. This result correlates with the observation that the first phenotypes of *FoxN3*-depleted embryos appear at NF stage 39 as reported by Schuff et al. (2007). Therefore we suggest that malformations of the muscles at the head/trunk interface and the heart are not due to migration defects of NCCs.

Morpholino-mediated knockdown of *FoxN3* delays heart development and leads to the absence of the interatrial septum

Our results show, that uni- and bilateral injection of *FoxN3*-MO delays heart morphogenesis compared to un-injected control embryos. In uni-laterally injected embryos, this delay disappears between NF stage 42 and 44. From these stages on, uni-laterally injected specimens develop similar to un-injected control specimens at the same NF stage. Bi-laterally injected specimens in contrast show absence of the interatrial septum and the pulmonary vein and weaker trabeculation. Additional malformations such as absent or reduced AV-valves and looping defects were also observed. The loss of the morphant phenotype and the subsequent normal cardiac development in uni-laterally injected specimens might be due to compensatory effects

from the un-injected contralateral side. Due to this we only refer to the phenotype of bilaterally injected specimens when discussing the results of *FoxN3* MO-mediated knockdown.

From NF stage 39 on, *FoxN3* morphants appear to be delayed in their development compared to un-injected control embryos by approximately two NF stages (Schmidt et al., 2011; Schuff et al., 2007). We confirm this observation concerning the early steps of heart morphogenesis, where cardiogenesis in *FoxN3* morphants is delayed by two NF stages between NF stages 39/40 and 46/47 compared to un-injected control embryos.

It has been proposed, that the craniofacial malformations in *FoxN3* morphants are due to incomplete differentiation of neural crest-derived skeletal elements. Mesoderm-derived parts of the head skeleton such as the otic capsule, the basihypobranchial and the parachordals appear unaffected (Schmidt et al., 2011). Malformations in the mesodermal head musculature are more or less a side effect mainly due to the skeletal defects or effects in the neural crest-derived connective tissue of these muscles (Schmidt et al., 2011). This is in contrast to the knockdown of *FoxN3* in mouse, where both NC and mesoderm-derived skeletal structures of the head are malformed (Samaan et al., 2010). To elucidate the mechanism by which *FoxN3* acts on cardiogenesis it therefore seems essential to know the exact contributions of NC and cranial mesoderm to the heart of *X. laevis*. It has been shown that NCCs only contribute to the aortic arches and are dispensable for heart development in *X. laevis* (Lee and Saint-Jeannet, 2011). However, an earlier study, using hetero-specific NC transplantations, reported NCCs in the outflow tract of *X. laevis* (Sadaghiani and Thiébaud, 1987). The heart itself is derived from two ventral mesodermal cell sub-populations of the cardiopharyngeal field, termed the first heart field (FHF) and the second heart field (SHF). The cells of the FHF contribute to the sinus venosus as well as to the atrial and the ventricular myocardium.

Cells of the SHF field contribute to the ventricular myocardium and the outflow tract (Lee and Saint-Jeannet, 2011). The interatrial septum, absent in *X. laevis FoxN3* morphants, is an outgrowth of the atrial myocardium while the trabeculae develop from the ventricular myocardium (Mohun et al., 2000). It has been shown in the mouse and the chicken, that a late population of migratory cells from the second heart field enters the heart, contributing to proper outflow tract septation and the interatrial septum in mouse (Hoffmann et al., 2009; Waldo et al., 2005). The origin of the interatrial septum in *X. laevis* has not been investigated so far. In the study by Lee and Saint-Jeannet (2011), lineage tracing of the heart fields was carried out and evaluated at NF stage 41. At this stage, the interatrial septum has not started to form in *X. laevis*. It is therefore possible that, as in the mouse, a migratory cell population of the SHF enters the heart of *X. laevis* later in development giving rise to the interatrial septum. Regardless if there is a physical contribution of NCCs to the heart in *X. laevis* or not it has been shown that NC ablation leads to defects in the primary heart tube at early stages (Martinsen et al., 2004; Nie and Bronner, 2015). We therefore propose that heart malformations of *FoxN3*-depleted *X. laevis* larvae might be due to signaling defects instead of lacking tissue contribution of NCCs.

***FoxN3* is involved in the development of the muscles in the head/trunk interface**

The origin of the cucullaris muscle in amphibians has long been controversial due its position at the head/trunk interface. Either an origin from the head mesoderm (Edgeworth, 1935; Rylkoff, 1924; Sefton et al., 2016) or the somites in the trunk (Piekarski and Olsson, 2007) has been proposed. Most recent data point to the head mesoderm as the source for the cucullaris muscle in amphibians (Sefton et al., 2016). However, the only data available are from a salamander (Urodela), the Mexican axolotl (*Ambystoma mexicanum*). No data on frogs (Anura), representing more than 80 % of all

extant amphibian species are available. Our results show that the cucullaris muscle, like most other head muscles, is malformed in *FoxN3* morphants of *X. laevis*. Trunk muscles, such as the epaxial and hypaxial musculature as well as the hypobranchial muscles are normally developed. Merely the hypobranchial geniohyoideus muscle appears a bit shorter and inserts on Meckel's cartilage in *FoxN3* morphants instead of on the infrarostral cartilage in un-injected controls (Schmidt et al., 2011). This might be a side-effect since the infrarostral normally develops from Meckel's cartilage but is absent in *FoxN3* morphants. Another muscle, the diaphragmatico-branchialis, was described recently and has not been considered in previous studies on *FoxN3* in *X. laevis*. This muscle develops late as the cucullaris muscle (Chapter 2), is innervated by the vagal nerve and, like the cucullaris muscle, spans the head/trunk interface (Naumann and Olsson, 2017). The diaphragmatico-branchialis is malformed in *FoxN3* morphants, indicating a head origin such as for the cucullaris muscle. The observation, that the cucullaris and diaphragmatico-branchialis muscles of *X. laevis* are governed by the same developmental mechanisms as the head musculature indirectly implies a head origin of both muscles. Our results also consolidate the link between the head and the heart. Both head muscle and heart defects can be explained by their common origin from the mesodermal cardiopharyngeal field.

An explanatory hypothesis on the role of *FoxN3* in craniofacial and heart development in *X. laevis*

Many aspects of the role of *FoxN3* in cell cycle control and embryonic development are still unknown. However, an explanatory hypothesis of how *FoxN3* knockdown leads to the craniofacial defects was proposed by Schuff et al. 2007. The proposed mechanism could also explain the cardiac malformations in *X. laevis FoxN3* morphants.

Ches1, the homolog of *FoxN3* in yeast, has been shown to act as a cell cycle checkpoint suppressor and promotes cell cycle arrest after DNA-damage at the transition from the G2- to the M-phase (Pati et al., 1997). It has been shown, that yeast *Ches1* and *Xenopus* *FoxN3* can bind to Sin3 and RPD3 proteins (Schuff et al., 2007; Scott and Plon, 2003) (Fig. 6A). Sin3 as well as RPD3 are co-repressors of histone deacetylase (HDAC) (Laduron et al., 2004; Schuff et al., 2007). HDAC is one of the major inhibitors of transcriptional activity by binding to DNA and promoting chromatin remodeling (Jones et al., 1998; Nan et al., 1998). However, HDAC alone does not interact with DNA but has to form protein complexes with e.g. Sin3 to exert its inhibitory function (Laduron et al., 2004). Genomic as well as Morpholino-mediated knockdown of HDAC in the zebrafish (*Danio rerio*) leads to smaller eyes, craniofacial defects (especially in the mandibular and branchial arches), weak myocardia and prevented cardiac looping, as well as smaller limb buds (Pillai et al., 2004; Yamaguchi et al., 2005). This phenotype is strikingly similar to the phenotypes produced by Morpholino-mediated *FoxN3* knockdown in *X. laevis* (Schmidt et al., 2011; Schuff et al., 2007). It was therefore proposed, that HDAC forms an active complex together with *FoxN3*, Sin3 and maybe RPD3 (Fig. 6B). This HDAC-complex binds to the DNA via *FoxN3* during the end of the G2-phase (Fig. 6C) (Schuff et al., 2007). The following chromatin remodeling inhibits transcription and leads to a stop at the checkpoint of the cell cycle (Fig. 6D) to repair of DNA damage prior to DNA replication and mitotic cell division Fig. 6E). After the knockdown of *FoxN3*, HDAC and its co-repressors Sin3 and RPD3 are not able to bind to the DNA and inhibit transcription (Fig. 6F). This prevents cell cycle stop at the G2/M-phase checkpoint (Fig. 6G) leading to reduced time for DNA repair and subsequent accumulation of DNA damage (Fig. 6H). Programmed cell death, or apoptosis, is one of the most prominent routes to remove cells with accumulated DNA damage that potentially could harm the organism by turning into cancer cells (Roos and

Kaina, 2006). This interpretation gains support by the increased levels of apoptosis (Schuff et al., 2007) and the decreased size of cranial cartilage and muscle anlagen (Schmidt et al., 2011) in *FoxN3* morphants of *X. laevis*. How can this mechanism explain the heart defects in *FoxN3* depleted embryos?

In early embryos of *X. laevis*, the FHF and SHF are located in the ventral region of the embryo. NCCs have already started migrating but do not reach that far ventral (Fig. 7A). After the cells of the FHF have started to differentiate and form the primary heart tube cells of SHF express *Fgf8* (Fig. 7B). *Fgf8* promotes cell proliferation in the SHF in inhibits migration and differentiation of these cells (Hutson et al., 2006; Waldo et al., 2005). In later embryos NCCs have migrated in the area of the SHF and inhibit the expression of *Fgf8*. This decreases cell proliferation and promotes migration of SHF cells into the heart tube (Fig. 7C) (Waldo et al., 2005). SHF cells arriving at the heart tube will start to differentiate and form the outflow tract (Lee and Saint-Jeannet, 2011) (Fig. 7D). These cells will then express *Sema3c* which will attract NCCs to enter the heart (Fig. 7E) (Kodo et al., 2017).

On the basis of this scenario we suggest three possible explanations for the heart malformations in *FoxN3*-depleted *X. laevis*. The first proposes, that the malformations might be due to a decreased signaling of the cardiac NCCs, a sub-population of the cranial NCCs. The second focuses on signals from the endocardium, the inner endodermal layer of the heart tube, and the pulmonary endoderm. The third proposes *FoxN3* depletion in the mesodermal cardiac progenitor cells.

The first possibility is based on a study of the cardiac NCCs in a specific part of the cardiopharyngeal field, the second heart field, in the chicken (Waldo et al., 2005). In this study it was shown, that cardiac NC ablation resulted in a shortened outflow tract and altered cardiac looping. This was surprising, since these malformations were

observed before the cardiac NCCs would enter the heart in normal development. Further investigations showed that the NCCs signal to the undifferentiated cells of the second heart field, which then start to migrate into the heart tube. Absence of the NC signal led to an increase in *Fgf8* expression and a subsequent higher mitosis rate in the second heart field. The dividing cells were not able to migrate into the heart tube, which led to the absence of structures derived from the second heart field in the chicken heart tube (Waldo et al., 2005). It is therefore possible that, as hypothesized by Schmidt et al. (2011), the apoptotic NCCs in *FoxN3* morphants do not signal to the second heart field. As a result, cells from the second heart field do not migrate into the developing heart tube of *X. laevis*. It has been shown that the second heart field of *X. laevis* contributes to the outflow tract and ventricular myocardium. A contribution to the interatrial septum has not been described since the lineage tracing investigation stopped at NF stage 41 (Lee and Saint-Jeannet, 2011). At this stage, the interatrial septum has not even started to develop. It is therefore possible that the interatrial septum of *X. laevis* is also derived from the second heart field. The second explanation is based on the delayed developmental timing. The interatrial septum and ventricular trabeculation develop relatively late between NF stage 42 and 46 (present study, Mohun et al., 2000). It is known that trabeculae formation is initiated by inductive signals from the endocardium and blood flow in the zebrafish (Peshkovsky et al., 2011). Additionally, it has been shown that inductive shh-signals from the developing pulmonary endoderm are essential for the formation of the interatrial septum in mouse (Hoffmann et al., 2009). It is therefore possible that the myocardial cells are not receptive for the inductive signals from the endoderm, which could lead to the reduction in trabeculation and the absence of the interatrial septum, developing even later than the trabeculae. The defect AV-valves, derivatives of the endocardium, in *X. laevis FoxN3* morphants could also indicate disturbances of the endoderm-mesoderm interaction in the heart. The third

possibility focuses on the mesodermal SHF. *FoxN3* is expressed in the animal half of *X. laevis* gastrulas and in the NC and visceral arches in later embryonic stages (Schuff et al., 2006). The mesoderm, giving rise to cranial and heart musculature (the cardiopharyngeal field) is located in the ventral animal half of late gastrulas of *X. laevis* (Wolpert et al., 2007). The knockdown of *FoxN3* and a subsequent increase in the rate of apoptosis in this area could result in a smaller amount of cells in the cardiopharyngeal field, which includes the primary and secondary heart fields. This in turn might lead to fewer cells contributing to the heart anlage. A decreased amount of progenitor cells could be one reason for the absence of the interatrial septum and the weaker ventricular trabeculation.

However, cardiogenesis is very different in amniote, amphibian and teleost model organisms as shown for the role of NC in heart development (Kirby et al., 1985; Lee and Saint-Jeannet, 2011; Poelmann et al., 1998; Sato and Yost, 2003; Tomita et al., 2005). It is therefore unclear if heart development in *X. laevis* is dependent upon the same signals as in the zebrafish, chicken or the mouse. Too little is known about the mechanisms of later heart morphogenesis in *X. laevis* and data on the process of trabeculation as well as the role of HDAC and shh in cardiogenesis are needed to decide between the proposed scenarios.

Conclusions

FoxN3 is involved in the development of muscles in the head/trunk interface of *X. laevis*, implying a cranial origin of the cucullaris and diaphragmatico-branchialis muscle in this species.

Morpholino-mediated knockdown of *FoxN3* delays heart development and leads to the absence of the interatrial septum. Other, more infrequent, cardiac defects such as a

decreased ventricular trabeculation, absent or reduced AV-valves and in-complete looping of the heart tube are also observed.

Acknowledgements

We thank Sandra Eisenberg for the care of the adult *X. laevis*. We further thank Katja Felbel for indispensable advice in the lab and Paul Lukas for giving access to additional serial sections of *X. laevis* for comparison. This project was funded by the Deutsche Forschungsgemeinschaft (Grant Number: DFG-OL 134/10-2 to LO).

References

- Böck P. 1989. Romeis mikroskopische technik. Urban & Schwarzenberg, München.
- Byth BC, Costa MT, Teshima IE, Wilson WG, Carter NP, Cox DW. 1995. Molecular analysis of three patients with interstitial deletions of chromosome band 14q31. *Journal of Medical Genetics* 32(7):564-567.
- Carlsson P, Mahlapuu M. 2002. Forkhead transcription factors: key players in development and metabolism. *Developmental Biology* 250(1):1-23.
- Diogo R, Kelly RG, Christiaen L, Levine M, Ziermann JM, Molnar JL, Noden DM, Tzahor E. 2015. A new heart for a new head in vertebrate cardiopharyngeal evolution. *Nature* 520(7548):466-473.
- Edgeworth FH. 1935. The cranial muscles of the vertebrates: Cambridge University Press, Cambridge.
- Ekker SC. 2000. Morphants: a new systematic vertebrate functional genomics approach. *Yeast* 17(4):302-306.
- Ericsson R, Cerny R, Falck P, Olsson L. 2004. Role of cranial neural crest cells in visceral arch muscle positioning and morphogenesis in the Mexican axolotl, *Ambystoma mexicanum*. *Developmental Dynamics* 231(2):237-247.
- Ericsson R, Knight R, Johanson Z. 2013. Evolution and development of the vertebrate neck. *Journal of Anatomy* 222(1):67-78.
- Gegenbaur C. 1889. Vergleichende Anatomie der Wirbelthiere: mit Berücksichtigung der Wirbellosen: W. Engelmann, Leipzig.
- Hall BK. 1999. The neural crest in development and evolution: Springer Science & Business Media.

- Harland RM. 1991. In situ hybridization: an improved whole-mount method for *Xenopus* embryos. *Methods in Cell Biology* 36:685-695.
- Hoffmann AD, Peterson MA, Friedland-Little JM, Anderson SA, Moskowitz IP. 2009. Sonic hedgehog is required in pulmonary endoderm for atrial septation. *Development* 136(10):1761-1770.
- Huang R, Zhi Q, Patel K, Wilting J, Christ B. 2000. Contribution of single somites to the skeleton and muscles of the occipital and cervical regions in avian embryos. *Anatomy and Embryology (Berl)* 202(5):375-383.
- Hutson MR, Zhang P, Stadt HA, Sato AK, Li Y-X, Burch J, Creazzo TL, Kirby ML. 2006. Cardiac arterial pole alignment is sensitive to FGF8 signaling in the pharynx. *Developmental Biology* 295(2):486-497.
- Jones PL, Veenstra GCJ, Wade PA, Vermaak D, Kass SU, Landsberger N, Strouboulis J, Wolffe AP. 1998. Methylated DNA and MeCP2 recruit histone deacetylase to repress transcription. *Nature genetics* 19(2):187-191.
- Karnitis SA, Burns K, Sudduth KW, Golden WL, Wilson WG. 1992. Deletion (14)(q24.3q32.1): evidence for a distinct clinical phenotype. *American Journal of Medical Genetics* 44(2):153-157.
- Kirby ML, Turnage KL, Hays BM. 1985. Characterization of conotruncal malformations following ablation of "cardiac" neural crest. *The Anatomical Record* 213(1):87-93.
- Klymkowsky MW, Hanken J. 1991. Whole-mount staining of *Xenopus* and other vertebrates. *Methods in Cell Biology* 36:419-441.
- Kodo K, Shibata S, Miyagawa-Tomita S, Ong S-G, Takahashi H, Kume T, Okano H, Matsuoka R, Yamagishi H. 2017. Regulation of Sema3c and the Interaction between Cardiac Neural Crest and Second Heart Field during Outflow Tract Development. *Scientific Reports* 7(1):6771.
- Kuratani S. 1997. Spatial distribution of postotic crest cells defines the head/trunk interface of the vertebrate body: embryological interpretation of peripheral nerve morphology and evolution of the vertebrate head. *Anatomy and Embryology (Berl)* 195(1):1-13.
- Laduron S, Deplus R, Zhou S, Kholmanskikh O, Godelaine D, De Smet C, Hayward SD, Fuks F, Boon T, De Plaen E. 2004. MAGE-A1 interacts with adaptor SKIP and the deacetylase HDAC1 to repress transcription. *Nucleic Acids Research* 32(14):4340-4350.

- Lee YH, Saint-Jeannet JP. 2011. Cardiac neural crest is dispensable for outflow tract septation in *Xenopus*. *Development* 138(10):2025-2034.
- Lescroart F, Hamou W, Francou A, Theveniau-Ruissy M, Kelly RG, Buckingham M. 2015. Clonal analysis reveals a common origin between nonsomite-derived neck muscles and heart myocardium. *Proceedings of the National Academy of Science U S A* 112(5):1446-1451.
- Martinsen BJ, Frasier AJ, Baker CV, Lohr JL. 2004. Cardiac neural crest ablation alters *Id2* gene expression in the developing heart. *Developmental Biology* 272(1):176-190.
- Matsuoka T, Ahlberg PE, Kessar N, Iannarelli P, Dennehy U, Richardson WD, McMahon AP, Koentges G. 2005. Neural crest origins of the neck and shoulder. *Nature* 436(7049):347-355.
- Metscher BD. 2009. MicroCT for comparative morphology: simple staining methods allow high-contrast 3D imaging of diverse non-mineralized animal tissues. *BMC Physiology* 9:11.
- Mohun TJ, Leong LM, Weninger WJ, Sparrow DB. 2000. The morphology of heart development in *Xenopus laevis*. *Developmental Biology* 218(1):74-88.
- Nan X, Ng H-H, Johnson CA, Laherty CD, Turner BM, Eisenman RN, Bird A. 1998. Transcriptional repression by the methyl-CpG-binding protein MeCP2 involves a histone deacetylase complex. *Nature* 393(6683):386-389.
- Naumann B, Olsson L. 2017. Three-dimensional reconstruction of the cranial and anterior spinal nerves in early tadpoles of *Xenopus laevis* (Pipidae, Anura). *Journal of Comparative Neurology*.
- Naumann B, Warth P, Olsson L, Konstantinidis P. 2017. The development of the cucullaris muscle and the branchial musculature in the Longnose Gar, (*Lepisosteus osseus*, Lepisosteiformes, Actinopterygii) and its implications for the evolution and development of the head/trunk interface in vertebrates. *Evolution and Development* 19(6):263-276.
- Nie S, Bronner ME. 2015. Dual developmental role of transcriptional regulator *Ets1* in *Xenopus* cardiac neural crest vs. heart mesoderm. *Cardiovascular Research* 106(1):67-75.
- Nieuwkoop PD, Faber J. 1994. Normal Table of *Xenopus laevis* (Daudin). A systematical and chronological survey of the development from the fertilized egg till the end of metamorphosis: Garland publishing, New York.

- Noden DM. 1983. The embryonic origins of avian cephalic and cervical muscles and associated connective tissues. *American Journal of Anatomy* 168(3):257-276.
- Pati D, Keller C, Groudine M, Plon SE. 1997. Reconstitution of a MEC1-independent checkpoint in yeast by expression of a novel human fork head cDNA. *Molecular and Cellular Biology* 17(6):3037-3046.
- Peshkovsky C, Totong R, Yelon D. 2011. Dependence of cardiac trabeculation on neuregulin signaling and blood flow in zebrafish. *Developmental Dynamics* 240(2):446-456.
- Piekarski N, Olsson L. 2007. Muscular derivatives of the cranialmost somites revealed by long-term fate mapping in the Mexican axolotl (*Ambystoma mexicanum*). *Evolution and Development* 9(6):566-578.
- Pillai R, Coverdale LE, Dubey G, Martin CC. 2004. Histone deacetylase 1 (HDAC-1) required for the normal formation of craniofacial cartilage and pectoral fins of the zebrafish. *Developmental Dynamics* 231(3):647-654.
- Poelmann R, Mikawa T, Groot GD. 1998. Neural crest cells in outflow tract septation of the embryonic chicken heart: differentiation and apoptosis. *Developmental dynamics* 212(3):373-384.
- Roos WP, Kaina B. 2006. DNA damage-induced cell death by apoptosis. *Trends in Molecular Medicine* 12(9):440-450.
- Rylkoff H. 1924. Die Entwicklung der Schultermuskeln bei urodelen Amphibien. *Zeitschrift für wissenschaftliche Zoologie* 122:118-171.
- Sadaghiani B, Thiébaud CH. 1987. Neural crest development in the *Xenopus laevis* embryo, studied by interspecific transplantation and scanning electron microscopy. *Developmental Biology* 124(1):91-110.
- Samaan G, Yugo D, Rajagopalan S, Wall J, Donnell R, Goldowitz D, Gopalakrishnan R, Venkatachalam S. 2010. Foxn3 is essential for craniofacial development in mice and a putative candidate involved in human congenital craniofacial defects. *Biochemical and Biophysical Research Communication* 400(1):60-65.
- Sato M, Yost HJ. 2003. Cardiac neural crest contributes to cardiomyogenesis in zebrafish. *Developmental Biology* 257(1):127-139.
- Schlade-Bartusiak K, Macintyre G, Zunich J, Cox DW. 2008. A child with deletion (14)(q24. 3q32. 13) and auditory neuropathy. *American Journal of Medical Genetics Part A* 146(1):117-123.

- Schmidt J, Piekarski N, Olsson L. 2013. Cranial muscles in amphibians: development, novelties and the role of cranial neural crest cells. *Journal of Anatomy* 222(1):134-146.
- Schmidt J, Schuff M, Olsson L. 2011. A role for FoxN3 in the development of cranial cartilages and muscles in *Xenopus laevis* (Amphibia: Anura: Pipidae) with special emphasis on the novel rostral cartilages. *Journal of Anatomy* 218(2):226-242.
- Schuff M, Rossner A, Donow C, Knochel W. 2006. Temporal and spatial expression patterns of FoxN genes in *Xenopus laevis* embryos. *The International Journal of Developmental Biology* 50(4):429-434.
- Schuff M, Rossner A, Wacker SA, Donow C, Gessert S, Knochel W. 2007. FoxN3 is required for craniofacial and eye development of *Xenopus laevis*. *Developmental Dynamics* 236(1):226-239.
- Scott KL, Plon SE. 2003. Loss of Sin3/Rpd3 histone deacetylase restores the DNA damage response in checkpoint-deficient strains of *Saccharomyces cerevisiae*. *Molecular and Cellular Biology* 23(13):4522-4531.
- Sefton EM, Bhullar BA, Mohaddes Z, Hanken J. 2016. Evolution of the head-trunk interface in tetrapod vertebrates. *Elife* 5:e09972.
- Theis S, Patel K, Valasek P, Otto A, Pu Q, Harel I, Tzahor E, Tajbakhsh S, Christ B, Huang R. 2010. The occipital lateral plate mesoderm is a novel source for vertebrate neck musculature. *Development* 137(17):2961-2971.
- Tokita M, Schneider RA. 2009. Developmental origins of species-specific muscle pattern. *Developmental Biology* 331(2):311-325.
- Tomita Y, Matsumura K, Wakamatsu Y, Matsuzaki Y, Shibuya I, Kawaguchi H, Ieda M, Kanakubo S, Shimazaki T, Ogawa S. 2005. Cardiac neural crest cells contribute to the dormant multipotent stem cell in the mammalian heart. *Journal of Cell Biology* 170(7):1135-1146.
- Waldo KL, Hutson MR, Stadt HA, Zdanowicz M, Zdanowicz J, Kirby ML. 2005. Cardiac neural crest is necessary for normal addition of the myocardium to the arterial pole from the secondary heart field. *Developmental Biology* 281(1):66-77.
- Wolpert L, Jessell T, Lawrence P, Meyerowitz E, Robertson E, Smith J. 2007. *Principles of Development*: Oxford university Press.

- Yamaguchi M, Tonou-Fujimori N, Komori A, Maeda R, Nojima Y, Li H, Okamoto H, Masai I. 2005. Histone deacetylase 1 regulates retinal neurogenesis in zebrafish by suppressing Wnt and Notch signaling pathways. *Development* 132(13):3027-3043.
- Yamamoto Y, Sawa R, Okamoto N, Matsui A, Yanagisawa M, Ikemoto S. 1986. Deletion 14q(q24.3 to q32.1) syndrome: significance of peculiar facial appearance in its diagnosis, and deletion mapping of Pi(alpha 1-antitrypsin). *Human Genetics* 74(2):190-192.
- Ziermann JM, Diogo R. 2013. Cranial Muscle Development in the Model Organism *Ambystoma mexicanum*: Implications for Tetrapod and Vertebrate Comparative and Evolutionary Morphology and Notes on Ontogeny and Phylogeny. *Anatomical Record* 296(7):1031-1048.

specimen #	NF stage	control/injected	sv	a	ias	avv	v	vt	ta	ss
XL001	46/47	control	2	2	2	2	2	2	2	2
XL002	46/47	control	2	2	2	2	2	2	2	2
XL003	46/47	control	2	2	2	2	2	2	2	2
XL004	46	bilateral	2	2	0	0	2	1	2	2
XL005	46	bilateral	2	2	0	0	2	1	2	2?
XL006	46	bilateral	2	2	1	0	2	1	2	2
XL007	46	bilateral	2	2	0	1	2	1	2	2
XL008	46	bilateral	?	1	0	?	2	1	?	?
XL009	44	control	2	2	1	2	2	2	2	2
XL010	44	control	2	2	1	2	2	2	2?	2?
XL011	44	control	?	2	1	2	2	2	2	2
XL012	44	control	2	2	1	2	2	2	2	2
XL013	44	bilateral	2	2	0	0	2	1	2	2
XL014	44	bilateral	2	1	0	0	1	0?	2	0
XL015	42	control	2	2	1	1	2	1	2	1
XL016	42	control	?	2	1	1?	2	1	2	1
XL017	42	unilateral	everything present but resembles stage 40 of controls sensu Mohun et al. (2000)							
XL018	42	unilateral	everything present but resembles stage 40 of controls sensu Mohun et al. (2000)							
XL019	42	unilateral	everything present but resembles stage 40 of controls sensu Mohun et al. (2000)							
XL020	42	bilateral	everything present but resembles stage 40 of controls sensu Mohun et al. (2000)							
XL021	42	unilateral	everything present but resembles stage 40 of controls sensu Mohun et al. (2000)							
XL022	40	control	normally developed as described by Mohun et al. (2000)							
XL023	39	unilateral	everything present but resembles stage 38 sensu Mohun et al. (2000)							
XL024	36	unilateral	everything present but resembles stage 32 sensu Mohun et al. (2000)							
XL025	36	unilateral	normally developed as described by Mohun et al. (2000)							
XL026	36	bilateral	everything present resembles stage 35 sensu Mohun et al. (2000); heart only slightly looped							
XL027	36	bilateral	everything present resembles stage 35 sensu Mohun et al. (2000); heart only slightly looped							
XL028	37	unilateral	everything present resembles stage 35 sensu Mohun et al. (2000)							
XL029	37	bilateral	normally developed as described by Mohun et al. (2000)							
XL030	46	unilateral	2	2	2	2	2	2	2	2
XL031	46	unilateral	2	2	2	2	2	2	2	2
XL032	46	unilateral	2	1	1	1	2	2	2	2
XL033	46	unilateral	2	1	2	2	2	2	2	2
XL034	40	bilateral	everything present but resembles stage 38 sensu Mohun et al. (2000)							
XL035	46/47	bilateral	2	2	1	0	2	1	2	2
XL036	46/47	bilateral	2	2	1	0	2	1	2	2
XL037	46/47	bilateral	2	2	1	0	2	1	2	2
XL038	36	control	normally developed as described by Mohun et al. (2000)							
XL039	36	control	normally developed as described by Mohun et al. (2000)							
XL040	37	control	normally developed as described by Mohun et al. (2000)							
XL041	37	control	normally developed as described by Mohun et al. (2000)							
XL042	39	control	normally developed as described by Mohun et al. (2000)							
XL043	40	control	normally developed as described by Mohun et al. (2000)							
XL044	40	control	normally developed as described by Mohun et al. (2000)							
XL045	46	control	2	2	2	2	2	2	2	2
XL046	46	control	2	2	2	2	2	2	2	2

Table 1: Total list of specimens. 0, absent; 1, not completely developed; 2; completely developed. The question mark indicates that the observed structure was not clearly visible. a, atrium; avv, atrioventricular-valves; ias, interatrial septum; ss, spiral septum; sv, sinus venosus; ta, Outflow tract; v, ventricle; vt, ventricular trabeculae.

A control

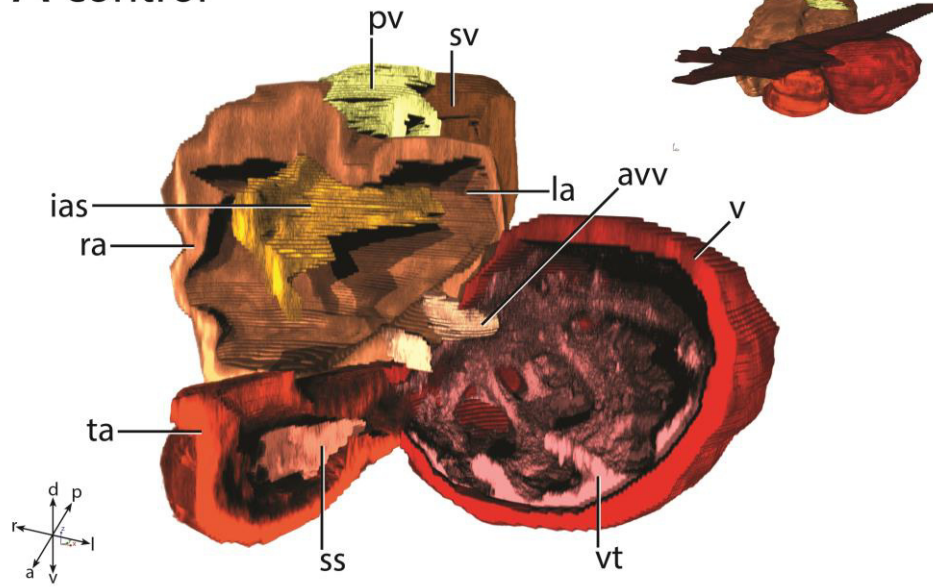
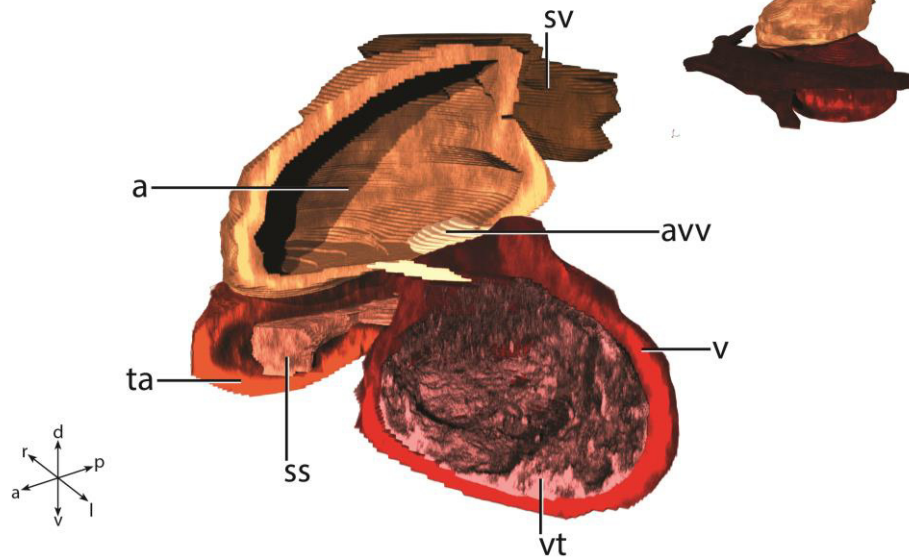
B *FoxN3*-MO

Figure 1: 3D volume reconstructions of hearts of *X. laevis* tadpoles based on digital z-stacks of fluorescent whole mount antibody stainings against desmin. The Sinus venosus (brown), atrium (light brown), ventricle (red) and outflow tract (orange) are clipped in different planes to view lumina and internal structures. Un-clipped whole heart renderings, including the posterior aortic arches (dark brown) in the same orientations are depicted in the upper right corners. The coordinate crosses in the lower left corner show the orientation of the hearts in relation to the body axes. A, un-injected control specimen at NF stage 46/47. B, bilaterally *FoxN3*-MO injected specimen at NF stage 46/47. a, atrium; avv, atrio-ventricular valves; ias, interatrial septum; la, left atrium; pv, pulmonary vein; ra, right atrium; ss, spiral septum; sv, sinus venosus; v, ventricle; vt, ventricular trabeculae.

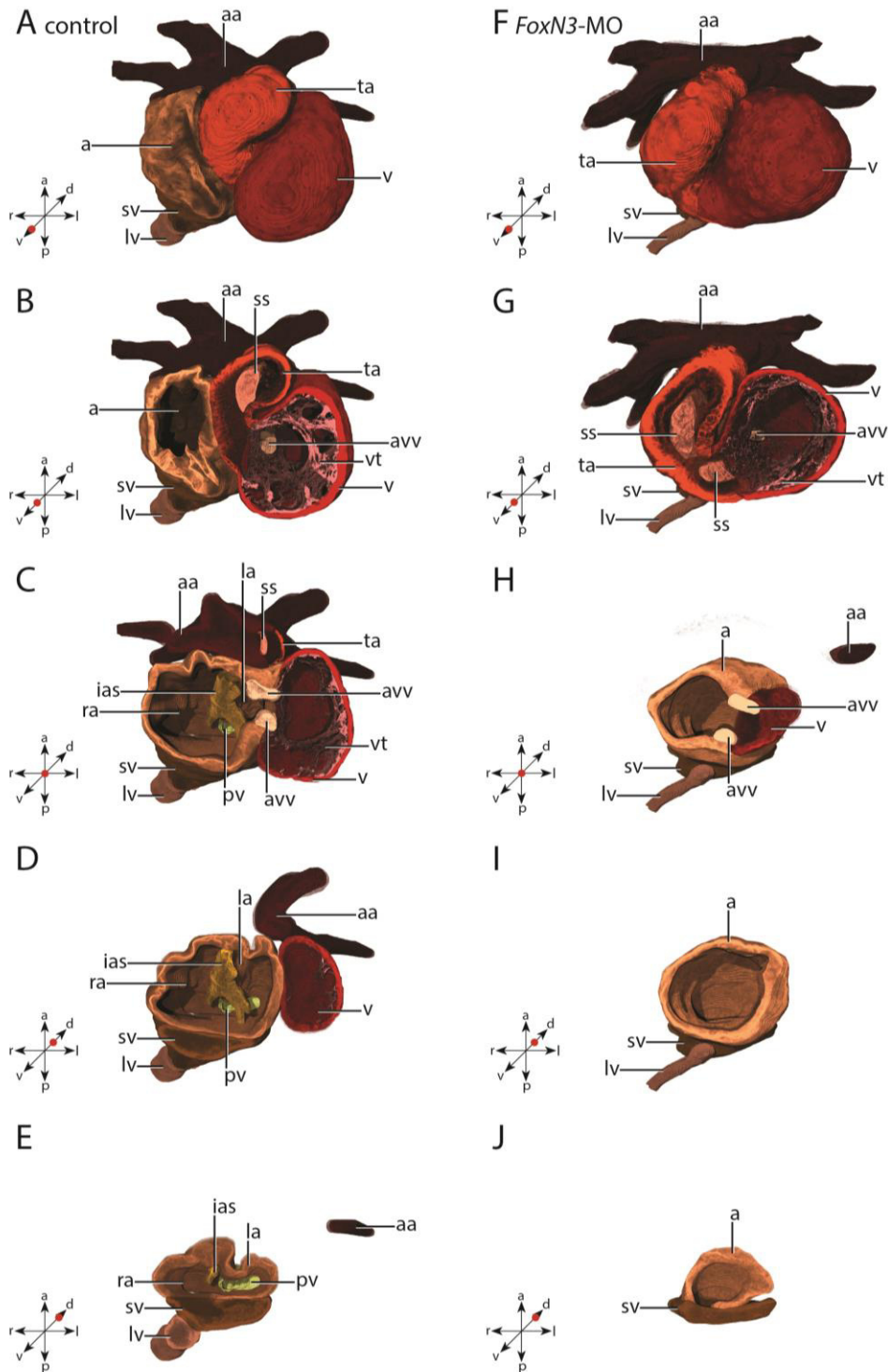


Figure 2: Different section planes of the same 3D reconstructions as shown in Figure 1 from a ventral view. A red dot in the coordinate crosses in the lower left corners indicate the position of the section plane along the dorsoventral axis. A-E, uninjected control specimen at NF stage 46/47. F-J, bilaterally *FoxN3-MO* injected specimen at NF stage 46/47. a, atrium; aa, aortic arches; avv, atrio-ventricular valves; ias, interatrial septum; la, left atrium; lv, liver vein; pv, pulmonary vein; ra, right atrium; ss, spiral septum; sv, sinus venosus; v, ventricle; vt, ventricular trabeculae.

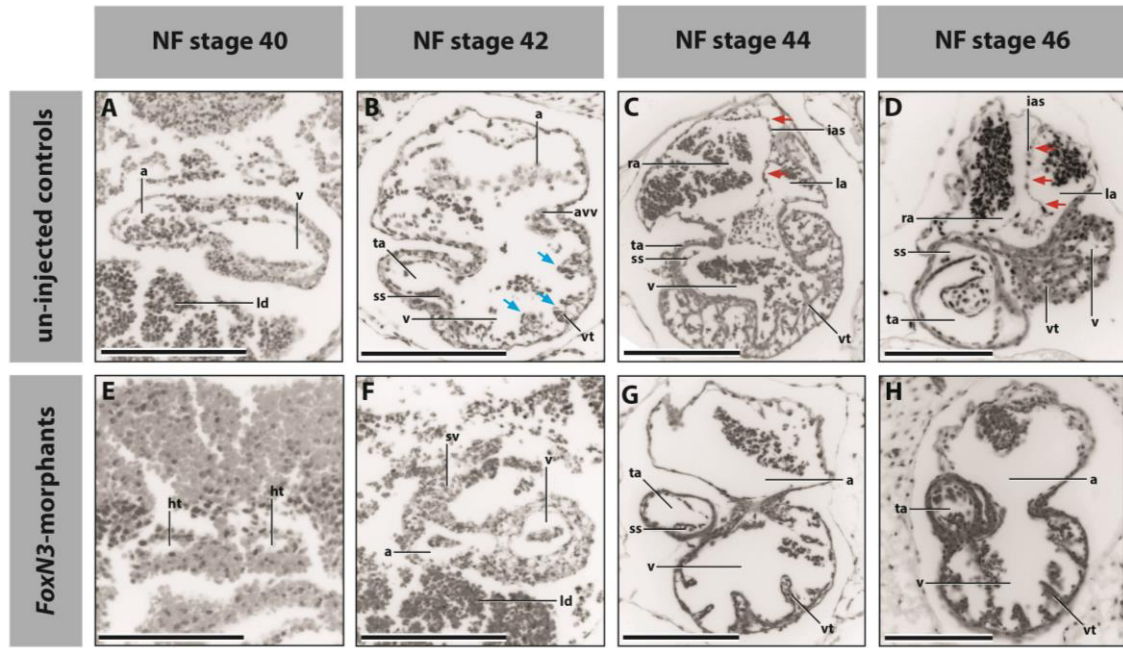


Figure 3: Histological cross sections through the developing heart of un-injected and FoxN3 morphant *X. laevis* at different developmental stages. Images of Azan stained sections are converted to grey scale to enhance contrast. A-D, un-injected control specimens. A, NF stage 40. B, NF stage 42. Blue arrows show the developing trabeculae. C, NF stage 44. Red arrows indicate the developing interatrial septum. D, NF stage 46. Red arrows indicate the interatrial septum. E-H, bilaterally *FoxN3*-MO injected specimens. E, NF stage 40. F, NF stage 42. G, NF stage 44. H, NF stage 46. The scale bar is 500 μ m. a, atrium; ia, interatrial septum; la, left atrium; ra, right atrium; ss, spiral septum; sv, sinus venosus; v, ventricle; vt, ventricular trabeculae.

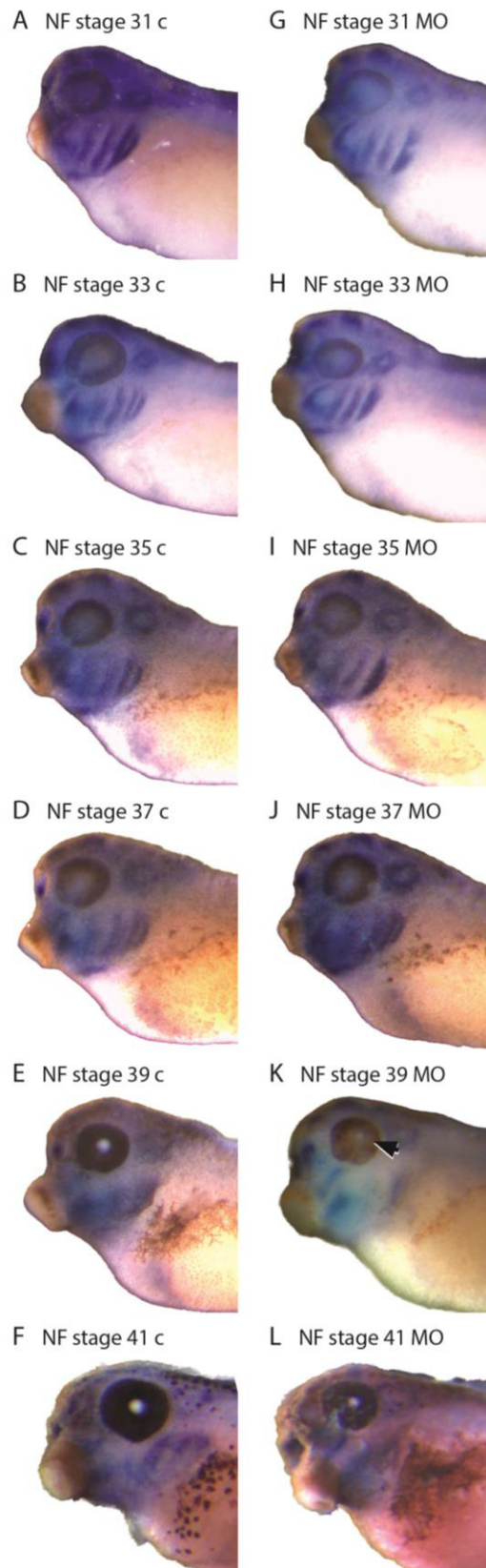


Figure 4: *In situ* hybridization of *Sox9* to visualize the migrating NCCs in *X. laevis* tadpoles at different NF stages in a lateral view. A-E, un-injected control specimens (c). A, NF stage 31. B, NF stage 33. C, NF stage 35. D, NF stage 37. E, NF stage 39. F, NF stage 41. F-K, bilaterally *FoxN3*-MO injected specimens (MO). G, NF stage 31. H, NF stage 33. I, NF stage 35. J, NF stage 37. K, NF stage 39. The arrow indicates the small eye of the *FoxN3*-MO-phenotype. L, NF stage 41.

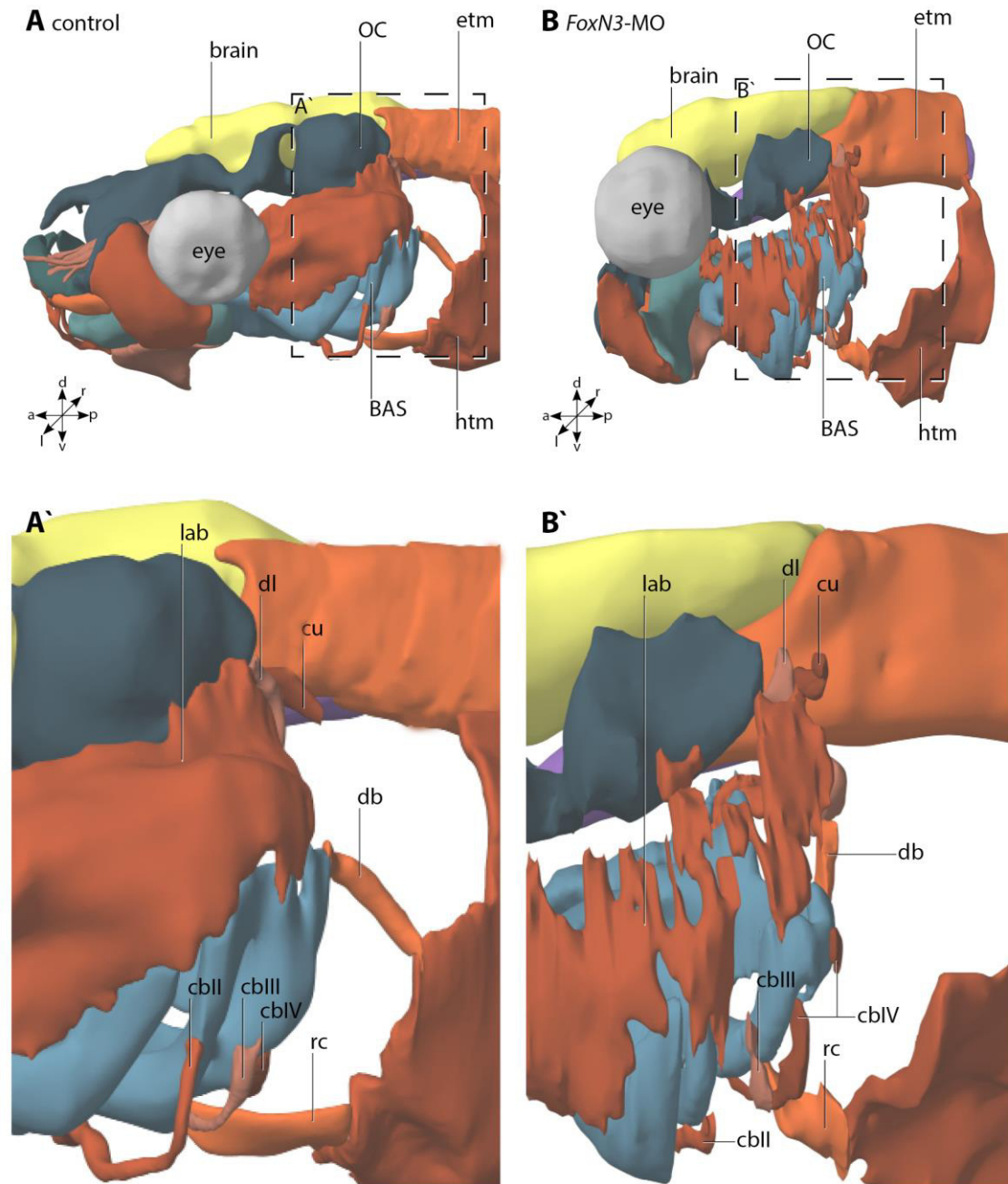


Figure 5: Lateral views of 3D surface reconstructions of μ CT scans of *X. laevis* tadpoles at NF stage 46/47. The brain is colored in yellow, the notochord in violet, the cartilaginous head skeleton in blue and muscles in flesh to light brown. The coordinate crosses in the lower left corner show the orientation of the hearts in relation to the body axes. A, un-injected control specimen. A', close up of the region in marked by the dashed line in A. B, bilaterally *FoxN3*-MO injected specimen. B', close up of the region in marked by the dashed line in B. b, brain; BAS, branchial arches; cbII-IV, constrictor branchialium II to IV; cu, cucullaris; db, diaphragmatico-branchialis; dl, dilatator larynges; etm, epaxonic trunk muscles; htm, hypaxonic trunk muscles; lab, levator arcus branchialium complex; OC, otic capsule; rc, rectus cervicis.

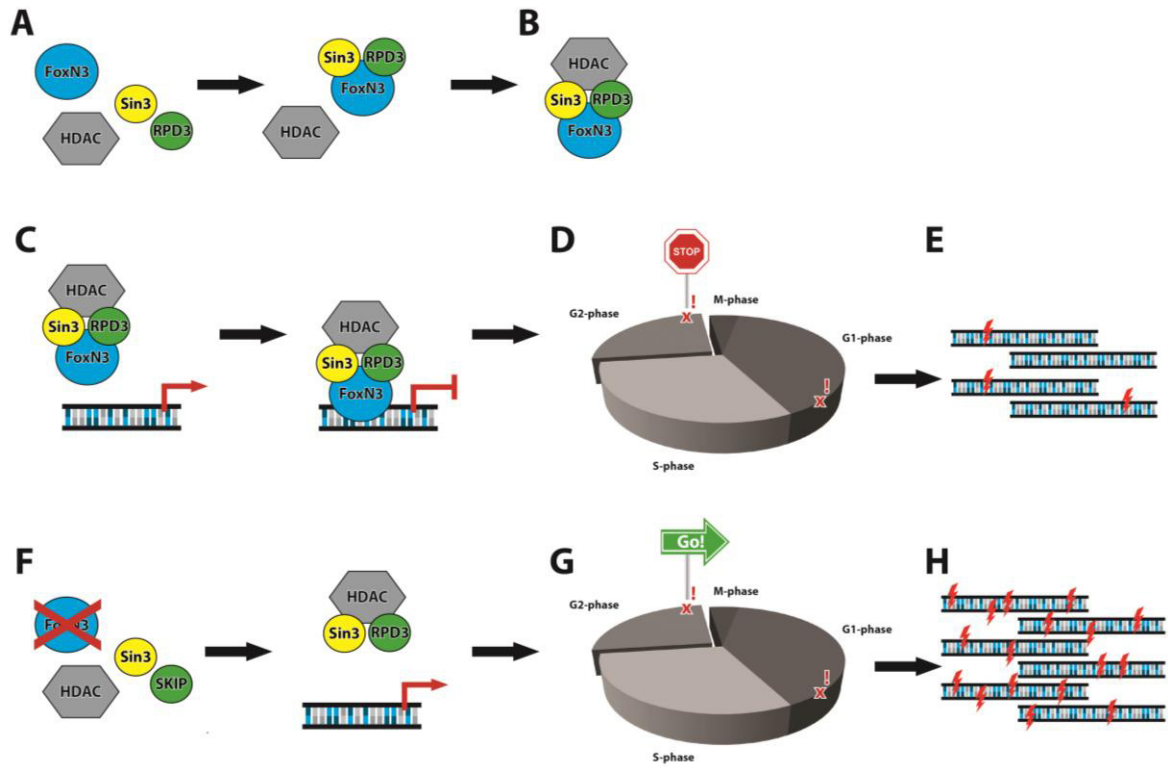


Figure 6: The interactions of FoxN3 with HDAC and its role in cell-cycle and DNA-repair. A, Sin3, RPD3 and FoxN3 form a complex. B, HDAC binds to the preformed complex. C, the HDAC-complex binds to the DNA via FoxN3 and inhibits transcription by histone deacetylation. D, this stops cell cycle progression and the G2/M check point. E, DNA damage can be repaired before cell cycle progression into M-phase. F, after knockdown of *FoxN3* the HDAC-complex can not bind to the DNA. G, the cell-cycle does not stop at the G2/M check point. H, DNA damage is accumulated resulting in higher rates of apoptosis. Red “x!” indicate checkpoints for DNA damage in the G1- and G2-phases. Red lightning bolts represent DNA damage.

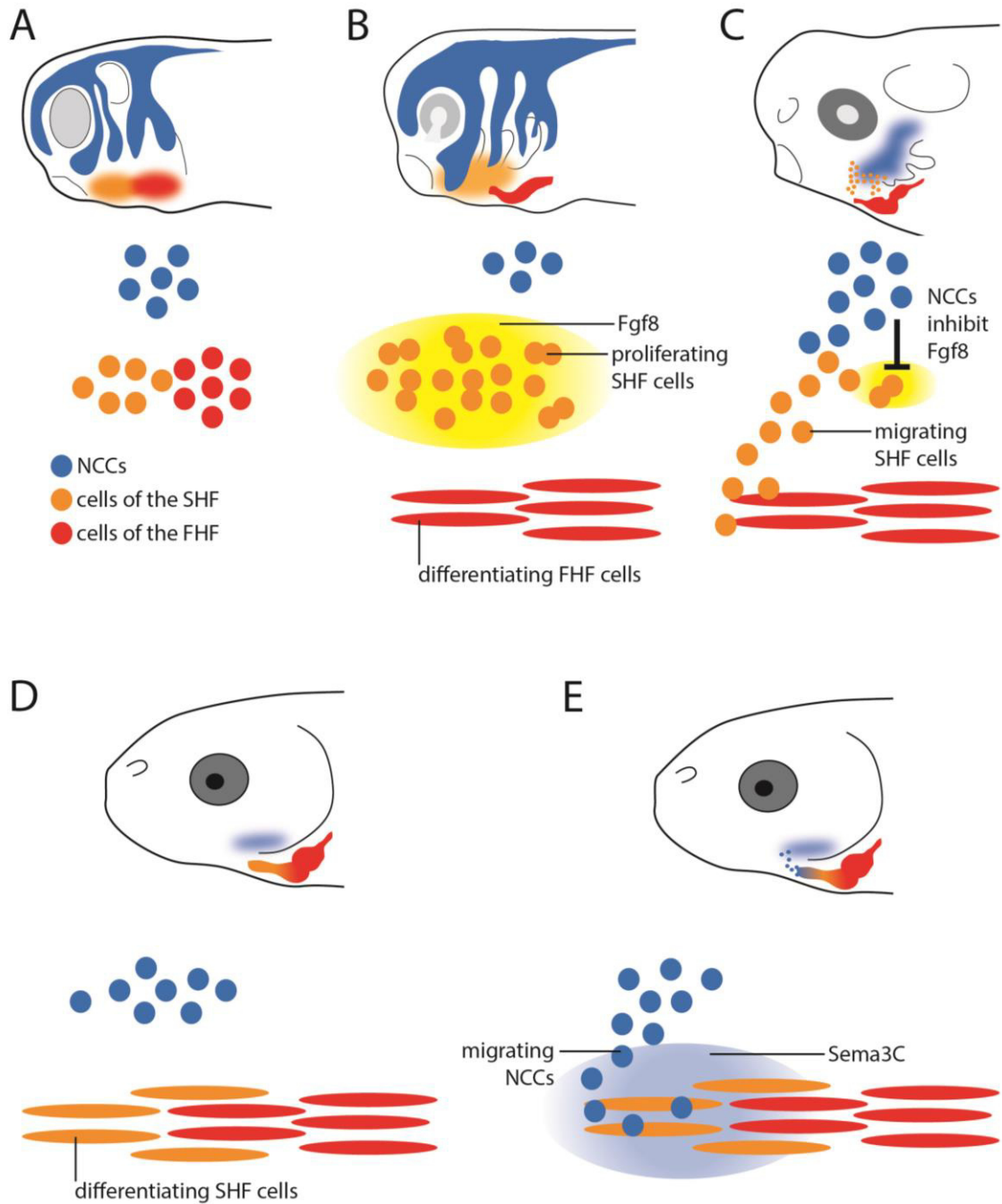


Figure 7: Schematic illustration of the proposed interactions of the cranial neural crest cells (NCCs; blue) with the cells of the first heart field (FHF; red) and second heart field (SHF; orange). A, early embryo of *X. laevis* showing the locations of the three different cell populations. B, Cells of the FHF start to form the primary heart tube. Cells of the SHF express Fgf8 leading to increased rates of proliferation. C, migrating NCCs inhibit Fgf8 expression in the SHF. SHF cells stop proliferation and migrate into the preformed heart tube. D, SHF cells differentiate and form the outflow tract. E, SHF cells start expression of Sema3C. Sema3C attracts NCCs and promotes migration towards the outflow tract.

Chapter 4

Naumann, & Olsson, L. **“Escaping” the new head – Cranial neural crest cells inhibit early cardiac myogenesis in the Mexican axolotl, *Ambystoma mexicanum* (Ambystomatidae: Urodela: Lissamphibia).** (*unpublished manuscript*).

“Escaping” the new head – Cranial neural crest cells inhibit early cardiac myogenesis in the Mexican axolotl, *Ambystoma mexicanum* (Ambystomatidae: Urodela: Lissamphibia)

Benjamin Naumann*, Lennart Olsson

Institut für Zoologie und Evolutionsforschung, Friedrich-Schiller-Universität, 07745 Jena, Germany

*author for correspondence: benjamin.naumann@uni-jena.de

Abstract

It is thought that the evolutionary success of vertebrates is mainly due to the emergence of epidermal placodes and the neural crest (NC) giving rise to a new head (Gans and Northcutt, 1983). This new head might have been a prerequisite to the evolution of a more active, predatory life-style in many vertebrates. This was only possible by the co-evolution of a more effective vascular system and a powerful chambered heart driving circulation, to facilitate the demand for higher metabolic and respiratory rates. While much is known about the developmental origin and differentiation of a chambered heart in amniotes such as chicken and mouse, information from more basal vertebrate taxa such as amphibians are scarce. In this study we describe the first data on the influence of cranial neural crest cells (NCCs) on the development of the early heart tube in the Mexican axolotl (*Ambystoma mexicanum*). We observed that the primary heart tube, derived from the first heart field (FHF), develops posteroventral to the head/trunk interface in the axolotl and many other vertebrates. It has been shown that NCCs are necessary for normal heart development both by direct and indirect interactions with cells derived from the second heart field (SHF). We transplanted cranial NCCs on top of the early heart primordium to test if factors secreted by these cells promote muscle

differentiation as is known for head muscles. Our results show, that cranial NCCs inhibit heart tube formation and muscle differentiation at early stages of heart development. At these early stages it is likely that only cells derived from the FHF are involved in heart tube formation. The inhibitory effect is compensated during later developmental stages, presumably when cells of the SHF enter the heart tube. We speculate that the FHF-derived heart tube can only develop outside of the head, due to the inhibitory effect of the cranial NC. This leads to the assumption that the development of a chambered heart in vertebrates is due to the evolution of the interaction between the NC and the SHF.

Keywords: axolotl, cardiac neural crest, cardiac muscle development, heart evolution

Introduction

Gans and Northcutt (1983) proposed that the evolutionary success of vertebrates is mainly due to the evolution of epidermal placodes and the cranial neural crest, giving rise to a “new head” (Diogo et al., 2015). Placodes are specific thickenings of the epidermis that give rise to many sense organs and ganglia of the vertebrate head (Schlosser, 2010; 2014). The cranial neural crest (NC) is a population of early migratory cells that contribute to the nervous, circulatory and musculoskeletal systems of the head (Hall, 1999; 2000). These innovations are thought to be prerequisites for a switch from a passive filter-feeding to a more active and later predatory life-style found in most vertebrates. The connected behavioral changes demanded a more powerful circulatory system to deal with the increased rates of metabolism and gas exchange (Diogo et al., 2015). A “new heart” (Diogo et al., 2015), sub-divided into muscularized chambers, co-evolved with the “new head” (Gans and Northcutt, 1983) to serve this function.

But what is the origin of this chambered heart? The vertebrate heart develops from two mesodermal cell populations (Jensen et al., 2013). The posterior first heart field (FHF) differentiates early and forms the primary heart tube. The second heart field (SHF) is located anterior to the FHF, differentiates later and contributes to the ventral head muscles, the outflow tract of the heart as well as parts of the ventricles and atria (Diogo et al., 2015; Tirosh-Finkel et al., 2006a; Tzahor, 2009; Tzahor and Evans, 2011). Studies on gene expression show that cells with expression profiles similar to the FHF and SHF of vertebrates also exist in Urochordates (Diogo et al., 2015). Cephalochordates in contrast exhibit only a cell population similar to the FHF (Holland et al., 2003). It therefore seems possible, that the SHF has evolved in the last common ancestor of urochordates and vertebrates (Delsuc et al., 2006).

Another cell population involved in vertebrate heart development is the “cardiac” NC. It has been shown that the cardiac NC is indispensable for normal outflow tract septation in the amniote model species mouse and chicken (Jensen et al., 2013; Kirby et al., 1983; Kirby et al., 1985; Kirby and Waldo, 1995; Martinsen et al., 2004; Waldo et al., 1998; Waldo et al., 2005; Yelbuz et al., 2002). In the zebrafish (*Danio rerio*), a teleost model species, cardiac neural crest cells (NCCs) contribute to every chamber and even differentiate into muscle fibers (Li et al., 2003; Sato and Yost, 2003). However, the embryonic development of amniotes as well as teleosts is considered to be highly derived and may not represent the plesiomorphic vertebrate condition. Unfortunately, data from more basal taxa such as sharks, bichirs, sturgeons and lungfishes do not exist. Data from amphibians as basal tetrapods are still scarce. It is controversial if NCCs contribute physically to the heart of the frog *Xenopus laevis* (Lee and Saint-Jeannet, 2011; Sadaghiani and Thiébaud, 1987). Despite the unclarities about a physical contribution, it has been shown that signaling interactions between NCCs and cardiac mesoderm are required for normal heart development (Martinsen et al., 2004; Nie and

Bronner, 2015). Most of these studies examining the role of NCCs in heart development focus on its interaction with cells derived from the SHF (Waldo et al., 2005). This is because the cardiac NCCs migrate late and enter the heart after cells of the SHF have already been added to the primary heart tube (Waldo et al., 2005).

The aim of this study is to explore interactions of NCCs with cells derived from the FHF in the Mexican axolotl (Tetrapoda: Lissamphibia: Urodela). This will clarify if NCCs play a role in early heart development, before cells of the SHF are added to the primary heart tube.

Materials and Methods

Axolotl embryos

Wildtype and GFP⁺ *Ambystoma mexicanum* embryos were obtained from the breeding colony of the Institut für Zoologie and Evolutionsforschung at the Friedrich Schiller University, Jena, Germany. Mating and subsequent spawning was induced in a separate tank (60 x 30 x 30 cm) with cold fresh water and crushed ice to lower the temperature down to 10°C. Embryos were staged according to the normal tables (Bordzilovskaya and Detlaff, 1989; Nye et al., 2003), de-jellied using watchmaker's forceps and transferred to agar-coated Petri dishes containing 20% Steinberg's Solution.

Neural crest labeling

For the injections embryos were immobilized by putting them into cavities cut in 2% agar-coated Petri dishes. CM-DiI stock solution (2 µg/µl in 100 % ethanol; Thermo Fisher Scientific) was diluted 1/20 in 0.1% sucrose-solution and 10-20 nl were injected into the neural folds of embryos between stages 18 and 20 using FEMTOJET (Eppendorf). Injections were done unilaterally into the neural fold overlaying somite one, two or three on either the right or the left side of the embryo. The success of the

injection experiments was checked between 30 to 60 minutes after the injection using a fluorescent stereo microscope (Stemi SV 11, Zeiss). Embryos were raised in the dark at 18 to 20°C until the desired stage, anesthetized and fixed in 4% para-formaldehyde (PFA) for paraffin sectioning. Nineteen embryos which showed a strong DiI-labeling in the neural fold and no other adjacent tissues were used for subsequent analysis. Injected embryos showing edema or abnormal development were not included in the analysis.

Paraffin sections

PFA-fixed specimens were de-hydrated through an ethanol series (30%, 50%, 70%, 80%, 90%, 96%, 99%, for 30 minutes each) and transferred to Neoclear (Sigma Aldrich). After 30 minutes, specimens were embedded in paraffin and sectioned into 7 µm transverse sections using a HM360 Microm (Germany). Sections were embedded in Mowiol and stored at 4°C. Counterstaining of the tissue was not required due to the autofluorescence of the tissue at 488 nm. Single sections were photographed with Zeiss microscope using the Spot software (Spot Imaging Inc.). Images of autofluorescence (488 nm) were converted to greyscale for a better visualization and brightness and contrast were adjusted using ImageJ.

Heterotopic neural crest cell transplantation

Two axolotl embryos, a donor (stage 25 to 27) and a host (stage 20-22), were placed side by side into cavities cut in 2% agarose-coated Petri dishes in 80% Steinberg's solution. Operations were carried out using sharpened minutiae needles (Fiebig Lehrmittel, Berlin, Germany, #1184-0001) glued into glass Pasteur pipets. The epidermis overlaying the branchial region was peeled off in the donor embryo (Fig. 1A) Neural crest cells from the posterior branchial stream were removed (Fig. 1A'). A piece of donor branchial neural crest stream was placed beside the host embryo. The

epidermis of the host overlaying the mesoderm of the heart field was peeled off (Fig. 1B) and the donor neural crest cells were placed on top of the mesoderm. The epidermis was then folded back and kept in place with a piece of glass coverslip for around five minutes (Fig. B'). Afterwards the operated host embryo was placed in a new agar-coated Petri dish containing 20% Steinberg's solution with 4% gentamicin (Thermo Fisher Scientific, #15750060). Care was taken, that the maximum time of embryos in 80% Steinberg's Solution was 15 minutes, because longer times results in malformations and increased lethality. In six surgeries GFP-positive neural crest cells were transplanted to a host and photographed after around two hours to test if transplanted neural crest cells were accepted by the host (Fig. 1C-C''). Neural crest transplantations were performed in 32 embryos, 15 of them survived and were used for analysis. As a first control experiment, pieces of ventral head mesoderm were transplanted from a donor embryo (stage 20-21) into a host as described for neural crest cells (mesoderm transplant). Mesoderm transplantations were performed in 19 embryos, eight of them survived and were used for analysis. As a second control experiment the epidermis of "host" embryos was peeled off and folded back after two to three minutes without receiving any donor cells. These sham operations were performed in 17 embryos, nine of them survived and were used for analysis. Photographs were taken using a Zeiss Axioplan microscope equipped with a digital camera, using the Zeiss "Axioplan" software. Subsequent, image adjustments were done in ImageJ.

Fluorescent whole mount antibody staining

Specimens were fixed in Dent's fixative for a minimum of one day and bleached in Dent's bleach (10% hydrogen peroxide in Dent's fixative) for 4 hours under a normal desk lamp. All incubations were carried out at room temperature (21 to 25°C). Antibody staining was conducted on whole mounts according to standard protocols (Klymkowsky

and Hanken, 1991). After bleaching, specimens were washed 3 times in PBS + 0.1 % TritonX-100 for 20 minutes each. They were then blocked for 2 hours in DAKO antibody diluent. Antibodies against desmin (Monosan, PS031) and acetylated alpha-tubulin (Sigma, T6793) were applied as primary antibodies (1:200 and 1:500 in DAKO antibody diluent) and incubated overnight. On the next day specimens were washed again 3 times in PBS + 0.1 % TritonX-100 for 20 minutes each and blocked in DAKO antibody diluent for 2 hours. Afterwards, Alexa568-anti-rabbit (Thermo Fisher Scientific, Product # R37120) and Alexa488-anti-mouse (Thermo Fisher Scientific, Product # A-11011) were applied as secondary antibodies (1:500 in DAKO antibody diluent) and incubated overnight. Stained specimens were dehydrated twice in 100 % methanol for 10 minutes each and cleared and stored in BABB (benzyl alcohol/ benzyl benzoate, 1/2). Digital stacks from the antibody stainings were obtained using a Zeiss LSM510 confocal microscope and processed with ZEN 2012.

Results

NCCs do not contribute to early heart development in the Mexican axolotl

To label pre-migratory NCCs, neural folds of axolotl embryos at stage 17 to 19 were injected on either the right or the left side. Injections were placed either at the level of the posterior cranial paraxial mesoderm and somite one (I in Fig. 2A) or somites two and three (II in Fig. 2A). A complete list of specimens is given in table 1.

Axolotl NCCs migrate as described in earlier studies (Epperlein et al., 2000; Ericsson et al., 2004; Falck et al., 2002). The branchial NCCs start to migrate around stage 22 (Fig. 2B and F). At around stage 32 they have reached the branchial arches and the anlagen of the external gills (Fig. 2C and G). At this stage, a population of NCCs posterior to the last branchial arch can be found in embryos injected in region II (Fig. 2G; blue arrows).

This region corresponds to the circumpharyngeal ridge first described in chicken embryos (Kuratani and Kirby, 1991). At stage 40/41, DiI positive NCCs have spread over the entire branchial region and the external gills (Fig. 2D and H). No DiI signal is visible in the region of the heart in whole mount specimens (Fig. 2E and I). In paraffin sections DiI signals are detectable in the neural tube, the ganglia of the vagal and posterior lateral line nerves, branchial branches of the vagal nerve and the connective tissue of the developing branchial levator muscles (Fig. 3A to E). No DiI-labeled cells were found in the heart of axolotl larvae at stage 40/41 (Fig. 3F).

Early heart tube formation starts posterior to the head/trunk interface

At stage 33/34, a strong signal of the desmin antibody is recognizable in the heart tube directly anterior to the yolk sac (Fig. 4A). The posterior cranial NCCs have migrated into the branchial arches and the circumpharyngeal ridge (see Fig. 2C, G). The circumpharyngeal crest cells demarcate the head/trunk interface. These NCCs are located dorsally to the developing heart tube.

At stage 41/42, NC derived neurons of the vagal and hypoglossal nerves are recognizable by a signal from the antibody against acetylated alpha-tubulin (Fig. 4B). The hypoglossal nerve runs anteriorly alongside and innervates the rectus cervicis muscle. The pattern of both the hypoglossal nerve and the rectus cervicis muscle on each side demarcates the triangular-shaped head/trunk interface (Fig. 4B, dashed line). The heart has undergone loop-formation and distinct chambers are recognizable. It is positioned posteroventral to the head/trunk interface (Fig. 4B). This pattern can also be observed at later developmental stages (e.g. stage 44/45, Fig. 4C).

Cranial NCCs inhibit muscle differentiation in the primary heart tube

To test if the early heart tube is able to differentiate in a “head environment” we transplanted pieces of branchial NC on top of the heart primordium. Sham operations and head mesoderm transplants were carried out as controls to exclude secondary effects of the surgical procedure and the added cell mass. The three different surgeries were compared to non-operated control embryos at the same stage. Specimens were fixed and investigated either at early, pre-heart beat stages (stage 33/34) or at later stages, when the heart has already started beating (stage 36/34).

In control embryos at stage 33/34 (Fig. 5A, n=5), the myocardium of the heart tube completely encloses the endocardium. The beginning of loop formation is indicated by a slight, left-side bending of the heart tube. A kink divides the heart into the posterior venous pole and the anterior arterial pole. A desmin signal can be detected, showing the highest intensity at the posterior venous pole. The desmin signal intensity decreases at the arterial pole. The heart tubes of stage-matched sham operated specimens (Fig. 5B, n=5) and specimens which received a head mesoderm transplant (Fig. 5C, n=5) appear similar to the non-operated controls. No heart tube was found in most specimens that received a cranial NC transplant (Figs. 5D and 6A, n=3/4). A desmin signal is only detectable in a small area in the position of the heart anlage at earlier stages. In one of the four specimens, a malformed heart tube has formed showing a weak desmin signal (Fig. 6B).

In control embryos at stage 36/37 (Fig. 5E, n=4), the heart has started beating. The myocardium has increased in thickness and a strong desmin signal can be observed over the entire heart tube. Loop-formation has progressed and the heart is now forming a left-sided, s-curve. The area of the later ventricle and atrium appear more inflated and are clearly distinguishable from the inflow and outflow areas. The hearts of stage-matched

sham operated specimens (Fig. 5F, n=4) and specimens which received a head mesoderm transplant (Fig. 54G, n=3) appear similar to the non-operated controls. Slightly different intensities of the desmin signals can be observed in different specimens of these three control experiments. This might be due to slight differences in the developmental stages of the heart (e.g. Fig. 5E and F). Specimens that received a branchial NC transplant (n=11) can be grouped in two different categories. Specimens of category one (n=4/11) show a delay in heart development compared to stage-matched control specimens (Figs. 5H, 6C). The heart tube has formed a left-sided s-shaped loop and shows a strong desmin signal. However, the regions that will give rise to the ventricle and atrium are clearly distinct but not inflated. The heartbeat frequency of these specimens was slower, compared to control specimens or specimens of category two. Specimens of category two (n=7/11) showed no difference in heart development compared to non-operated control embryos (Fig. 6D).

Discussion

The development and evolution of the chambered heart in vertebrates has been researched extensively (Jensen et al., 2013; Rickert-Sperling et al., 2016). Studies in amniote and teleost model organisms have shown that at least two mesodermal cell populations, the FHF and SHF, and also the cardiac NCCs are involved in heart development (Diogo et al., 2015; Jiang et al., 2000; Kaartinen et al., 2004; Kang et al., 2009; Kirby et al., 1983; Kirby et al., 1985; Kirby and Waldo, 1995; Kodo et al., 2017; Li et al., 2003; Martinsen et al., 2004; Miyagawa-Tomita et al., 2016; Rickert-Sperling et al., 2016; Sato et al., 2006; Sato and Yost, 2003; Tirosh-Finkel et al., 2006b; Tomita et al., 2005; Tzahor, 2009; Tzahor and Lassar, 2001; Yelbuz et al., 2002; Yelbuz et al., 2003). Only a few studies examine the contribution of the cardiac neural crest to the heart of the amphibian model species *Xenopus laevis* (Lee and Saint-Jeannet, 2011;

Martinsen et al., 2004; Sadaghiani and Thiébaud, 1987). Interestingly, these studies report different results. Sadaghiani and Thiébaud, carrying out heterospecific NC transplantations, reported NC derived cells in the outflow tract of *X. laevis* at NF stage 39/40 (Sadaghiani and Thiébaud, 1987). Lee and Saint-Jeannet, carrying out fluorophore-marked NC transplantations, reported the absence of NC-derived cells in the outflow tract of *X. laevis* at NF stage 41 (Lee and Saint-Jeannet, 2011). Martinsen and colleagues, by ablating the cranial and parts of the trunk NC, reported abnormalities already at early stages of heart tube system development (Martinsen et al., 2004). All these studies share the problem that the investigation stops at a developmental stage (NF stage 41 latest) when the tadpole heart is not completely developed. In *X. laevis* this is the case at NF stage 46 (Kolker et al., 2000; Mohun et al., 2000), and a later contribution of NCCs to the heart can therefore not be excluded. In 2012 Epperlein and colleagues reported a NC contribution to “the truncus arteriosus and septa of the heart” in two months old axolotl juveniles (Epperlein et al., 2012). However, a detailed anatomical description is missing. Most of these studies have in common that they investigate mid to late stages of heart development when the primary heart tube has already formed and cells derived from the SHF enter the heart tube.

In the present study we examined the interactions of cardiac NCCs and mesodermal heart precursors in the Mexican axolotl. We showed that the NC does not contribute physically to early heart tube formation. Furthermore, we described that the formation of the primary heart tube starts posteroventrally to the posterior branchial arches and the circumpharyngeal ridge demarcating the vertebrate head/trunk interface (Kuratani, 1997). It thus develops in a region free of cranial neural crest cells.

By transplanting cranial NC on top of the heart primordium we showed that cranial NCCs inhibit myogenesis at early stages of heart development (stage 33/34). This effect

seems to be compensated in later stages of heart development (stage 36/37). The compensatory effect might have different reasons. (1) Myogenesis in the heart tube increases after the inhibitory effect of NCCs has faded. This could be caused either by cells derived from the FHF itself or by invading cells from the SHF. This possibility would represent a regenerative effect of the developing heart. (2) Slightly different sizes of NC transplants could also cause different results. This would represent a dose-dependent effect of factors secreted by NCCs on the differentiating heart muscle precursors. In our view the first option might be more likely because of the severe phenotypes of early stages of heart development (stage 33/34). However, a larger sample size and data from between stages 33 and 47 are needed to decide which effect plays the major role.

Due to our observations that cranial NCCs inhibit heart muscle differentiation in the primary heart tube, we propose a speculative but testable scenario for the development and evolution of the amphibian heart. At a late neurula stage, the anterior SHF and the posterior FHF are located ventral to the cranial NC (Fig. 7A) (Lee and Saint-Jeannet, 2011). During early morphogenesis of the head and the onset of cranial NCC migration the FHF is displaced posteroventrally (Fig. 7B). The new position of the FHF is therefore posterior to the head/trunk interface. Later, the SHF becomes separated from the FHF by the formation of the branchial arches (Fig. 7C). NCCs migrate into the branchial arches and promote differentiation of the cranial musculature from cells of the cranial paraxial mesoderm and the SHF (Tzahor, 2009). The posterior-most cranial NCCs, the circumpharyngeal crest cells, settle in the circumpharyngeal ridge. They do not migrate further ventrally or posteriorly (Kuratani, 1997) maybe because this pathway is blocked by the pharyngeal mesenchyme. It has been shown that signals from the NC, the neural tube, the pharyngeal endoderm, as well as the surface ectoderm are integrated to first keep cells of the SHF in a proliferative state and promote

differentiation at later developmental stages (Lazic and Scott, 2011). In our model, the FHF-derived primary heart tube develops outside of the head, in an environment free from NCCs and maybe other signaling tissues in the head (Fig. 7C). This results in heart muscle differentiation and morphogenesis of the primary heart tube at relatively early developmental stages. Later, cells from the SHF migrate towards and enter the primary heart tube (Fig. 7D) (Sato et al., 2006). They form the complete outflow tract and partly contribute the myocardium of the ventricle (Lee and Saint-Jeannet, 2011). Attracted by Sema3C expressed by SHF cells, cardiac NCCs migrate through the pharyngeal arch arteries and enter the outflow tract (Fig. 7E) (Kodo et al., 2017). In contrast to amniotes, the NCC contribution to the amphibian outflow tract takes place at very late stages of heart development. However, as in amniotes, the cardiac NC later contributes to the formation of the outflow tract in both *Xenopus* (Sadaghiani and Thiébaud, 1987) and the axolotl (Epperlein et al., 2012) (Fig. 7F).

This scenario can be tested by preparing long-term fate maps of the FHF, SHF and cardiac NC in *Xenopus* and the axolotl. A fate map of the FHF, SHF and cardiac NC in *Xenopus* has been prepared in an earlier study (Lee and Saint-Jeannet, 2011). Unfortunately, this study does not examine the venous pole of the heart and stops at a stage when heart development is not completed. We think that the reported absence of NCCs in the outflow tract of *Xenopus* might be an artifact caused by a too early examination of the specimens in this study. More detailed fate maps in *Xenopus* and axolotl and details about the dynamics of NC-heart interactions are needed to draw robust scenarios about heart development and evolution in amphibians and vertebrates in general.

Acknowledgements

This project was funded by the Deutsche Forschungsgemeinschaft (Grant Number: DFG-OL 134/10-2 to LO).

References

- Bordzilovskaya NP, Detlaff TA. 1989. Table of stages of the normal development of axolotl embryos and the prognostication of timing of successive developmental stages at various temperatures. *Axolotl Newsletter* 7:2-22.
- Delsuc F, Brinkmann H, Chourrout D, Philippe H. 2006. Tunicates and not cephalochordates are the closest living relatives of vertebrates. *Nature* 439(7079):965.
- Diogo R, Kelly RG, Christiaen L, Levine M, Ziermann JM, Molnar JL, Noden DM, Tzahor E. 2015. A new heart for a new head in vertebrate cardiopharyngeal evolution. *Nature* 520(7548):466-473.
- Epperlein H, Meulemans D, Bronner-Fraser M, Steinbeisser H, Selleck M. 2000. Analysis of cranial neural crest migratory pathways in axolotl using cell markers and transplantation. *Development* 127(12):2751-2761.
- Epperlein HH, Khattak S, Knapp D, Tanaka EM, Malashichev YB. 2012. Neural crest does not contribute to the neck and shoulder in the axolotl (*Ambystoma mexicanum*). *PLoS One* 7(12):e52244.
- Ericsson R, Cerny R, Falck P, Olsson L. 2004. Role of cranial neural crest cells in visceral arch muscle positioning and morphogenesis in the Mexican axolotl, *Ambystoma mexicanum*. *Developmental Dynamics* 231(2):237-247.
- Falck P, Hanken J, Olsson L. 2002. Cranial neural crest emergence and migration in the Mexican axolotl (*Ambystoma mexicanum*). *Zoology* 105(3):195-202.
- Gans C, Northcutt RG. 1983. Neural crest and the origin of vertebrates: a new head. *Science* 220(4594):268-273.
- Hall BK. 1999. *The neural crest in development and evolution*: Springer Science & Business Media.
- Hall BK. 2000. The neural crest as a fourth germ layer and vertebrates as quadroblastic not triploblastic. *Evolution and Development* 2(1):3-5.

- Holland ND, Venkatesh TV, Holland LZ, Jacobs DK, Bodmer R. 2003. *AmphiNk2-tin*, an amphioxus homeobox gene expressed in myocardial progenitors: insights into evolution of the vertebrate heart. *Developmental Biology* 255(1):128-137.
- Jensen B, Wang T, Christoffels VM, Moorman AF. 2013. Evolution and development of the building plan of the vertebrate heart. *Biochimica et Biophysica Acta* 1833(4):783-794.
- Jiang X, Rowitch DH, Soriano P, McMahon AP, Sucov HM. 2000. Fate of the mammalian cardiac neural crest. *Development* 127(8):1607-1616.
- Kaartinen V, Dudas M, Nagy A, Sridurongrit S, Lu MM, Epstein JA. 2004. Cardiac outflow tract defects in mice lacking *ALK2* in neural crest cells. *Development* 131(14):3481-3490.
- Kang J, Nathan E, Xu SM, Tzahor E, Black BL. 2009. *Isl1* is a direct transcriptional target of Forkhead transcription factors in second-heart-field-derived mesoderm. *Developmental Biology* 334(2):513-522.
- Kirby ML, Gale TF, Stewart DE. 1983. Neural crest cells contribute to normal aorticopulmonary septation. *Science* 220(4601):1059-1061.
- Kirby ML, Turnage KL, Hays BM. 1985. Characterization of conotruncal malformations following ablation of "cardiac" neural crest. *The Anatomical Record* 213(1):87-93.
- Kirby ML, Waldo KL. 1995. Neural crest and cardiovascular patterning. *Circulation Research* 77(2):211-215.
- Klymkowsky MW, Hanken J. 1991. Whole-mount staining of *Xenopus* and other vertebrates. *Methods in Cell Biology* 36:419-441.
- Kodo K, Shibata S, Miyagawa-Tomita S, Ong S-G, Takahashi H, Kume T, Okano H, Matsuoka R, Yamagishi H. 2017. Regulation of *Sema3c* and the Interaction between Cardiac Neural Crest and Second Heart Field during Outflow Tract Development. *Scientific Reports* 7(1):6771.
- Kolker SJ, Tajchman U, Weeks DL. 2000. Confocal imaging of early heart development in *Xenopus laevis*. *Developmental Biology* 218(1):64-73.
- Kuratani S. 1997. Spatial distribution of postotic crest cells defines the head/trunk interface of the vertebrate body: embryological interpretation of peripheral nerve morphology and evolution of the vertebrate head. *Anatomy and Embryology (Berl)* 195(1):1-13.

- Kuratani SC, Kirby ML. 1991. Initial migration and distribution of the cardiac neural crest in the avian embryo: an introduction to the concept of the circumpharyngeal crest. *Developmental Dynamics* 191(3):215-227.
- Lazic S, Scott IC. 2011. Mef2cb regulates late myocardial cell addition from a second heart field-like population of progenitors in the zebrafish. *Developmental Biology* 354(1):123-133.
- Lee YH, Saint-Jeannet JP. 2011. Cardiac neural crest is dispensable for outflow tract septation in *Xenopus*. *Development* 138(10):2025-2034.
- Li YX, Zdanowicz M, Young L, Kumiski D, Leatherbury L, Kirby ML. 2003. Cardiac neural crest in zebrafish embryos contributes to myocardial cell lineage and early heart function. *Developmental Dynamics* 226(3):540-550.
- Martinsen BJ, Frasier AJ, Baker CV, Lohr JL. 2004. Cardiac neural crest ablation alters Id2 gene expression in the developing heart. *Developmental Biology* 272(1):176-190.
- Miyagawa-Tomita S, Arima Y, Kurihara H. 2016. The “Cardiac Neural Crest” Concept Revisited. *Etiology and Morphogenesis of Congenital Heart Disease: Springer*. p 227-232.
- Mohun TJ, Leong LM, Weninger WJ, Sparrow DB. 2000. The morphology of heart development in *Xenopus laevis*. *Developmental Biology* 218(1):74-88.
- Nie S, Bronner ME. 2015. Dual developmental role of transcriptional regulator Ets1 in *Xenopus* cardiac neural crest vs. heart mesoderm. *Cardiovascular Research* 106(1):67-75.
- Nye HL, Cameron JA, Chernoff EA, Stocum DL. 2003. Extending the table of stages of normal development of the axolotl: limb development. *Developmental Dynamics* 226(3):555-560.
- Rickert-Sperling S, Kelly RG, Driscoll DJ. 2016. *Congenital Heart Diseases: The Broken Heart*. Vienna: Springer <http://doi.org/10.1007/978-3-7091-1883-2>.
- Sadaghiani B, Thiébaud CH. 1987. Neural crest development in the *Xenopus laevis* embryo, studied by interspecific transplantation and scanning electron microscopy. *Developmental Biology* 124(1):91-110.
- Sato M, Tsai H-J, Yost HJ. 2006. Semaphorin3D regulates invasion of cardiac neural crest cells into the primary heart field. *Developmental biology* 298(1):12-21.
- Sato M, Yost HJ. 2003. Cardiac neural crest contributes to cardiomyogenesis in zebrafish. *Developmental Biology* 257(1):127-139.

- Schlosser G. 2010. Making senses: development of vertebrate cranial placodes. *International review of cell and molecular biology*: Elsevier. p 129-234.
- Schlosser G. 2014. Early embryonic specification of vertebrate cranial placodes. *Wiley Interdisciplinary Reviews: Developmental Biology* 3(5):349-363.
- Tirosh-Finkel L, Elhanany H, Rinon A, Tzahor E. 2006a. Mesoderm progenitor cells of common origin contribute to the head musculature and the cardiac outflow tract. *Development* 133(10):1943-1953.
- Tirosh-Finkel L, Elhanany H, Rinon A, Tzahor E. 2006b. Mesoderm progenitor cells of common origin contribute to the head musculature and the cardiac outflow tract. *Development* 133(10):1943-1953.
- Tomita Y, Matsumura K, Wakamatsu Y, Matsuzaki Y, Shibuya I, Kawaguchi H, Ieda M, Kanakubo S, Shimazaki T, Ogawa S. 2005. Cardiac neural crest cells contribute to the dormant multipotent stem cell in the mammalian heart. *Journal of Cell Biology* 170(7):1135-1146.
- Tzahor E. 2009. Heart and craniofacial muscle development: a new developmental theme of distinct myogenic fields. *Developmental Biology* 327(2):273-279.
- Tzahor E, Evans SM. 2011. Pharyngeal mesoderm development during embryogenesis: implications for both heart and head myogenesis. *Cardiovascular Research* 91(2):196-202.
- Tzahor E, Lassar AB. 2001. Wnt signals from the neural tube block ectopic cardiogenesis. *Genes & development* 15(3):255-260.
- Waldo K, Miyagawa-Tomita S, Kumiski D, Kirby ML. 1998. Cardiac neural crest cells provide new insight into septation of the cardiac outflow tract: aortic sac to ventricular septal closure. *Developmental Biology* 196(2):129-144.
- Waldo KL, Hutson MR, Stadt HA, Zdanowicz M, Zdanowicz J, Kirby ML. 2005. Cardiac neural crest is necessary for normal addition of the myocardium to the arterial pole from the secondary heart field. *Developmental Biology* 281(1):66-77.
- Yelbuz TM, Waldo KL, Kumiski DH, Stadt HA, Wolfe RR, Leatherbury L, Kirby ML. 2002. Shortened outflow tract leads to altered cardiac looping after neural crest ablation. *Circulation* 106(4):504-510.
- Yelbuz TM, Waldo KL, Zhang X, Zdanowicz M, Parker J, Creazzo TL, Johnson GA, Kirby ML. 2003. Myocardial volume and organization are changed by failure of

addition of secondary heart field myocardium to the cardiac outflow tract.
Developmental Dynamics 228(2):152-160.

specimen #	injection site		analyzed stage
	left	right	
Ani065	I		40
Ani088		I	41
Ani092		II	40
Ani096		I	41
Ani106	II		40
Ani114	II		41
Ani115		I	40
Ani116	I		40/41
Ani123		II	40
Ani126		II	41
Ani128	II		41
Ani131	II		41
Ani139		I	40
Ani155	I		40
Ani167	I		41
Ani168	II		41
Ani170		II	41/42
Ani176		I	41

Table 1: Specimens list of cranial fold injections. I, DiI injection in region I (Fig. 2A); II DiI injection in region II (Fig. 2A).

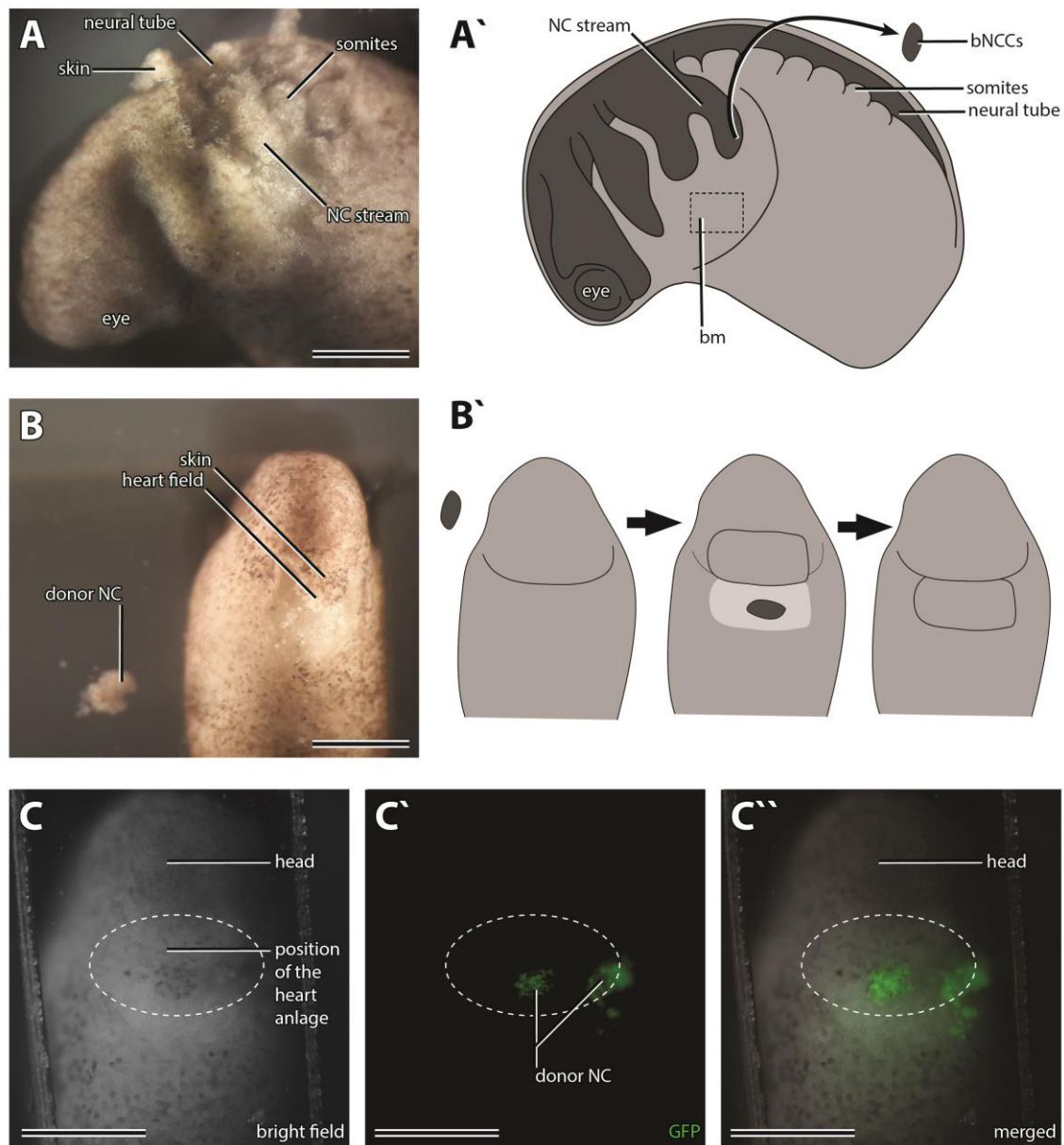


Figure 1: Experimental procedure of neural crest cell transplantations. A, micrograph of an axolotl embryo at stage 26 serving as the donor for neural crest transplantation. The skin overlaying the branchial region has been peeled off to make it possible to ablate the branchial neural crest stream. A'. Schematic illustration of branchial neural crest stream ablation in donor axolotl embryo. The dashed line indicates the region where cranial mesoderm has been removed in control surgeries. B, host axolotl embryo at stage 21/22 from a ventral view. The skin overlaying the heart anlage has been peeled off. Donor branchial neural crest cells are positioned beside the host embryo. B', schematic illustration of the transplantation procedure. C to C'', ventral views of donor embryos two hours after transplantation. bNCCs, branchial neural crest cells; bm, branchial mesoderm; NC, neural crest. Scale bar is 500 μ m.

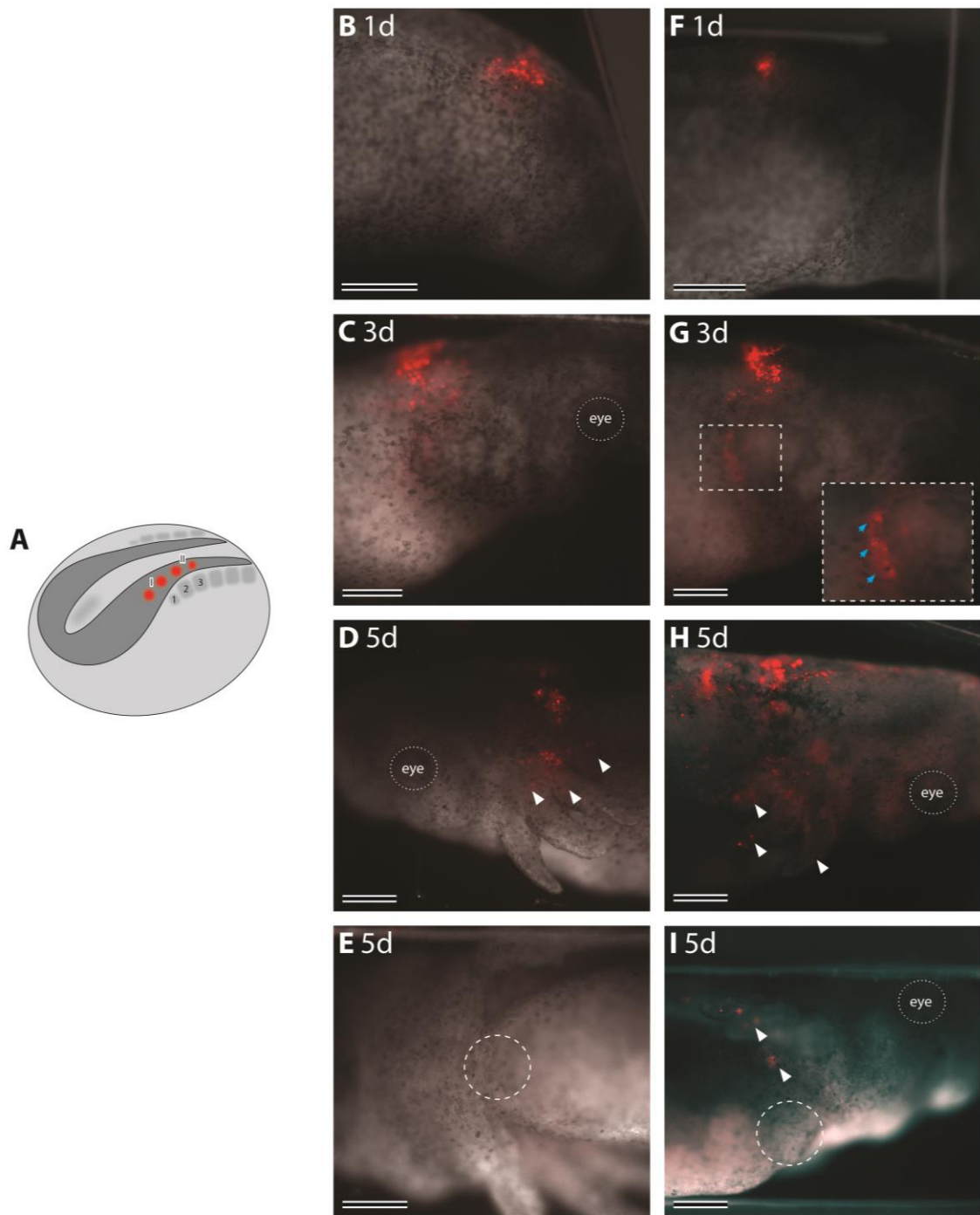


Figure 2: DiI injection of cranial neural crest cells. A, schematic illustration of an axolotl neurula at stage 18. Red dots indicate the sites of DiI injection. Either the region overlaying the unsegmented head mesoderm and somite one (I), or the region overlaying somite two and three (II) was injected. Arabic numbers refer to somite identity. B, lateral view of an axolotl embryo injected in region I at stage 25 (1 day after injection). C, lateral view of an axolotl embryo injected in region I at stage 32 (3 days after injection). D, lateral view of an axolotl embryo injected in region I at stage 40/41 (5 days after injection). E, ventral view of the specimen in D. F, lateral view of an axolotl embryo injected in region II at stage 25 (1 day after injection). G, lateral view of an axolotl embryo injected in region II at stage 32 (3 days after injection). H, lateral view of an axolotl embryo injected in region II at stage 40/41 (5 days after injection). I, ventral view of the specimen in D. White arrows indicate DiI signals in migrating neural crest cells. Blue arrows indicate the circumpharyngeal crest cells. Scale bar is 500 μm .

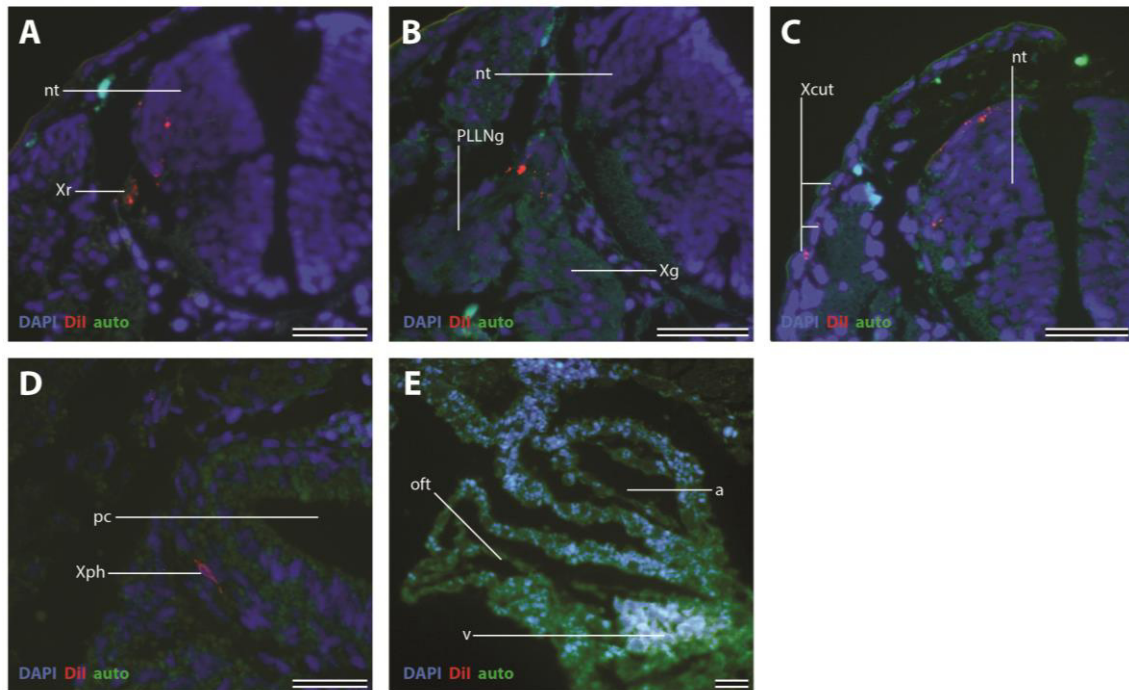


Figure 3: Cross section of axolotl larvae injected with DiI at stage 40/41. A, DiI signal in the neural tube and the root of the vagal nerve. B, DiI signal in the stems of the vagal and posterior lateral line nerve. C, DiI signal in cutaneous branches of the vagal nerve and the neural tube. D, DiI signal in a pharyngeal of the vagal nerve. E, no signal can be found in the outflow tract or other parts of the heart. Xcut, cutaneous rami of the vagal nerve; Xg, ganglion of the vagal nerve; Xph, pharyngeal ramus of the vagal nerve; Xr, root of the vagal nerve; nt, neural tube; pc, pharyngeal cavity; PLLNg, ganglion of the posterior lateral line nerve. Scale bar is 100 μ m.

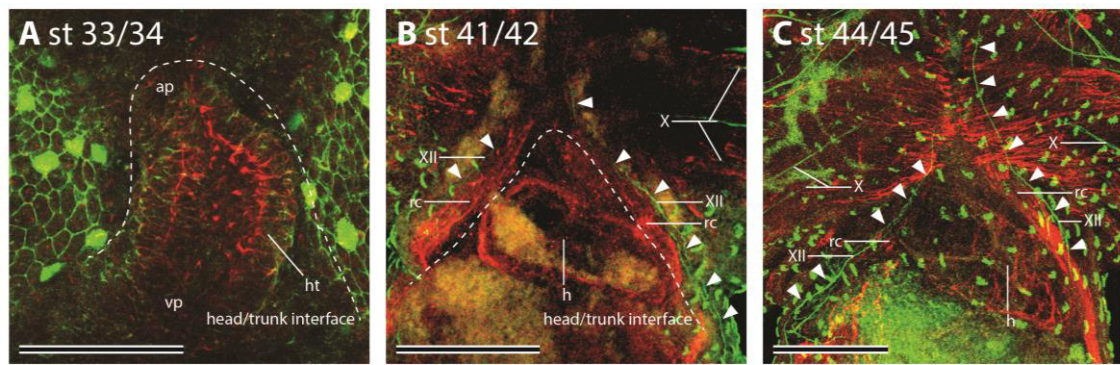


Figure 4: Ventral views of the posterior head region of whole mount antibody stainings of axolotl larvae at different developmental stages. Muscles are stained with an antibody against desmin (red) and nerves are stained with an antibody against acetylated alpha-tubulin (green). A, stage 33/34. B, stage 41/42. C, stage 44/45. White arrows indicate the hypoglossal nerve. The dashed line marks the head/trunk interface. X, vagal nerve; XII, hypoglossal nerve; ap, arterial pole; h, heart; ht, heart tube; rc, rectus cervicis; vp, venous pole. Scale bar is 300 μm .

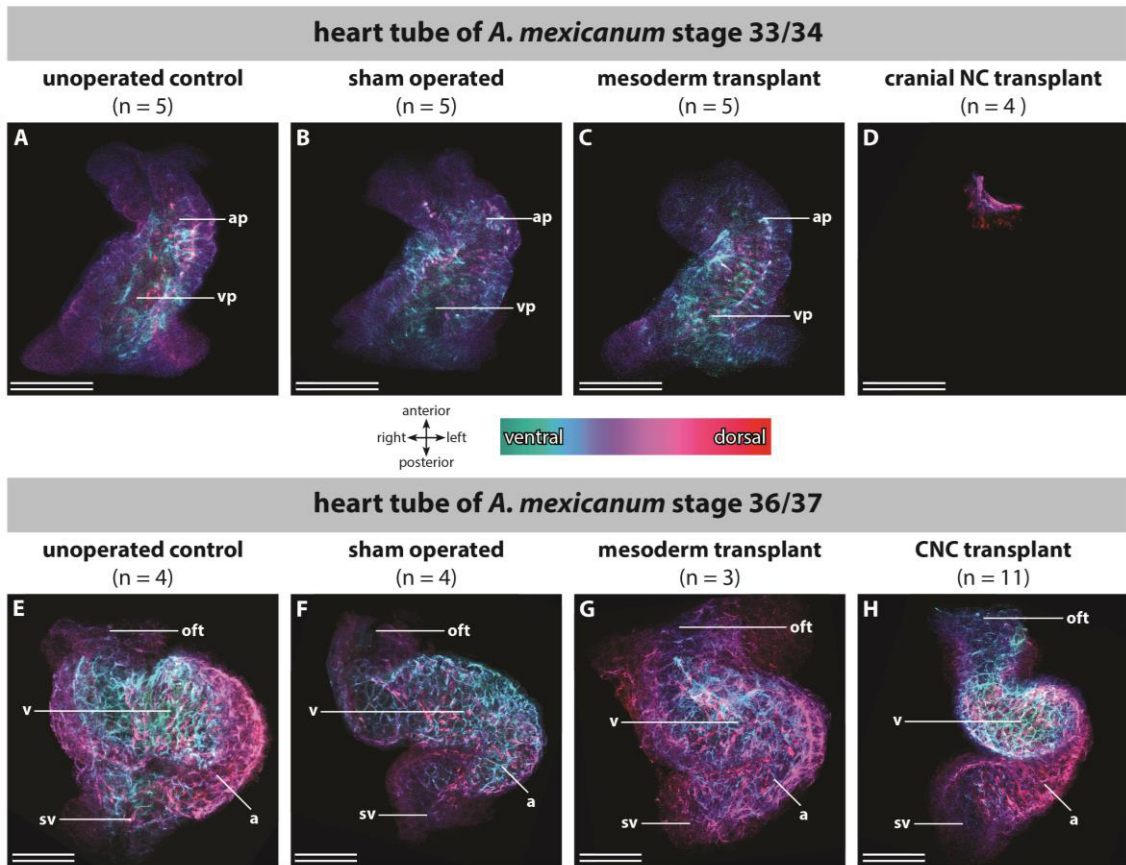


Figure 5: Ventral views of the heart tubes of axolotl larvae stained with an antibody against desmin. The images are shown in a depth coding view where cold colors are close to the observer (ventral) and warm colors are far from the observer (more dorsal). A to B, axolotl larvae at stage 33/34 before the heart starts beating. A, control. B, sham operated. C, host embryo that received a cranial mesoderm transplant from a donor embryo at stage 26. D, host embryo that received a cranial neural crest cell transplant from a donor embryo at stage 26. E to H, axolotl larvae at stage 36/37 after the heart has started beating. E, control. F, sham operated. G, host embryo that received a cranial mesoderm transplant from a donor embryo at stage 26. H, host embryo that received a cranial neural crest cell transplant from a donor embryo at stage 26. a, atrium; ap, arterial pole; oft, outflow tract; sv, sinus venosus; v, ventricle; vp, venous pole. Scale bar is 200 μm .

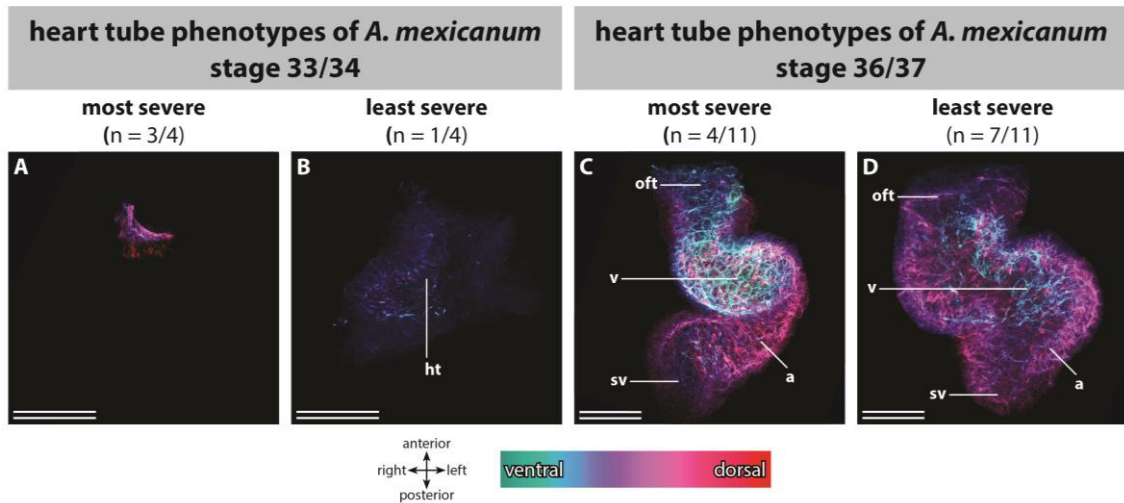


Figure 6: Ventral views of the heart tubes of axolotl larvae stained with an antibody against desmin. The images are shown in a depth coding view where cold colors are close to the observer (ventral) and warm colors are far from the observer (more dorsal). Host embryos that received a cranial neural crest cell transplant from a donor embryo at stage 26. A and B, axolotl larvae at stage 33/34. A, most severe phenotype. B, least severe phenotype. C and D, axolotl larvae at stage 36/37. C, most severe phenotype. D, least severe phenotype. Scale bar is 200 μm .

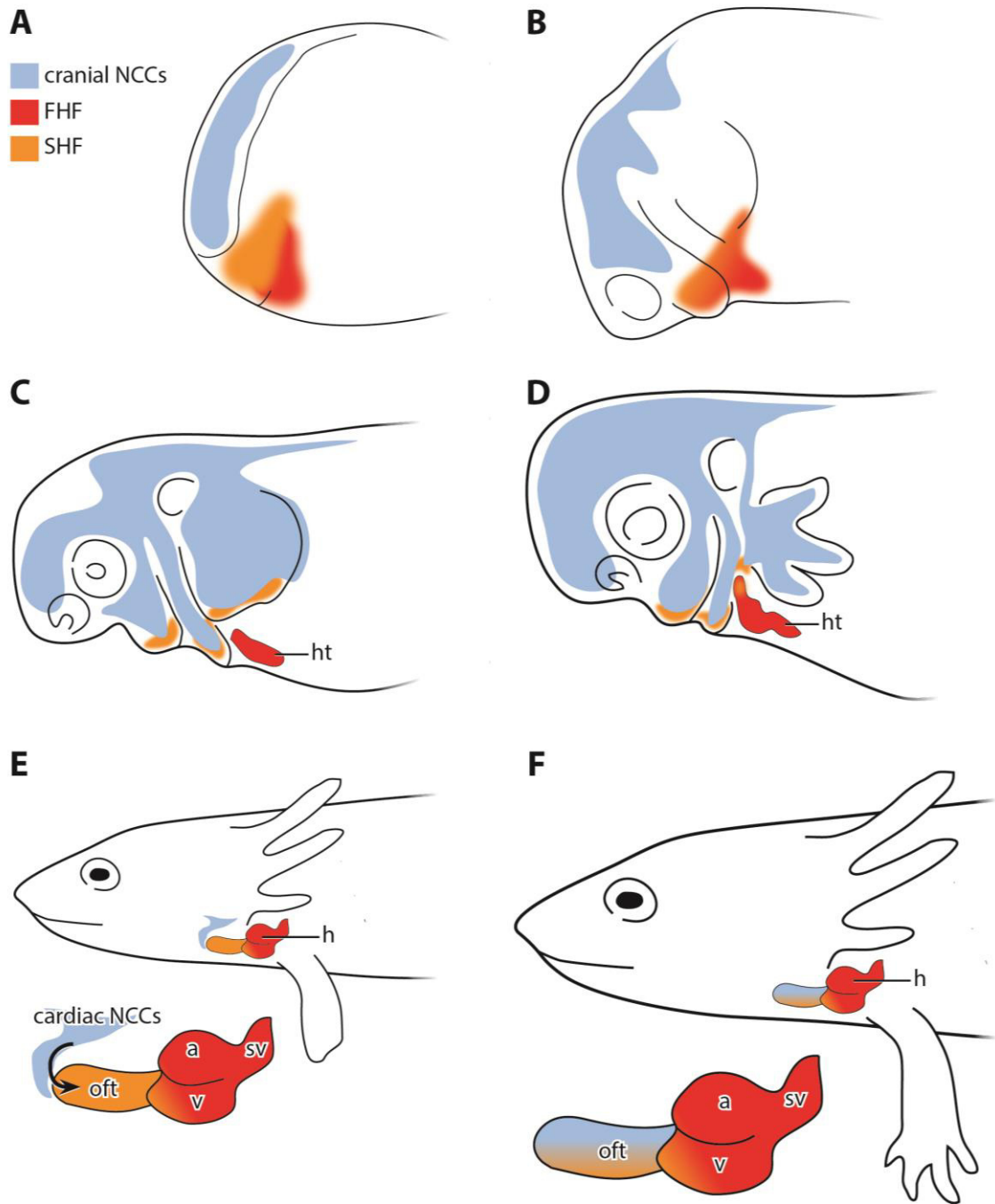


Figure 7: Schematic diagram of heart development in amphibians. Cranial neural crest cells (NCCs) are colored in light blue, cells of the first heart field (FHF) in red and cells of the second heart field (SHF) in orange. A, late neurula stage. B, “tadpole” stage. C, early larval stage. D, mid larval stage. E, late larval stage. F, early juvenile stage. A, atrium; h, heart; ht, heart tube; oft, outflow tract; sv, sinus venosus; v, ventricle.

Discussion

Head, trunk and in between – The developmental and evolutionary pattern of the hypobranchial and cucullaris muscles

The head/trunk interface is the domain of the vertebrate body where the cucullaris and the hypobranchial muscles develop (Ericsson et al., 2013). Since the early 20th century there has been controversy about the developmental origin and evolution of the cucullaris muscle (Edgeworth, 1911; 1929; 1935). The hypobranchial muscles in contrast were often regarded as highly conservative and “unproblematic” in comparison to the cucullaris. However, recent studies show that there are still open questions about the development and evolution of the hypobranchial musculature as there are for the cucullaris (Ericsson et al., 2013).

The hypobranchial muscles

The hypobranchial muscles are present in jaw-less (Cyclostomata) as well as jawed vertebrates (Gnathostomata). They are always innervated by the spinal hypoglossal nerve (Edgeworth, 1935). In cyclostomes they connect the head to the hypaxial trunk musculature (Oisi et al., 2015) while in gnathostomes they connect the head to the pectoral girdle (Edgeworth, 1935; Ericsson et al., 2013; Gegenbaur, 1889). Based on the precise anatomical/morphological studies of outstanding morphologists in the 19th and early 20th century, it was thought that they always originate from the anterior-most somites only and are therefore of pure trunk origin (Edgeworth, 1935; Fürbringer, 1874; Gegenbaur, 1889). Thus, the hypobranchial musculature prevailed as highly conserved in contrast to the dorsal cucullaris/trapezius muscle group. However, this conserved character of the hypobranchial musculature fades when recent developmental data are taken into account.

It has been shown that the hypobranchial muscles originate from both, the head mesoderm and the somites, in mouse (Czajkowski et al., 2014) and chicken (Harel et al., 2009; Theis, 2010; Theis et al., 2010). The migratory muscle precursors giving rise to the hypobranchial muscles are derived from *Pax3*-positive somitic mesoderm (Czajkowski et al., 2014; Harel et al., 2009; Theis et al., 2010). However, *Mesp1*-positive cells derived from cranial mesoderm are also present in these muscles (Czajkowski et al., 2014). Despite the mixed origin of the hypobranchial musculature, a governance by the trunk myogenic program seems to be predominant (Minchin et al., 2013). The connective tissue of the hypobranchial muscles in mouse and chicken seems to be derived from the cranial neural crest (NC) (Hosokawa et al., 2010; Matsuoka et al., 2005; Theis, 2010). Additionally, a role for lateral plate mesoderm in the migration of these muscle has also been reported (Lours-Calet et al., 2014).

The hypobranchial muscles of amphibians are derived from somitic mesoderm as has been shown by fate mapping studies of the anterior-most somites in *Ambystoma mexicanum* (Piekarski and Olsson, 2007) and gene expression studies in *X. laevis* (Lours-Calet et al., 2014). Transplantation experiments of GFP-positive cranial mesoderm showed no contribution to the hypobranchial muscles. The connective tissue of these muscles seems to be NC-derived. In studies on GFP-labeled NC-transplants in the Mexican axolotl a positive labeling of the connective tissue of the hypobranchial muscles cannot be seen in the depicted images by Epperlein et al. (2012) and Ericsson et al. (2004) but is visible in the study of Davidian and Malashichev (2014). Ablation of cranial NC streams in the fire-bellied toad, *Bombina orientalis* does not affect the hypobranchial muscles (Olsson et al., 2001). Thus it seems that the NC giving rise to the connective tissue of the hypobranchial muscles in amphibians is located at the level of the anterior-most somites. However, a detailed long-term fate mapping of the NC has to be carried out to answer this question. It has been shown that the migratory muscle

precursors that give rise to the hypobranchial muscles are *Pax3*-positive in *X. laevis* (Martin and Harland, 2001). Additionally, *FoxN3* morphants of *X. laevis* show severe patterning defects of the head muscles while the hypobranchial muscles are almost normal developed (Chapter 4). As in amniotes, this indicates that hypobranchial muscle development is governed by the trunk myogenic program.

Unfortunately, no detailed data about the connective tissue component and a possible cranial mesodermal contribution are available from non-tetrapod vertebrates.

Another interesting question is the number of somites that contribute in the formation of the hypobranchial musculature. These so-called occipital somites are different from the more posterior trunk somites in different ways. First, they give rise to the previously described migratory muscle precursors that migrate anteroventrally into the head. Second, they do not form distinct vertebrae but fuse to the neurocranium to form the occipital bone (Edgeworth, 1935). Third, they do not have an intermediate mesoderm giving rise to the pronephros. In the chicken, either four (Noden, 1983b) or five (Couly et al., 1993; Huang et al., 2000) somites contribute to the formation of the hypobranchial muscles. This seems to fit to the position of the pronephric glomerulus, the anterior-most component of the pronephros, at the border between somite five and six. In the axolotl, three somites give rise to the hypobranchial rectus cervicis and geniohyoideus muscles (Piekarski and Olsson, 2007). This corresponds to the position of the pronephric glomerulus at the border between somite three and four (own observations). In the shark (*Scyliorhinus torazame*) five somites can be counted to give rise to migratory muscle precursors migrating anteriorly to form the hypobranchial muscles (Adachi et al., 2018). The position of the pronephric glomerulus at the border between somite five and six in the closely related species *S. canicula* (Ballard et al., 1993) fits to this observation. In the basal actinopterygian species *Lepisosteus osseus* a

contribution of up to seven somites has been reported (Edgeworth, 1935) which does not fit with the observed position of the pronephric glomerulus at the border between somite three to four (own observations). In re-examination of the development of the branchial muscles in this species, we could show that the hypobranchial muscles develop from three to four somites instead of up to seven (Chapter 1). The same is true for the Siberian sturgeon (*Acipenser baerii*), another basal actinopterygian species (unpublished data). Thus, the unique identity of the occipital somites seems to be conserved at least in gnathostomes. However, the differing numbers between higher taxa indicate that there is some developmental and evolutionary variability. Recently a study by Adachi and colleagues proposed that a heterotopic rearrangement of the pericardium and posterior pharyngeal arches in the gnathostome developmental program may have occurred (Adachi et al., 2018). The anterior shift of the pericardium might have caused a relocation of the hypobranchial muscles from a primary position distal to the visceral arches (Cyclostomata) to a proximal position in regard to the mandibular and hyoid arch (Gnathostomata). This new position is in accordance with the evolutionary emergence of a tongue (Adachi et al., 2018). The hypobranchial musculature of this tongue might have acquired the potential to differentiate into more than five distinct muscles by the addition of cranial mesoderm in the amniote lineage (Czajkowski et al., 2014; Theis, 2010). However, if the cranial mesodermal component of the hypobranchial musculature is a synapomorphy of amniotes or if this trait is more widespread among vertebrates remains unclear.

In summary it can be said that the hypobranchial muscles are not as conserved and “simple” as stated by some authors. These muscles have experienced as much evolutionary change as the muscles spanning the dorsal aspect of the head/trunk interface (e.g. the cucullaris/trapezius muscle). Major events in the evolution of the hypobranchial muscles are shown in Figure 10 (“hm”-numbers).

Discussion

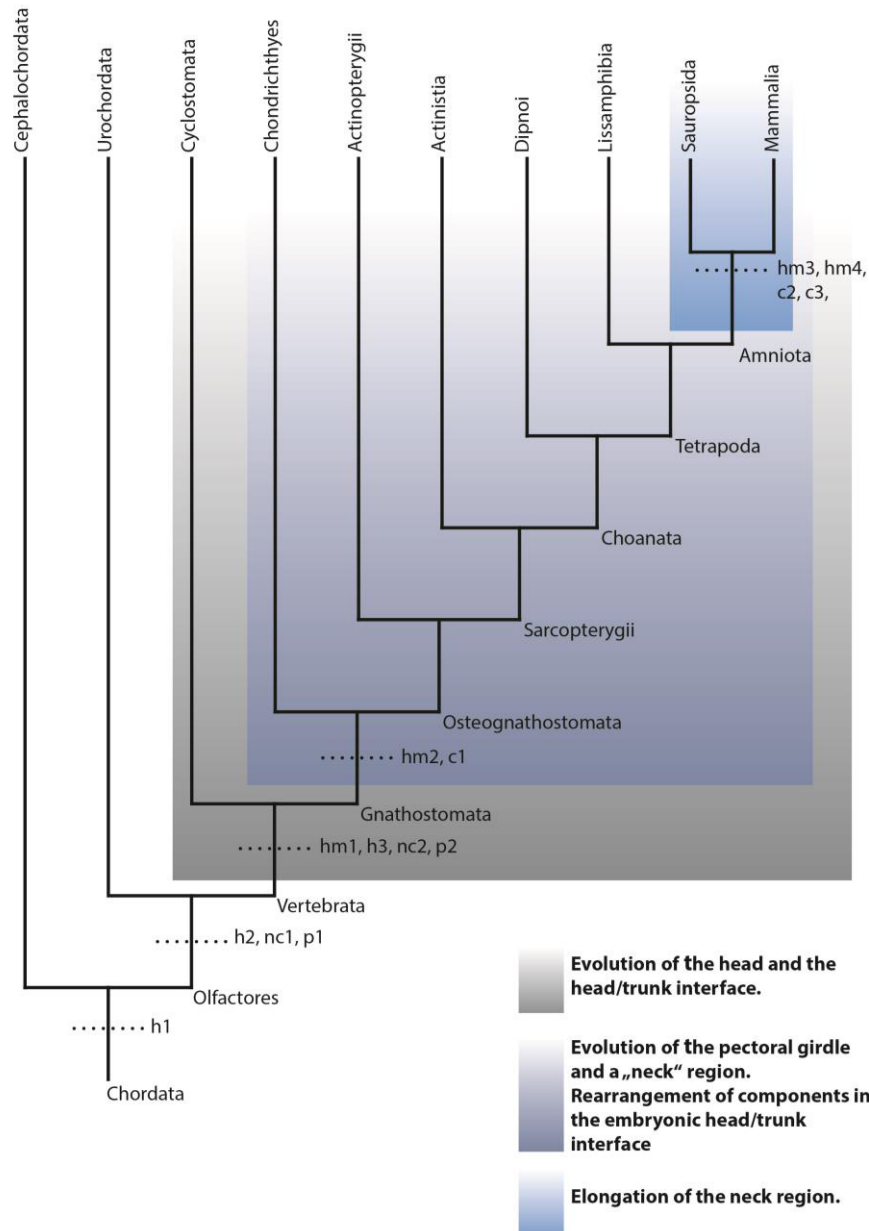


Figure 10: A cladogram of extant chordates showing major events connected to the evolution of the head and the head/trunk interface in vertebrates. c1: A cucullaris muscle derived from cranial *Mesp1*-positive cranial mesoderm innervated by the vagal nerve and connecting the head to the pectoral girdle. c2: Addition of a *Pax3*-positive mesodermal component from the somites to the cucullaris/trapezius and split into several distinct muscle portions. c3: Innervation of the cucullaris/trapezius muscle by the accessory nerve and additional spinal nerves in some taxa. h1: *Ilset1*-positive contractile vessel in the ventral body region (primary heart tube derived from the first heart field?). h2: *Nkx2-5*-positive cells (second heart field) that contribute to the heart tube. h3: Role of Neural crest in heart development and the evolution of a chambered heart. hm1: Hypobranchial musculature originating from migratory muscle precursors of the anterior somites and connecting the head to the hypaxial trunk musculature. hm2: Origin of the hypobranchial muscles from the pectoral girdle. hm3: heterotopic rearrangement of the pericard and a relocation of the hypobranchial muscles. hm4: Addition of a *Mesp1*-positive component from the cranial mesoderm to the hypobranchial muscles and split into several distinct muscles in the tongue. nc1: *Hnk1*-positive migratory pigment cells (pre-neural crest cells?). nc2: Neural crest cells that contribute to the cranial skeleton, peripheral nervous system and connective tissue of the head muscles. p1: Placode-like epidermal thickenings at the oral and atrial siphon expressing eg. *Pax*, *Six*, *Fox*, *Eya* and *Neurogenin* genes. p2: Placodes that interact with neural crest cells.

The cucullaris/trapezius muscle

The embryonic origin of the cucullaris muscle has puzzled vertebrate developmental morphologists since the early 20th century. The cucullaris muscle spans the dorsal aspect of the vertebrate head/trunk interface. It originates from the posterior cranium or occipital bone and inserts on the cleithrum or scapula of the pectoral girdle (Gegenbaur, 1889). In amniotes, the cucullaris is split into several distinct portions and is often referred to as the trapezius or trapezius-complex. Its innervation by a branch of the vagal nerve in non-amniote gnathostomes and the accessory nerve, regarded as a separated component of the vagus, in amniotes led anatomists to propose a cranial origin of this muscle (Edgeworth, 1935; Gegenbaur, 1889). Observations of a spinal innervation of the trapezius in some amniote taxa called this interpretation into question (Fürbringer, 1874; Gegenbaur, 1889). This debate continues when developmental data are taken into account. While early histological studies proposed an origin from the unsegmented cranial mesoderm (Edgeworth, 1911; 1929; 1935) the advent of new cell lineage tracing studies brought a somitic origin back to the discussion (Couly et al., 1993; Huang et al., 2000; Noden, 1983b; Piekarski and Olsson, 2007). Recently, improved fate mapping experiments in chicken (Theis et al., 2010) and the Mexican axolotl (Sefton et al., 2016) have turned the view back to a cranial origin with 10% of somite-derived myocytes in chicken (Theis et al., 2010). Genetic cell lineage studies in the mouse showed that the majority of the trapezius myocytes is derived from *Mesp1*-positive cranial mesodermal cells (Lescroart et al., 2015). However, *Pax3*-positive myocytes indicating an additional somitic contribution were also detected (Lescroart et al., 2015). The predominant cranial component of the amniote trapezius muscle is in accordance with the connective tissue origin from the NC (Matsuoka et al., 2005; Theis, 2010; Theis et al., 2010). In the axolotl in contrast, neural crest cells (NCCs) do not contribute to the connective tissue of the cucullaris muscle (Epperlein et al., 2012).

What all examined tetrapod taxa have in common is that the cucullaris develops late compared to other head and trunk muscles (Ericsson et al., 2013; Naumann et al. 2017). In Chapter 2 we could confirm this statement for an anuran species (*X. laevis*) for the first time. Additionally, we described another muscle, the diaphragmatico-branchialis muscle (Schlosser and Roth, 1995) originating from the cranial mesoderm. It spans the dorsal aspect of the head/trunk interface of *X. laevis* (Naumann and Olsson, 2017). As the cucullaris, the diaphragmatico-branchialis develops late compared to other head and trunk muscles. The data indicate that the temporal developmental pattern of the tetrapod cucullaris muscle is highly conserved. Even if a new developmental trajectory, such as the anuran tadpole with a high degree of morphological changes, is introduced into ontogeny.

Unfortunately, only descriptive developmental data are available from non-tetrapod taxa (Edgeworth, 1935; Naumann et al., 2017; Noda et al., 2017; Ziermann et al., 2017). In Chapter 1 we re-examined the development of the cucullaris muscle in the basal actinopterygian species *L. osseus* (Naumann et al., 2017). In this study we focused on the development of the posterior branchial and hypobranchial muscles. Our results show that the cucullaris muscle has been misidentified in this species in earlier studies (Edgeworth, 1935). This might be due to its delayed development, which is similar to the developmental pattern of the cucullaris in tetrapods. Additionally, we showed that another muscle in the dorsal head/trunk interface, the retractor dorsalis, develops from the cranial mesoderm and differentiates similarly late as the cucullaris. The origin of this muscle has been assigned to either the cranial mesoderm or the anterior somites (Edgeworth, 1929; 1935).

In summary the data indicate, that the delayed developmental pattern of the cucullaris muscle is not unique to it. Rather it seems that it is a general pattern of muscles derived

from the cranial mesoderm and spanning the head/trunk interface (Naumann et al., 2017a). A mechanism to explain this observation has been put forward by Theis and colleagues (Theis, 2010; Theis et al., 2010). The authors propose that the trunk myogenic program inhibits differentiation in the head-derived cucullaris/trapezius muscle. Only after the trunk myogenic program is down-regulated, muscle fiber differentiation is initiated in the cucullaris muscle. The developmental mechanism is described in detail in the discussion of Chapter 1. Major events in the evolution of the cucullaris/trapezius muscle are shown in Figure 10 (“c”-numbers).

The role of the cardiac neural crest in amphibian heart development

Data on the role of NCCs in amphibian heart development are scarce and only available from *X. laevis* and the Mexican axolotl. The role and contribution of the NC in *X. laevis* heart development are ambiguous. Sadaghini and Thiebaud, by carrying out transplantations of the rhombencephalic NC using *X. laevis*-*X. borealis* chimeras, reported the presence of a few NCCs in the Truncus arteriosus (outflow tract) in larvae at stage NF stage 39/40. In a later study by Martinsen and co-workers, by ablating the whole cranial and anterior trunk NC, a broad range of cardiac defects such as abnormal looping in *X. laevis* at NF stage 33 was reported (Martinsen et al., 2004). The most recent study, by Lee and colleagues, in which red fluorescent protein expressing NCCs from the level of the branchial arches were transplanted, revealed no contribution of NCCs to the heart tube. They only contribute to the branchial arch arteries and the aortic sac of *X. laevis* at NF stage 41 (Lee and Saint-Jeannet, 2011). In the axolotl, transplantation of GFP-positive neural NC to wild type host embryos resulted in a brightly labeled outflow tract in two months old juveniles (Epperlein et al., 2012).

Several problems arise from the data set of *X. laevis*. (1) All studies stopped at stages when heart development is still in process. Sadaghiani et al. stopped at NF stage 39/40

and Lee et al. at NF stage 41. At stage 41 the myocardia of the outflow tract and ventricle are still thickening, the spiral septum and the trabeculae have only begun to form and development of the interatrial septum has not even begun (Kolker et al., 2000; Mohun et al., 2000). It is therefore not possible to exclude a contribution of NCCs to late events of heart development. (2) None of these studies maps the cardiac NC throughout different stages of heart development. Therefore, a transient contribution of NCCs at early stages might have been missed. Such a phenomenon has been observed in the outflow tract and the conductive system of chicken embryos (Poelmann and Gittenberger-de Groot, 1999; Poelmann et al., 1998), Furthermore, a late “dormant” population of cardiac NCCs resting in the posterior head region might have been overlooked. Such a late NCC population has been described in the zebrafish (Cavanaugh et al., 2015) and could also exist in *X. laevis*. (3) The cardiac NC could influence heart patterning by signaling molecules without physically contributing cells to structures of the heart. As shown by Martinsen and colleagues, heart defects after NC ablation were observed at NF stage 33. At this stage, the heart tube is still in an early stage of development shortly before the onset of loop-formation. Alterations in heart development observed by the authors are a ventrally elongated heart, without proper tube formation and an enlarged pericardial cavity (Martinsen et al., 2004). The myocardium appears hypertrophied in NC ablated embryos compared to controls (compare Fig. 7C to E in Martinsen et al., 2004), though this has not been mentioned by the authors. Hypertrophy of the myocardium could explain the ventral elongation and absence of a proper lumen within the “heart tube” (Fig. 7E and F in Martinsen et al. 2004). These results allow the interpretation that NCCs, directly or indirectly, inhibit cardiomyogenesis in cells derived from the FHF. The inhibitory effect of NCCs prevents myocardial hypertrophy and leads to a “normal” functional heart tube. This is supported by our observation of decreased desmin expression in the heart tube after

transplantation of NCCs on top of the heart field of the axolotl (Chapter 4). Another indication of a possible role of cranial NCCs in amphibian heart development can be inferred from the heart phenotype in *FoxN3* morphants of *X. laevis*. As reported in Chapter 3, the hearts of *FoxN3* morphants show decreased trabeculation, valve defects and abnormal looping, in addition to the absence of the interatrial septum (Chapter 3). The ventricular trabeculae of *X. laevis* are derived from the FHF and SHF (Lee and Saint-Jeannet, 2011). Unfortunately, the dynamics of invasion of cells from the SHF into the heart tube is not known in *X. laevis*, but has been described in the chicken. In chicken embryos in which the cardiac NC is ablated, the SHF fails to add cells to the outflow tract and linear heart tube, resulting in altered loop formation (Waldo et al., 2005; Yelbuz et al., 2002; Yelbuz et al., 2003). This might be due to the overexpression of *Fgf8* in the SHF after NC ablation, resulting in increased cell proliferation of SHF cells. An increased proliferative activity prevents migration of these SHF cells into the linear heart tube. The absence of SHF cells in the heart tube leads to weaker myocardia and consequently to altered loop formation (Waldo et al., 2005). Recently, a study by Kodo and co-workers showed that the SHF also influences the migration of cranial NCCs into the outflow tract. *Fgf8* expression from the SHF inhibits expression of *Sema3c* in the NCCs. *Sema3C* is important for proper aggregation of NCCs but prevents their migration into the heart (Kodo et al., 2017). Assuming that a similar interaction of cardiac NCCs and the SHF exists in *X. laevis*, it is possible to interpret the heart defects of *FoxN3* morphants (Chapter 3) as a result of the reduction of cranial NCCs. A reduced amount of NCCs cells could result in an increase in *Fgf8* expression and the subsequent inhibition of SHF cell migration into the heart tube.

In Summary, the data on heart morphology and development in *FoxN3* morphants of *X. laevis* add further evidence to an early interaction of cardiac NCCs with cells from the SHF (Chapter 3). An inhibitory effect of cranial NCCs on muscle fiber formation in

cells of the primary heart tube (FHF-derived) allows the speculation that the FHF is evolutionary older than the SHF and NCCs (Chapter 4). Major events in the evolution of the FHF, SHF and the cranial NC are shown in Figure 10 (“h”- and “nc”-numbers).

Development and evolution of the muscles in the vertebrate head/trunk interface – “escaping” the circumpharyngeal crest

As stated before, the vertebrate head/trunk interface offers a unique possibility to study the anatomical structures that develop in the presence of two completely different patterning mechanisms. The head/trunk interface is defined by the migratory route of the posterior-most cranial NCCs, the so-called circumpharyngeal crest (Kuratani, 1997; Kuratani et al., 2018; Kuratani and Kirby, 1991). The four chapters of this study focus on the development and evolution of different muscle groups in this body region: The muscles of the dorsal aspect of the interface (e.g. the cucullaris) and the muscles of the ventral aspect, the hypobranchial musculature and the heart.

The muscles of the dorsal aspect of the head/trunk interface and the heart originate from a common *Mesp1*-positive cell population in the head mesoderm (Diogo et al., 2015). During development they grow out of the head, bridging the head/trunk interface and settle into the trunk. The hypobranchial muscles originate from *Pax3*-positive mesoderm of the occipital somites in the trunk (Ericsson et al., 2013), migrate along the head/trunk interface until they cross it and settle into the head. As shown in Chapter 1 and 2, the cucullaris as well as the retractor dorsalis of *L. osseus* (Chapter 1) and the diaphragmatico-branchialis of *X. laevis* (Chapter 2) develop late compared to other head muscles. It has been proposed that this is due to the head myogenic program and the absence of cranial NCCs posterior to the head/trunk interface (Naumann et al., 2017; Theis et al., 2010). The inhibition of head muscle differentiation by the trunk environment might have been responsible for the generation of more cells in the anlage

of these muscles. This in turn might have enabled the cucullaris/trapezius anlage to bridge the distance between the head and the pectoral girdle (Theis, 2010; Theis et al., 2010). The same might be true for the retractor dorsalis muscle of *L. osseus* reaching from the branchial skeleton up to the fourth trunk vertebra (Naumann et al., 2017). In amniotes, an additional somatic component added to the cucullaris/trapezius muscle might have played a role in the elongation of the neck and the split of the formerly simple cucullaris muscles into several portions. So the “escape” from the cranial NC by some dorsal cranial muscles might have been an important process in the evolution of the vertebrate neck.

The hypobranchial musculature of amniotes is split into several distinct muscles, while often only one to two hypobranchial muscles are present in non-amniotes. The acquisition of a *Mesp1*-positive cranial component to this somatic musculature (Czajkowski et al., 2014; Theis, 2010) might have played a role in this split. Furthermore, it seems that the development of the hypobranchial muscles in amniotes such as chicken and mouse is much more dependent on NCCs than in non-amniotes such as *Bombina* (Olsson et al., 2001), *Xenopus* (Chapter 3) and axolotl (Epperlein et al., 2012). However, this suggestion is based on only a few data for a small set of taxa. It is necessary to do more complete and dynamic NC and mesoderm fate mapping in the taxa discussed above as well as other non-tetrapod taxa to test this assumption.

The early vertebrate heart tube develops from cells of the FHF. Due to its position posteroventral to the circumpharyngeal ridge, muscle precursors of the primary heart tube differentiate in the absence of cranial NCCs. It has been shown in many studies that the cranial NC interacts with the SHF in the development of the chambered vertebrate heart (see Chapter 3 and 4). However FHF cells seem to be inhibited by NC and are not able to form a primary heart tube serving as a scaffold for further heart

development (Chapter 4). Therefore, the “escape” of the FHF cells from the cranial NC might have been important to develop a primary heart scaffold, which was then modified by cell populations from the new head to form the vertebrate chambered heart.

In summary, it seems that extensive changes in the position and the nature of interactions of embryonic structures situated in the head/trunk interface have shaped the evolution of the vertebrate body plan. Regarding the muscles developing in the head/trunk interface, it seems that three major evolutionary events were due to newly acquired interactions of their embryonic precursors. (1) The evolution of the chambered heart and a head in the last common ancestor of all vertebrates. This might have been due to the acquisition of a new interaction between parts of the cardiopharyngeal field (cranial mesoderm, and SHF) and NCCs (Fig. 10; grey gradient). Additionally, the interaction of epidermal placodes with NCCs, giving rise to the extensive peripheral nervous system of the head is first seen in basal vertebrates (Fig. 10, “p”-numbers). (2) The evolution of a pectoral girdle carrying paired appendages and a “neck”-region in Gnathostomata. Simultaneously, a cranial cucullaris muscle, connecting the head to the pectoral girdle, and a heterotopic shift of the hypobranchial musculature resulting in a proximally situated tongue can be observed (Fig. 10). (3) The acquisition of a *Pax3*-positive somitic component to the cucullaris/trapezius muscle and of a *Mesp1*-positive cranial component to the hypobranchial muscles can be observed. This is correlated with an extension of the neck region and a split into several distinct portions in these two muscle groups (Fig. 10).

These observations indicate that interfaces in biology offer a great potential to be the places of evolutionary innovation by the establishment of new interactions between pre-existing (“old”) components. As nicely stated by Shigeru Kuratani for the vertebrate head/trunk interface as an example:

“Even when the embryonic components are conserved, changes in ratio and length results in invention of a new interaction that will potentially serve as a novel embryonic environment in which cells will differentiate. Thus the embryonic distribution of the NC cells is one of the fundamental and best proxies for the developmental background of the evolution of body plans in vertebrate lineages.” (Kuratani et al., 2018).

Method and techniques applied

The method used in this study and one of the main methods on which developmental morphology and evolutionary developmental biology are based on is the comparison. As stated by Peter Warth, the comparison is a powerful tool to unravel similarities and differences. This is especially true when it is conducted with data gained by the application of new techniques (Warth, 2017).

In Chapter 1, 2 and 3 classical histological sectioning and azan-staining were combined with modern state-of-the-art techniques (Naumann and Olsson, 2017; Naumann et al., 2017). We used fluorescent whole mount antibody staining (FWMABS) to stain different tissues such as muscle, cartilage and nerves which allows following the development of structures composed of these tissues in great detail. This is of special interest in studies on the development of soft tissues such as muscle and nerves (Hilton et al., 2015; Konstantinidis et al., 2015). The FWMABS were than combined with confocal laser scanning microscopy (CLSM) to obtain digital z-stacks from different specimens. In contrast to classical histological sectioning, laser scanning microscopy is non-destructive. This allows observing filigreed structures, such as the cucullaris muscle of *L. osseus*, without artefacts that can be introduced to the sample by the sectioning process. A disadvantage of the combination of FWMABS and CLSM is the limited sample size. Only small (maximum 20 mm), un-ossified specimens can be analysed with a maximum penetration depth of around 2 mm. However, most early

developmental stages of vertebrate embryos fit these requirements. A second step was the preparation of a 3-dimensional (3D) model. This can be done on the basis of histological sections as well as digital sections obtained from FWMABS or micro-computed tomography (μ CT). The advantage of digital sections is their perfect alignment while histological sections are often distorted and cannot be aligned perfectly to each other. 3D models are sometimes misjudged for having only an illustrative value. Even a pure illustrative value would be worth preparing the model since, in combination with 3D pdf, it offers the viewer an easy possibility to follow the observations of the investigator (Naumann and Olsson, 2017). What is often neglected is the process of preparing the model which requires a deep examination of the sample. During this process, called segmentation, the investigator has to precisely retrace the different structures that shall be illustrated in the model. Thus a 3D model is a powerful new way to (1) makes it easier for the investigator to understand the anatomical conditions of a specimen and (2) makes it easier to transport observations to the viewer. However, presently a combination of histological sectioning and either FWMABS or μ CT must be used according to the requirements of the study.

In Chapter 3, Morpholino (MO)-mediated knockdown of *FoxN3* in *X. laevis* embryos and larvae produced by Schmidt et al. 2011 were re-examined. The aim was to investigate the morphant heart development and anatomy. Recently, the use of MO-mediated knockdown has been criticized due to evidence for off-target effects and subsequent false-positive results (Eisen and Smith, 2008; Kok et al., 2015). However, as stated by Eisen and Smith, MO can still serve as a versatile tool to study the role of developmental genes if adequate control experiments are conducted (Eisen and Smith, 2008). The *FoxN3*-MO used by Schmidt et al. (2011) has been tested in a preceding study (Schuff et al., 2007). In this study Schuff et al. injected *Xenopus* embryos with either an intact *FoxN3*/GFP or *FoxN3*^{Res}/GFP reporter construct. The *FoxN3*^{Res}/GFP

construct was prepared carrying silent mutations in the putative MO binding site. The *FoxN3*-MO was only able to stop GFP expression in embryos injected with the *FoxN3*/GFP construct. A control-MO against the *human beta-globin* gene did not stop GFP expression in neither of the constructs (Schuff et al., 2007). Additional control experiments could be carried out such as the injection of another similar but not identical *FoxN3*-MO and *FoxN3* insitu hybridisations and quantitative PCR to screen the degree of down-regulation of the *FoxN3* gene. The latter two control experiments have been already carried out by Jennifer Schmidt (personal communication), adding further evidence for the specificity of the used *FoxN3*-MO.

In Chapter 4, DiI was injected in-vivo into neural folds to label NCCs and their derivatives in the Mexican axolotl. DiI is a lipophilic fluorescent dye that accumulates in cell membranes at the injection site. In developmental biology, the injection of such fluorescent dyes has been and still is an extensively used technique to examine cell movements and fates (Lee and Saint-Jeannet, 2011; Minarik et al., 2017; Olsson et al., 2001; Piekarski and Olsson, 2007). Despite its extensive use, this technique has some obvious problems. Starting from a high concentration, the dye is diluted by subsequent cell divisions, which in combination with photo bleaching decreases signal intensity. This becomes critical when the origin of late-developing anatomical structures is examined. Furthermore, not every cell at the injection site will be labelled by the dye. This may lead to false-negative results if the examined anatomical structure is derived from a very small cell population. Of course this problem can often be solved by an increase in sample size. A technique that allows a better long-term cell labelling is the transplantation of GFP expressing donor tissue into GFP-negative host embryos (Piekarski and Olsson, 2007; Sefton et al., 2015). GFP-tissue-transplants are homogeneously labelled and signal intensity does not decrease due to cell divisions or photo bleaching. It is therefore necessary to prepare GFP-positive NC as well as heart

field transplants to (1) exactly trace the migration dynamics and fate of the cardiac NC in the Mexican axolotl and (2) examine if the position of the FHF and SHF are similar in *X. laevis* (Lee and Saint-Jeannet, 2011). However, tissue disturbance by the transplantation procedure itself might have an influence on the experimental outcome. Micro-surgical procedures and tissue crafts have a long-standing tradition in developmental biology (Spemann, 2013). What is critical for high quality micro-surgeries is practice of the specific surgery (e.g. NC to heart transplantations in Chapter4). It has to be assured that the surgical procedure is well established before specimens are integrated into the sample set and analysed in the context of the study. Another important thing is to prepare controls. In the case of the transplantation experiments in Chapter 4, sham operations were prepared to eliminate effects of the surgical procedure itself. Additionally, transplants from cranial mesoderm were prepared to trace the effect specifically to the NCCs and eliminate an effect of the introduction of additional cells to the heart primordium. However, the sample size is still relatively small. More transplantations have to be made to verify the preliminary results and minimize stochastic effects.

A short note on the role of serendipity shaping this thesis

Obviously, the topic of Chapter 2 in this thesis is somehow different compared to Chapter 1, 3 and 4. However, it played a crucial role in the process of producing this thesis. One of the initial questions was to examine the role of *FoxN3* in cranial nerve development. It has been reported in an earlier study, that some branches of the trigeminal as well the entire hypoglossal nerve are absent in *FoxN3* morphants of *X. laevis* (Schuff et al., 2007). When I started to work on this question it became obvious that no complete description of the cranial nerves of *X. laevis* tadpoles existed. A nice work by Paterson provided a detailed description of the pre-otic cranial nerves but lacks details about the post-otic cranial nerves as well as the anterior spinal nerves that form

the hypoglossal nerve (Paterson, 1939). It was therefore necessary to describe the “normal” anatomy of the cranial nerves before analyzing the nerve phenotypes of *FoxN3* morphants. By tracing the posterior branches of the vagal nerve I found the cucullaris muscle and the diaphragmatico-branchialis muscle both crossing the head/trunk interface. While the cucullaris has been described earlier (Ziermann and Diogo, 2014), the diaphragmatico-branchialis muscle has previously only been described in tadpoles of *Discoglossus pictus* before (Schlosser and Roth, 1995). The developmental pattern of the cranial muscles of *X. laevis* has been described in detail in an earlier study (Ziermann and Olsson, 2007). However, the cucullaris and diaphragmatico-branchialis were not included in this study. A comparison of the development of these two muscles (Chapter 2 Supplementary) with data from other tetrapods (Theis, 2010; Ziermann and Diogo, 2013) revealed a similar pattern. This adds further evidence to the explanatory scenario of the muscles spanning the head/trunk interface discussed in Chapter 1.

After the anatomy of the post-otic cranial and anterior spinal nerves has been described it became apparent that it was not possible to describe the cranial nerve morphology in serial sections of *FoxN3* morphants from the samples of Schmidt et al. (2011). However, when trying to trace the nerves in the sections I noticed differences in the heart morphologies of morphants and un-injected control larvae. Inspired by the re-discovered close developmental link between the heart and the head (Diogo et al., 2015), we decided to analyze the heart development in *FoxN3* morphants. The malformations found can be explained by interactions between cranial NCCs and the SHF which had been described in studies on chicken embryos (Waldo et al., 2005). This indicates that regulatory interactions between the cranial NC and the SHF are conserved among tetrapods and support the close link between the cells of the SHF and the cranial muscles (Chapter 3, Diogo et al., 2015).

However, the study on cranial nerve morphology of *X. laevis* tadpoles (Chapter 2) can serve as a basis to evaluate data on nerve malformations from experimental studies in *X. laevis*. Furthermore, the data can be compared to data from tadpoles of other frog species (Schlosser and Roth, 1995; 1997a; Schlosser and Roth, 1997b) to gain more information about the evolution of the cranial nerves in Anura. This is of particular value when data about the developmental morphology of the cranial nerves in *X. laevis* become available. Due to this, the cranial nerve anatomy of *X. laevis* is not discussed further in this thesis.

The two cases mentioned above involve a moment of serendipity. The word Serendipity has been borrowed from the fairy tale “The three princes of Serendip” by the English writer Horac Walpole. He defined it as “... making discoveries, by accident and sagacity, of things which they were not in quest of...” (Bosenman, 1988). Bosenman also states that after such a serendipitous moment logical and systematic scientific work has to follow to unravel the whole extent of the scientific discovery. Regarding developmental biology, the awareness of this principle urges an embryologist to always be knowledgeable about as many structures as possible regarding the organisms under investigation. I really appreciate the concluding notion of Bosenman’s article that: “By realizing that discovery involves a dynamic interplay between conventional scientific methods and chance in all of its forms, and by cultivating an aptitude for serendipity, scientists can greatly enhance their investigative powers.” (Bosenman, 1988).

References

- Allis, EP. 1897. The cranial muscles and first spinal nerves in *Amia calva*. *Journal of Morphology* 12:487-772
- Altmann JS, Dawes, EA. 1983. A cobalt study of medullary sensory projections from lateral line nerves, associated cutaneous nerves, and the VIIIth nerve in adult *Xenopus*. *Journal of Comparative Neurology* 213(3):310-326.
- Adachi N, Pascual-Anaya J, Hirai T, Higuchi S, Kuratani S. 2018. Development of hypobranchial muscles with special reference to the evolution of the vertebrate neck. *Zoological Letters* 4(1):5.
- Ballard WW, Mellinger J, Lechenault H. 1993. A series of normal stages for development of *Scyliorhinus canicula*, the lesser spotted dogfish (Chondrichthyes: Scyliorhinidae). *Journal of Experimental Zoology Part A: Ecological Genetics and Physiology* 267(3):318-336.
- Benedetti, E. 1933. Il cervello ei nervi cranici del *Proteus anguines* Laur. Stabilimento tipografica nazionale.
- Böck P. 1989. Romeis mikroskopische technik. Urban & Schwarzenberg, München.
- Bonner JT, Dawid I, Gerhart J, Maderson P, Davidson E, Freeman G, Gould S, Horn H, Oster G, Sauer H. 2012. Evolution and Development: Report of the Dahlem Workshop on Evolution and Development Berlin 1981, May 10–15: Springer Science & Business Media.
- Bordzilovskaya NP, Detlaff TA. 1989. Table of stages of the normal development of axolotl embryos and the prognostication of timing of successive developmental stages at various temperatures. *Axolotl Newsletter* 7:2-22.
- Bosenman MF. 1988. Serendipity and scientific discovery. *The Journal of Creative Behavior* 22(2):132-138.
- Bothe I, Dietrich S. 2006. The molecular setup of the avian head mesoderm and its implication for craniofacial myogenesis. *Developmental Dynamics* 235(10):2845-2860.
- Buckingham M. 2017. Gene regulatory networks and cell lineages that underlie the formation of skeletal muscle. *Proceedings of the National Academy of Sciences* 114(23):5830-5837.
- Buckingham M, Relaix F. 2007. The role of Pax genes in the development of tissues and organs: Pax3 and Pax7 regulate muscle progenitor cell functions. *Annual Review of Cell and Developmental Biology* 23:645-673.

References

- Byth BC, Costa MT, Teshima IE, Wilson WG, Carter NP, Cox DW. 1995. Molecular analysis of three patients with interstitial deletions of chromosome band 14q31. *Journal of Medical Genetics* 32(7):564-567.
- Canatella DC, De Sa RO. 1993. *Xenopus laevis* as a model organism. *Systematic Biology* 42(4):476-507.
- Carlsson P, Mahlapuu M. 2002. Forkhead transcription factors: key players in development and metabolism. *Developmental Biology* 250(1):1-23.
- Cavanaugh AM, Huang J, Chen J-N. 2015. Two developmentally distinct populations of neural crest cells contribute to the zebrafish heart. *Developmental Biology* 404(2):103-112.
- Cervino A, Paz D, Frontera J. 2017. Neuronal degeneration and regeneration induced by axotomy in the olfactory epithelium of *Xenopus laevis*. *Developmental Neurobiology* 77(11):1308-1320.
- Cline HT, Kelly D. 2012. *Xenopus* as an experimental system for developmental neuroscience. Introduction to a special issue. *Developmental Neurobiology* 72(4):463-464.
- Coghill GE. 1902. The cranial nerves of *Amblystoma tigrinum*. *Journal of comparative Neurology* 12:207-289.
- Couly GF, Coltey PM, Le Douarin NM. 1993. The triple origin of skull in higher vertebrates: a study in quail-chick chimeras. *Development* 117(2):409-429.
- Czajkowski MT, Rassek C, Lenhard DC, Bröhl D, Birchmeier C. 2014. Divergent and conserved roles of Dll1 signaling in development of craniofacial and trunk muscle. *Developmental Biology* 395(2):307-316.
- Davidson E, Levin M. 2005. Gene regulatory networks. National Academy of Sciences.
- Delsuc F, Brinkmann H, Chourrout D, Philippe H. 2006. Tunicates and not cephalochordates are the closest living relatives of vertebrates. *Nature* 439(7079):965.
- Diogo R, Kelly RG, Christiaen L, Levine M, Ziermann JM, Molnar JL, Noden DM, Tzahor E. 2015. A new heart for a new head in vertebrate cardiopharyngeal evolution. *Nature* 520(7548):466-473.
- Dong W, Lee RH, Xu H, Yang S, Pratt KG, Cao V, ...Aizenmann CD. 2009. Visual avoidance in *Xenopus* tadpoles is correlated with the maturation of visual responses in the optic tectum. *Journal of Neurophysiology* 101(2):803-815.

References

- Edgeworth FH. 1911. Memoirs: On the morphology of the cranial muscles in some vertebrates. *Journal of Cell Science* 2(222):167-316.
- Edgeworth FH. 1929. The development of some of the cranial muscles of ganoid fishes. *Philosophical Transactions of the Royal Society of London Series B, Containing Papers of a Biological Character* 217:39-89.
- Edgeworth FH. 1935. *The cranial muscles of the vertebrates*: Cambridge University Press, Cambridge.
- Edwards-Faret G, Muñoz R, Méndez-Olivos EE, Lee-Liu D, Tapia VS, Larrain J. 2017. Spinal cord regeneration in *Xenopus laevis*. *Nature Protocols* 12(2):372-389.
- Eisen JS, Smith JC. 2008. Controlling morpholino experiments: don't stop making antisense. *Development* 135(10):1735-1743.
- Ekker SC. 2000. Morphants: a new systematic vertebrate functional genomics approach. *Yeast* 17(4):302-306.
- Epperlein H, Meulemans D, Bronner-Fraser M, Steinbeisser H, Selleck M. 2000. Analysis of cranial neural crest migratory pathways in axolotl using cell markers and transplantation. *Development* 127(12):2751-2761.
- Epperlein HH, Khattak S, Knapp D, Tanaka EM, Malashichev YB. 2012. Neural crest does not contribute to the neck and shoulder in the axolotl (*Ambystoma mexicanum*). *PLoS One* 7(12):e52244.
- Ericsson R, Cerny R, Falck P, Olsson L. 2004. Role of cranial neural crest cells in visceral arch muscle positioning and morphogenesis in the Mexican axolotl, *Ambystoma mexicanum*. *Developmental Dynamics* 231(2):237-247.
- Ericsson R, Knight R, Johanson Z. 2013. Evolution and development of the vertebrate neck. *Journal of Anatomy* 222(1):67-78.
- Falck P, Hanken J, Olsson L. 2002. Cranial neural crest emergence and migration in the Mexican axolotl (*Ambystoma mexicanum*). *Zoology* 105(3):195-202.
- Francis ETB. 1934. *The anatomy of the salamander (Vol 2)*. Clarendon Press.
- Frankenhaeuser B, Huxley A. 1964. The action potential in the myelinated nerve fiber of *Xenopus laevis* as computed on the basis of voltage clamp data. *The Journal of Physiology* 171(2):302-315.
- Frost DR, Grant T, Faivovich J, Bain RH, Haas A, Haddad CFB, ... Wheeler WC. 2006. The amphibian tree of life. *Bulletin of the American Museum of Natural History* 297:8-370.

- Fürbringer M. 1874. Zur vergleichenden Anatomie der Schultermuskeln. II Theil. Jenaische Zeitschrift für Naturwissenschaften 8:175-280.
- Gans C, Northcutt RG. 1983. Neural crest and the origin of vertebrates: a new head. Science 220(4594):268-273.
- Gaupp G. 1896/1899. Anatomie des Frosches. 1. Abteilung: Lehre vom Skelet und dem Muskelsystem. (3rd ed.). 2. Abteilung: Lehre vom Nerven- und Gefäßsystem. (2nd ed.). Braunschweig, Vieweg.
- Gegenbaur C. 1889. Vergleichende Anatomie der Wirbelthiere: mit Berücksichtigung der Wirbellosen: W. Engelmann, Leipzig.
- Gilbert SF. 2013. Developmental Biology: Palgrave.
- Goethe Jv. 1820. Das Schädelgerüst aus sechs Wirbelknochen aufgebaut. Zur Naturwissenschaft überhaupt, besonders zur Morphologie II 2.
- Goodrich ES. 1930. Studies on the structure & development of vertebrates: Macmillan and C., Limited, London.
- Gouchie G, Roberts L, Wassersug RJ. 2008. The effect of mirrors on African clawed frog (*Xenopus laevis*) larval growth, development and behavior. Behavioral Ecology and Sociobiology 62(11):1821-1829.
- Graham A, Koentges G, Lumsden A. 1996. Neural crest apoptosis and the establishment of craniofacial pattern: an honorable death. Molecular and Cellular Neuroscience 8(2):76-83.
- Grande L. 2010. An empirical synthetic pattern study of gars (Lepisosteiformes) and closely related species, based mostly on skeletal anatomy. The resurrection of Holostei. Copeia 10(2A).1.
- Green SA, Simoes-Costa M, Bronner ME. 2015. Evolution of vertebrates as viewed from the crest. Nature 520(7548):474-482.
- Greenwood PH, Lauder GV. 1981. Protractor pectoralis muscle and the classification of teleost fishes. Bulletin. Zoology of the British Museum (Natural History), Department of Zoology.
- Gross JB, Hanken J. 2008. Review of fate-mapping studies of osteogenic cranial neural crest in vertebrates. Developmental Biology 317(2):389-400.
- Haas A. 2001. Mandibular arch musculature of anuran tadpoles, with comments on homologies of amphibian jaw muscles. Journal of Morphology 247(1):1-33.
- Haeckel E. 1866. bd. Allgemeine Entwicklungsgeschichte der Organismen: G. Reimer.

- Hall BK. 1999. The neural crest in development and evolution: Springer Science & Business Media.
- Hall BK. 2000. The neural crest as a fourth germ layer and vertebrates as quadroblastic not triploblastic. *Evolution and Development* 2(1):3-5.
- Hall BK. 2012. *Evolutionary developmental biology*: Springer Science & Business Media.
- Harel I, Nathan E, Tirosh-Finkel L, Zigdon H, Guimarães-Camboa N, Evans SM, Tzahor E. 2009. Distinct origins and genetic programs of head muscle satellite cells. *Developmental Cell* 16(6):822-832.
- Harland RM. 1991. In situ hybridization: an improved whole-mount method for *Xenopus* embryos. *Methods in Cell Biology* 36:685-695.
- Hilton EJ, Schnell NK, Konstantinidis P. 2015. When tradition meets technology: systematic morphology of fishes in the early 21st Century. *Copeia* 103(4):858-873.
- His W. 1868. Untersuchungen über die erste Anlage des Wirbelthierleibes: die erste Entwicklung des Hühnchens im Ei: FCW Vogel.
- Hoffmann AD, Peterson MA, Friedland-Little JM, Anderson SA, Moskowitz IP. 2009. Sonic hedgehog is required in pulmonary endoderm for atrial septation. *Development* 136(10):1761-1770.
- Holland ND, Venkatesh TV, Holland LZ, Jacobs DK, Bodmer R. 2003. *AmphiNk2-tin*, an amphioxus homeobox gene expressed in myocardial progenitors: insights into evolution of the vertebrate heart. *Developmental Biology* 255(1):128-137.
- Hosokawa R, Oka K, Yamaza T, Iwata J, Urata M, Xu X, Bringas P, Nonaka K, Chai Y. 2010. TGF- β mediated FGF10 signaling in cranial neural crest cells controls development of myogenic progenitor cells through tissue-tissue interactions during tongue morphogenesis. *Developmental Biology* 341(1):186-195.
- Huang R, Zhi Q, Patel K, Wilting J, Christ B. 2000. Contribution of single somites to the skeleton and muscles of the occipital and cervical regions in avian embryos. *Anatomy and Embryology (Berl)* 202(5):375-383.
- Hutson MR, Zhang P, Stadt HA, Sato AK, Li Y-X, Burch J, Creazzo TL, Kirby ML. 2006. Cardiac arterial pole alignment is sensitive to FGF8 signaling in the pharynx. *Developmental Biology* 295(2):486-497.
- Jacobson AG. 1993. Somitomeres: mesodermal segments of the head and trunk. *The Skull* 1:42-76.

References

- Jensen B, Wang T, Christoffels VM, Moorman AF. 2013. Evolution and development of the building plan of the vertebrate heart. *Biochimica et Biophysica Acta* 1833(4):783-794.
- Jeong J, Mao J, Tenzen T, Kottmann AH, McMahon AP. 2004. Hedgehog signaling in the neural crest cells regulates the patterning and growth of facial primordia. *Genes & Development* 18(8):937-951.
- Jessen HL. 1972. Schultergürtel und Pectoralflosse bei Actinopterygiern [Shoulder girdle and pectoral fin in actinopterygians] *Fossils and Strata* 1:1-101.
- Jiang X, Rowitch DH, Soriano P, McMahon AP, Sucov HM. 2000. Fate of the mammalian cardiac neural crest. *Development* 127(8):1607-1616.
- Jones PL, Veenstra GCJ, Wade PA, Vermaak D, Kass SU, Landsberger N, Strouboulis J, Wolffe AP. 1998. Methylated DNA and MeCP2 recruit histone deacetylase to repress transcription. *Nature genetics* 19(2):187-191.
- Kaartinen V, Dudas M, Nagy A, Sridurongrit S, Lu MM, Epstein JA. 2004. Cardiac outflow tract defects in mice lacking ALK2 in neural crest cells. *Development* 131(14):3481-3490.
- Kang J, Nathan E, Xu SM, Tzahor E, Black BL. 2009. *Isl1* is a direct transcriptional target of Forkhead transcription factors in second-heart-field-derived mesoderm. *Developmental Biology* 334(2):513-522.
- Karnitis SA, Burns K, Sudduth KW, Golden WL, Wilson WG. 1992. Deletion (14)(q24.3q32.1): evidence for a distinct clinical phenotype. *American Journal of Medical Genetics* 44(2):153-157.
- Katz LC, Potel MJ, Wassersug RJ. 1981. Structure and mechanism of schooling in tadpoles of the clawed frog, *Xenopus laevis*. *Animal Behavior* 29(1):20-33.
- Kirby ML, Gale TF, Stewart DE. 1983. Neural crest cells contribute to normal aorticopulmonary septation. *Science* 220(4601):1059-1061.
- Kirby ML, Turnage KL, Hays BM. 1985. Characterization of conotruncal malformations following ablation of "cardiac" neural crest. *The Anatomical Record* 213(1):87-93.
- Kirby ML, Waldo KL. 1995. Neural crest and cardiovascular patterning. *Circulation research* 77(2):211-215.
- Klymkowsky MW, Hanken J. 1991. Whole-mount staining of *Xenopus* and other vertebrates. *Methods in Cell Biology* 36:419-441.

- Kodo K, Shibata S, Miyagawa-Tomita S, Ong S-G, Takahashi H, Kume T, Okano H, Matsuoka R, Yamagishi H. 2017. Regulation of *Sema3c* and the Interaction between Cardiac Neural Crest and Second Heart Field during Outflow Tract Development. *Scientific Reports* 7(1):6771.
- Kok FO, Shin M, Ni C-W, Gupta A, Grosse AS, van Impel A, Kirchmaier BC, Peterson-Maduro J, Kourkoulis G, Male I. 2015. Reverse genetic screening reveals poor correlation between morpholino-induced and mutant phenotypes in zebrafish. *Developmental Cell* 32(1):97-108.
- Kolker SJ, Tajchman U, Weeks DL. 2000. Confocal imaging of early heart development in *Xenopus laevis*. *Developmental Biology* 218(1):64-73.
- Konstantinidis P, Warth P, Naumann B, Metscher B, Hilton EJ, Olsson L. 2015. The developmental pattern of the musculature associated with the mandibular and hyoid arches in the Longnose gar, *Lepisosteus osseus* (Actinopterygii, Ginglymodi, Lepisosteiformes). *Copeia* 103(4):920-932.
- Kuratani S. 1997. Spatial distribution of postotic crest cells defines the head/trunk interface of the vertebrate body: embryological interpretation of peripheral nerve morphology and evolution of the vertebrate head. *Anatomy and Embryology (Berl)* 195(1):1-13.
- Kuratani S. 2003. Evolutionary developmental biology and vertebrate head segmentation: a perspective from developmental constraint. *Theory in Biosciences* 122(2-3):230-251.
- Kuratani S. 2008. Evolutionary developmental studies of cyclostomes and the origin of the vertebrate neck. *Development, Growth and Differentiation* 50 Suppl 1:S189-194.
- Kuratani S, Kusakabe R, Hirasawa T. 2018. The neural crest and evolution of the head/trunk interface in vertebrates. *Developmental Biology*.
- Kuratani SC, Kirby ML. 1991. Initial migration and distribution of the cardiac neural crest in the avian embryo: an introduction to the concept of the circumpharyngeal crest. *Developmental Dynamics* 191(3):215-227.
- Laduron S, Deplus R, Zhou S, Kholmanskikh O, Godelaine D, De Smet C, Hayward SD, Fuks F, Boon T, De Plaen E. 2004. MAGE-A1 interacts with adaptor SKIP and the deacetylase HDAC1 to repress transcription. *Nucleic Acids Research* 32(14):4340-4350.

- Lazic S, Scott IC. 2011. Mef2cb regulates late myocardial cell addition from a second heart field-like population of progenitors in the zebrafish. *Developmental Biology* 354(1):123-133.
- Lee YH, Saint-Jeannet JP. 2011. Cardiac neural crest is dispensable for outflow tract septation in *Xenopus*. *Development* 138(10):2025-2034.
- Lee-Liu D, Méndez-Olivos EE, Muñoz R, Larrain J. 2016. The African clawed frog *Xenopus laevis*: A model organisms to study regeneration of the central nervous system. *Neuroscience Letters* 652: 82-93.
- Lescroart F, Hamou W, Francou A, Theveniau-Ruissy M, Kelly RG, Buckingham M. 2015. Clonal analysis reveals a common origin between nonsomite-derived neck muscles and heart myocardium. *Proceedings of the National Academy of Sciences U S A* 112(5):1446-1451.
- Li YX, Zdanowicz M, Young L, Kumiski D, Leatherbury L, Kirby ML. 2003. Cardiac neural crest in zebrafish embryos contributes to myocardial cell lineage and early heart function. *Developmental Dynamics* 226(3):540-550.
- Lours-Calet C, Alvares LE, El-Hanfy AS, Gandesha S, Walters EH, Sobreira DR, Wotton KR, Jorge EC, Lawson JA, Lewis AK. 2014. Evolutionarily conserved morphogenetic movements at the vertebrate head–trunk interface coordinate the transport and assembly of hypopharyngeal structures. *Developmental Biology* 390(2):231-246.
- Long WL, Ballard WW. 2001. Normal embryonic stages of the longnose gar, *Lepisosteus osseus*. *BMC Developmental Biology* 1,6.
- Love AC. 2003. Evolutionary morphology, innovation, and the synthesis of evolutionary and developmental biology. *Biology and Philosophy* 18(2):309-345.
- Martin BL, Harland RM. 2001. Hypaxial muscle migration during primary myogenesis in *Xenopus laevis*. *Developmental Biology* 239(2):270-280.
- Martinsen BJ, Frasier AJ, Baker CV, Lohr JL. 2004. Cardiac neural crest ablation alters Id2 gene expression in the developing heart. *Developmental Biology* 272(1):176-190.
- Matsuoka T, Ahlberg PE, Kessarar N, Iannarelli P, Dennehy U, Richardson WD, McMahon AP, Koentges G. 2005. Neural crest origins of the neck and shoulder. *Nature* 436(7049):347-355.

- McKeown CR, Sharma P, Sharipov HE, Shen W, Cline HT. 2013. Neurogenesis is required for behavioral recovery after injury in the visual system of *Xenopus laevis*. *Journal of Comparative Neurology* 521(10):2262–2278.
- Meier S. 1981. Development of the chick embryo mesoblast: morphogenesis of the prechordal plate and cranial segments. *Developmental Biology* 83(1):49-61.
- Metscher BD. 2009. MicroCT for comparative morphology: simple staining methods allow high-contrast 3D imaging of diverse non-mineralized animal tissues. *BMC Physiology* 9:11.
- Minarik M, Stundl J, Fabian P, Jandzik D, Metscher BD, Psenicka M, Gela D, Osorio-Pérez A, Arias-Rodriguez L, Horáček I. 2017. Pre-oral gut contributes to facial structures in non-teleost fishes. *Nature* 547(7662):209.
- Minchin JE, Williams VC, Hinitz Y, Low S, Tandon P, Fan C-M, Rawls JF, Hughes SM. 2013. Oesophageal and sternohyal muscle fibres are novel Pax3-dependent migratory somite derivatives essential for ingestion. *Development* 140(14):2972-2984.
- Minoux M, Rijli FM. 2010. Molecular mechanisms of cranial neural crest cell migration and patterning in craniofacial development. *Development* 137(16):2605-2621.
- Miyagawa-Tomita S, Arima Y, Kurihara H. 2016. The “Cardiac Neural Crest” Concept Revisited. *Etiology and Morphogenesis of Congenital Heart Disease: Springer*. p 227-232.
- Mohun TJ, Leong LM, Weninger WJ, Sparrow DB. 2000. The morphology of heart development in *Xenopus laevis*. *Developmental Biology* 218(1):74-88.
- Mootosamy RC, Dietrich S. 2002. Distinct regulatory cascades for head and trunk myogenesis. *Development*, 129(3):573–583.
- Moreno M, Tapia K, Larrain J. 2014. Neural regeneration in *Xenopus* tadpoles during metamorphosis. In M. Kloc & J. Z. Kubiak (Eds.), *Xenopus Development*:293–308. Oxford: John Wiley & Sons.
- Nakae M, Sasaki K. 2004. Homologies of the adductor mandibulae muscles in Tetraodontiformes as indicated by nerve branching patterns. *Ichthyological Research* 51(4):327–336.
- Nan X, Ng H-H, Johnson CA, Laherty CD, Turner BM, Eisenman RN, Bird A. 1998. Transcriptional repression by the methyl-CpG-binding protein MeCP2 involves a histone deacetylase complex. *Nature* 393(6683):386-389.

References

- Nathan E, Monovich A, Tirosh-Finkel L, Harrelson Z, Rousso T, Rinon A, Harel I, Evans SM, Tzahor E. 2008. The contribution of Islet1-expressing splanchnic mesoderm cells to distinct branchiomic muscles reveals significant heterogeneity in head muscle development. *Development* 135(4):647-657.
- Naumann B, Olsson L. 2017. Three-dimensional reconstruction of the cranial and anterior spinal nerves in early tadpoles of *Xenopus laevis* (Pipidae, Anura). *Journal of Comparative Neurology*.
- Naumann B, Warth P, Olsson L, Konstantinidis P. 2017. The development of the cucullaris muscle and the branchial musculature in the Longnose Gar, (*Lepisosteus osseus*, Lepisosteiformes, Actinopterygii) and its implications for the evolution and development of the head/trunk interface in vertebrates. *Evolution and Development* 19(6):263-276.
- Nie S, Bronner ME. 2015. Dual developmental role of transcriptional regulator Ets1 in *Xenopus* cardiac neural crest vs. heart mesoderm. *Cardiovascular Research* 106(1):67-75.
- Nieuwkoop PD, Faber J. 1994. *Normal Table of Xenopus laevis* (Daudin). A systematical and chronological survey of the development from the fertilized egg till the end of metamorphosis: Garland publishing, New York.
- Noda M, Miyake T, Okabe M. 2017. Development of cranial muscles in the actinopterygian fish Senegal bichir, *Polypterus senegalus* Cuvier, 1829. *Journal of Morphology*.
- Noden DM. 1983a. The embryonic origins of avian cephalic and cervical muscles and associated connective tissues. *American Journal of Anatomy* 168(3):257-276.
- Noden DM. 1983b. The embryonic origins of avian cephalic and cervical muscles and associated connective tissues. *Developmental Dynamics* 168(3):257-276.
- Noden DM. 1983c. The role of the neural crest in patterning of avian cranial skeletal, connective, and muscle tissues. *Developmental Biology* 96(1):144-165.
- Noden DM, Schneider RA. 2006. Neural crest cells and the community of plan for craniofacial development. *Neural crest induction and differentiation*: Springer. p 1-23.
- Norris HW. 1913. The cranial nerves of *Siren lacertina*. *Journal of Morphology* 24:245–316.
- Norris HW, Hughes SP. 1918. The cranial and anterior spinal nerves of caecilian amphibians. *Journal of Morphology* 31(3):489–560.

References

- Northcutt RG. 1993. A reassessment of Goodrich's model of cranial nerve phylogeny. *Acta Anatomica* 148(2–3):71–80.
- Northcutt RG. 1989. The phylogenetic distribution and innervation of craniate mechanoreceptive lateral lines. In S. Coombs, P. Görner, & H. Münz (Eds.), *Neurobiology and Evolution of the Lateral Line System* (pp. 17–78). New York: Springer.
- Northcutt RG, Bemis WE. 1993. Cranial nerves of the coelacanth, *Latimeria chalumnae* [Osteichthyes: Sarcopterygii: Actinistia], and comparisons with other craniata. *Brain, Behavior and Evolution* 42(Suppl 1):1–76.
- Nye HL, Cameron JA, Chernoff EA, Stocum DL. 2003. Extending the table of stages of normal development of the axolotl: limb development. *Developmental Dynamics* 226(3):555-560.
- Oisi Y, Fujimoto S, Ota KG, Kuratani S. 2015. On the peculiar morphology and development of the hypoglossal, glossopharyngeal and vagus nerves and hypobranchial muscles in the hagfish. *Zoological Letters* 1:6.
- Oka Y, Takeuchi H, Satou M, Ueda K. 1987. Cobaltic lysine study of the morphology and distribution of the cranial nerve efferent neurons (motoneurons and preganglionic parasympathetic neurons) and rostral spinal motoneurons in the Japanese toad. *The Journal of Comparative Neurology* 259(3):400–423.
- Olsson L, Ericsson R, Cerny R. 2005. Vertebrate head development: segmentation, novelties, and homology. *Theory in Biosciences* 124(2):145-163.
- Olsson L, Falck P, Lopez K, Cobb J, Hanken J. 2001. Cranial neural crest cells contribute to connective tissue in cranial muscles in the anuran amphibian, *Bombina orientalis*. *Developmental Biology* 237(2):354-367.
- Paterson NF. 1939. The head of *Xenopus laevis*. *Journal of Cell Science* s2-81(322):161-232.
- Pati D, Keller C, Groudine M, Plon SE. 1997. Reconstitution of a MEC1-independent checkpoint in yeast by expression of a novel human fork head cDNA. *Molecular and Cellular Biology* 17(6):3037-3046.
- Peshkovsky C, Totong R, Yelon D. 2011. Dependence of cardiac trabeculation on neuregulin signaling and blood flow in zebrafish. *Developmental Dynamics* 240(2):446-456.

- Piekarski N, Olsson L. 2007. Muscular derivatives of the cranialmost somites revealed by long-term fate mapping in the Mexican axolotl (*Ambystoma mexicanum*). *Evolution and Development* 9(6):566-578.
- Pieper M, Eagleson G, Wosniok W, Schlosser G. 2011. Origin and segregation of cranial placodes in *Xenopus laevis*. *Developmental Biology* 360(2):257–275.
- Pillai R, Coverdale LE, Dubey G, Martin CC. 2004. Histone deacetylase 1 (HDAC-1) required for the normal formation of craniofacial cartilage and pectoral fins of the zebrafish. *Developmental Dynamics* 231(3):647-654.
- Poelmann R, Gittenberger-de Groot A. 1999. A subpopulation of apoptosis-prone cardiac neural crest cells targets to the venous pole: multiple functions in heart development? *Developmental Biology* 207(2):271-286.
- Poelmann R, Mikawa T, Groot GD. 1998. Neural crest cells in outflow tract septation of the embryonic chicken heart: differentiation and apoptosis. *Developmental Dynamics* 212(3):373-384.
- Porro LB, Richards CT. 2017. Digital dissection of the model organism *Xenopus laevis* using contrast-enhanced computed tomography. *Journal of Anatomy* 231:169–191.
- Pratt KG, Khakhalin AS. 2013. Modeling human neurodevelopmental disorders in the *Xenopus tadpole*: From mechanisms to therapeutic targets. *Disease Models and Mechanisms* 6(5):1057–1065.
- Pyron RA, Wiens JJ. 2011. A large-scale phylogeny of Amphibia including over 2800 species, and a revised classification of extant frogs, salamanders, and caecilians. *Molecular Phylogenetics and Evolution* 61(2):543–583.
- Rickert-Sperling S, Kelly RG, Driscoll DJ. 2016. *Congenital Heart Diseases: The Broken Heart*. Vienna: Springer.
- Rinon A, Lazar S, Marshall H, Büchmann-Møller S, Neufeld A, Elhanany-Tamir H, Taketo MM, Sommer L, Krumlauf R, Tzahor E. 2007. Cranial neural crest cells regulate head muscle patterning and differentiation during vertebrate embryogenesis. *Development* 134(17):3065-3075.
- Quinzio S, Fabrezi M. 2014. The lateral line system in anuran tadpoles: Neuromast morphology, arrangement, and innervation. *The Anatomical Record* 297(8):1508–1522.
- Rios AC, Marcelle C. 2009. Head muscles: aliens who came in from the cold? *Developmental Cell* 16(6):779-780.

References

- Roberts A, Walford A, Soffe S, Yoshida M. 1999. Motoneurons of the axial swimming muscles in hatchling *Xenopus tadpoles*: Features, distribution, and central synapses. *Journal of Comparative Neurology* 411(3):472–486.
- Roos WP, Kaina B. 2006. DNA damage-induced cell death by apoptosis. *Trends in Molecular Medicine* 12(9):440-450.
- Rylkoff H. 1924. Die Entwicklung der Schultermuskeln bei urodelen Amphibien. *Zeitschrift für wissenschaftliche Zoologie* 122:118-171.
- Sadaghiani B, Thiébaud CH. 1987. Neural crest development in the *Xenopus laevis* embryo, studied by interspecific transplantation and scanning electron microscopy. *Developmental Biology* 124(1):91-110.
- Samaan G, Yugo D, Rajagopalan S, Wall J, Donnell R, Goldowitz D, Gopalakrishnan R, Venkatachalam S. 2010. Foxn3 is essential for craniofacial development in mice and a putative candidate involved in human congenital craniofacial defects. *Biochemical and Biophysical Research Communications* 400(1):60-65.
- Sambasivan R, Kuratani S, Tajbakhsh S. 2011a. An eye on the head: the development and evolution of craniofacial muscles. *Development* 138(12):2401-2415.
- Sambasivan R, Kuratani S, Tajbakhsh S. 2011b. An eye on the head: the development and evolution of craniofacial muscles. *Development* 138(12):2401-2415.
- Santagati F, Rijli FM. 2003. Cranial neural crest and the building of the vertebrate head. *Nature Reviews Neuroscience* 4(10):806-818.
- Sato M, Tsai H-J, Yost HJ. 2006. Semaphorin3D regulates invasion of cardiac neural crest cells into the primary heart field. *Developmental Biology* 298(1):12-21.
- Sato M, Yost HJ. 2003. Cardiac neural crest contributes to cardiomyogenesis in zebrafish. *Developmental Biology* 257(1):127-139.
- Schlade-Bartusiak K, Macintyre G, Zurich J, Cox DW. 2008. A child with deletion (14)(q24. 3q32. 13) and auditory neuropathy. *American Journal of Medical Genetics Part A* 146(1):117-123.
- Schlosser G. 2010. Making senses: development of vertebrate cranial placodes. *International review of cell and molecular biology*: Elsevier. p 129-234.
- Schlosser G. 2014. Early embryonic specification of vertebrate cranial placodes. *Wiley Interdisciplinary Reviews: Developmental Biology* 3(5):349-363.
- Schlosser G, Ahrens K. 2004. Molecular anatomy of placode development in *Xenopus laevis*. *Developmental Biology* 271(2):439–466.

References

- Schlosser G, Northcutt RG. 2000. Development of neurogenic placodes in *Xenopus laevis*. *The Journal of Comparative Neurology* 418 (2):121–146.
- Schlosser G, Roth G. 1995. Distribution of cranial and rostral spinal nerves in tadpoles of the frog *Discoglossus pictus* (Discoglossidae). *Journal of Morphology* 226(2):189–212.
- Schlosser G, Roth G. 1995. Distribution of cranial and rostral spinal nerves in tadpoles of the frog *Discoglossus pictus* (Discoglossidae). *Journal of Morphology* 226(2):189-212.
- Schlosser G, Roth G. 1997a. Evolution of nerve development in frogs. II. Modified development of the peripheral nervous system in the direct-developing frog *Eleutherodactylus coqui* (Leptodactylidae). *Brain, Behavior and Evolution* 50(2):94-128.
- Schlosser G, Roth G. 1997b. Evolution of Nerve Development in Frogs; pp. 61–73. *Brain, Behavior and Evolution* 50(2):61-73.
- Schmidt J, Piekarski N, Olsson L. 2013. Cranial muscles in amphibians: development, novelties and the role of cranial neural crest cells. *Journal of Anatomy* 222(1):134-146.
- Schmidt J, Schuff M, Olsson L. 2011. A role for FoxN3 in the development of cranial cartilages and muscles in *Xenopus laevis* (Amphibia: Anura: Pipidae) with special emphasis on the novel rostral cartilages. *Journal of Anatomy* 218(2):226-242.
- Schuff M, Rossner A, Donow C, Knochel W. 2006. Temporal and spatial expression patterns of FoxN genes in *Xenopus laevis* embryos. *International Journal of Developmental Biology* 50(4):429-434.
- Schuff M, Rossner A, Wacker SA, Donow C, Gessert S, Knochel W. 2007. FoxN3 is required for craniofacial and eye development of *Xenopus laevis*. *Developmental Dynamics* 236(1):226-239.
- Scott KL, Plon SE. 2003. Loss of Sin3/Rpd3 histone deacetylase restores the DNA damage response in checkpoint-deficient strains of *Saccharomyces cerevisiae*. *Molecular and Cellular Biology* 23(13):4522-4531.
- Sefton EM, Bhullar BA, Mohaddes Z, Hanken J. 2016. Evolution of the head-trunk interface in tetrapod vertebrates. *Elife* 5:e09972.

- Sefton EM, Piekarski N, Hanken J. 2015. Dual embryonic origin and patterning of the pharyngeal skeleton in the axolotl (*Ambystoma mexicanum*). *Evolution and Development* 17(3):175-184.
- Shelton PM. 1970. The lateral line system at metamorphosis in *Xenopus laevis* (Daudin). *Journal of Embryology and Experimental Morphology* 24(3):511–524.
- Simmons AM, Costa LM, Gerstein HB. 2004. Lateral line mediated rheotactic behavior in tadpoles of the African clawed frog (*Xenopus laevis*). *Journal of Comparative Physiology A* 190(9):747–758.
- Song JK, Boord RL. 1993. Motor components of the trigeminal nerve and organization of the mandibular arch muscles in vertebrates. Phylogenetically conservative patterns and their ontogenetic basis. *Cells Tissues Organs* 148(2–3):139–149.
- Song JK, Northcutt RG. 1991. The primary projections of the lateral-line nerves of the Florida gar, *Lepisosteus platyrhincus*. *Brain, Behavior and Evolution* 37(1):38–63.
- Spemann H. 2013. *Experimentelle Beiträge zu einer Theorie der Entwicklung*: Springer-Verlag.
- Strong OS. 1895. The cranial nerves of Amphibia. *Journal of Morphology* 10:101–230.
- Tada MN, Kuratani S. 2015. Evolutionary and developmental understanding of the spinal accessory nerve. *Zoological Letters* 1:4.
- Theis S. 2010. *Origin and development of cucullaris/trapezius-sternocleidomastoid muscles in birds, mammals and reptiles*: Albert-Ludwig-Universität Freiburg im Bresigau.
- Theis S, Patel K, Valasek P, Otto A, Pu Q, Harel I, Tzahor E, Tajbakhsh S, Christ B, Huang R. 2010. The occipital lateral plate mesoderm is a novel source for vertebrate neck musculature. *Development* 137(17):2961-2971.
- Tirosh-Finkel L, Elhanany H, Rinon A, Tzahor E. 2006a. Mesoderm progenitor cells of common origin contribute to the head musculature and the cardiac outflow tract. *Development* 133(10):1943-1953.
- Tirosh-Finkel L, Elhanany H, Rinon A, Tzahor E. 2006b. Mesoderm progenitor cells of common origin contribute to the head musculature and the cardiac outflow tract. *Development* 133(10):1943-1953.
- Tokita M, Schneider RA. 2009. Developmental origins of species-specific muscle pattern. *Developmental Biology* 331(2):311-325.

References

- Tomita Y, Matsumura K, Wakamatsu Y, Matsuzaki Y, Shibuya I, Kawaguchi H, Ieda M, Kanakubo S, Shimazaki T, Ogawa S. 2005. Cardiac neural crest cells contribute to the dormant multipotent stem cell in the mammalian heart. *Journal of Cell Biology* 170(7):1135-1146.
- Trainor PA, Krumlauf R. 2001. Hox genes, neural crest cells and branchial arch patterning. *Current Opinion in Cell Biology* 13(6):698-705.
- Tzahor E. 2009. Heart and craniofacial muscle development: a new developmental theme of distinct myogenic fields. *Developmental Biology* 327(2):273-279.
- Tzahor E, Evans SM. 2011. Pharyngeal mesoderm development during embryogenesis: implications for both heart and head myogenesis. *Cardiovascular Research* 91(2):196-202.
- Tzahor E, Kempf H, Mootosamy RC, Poon AC, Abzhanov A, Tabin CJ, Dietrich S, Lassar AB. 2003. Antagonists of Wnt and BMP signaling promote the formation of vertebrate head muscle. *Genes and Development* 17(24):3087-3099.
- Tzahor E, Lassar AB. 2001. Wnt signals from the neural tube block ectopic cardiogenesis. *Genes and Development* 15(3):255-260.
- Wagner GP. 2007. The developmental genetics of homology. *Nature Reviews Genetics* 8(6):473.
- Wagner GP. 2014. *Homology, genes, and evolutionary innovation*: Princeton University Press.
- Wake DB, Roth G, Wake MH. 1983. Tongue evolution in lungless salamanders, family plethodontidae. III. Patterns of peripheral innervation. *Journal of Morphology* 178(3):207-224.
- Wake MH. 1992. Patterns of peripheral innervation of the tongue and hyobranchial apparatus in caecilians (Amphibia: Gymnophiona). *Journal of Morphology* 212(1):37-53.
- Wake MH. 1993. Evolutionary diversification of cranial and spinal nerves and their targets in the gymnophione amphibians. *Cells Tissues Organs* 148(2-3):160-168.
- Waldo K, Miyagawa-Tomita S, Kumiski D, Kirby ML. 1998. Cardiac neural crest cells provide new insight into septation of the cardiac outflow tract: aortic sac to ventricular septal closure. *Developmental Biology* 196(2):129-144.
- Waldo KL, Hutson MR, Stadt HA, Zdanowicz M, Zdanowicz J, Kirby ML. 2005. Cardiac neural crest is necessary for normal addition of the myocardium to the

- arterial pole from the secondary heart field. *Developmental Biology* 281(1):66-77.
- Warth P. 2017. Development of the muscles and the skeleton of the head in certain actinopterygian fishes. unpublished PhD thesis: Friedrich-Schiller-Universität Jena.
- Wassersug R, Hessler CM. 1971. Tadpole behaviour: Aggregation in larval *Xenopus laevis*. *Animal Behaviour* 19(2):386–389.
- Wiedersheim R, Weismann A. 1904. Über das Vorkommen eines Kehlkopfes bei Ganoiden und Dipnoern: sowie über die Phylogenie der Lunge. Verlag von Gustav Fischer.
- Winterbottom R. 1974. Descriptive synonymy of striated muscles of Teleostei. *Proceedings of the Academy of Natural Sciences of Philadelphia* 125(12):225–317.
- Wolpert L, Jessell T, Lawrence P, Meyerowitz E, Robertson E, Smith J. 2007. *Principles of Development*: Oxford University Press.
- Yamaguchi M, Tonou-Fujimori N, Komori A, Maeda R, Nojima Y, Li H, Okamoto H, Masai I. 2005. Histone deacetylase 1 regulates retinal neurogenesis in zebrafish by suppressing Wnt and Notch signaling pathways. *Development* 132(13):3027-3043.
- Yamamoto Y, Sawa R, Okamoto N, Matsui A, Yanagisawa M, Ikemoto S. 1986. Deletion 14q(q24.3 to q32.1) syndrome: significance of peculiar facial appearance in its diagnosis, and deletion mapping of Pi(alpha 1-antitrypsin). *Human Genetics* 74(2):190-192.
- Yelbuz TM, Waldo KL, Kumiski DH, Stadt HA, Wolfe RR, Leatherbury L, Kirby ML. 2002. Shortened outflow tract leads to altered cardiac looping after neural crest ablation. *Circulation* 106(4):504-510.
- Yelbuz TM, Waldo KL, Zhang X, Zdanowicz M, Parker J, Creazzo TL, Johnson GA, Kirby ML. 2003. Myocardial volume and organization are changed by failure of addition of secondary heart field myocardium to the cardiac outflow tract. *Developmental Dynamics* 228(2):152-160.
- Young SH, Poo MM. 1983. Rapid lateral diffusion of extra junctional acetylcholine receptors in the developing muscle membrane of *Xenopus tadpole*. *Journal of Neuroscience* 3(1):225–231.

References

- Zhu M, Ahlberg PE, Pan Z, Zhu Y, Qiao T, Zhao W, Jia L, Lu J. 2016. A Silurian maxillate placoderm illuminates jaw evolution. *Science* 354(6310):334-336.
- Ziermann JM, Diogo R. 2013. Cranial Muscle Development in the Model Organism *Ambystoma mexicanum*: Implications for Tetrapod and Vertebrate Comparative and Evolutionary Morphology and Notes on Ontogeny and Phylogeny. *Anatomical Record* 296(7):1031-1048.
- Ziermann JM, Diogo R. 2014. Cranial muscle development in frogs with different developmental modes: direct development versus biphasic development. *Journal of Morphology* 275(4):398-413.
- Ziermann JM, Freitas R, Diogo R. 2017. Muscle development in the shark *Scyliorhinus canicula*: implications for the evolution of the gnathostome head and paired appendage musculature. *Frontiers in Zoology* 14(1):31.
- Ziermann JM, Olsson L. 2007. Patterns of spatial and temporal cranial muscle development in the African clawed frog, *Xenopus laevis* (Anura: Pipidae). *Journal of Morphology* 268(9):791-804.

Eigenständigkeitserklärung (Declaration of authorship)

Ich erkläre hiermit, dass mir die Promotionsordnung der Fakultät für Pharmazie und Biologie der Friedrich-Schiller-Universität Jena bekannt ist. Die vorliegende Dissertationsschrift wurde selbstständig, ohne die Hilfe Dritter und ohne Benutzung anderer als der angegebenen Hilfsmittel angefertigt. Die aus anderen Quellen direkt oder indirekt übernommenen Daten und Konzepte sind unter Angabe der Quellen gekennzeichnet. Alle Personen die Beiträge zum Material, zur Auswertung dieses oder zur Herstellung der Manuskripte geleistet haben sind jeweils als Autoren aufgeführt:

Prof. Dr. Lennart Olsson¹, Dr. Peter Warth¹, Dipl. Bio. Jennifer Schmidt¹, Dr. Peter Konstantinidis²

¹Institut für Zoologie und Evolutionsforschung, Friedrich-Schiller-Universität, Jena, Germany

²Department of Fisheries and Wildlife, Oregon State University, Corvallis, Oregon, USA

Die Hilfe des Promotionsberaters wurde nicht in Anspruch genommen und es wurden Dritten weder mittelbar noch unmittelbar durch geldwerte Leistungen für Arbeiten entlohnt die im Zusammenhang mit dem Inhalt dieser Dissertation stehen. Die Dissertationsschrift wurde nicht bereits zuvor als Prüfungsarbeit für eine Staatliche oder andere wissenschaftliche Prüfung eingereicht.

CURRICULUM VITAE

Name: Benjamin Naumann

Date of birth: 02.03.1990 in Sömmerda

Citizenship: german

Marital status: unmarried, no children

Address: Magdelstieg 19, 07745 Jena, Germany

Educational background:

since 2014 - PhD student at the University of Jena

PhD thesis: “Head, trunk and in between - The evolution and development of muscles in the head/trunk interface of vertebrates”

2011-2014 – M.Sc. in Biology, Section: “Evolution, Ecology and Systematics”,
University of Jena (1,1)

Master thesis: “The development of the cucullaris and the hypobranchial muscles in the Mexican axolotl and the zebrafish” (1,0)

2008-2011 – B.Sc. in Biology, University of Jena (1,6)

Bachelor thesis: “The development of the cucullaris muscle in the Mexican axolotl”
(1,1)

2008 Diploma from german secondary school (Prof. Fritz Hofmann Gymnasium;
Abiturnote 1,6); Seminar topic: “Kurioses Haustier oder Wissenschaftswunder? –
Eine aktuelle Untersuchung zum Stand der Regenerationsforschung am
Mexikanischen Axolotl (*Ambystoma mexicanum*)” (“Strange pet or scientific
marvel? – An actual review on the regenerative research in the Mexican axolotl
(*Ambystoma mexicanum*).”)

Main research interests:

Development and evolution of the vertebrate head

Developmental morphology of the peripheral nervous system in basal vertebrates

Evolution and development of the vertebrate heart

Evolutionary morphology of the diplopod head

Functional morphology of the copulatory organs in diplopods

Publications:

- Konstantinidis, P., Warth, P., **Naumann, B.**, Metscher, B., Hilton, E.J., Olsson, L. (2015). The Developmental Pattern of the Musculature Associated with the Mandibular and Hyoid Arches in the Longnose Gar, *Lepisosteus osseus* (Actinopterygii, Ginglymodi, Lepiosteiformes). *Copeia* 103: 920-932
- Warth, P., Konstantinidis, P., Hilton, E.J., **Naumann, B.** & Olsson, L. (2016). Development of the skull and pectoral girdle in Siberian sturgeon, *Acipenser baerii*, and Russian sturgeon, *Acipenser gueldenstaedtii* (Acipenseriformes: Acipenseridae). *Journal of Morphology* 278: 418-442.
- Schweiger, S., **Naumann, B.**, Larson, J.G., Möckel, L. & Müller, H. (2017). Direct development in the African squeaker frogs (Anura: Arthroleptidae: *Arthroleptis*) reveals a mosaic of derived and plesiomorphic characters. *Organisms, Diversity and Evolution* (2017) 17: 693.
- Naumann, B.**, Warth, P., Olsson, L., & Konstantinidis, P. (2017). The development of the cucullaris muscle and the branchial musculature in the Longnose Gar (*Lepisosteus osseus*, Lepiosteiformes, Actinopterygii) and its implications for the evolution and development of the head/trunk interface in vertebrates. *Evolution & Development*, 19(6), 263-276.
- Warth, P., Hilton, E. J., **Naumann, B.**, Olsson, L., & Konstantinidis, P. (2017). Development of the muscles associated with the mandibular and hyoid arches in the Siberian sturgeon, *Acipenser baerii* (Acipenseriformes: Acipenseridae). *Journal of Morphology*.
- Naumann, B.** & Olsson, L. (2017). Three-dimensional reconstruction of the cranial and anterior spinal nerves in early tadpoles of *Xenopus laevis* (Pipidae, Anura). *Journal of Comparative Neurology*.

Publications in preparation:

- Naumann, B.**, Akkari, N., Reip, H. S., Neubert, D. (*in prep.*). Inside the head of a cybertype – 3D reconstruction of the head muscles of *Ommatoiulus avatar* Akkari and Enghoff, 2015 (Diplopoda: Julidae) and insights on the head musculature of Juliformia.

Teaching experience:

WS 2009/10; 2010/11; 2011/12 - Tutorium Systematic Zoology (Bachelor)

SS 2010 - Tutorium General Zoology (Bachelor)

WS 2012/13; 2013/14; 2016/17; 2017/2018 - Practical course in animal anatomy (Bachelor)

WS 2013/14; 2014/15; 15/16; 16/17 - Practical course in histology and embryology (Bachelor)

SS 2014 - Practical course in zoological biodiversity (Bachelor)

SS 2015; 2016; 2017 – Methods in invertebrate morphology (Bachelor)

WS 2016/17 - Practical course in fluorescence microscopy, laser scanning microscopy and 3D reconstruction (Master)

Funded proposals:

“In vivo time-lapse tomography of neurulation in developing sturgeons”, I-20140659, 2014, DESY, Hamburg, Germany (approx. 28.800 €)

“Neurulation in developing fishes studied by in vivo time-lapse tomography”, I-20160119, 2015, DESY, Hamburg, Germany (approx. 50.200 €)

“Dispersal and re-aggregation of embryonic precursor cells in early fish embryos studied by in vivo time-lapse tomography”, I-20170159, 2017, DESY, Hamburg, Germany (approx. 43.200 €)

“3D-visualization of the connective tissue architecture in developing fin and limb buds”, I-20170907, 2018, DESY, Hamburg, Germany (approx. 13.800 €)

Research experience:

2009-2011 - Max-Planck-Institut for Chemical Ecology, Department of Molecular Ecology (I. T. Baldwin)

Tasks: DNA/RNA extraction, phytohormone extraction, plant crossings, preparation of samples for HPLC, PCR/qRT-PCR, molecular cloning, ecological greenhouse experiments using *Manduca sexta* and *Nicotiana attenuata*.

2011-2014 - Max-Planck-Institut for Chemical Ecology, Department of Evolutionary Neuroethnology (B. Hansson)

Tasks: DNA/RNA extraction, fluorescent *in situ* hybridization, PCR/qRT-PCR, preparation of chemical competent *E. coli* cells, molecular cloning (e.g. gateway

cloning) in *Drosophila*, *Manduca sexta* and the land hermit crab (*Coenorhiza*),
assistance in electro-physiological experiments using odorants

2016, June - Ichthyological field work at the Virginia Institut for Marine Science
(VIMS), Virginia, USA

since 2018 – Leibniz Institute on Aging, Department of Molecular Genetics (C. Englert)
Task: Anatomical characterization of a mutant zebrafish line

Attended practical courses:

2006 - Max-Planck-Institut for Chemical Ecology, Department of Molecular Ecology (1
week)

2007 - Summer school for chemo and bio sensory technology for secondary school
students (1 week)

2008 - Max-Planck-Institut for Chemical Ecology, S1 greenhouse (4 weeks)

2009 - Practical work about the lateral line organs of juvenile caecilians (2 weeks)

2016 - “Proposal Writing and Funding”, Dr FSU, Jena, Germany (2 days)

2018 - “Research funding in Germany”, Dr FSU, Jena, Germany (0.5 days)

Field trips and field work:

2011, 2012 - Entomological field trip, Lago di Trassimeno, Italy

2011, 2012, 2013, 2014, 2016 - Marine biological field trip, Station bioloquige de
Roscoff, France

2014 - Entomological field trip, Bast, Croatia

2015 - Herpetological field work, Kwazulu-Natal, South Africa

2016 - Entomological field trip, Rovinji, Croatia;

Ichthyological field work in Virginia USA

2017 - Entomological field trip, Rovinji, Croatia

Conferences:

2013 - 106th Annual Meeting of the German Zoological Society (DZG), Munich,
Germany

Poster: “Die Entwicklung des Cucullaris-Muskels des Axolotls (*Ambystoma
mexicanum*)“ (Poster price)

2014 - 5th Meeting of the European Society for Evolutionary Developmental Biology
(EED), Vienna, Austria

Poster: “Developmental studies of the cucullaris muscle in the Mexican axolotl (*Ambystoma mexicanum*).

Forum for Graduate Students, DZG, Sub-division of Morphology, Hamburg, Germany

Talk: “Die Entwicklung der Kopfmuskulatur des Gemeinen Knochenhechtes, *Lepisosteus osseus* (Ginglymodi, Actinopterygii)“

2015 - EMBO Workshop on integrative perspectives of musculo-skeletal development, Ein Gedi, Israel

Talk: “The evolution and development of the pectoral girdle”

Forum for Graduate Students, DZG, Sub-division of Morphology, Jena, Germany (Organization Team)

Talk: “Die Entwicklung der branchiomeren Cranialnerven und Kopfmuskulatur des Türkisen Prachtgrundkärpflings, *Nothobranchius furzeri*”

2016 - International Congress of Vertebrate Morphology (ICVM), Washington D.C., USA

Talk: “The development and evolution of the cranial nerves and head muscles in two actinopterygian fishes, the Longnose gar (*Lepisosteus osseus*) and the Turquoise killifish (*Nothobranchius furzeri*)”

6th Meeting of the European Society for Evolutionary Developmental Biology (EED), Uppsala, Sweden

Poster: “New hearts for new heads FoxN3 is involved in the development of a 3-chambered heart in *Xenopus laevis* (Anura, Lissamphibia)”

Poster at the 2nd Nothobranchius Symposium, Jena, Germany

“A look beneath the surface: Cranial nerve development of *Nothobranchius furzeri* & the EvoDevo of the trigeminal nerve”

2017- Posters at the 17th International Congress of Myriapodology, Krabi, Thailand

Poster 1: “The taxonomic value of the vulvae in millipedes of the family Julidae (Diplopoda)”

Poster 2: “One for a thousand? - The evolution of the musculo-skeletal system of the diplopod head”

Popular science articles about conducted research:

“Head, trunk and in between – Understanding the origin of muscles that join head and trunk.” (2017), Research Highlights, *Nature*, 550, 432-433.

“Muskelentwicklung bei Fischen liefert Erkenntnisse über die Evolution der Landwirbeltiere. Evolutionsbiologen identifizieren wichtigen Muskel bei ursprünglichen Fischen“ (2017), *Nachrichten aus der Forschung*, Friedrich-Schiller-Universität, Jena, Germany.

Acknowledgements

I am very thankful to my doctoral adviser Prof. Lennart Olsson. He always gave me the opportunity to freely follow all the questions that appeared during my work and had always an open ear and constructive criticism. I am especially thankful that he gave me the possibility to attend many conferences and meet scientists working in the same field.

I thank Prof. Martin Fischer for the financial support at the beginning of my dissertation, for agreeing to evaluate it and for his valuable advice and challenging conversations during the past years.

I also want to thank Prof. Shigeru Kuratani for agreeing to be my external reviewer.

I thank Dr. Peter Warth for giving me the opportunity to join his research on sturgeons, for pushing me during long lab-nights, for critical reading of this manuscript and for simply becoming a really good friend over the years.

I am grateful to Dr. Peter Konstantinidis who introduced me into the world of Actinops and gave me the opportunity to work on *Lepisosteus* in the lab as well as in the field. Dr. Hendrik Müller always had good advice and allowed me to join his field work in South Africa which created unforgettable moments and started my interest in direct development in amphibians. I thank Dr. Hans Pohl for invaluable advice when it comes to the work on illustrations. I thank Dr. Benjamin Wipfler and David Neubert for their help with different 3D reconstruction softwares. Furthermore I would like to thank Katja Felbel for her help with the histological sections and the tasty wake-up coffee at lab-mornings. I would also like to thank the “selfless” Lars and the “well-organized” Susan for being some of the best office buddies and friends. Dr. Jörg Hammel and Dr. Julian Moosmann invested much time in μ CT scanning and in-vivo phase contrast

Acknowledgements

imaging during our experiments at the DESY. Furthermore, I would like to thank the whole team at the P05 for making these experiments possible.

Many more people from different research institutions helped me during the past years. I therefore would like to thank these people for good discussions, advice concerning special techniques, embryo material and the most important a nice and inspiring working atmosphere: Jennifer Schmidt, Patrick Arnold, Paul Lukas, Julian Sartori, Michael Richter, Prof. Christoph Englert and his lab members, Prof. Rolf Beutel and Sandra Rüdiger. I would also like to thank Dr. Eric Hilton for the opportunity to stay at the Virginia Institute of Marine Science and Dr. Kristene Parsons, CJ Sweetman and Cindy Marin-Martinez for their support during the time there.

I am deeply grateful that all the people mentioned allowed me to learn from them and each time maybe become a slightly better scientist.

The greatest thanks go to my parents and family! They always supported me with great endurance and love! Thanks to you all, I am grateful to have you!!!